Unravelling the Host Immunomodulation by Two Gram-negative Enteric Bacterial Ligands

Aakanksha Gulati

A thesis submitted for the partial fulfillment of
the degree of Doctor of Philosophy

Department of Biological Sciences
Indian Institute of Science Education and Research Mohali
Knowledge city, Sector 81, SAS Nagar, Manauli PO, Mohali 140306, Punjab, India.

September, 2019

I would like to dedicate my thesis to my mother, without whose support I would not have achieved anything.

Declaration

The work presented in this thesis has been carried out by me under the guidance of Dr. Arunika Mukhopadhaya at the Indian Institute of Science Education and Research Mohali. This work has not been submitted in part or in full for a degree, a diploma, or a fellowship to any other university or institute. Whenever contributions of others are involved, every effort is made to indicate this clearly, with due acknowledgement of collaborative research and discussions. This thesis is a bona fide record of original work done by me and all sources listed within have been detailed in the bibliography.

Date:
Place:

Aakanksha Gulati

In my capacity as the supervisor of the candidate's thesis work, I certify that the above statements by the candidate are true to the best of my knowledge.

Date:
Place:

Dr. Arunika Mukhopadhaya

Acknowledgements

I would like to thank my guide, Dr. Arunika Mukhopadhaya, who has helped me throughout my PhD. She guided me through my problems and was available for any advice that I needed. She also helped me improve my presentation and writing skills. She was open to new ideas and suggestions and encouraged me to try newer things.

I would also like to thank my doctoral committee members, Dr. Rachna Chaba and Dr. Mahak Sharma for their constant evaluation and suggestions, which helped me improve my perspective and my research work. They also provided me with some strains and materials for my research work. I would also like to thank Dr. Kausik Chattopadhyay for his suggestions and support all through my PhD. He was always available for any kind of guidance I required. I also thank Dr. Shravan Mishra and his lab members for helping me with yeast two hybrid based experiments. I also thank Dr. Francisco Ramos-Morales (University of Seville, Spain), Dr. Rajesh Ramachandran and Dr. Ram Yadav (IISER Mohali) for providing me with materials for my research work.

I would like to thank my seniors Dr. Sanica Sakharwade, Dr. Shelly Gupta, Dr. Barkha Khilwani, Dr. Karan Paul and Dr. Junaid Khan, who taught me various technques in the initial years of my PhD. I would like to extend my thanks and love to my lab members- Krishna, Vinica, Deepinder, Arpita, Shraddha, Yogesh, Shashi and Shilpa, who have constantly been there and have helped me improve upon me as a person. They have always tried to cheer me up in my tougher times and have accompanied me for tea breaks. They filled life into my living. I feel lucky and proud to have found friends in my lab mates. I would also like to thank Dr. Ranjai Kumar and Rhythm Shukla for their support and contribution to my thesis work. I would also thank members of Dr. Kausik Chattopadhyay's lab for helping me in troubleshooting for some of the experiments. I would like to thank Dr. Ritam Sinha for teaching me animal handling.

I would like to thank Indian Institute of Science Education and Research Mohali for giving me the opportunity and the facilities to do my PhD. I would also thank Indian Council of Medical Research (ICMR) for funding me for the PhD programme.

I would like to extend my heartfelt thanks to my parents and my brother for always supporting me and motivating me throughout. I would especially like to thank my mother, who was also my best

friend, for giving wings to my dreams and helping me grow into the person I now am. She stood by me like a wall and always caught me when I was about to fall.

I would like to thank my friends especially Prince Saini and Gaurav Rose for being patient with me and always extending an ear when I needed. Their advices helped me improve upon myself as a person and a researcher.

Abstract

Bacteria while infecting a host brings a group of arsenals with it in terms of antigens/ligands to pathogenize the host. Host immune cells on the other hand induce innate immune (pro-inflammatory) responses and adaptive immune responses against them to win the battle and clear out infections. In the thesis work, we have studied two of these bacterial ligands namely, *Vibrio parahaemolyticus* OmpU (VpOmpU) and SteA of *Salmonella enterica* Typhimurium for their role in modulation of host innate immune responses.

V. parahaemolyticus is a non-invasive, marine bacterium, which causes severe gastroenteritis in humans upon consumption of raw or undercooked sea food. The role of VpOmpU in pathogenesis of *V. parahaemolyticus* was not explored till date. In our attempt to characterize VpOmpU for modulation of host's innate immune responses, we have observed that it induces pro-inflammatory responses in macrophages and monocytes via TLR2-MyD88-IRAK-1-MAPkinases-AP-1 and NF-κB pathway. TLR2 forms hetero-dimer either with TLR1 or TLR6 to recognize different ligands. We have shown that VpOmpU is recognized by both TLR1/2 and TLR2/6 hetero-dimer in macrophages. This is the first report of a natural ligand recognized by both TLR1/2 and TLR2/6 hetero-dimers.

Salmonella enterica Typhimurium is an invasive Gram negative bacterium which has been known to cause gastroenteritis in humans known as salmonellosis and typhoid-like disease in mice. It is equipped with a specialized machinery called the type-3 secretion system through which it translocate various effector proteins directly into the host cytoplasm. These effectors then modulate various host-responses and help the bacteria to survive in the host. We are showing that, SteA, an effector protein of *S.* Typhimurium suppresses host-immune responses by interfering with NF-κB activation. We have further elucidated the mechanism that SteA employs to suppress this pathway.

So far, the two enteric bacterial ligands that we have studied in the thesis work have differential effect on host's immune responses, such as, VpOmpU activates, whereas, SteA suppresses host's immune system.

These observations suggest the complexity inflicted by the antigens/ligands in the bacterial pathogenesis and, this underscores the need to study in great detail, the role of bacterial ligands in host modulation, to be able to design effective therapy or vaccine.

Synopsis

Synopsis: Unravelling the host immunomodulation by two gram negative enteric bacterial ligands.

Introduction

Various Gram-negative bacteria infect humans and cause enteric diseases. These bacteria employ various strategies to infect the host and in turn the host also deploys its immune system to fight off the infection and kill the invading bacteria. The human immune system consists of the innate immune system and the adaptive immune system. The innate immune cells sense the bacterial invasion first, they recognize specific patterns on the bacteria and induce a pro-inflammatory response. This, further leads to the secretion of various cytokines to inform other immune cells of the infection. The innate immune response also activates the adaptive immune system. The bacteria also modulate the host immune system in various ways to be able to establish an infection. In this study, we have studied how OmpU, an outer membrane protein of *Vibrio parahaemolyticus* and SteA, a translocation effector of *Salmonella enterica* Typhimurium as modulate host's innate immune responses.

Aim 1- To study the host immunomodulation by OmpU of *Vibrio parahaemolyticus*

Aim 2- To study the host immunomodulation by SteA of *Salmonella enterica* Typhimurium

Aim 1: To study the host immunomodulation by OmpU of *Vibrio parahaemolyticus*

Vibrio parahaemolyticus is a gram negative, non-invasive bacteria which is majorly found in the marine and estuarine waters. *V. parahaemolyticus* is known to infect humans and cause acute gastroenteritis upon consumption of raw or undercooked sea food, in addition to this, *V. parahaemolyticus* infection may also lead to septicaemia and death. Its pathogenesis is mainly attributed to haemolysins- Thermostable Direct Haemolysin (TDH) and TDH- related Haemolysin (TRH). The strains deficient in the major toxins TDH and TRH have also been found to be virulent indicating additional factors involved in its virulence. Some factors such as Thermolabile Haemolysin (TLH) and effectors secreted by the type-III secretion system and the type-VI secretion systems have also been implicated in its virulence, although to a much lesser extent. *V. parahaemolyticus* is also equipped with a master regulon called ToxRS which regulates many of

the virulence genes including TDH and TRH. In addition to these, ToxRS has also been known to regulate a major outer membrane protein OmpU, indicating its requirement in the pathogenesis. OmpU is a porin present across *Vibrio* sp. and has been found to have varied roles towards host responses in different species. For example, OmpU of *V. vulnificus* has been found to have a role in adhesion, in *V. splendidus*, OmpU helps in both adhesion and invasion. Also, OmpU of *V. cholerae* has been shown to induce programmed cell death. Additionally, OmpU from some of the *Vibrio* species have been shown to be immunogenic. Pertaining to this, OmpU from *V. alginolyticus* and *V. harveyi* have also been developed as a vaccine candidate. OmpU of *V. parahaemolyticus* (VpOmpU) has also been found to be immunogenic in yellow croaker fish. However, a detailed immunological characterization of the cellular responses evoked by VpOmpU has not been carried out as yet. Therefore, we were interested in understanding how OmpU modulates immune cells such as macrophages and monocytes. Towards this, we have formulated the following objectives:

1) To purify OmpU from *Vibrio parahaemolyticus*

2) To check if OmpU modulates innate immune cells

3) To probe how OmpU is recognized by the innate immune cells

4) To understand the underlying signalling mechanism of innate-immunomodulation

Objective 1- To purify OmpU from *Vibrio parahaemolyticus*

OmpU is present across *Vibrio* species and has been characterized as a porin protein in many of the species. However, VpOmpU has not been characterized as a functional porin till date. To be able to characterize VpOmpU as a porin and to probe its role in host-modulation, we purified it from the outer membrane of *Vibrio parahaemolyticus*. We employed detergent based extraction of all the outer membrane proteins of *V. parahaemolyticus* and then subjected them to anion exchange and size exclusion chromatography to purify VpOmpU from the outer membrane. Further, we did a Far-UV Circular Dichroism analysis of VpOmpU and found it to majorly consist of β-sheets. This result is in accordance with the predicted structure of VpOmpU generated using the crystal structure of *Vibrio cholerae* OmpU (70 % similarity to the sequence of VpOmpU).

Then, using liposome swelling assay we confirmed that VpOmpU acts as a porin, similar to the other OmpU proteins.

Objective 2- To check if OmpU modulates innate immune cell functions

The innate immune system of the host is the first to recognize an intrusion by a pathogen. The innate immune cells namely the monocytes and macrophages, then secrete various cytokines to signal other cells about the infection. Therefore, we first checked whether VpOmpU could elicit an immune response in monocytes and macrophages. Towards this, we used THP-1 (human monocytic cell line) and RAW 264.7 (murine macrophage cell line). We observed that, in response to VpOmpU, both RAW 264.7 macrophages and THP-1 monocytes produce pro-inflammatory cytokines namely TNFα and IL-6. In addition to these, RAW 264.7 macrophages produce Nitric oxide in response to VpOmpU. Altogether, these results indicated that VpOmpU elicits a pro-inflammatory response in monocytes and macrophages.

Objective 3- To probe how OmpU is recognized by the innate immune cells

To be able to sense pathogens, monocytes and macrophages have been equipped with specialized receptors called the Pattern Recognition Receptors (PRR) which identify distinct patterns or moieties on the pathogen called the PAMPs or Pathogen associated molecular patterns. This PAMP-PRR interaction then leads to the activation of a signalling cascade resulting in the production of various cytokines. Since, VpOmpU induced the production of pro-inflammatory cytokines by macrophages and monocytes, it must have been recognized as a PAMP by a PRR present on these cells. There are four classes of PRRs namely- Toll- like receptors (TLR), Nucleotide-binding Leucine rich repeat containing receptors (NLR), RIG-like receptors (RLR) and C-type lectin receptors (CLR). Each of these PRR class is specialized in recognizing specific patterns from the pathogens i.e. bacteria, fungi, virus or parasites. Of these, TLRs are known majorly to recognize bacterial PAMPs. There are various TLRs in a cell localized either on the cell surface or in the endosomes. These TLRs either homo-dimerize or hetero-dimerize to recognize and induce a downstream signalling cascade. Therefore, to induce VpOmpU-mediated pro-inflammatory response, we probed whether TLRs could recognize VpOmpU as a PAMP. Interestingly, we found that VpOmpU is being recognized by different TLR- dimers in monocytes and macrophages i.e. it is being recognized by TLR1/2 dimer in monocytes and by both TLR1/2 and TLR2/6 dimers in macrophages. This result is intriguing since these TLR pairs are specialized

to recognize different patterns, yet VpOmpU is being recognized by both TLR2 heterodimers in macrophages, but not in monocytes. Till date, apart from VpOmpU, no other natural PAMP had been demonstrated to show itself differentially in different cell types.

Objective 4- To understand the underlying signalling mechanism of innate-immunomodulation

Upon TLR activation, a downstream signalling cascade is initiated leading to the activation of transcription factors which transcribe genes related to pro-inflammatory responses. In our study, we have observed that upon recognition of VpOmpU, the TLRs on both macrophages and monocytes recruit MyD88 which is an adaptor molecule. MyD88 further recruits IRAK-1, a kinase which phosphorylates downstream molecules leading to the degradation of IκB (inhibitor of NF-κB) and the activation of MAP-kinases (p38 and JNK). This further activates the sub-units of both NF-κB and AP-1 transcription factors. In RAW 264.7 cells, c-Rel (sub-unit of NF-κB) and JunB, c-Jun and c-Fos (sub-units of AP-1) were activated and in THP-1 cells, p65 (sub-unit of NF-κB) and JunB, c-Jun, JunD and c-Fos (sub-units of AP-1) were found to be activated in response to VpOmpU. Using TLR2-deficient mice, we also observed that the activation of MAP-kinases is dependent on the TLR2-mediated recognition of VpOmpU.

Conclusion

This study showed that VpOmpU elicits a pro-inflammatory response in monocytes and macrophages. VpOmpU is recognized by TLR1/2 heterodimers in THP-1 cells and by TLR1/2 and TLR2/6 dimers in RAW 264.7 cells. The activation of TLRs further leads to a MyD88-IRAK1 dependent activation of p38 and JNK MAP-kinases leading to the activation of NF-κB and AP-1 transcription factors.

Aim 2- To study the host immunomodulation by SteA of *Salmonella enterica* Typhimurium

Salmonella enterica Typhimurium is a Gram-negative, invasive bacterium which causes gastroenteritis in humans and typhoid-like disease in mice. Due to a high similarity (about 85 %) with the typhoid causing bacteria *S. typhi,* it is widely used as a laboratory strain to study typhoid. For its infection, *S.* Typhimurium uses a needle like machinery called the type-3 secretion system

(T3SS) to secrete about 40 effectors directly into the cytoplasm of the host cells. Many of these effectors have been characterized to have roles in modulating host functions to help the invasion and survival of the bacteria inside the host cell. Upon invasion, the bacteria forms a *Salmonella* containing vacuole (SCV) where the bacteria are protected from the cellular environment and can multiply. *S.* Typhimurium is known to utilize two T3SS i.e. T3SS1 and T3SS2 assemblies for its infection. Both these T3SS secrete different set of effector proteins. The T3SS1 is used in the early phases of infection and thus translocates effectors which help in invasion and suppression of immune responses. On the other hand, T3SS2 is required at later stages of infection and translocates effectors required for SCV maintenance, replication and dissemination of the bacteria. Interestingly, some of the effector proteins have dual roles and are secreted by both the T3SS1 and T3SS2. One such effector is *Salmonella* translocated effector A (SteA). The role of SteA in the later phases of infection has been established in the control of membrane dynamics of the SCV. However, its role in the early phases of infection remains unknown. Towards this, we wanted to explore the role of SteA in the early phases of infection and thus have formulated the following objectives:

1) To probe if SteA has a role in virulence of *S.* Typhimurium

2) How SteA affects the immune responses?

3) To probe the mechanism underlying the SteA-mediated effect on immune responses

Objective 1: To probe if SteA has a role in virulence of *S.* Typhimurium

S. Typhimurium causes typhoid-like disease in mice. So, first we deleted *steA* from the genome of *S.* Typhimurium and compared the survival of BALB/c mice upon infection with wild type *S.* Typhimurium (wt) or the deletion mutant of *steA* (Δ*steA*). The mice infected with Δ*steA* were found to have a lower survival than those infected with wt. Also, the mice infected with Δ*steA* showed signs of septic shock syndrome such as pilorected fur, decrease in activity, decrease in response to stimuli and closing of the eye. This indicated that SteA might play a role in virulence by modulating the host-immune responses.

Objective 2: How SteA affects the immune responses?

To further understand whether there is a heightened immune responses, we have isolated cells from the infected spleen and observed higher gene expression of the pro-inflammatory cytokine TNFα in Δ*steA* compared to the wt and the complement strains. Further, we observed an increased TNFα production in response to Δ*steA* than the wt in both murine macrophage cell line RAW 264.7 and the bone marrow derived macrophages (BMDM). The generation of an immune response by macrophages employs a signalling cascade leading to the activation of NF-κB and AP-1 transcription factors. The activation of AP-1 is mediated by the phosphorylation of MAP-kinases. To understand how SteA affects the pro-inflammatory response, we checked the phosphorylation status of MAP-kinases and the activation status of NF-κB after infection of RAW 264.7 cells with wt and Δ*steA* strains. We found no difference in the phosphorylation of the MAP-kinases in wt and Δ*steA* infected cells. However, an increased activation of NF-κB was observed in Δ*steA* infected RAW 264.7 cells as compared to the wt infected cells. These data showed that, SteA acts on the NF-κB pathway to suppress the immune responses.

Objective 3: To probe the mechanism underlying the SteA-mediated effect on immune responses

For the activation of NF-κB, a signalling cascade phosphorylates IKK complex which further phosphorylates IκB. IκB is the inhibitor of NF-κB and is bound to it in the inactivated state. The phosphorylation of IκB leads to its degradation, rendering NF-κB active. We checked the phosphorylation status of IKK and the total IκB levels in cells infected with wt and Δ*steA* strains. We observed no difference in the phosphorylation status of IKK in wt or Δ*steA* infected cells. However, total IκB levels were much lower in cells infected with Δ*steA* than the wt.

The degradation of IκB is a result of its poly-ubiquitination. Ubiquitination is a multi-step pathway which eventually utilizes an E3 Ligase complex to add the poly-ubiquitin chains to the substrate. We further found that SteA interferes with the ubiquitination pathway of IκB. We also observed that SteA does not interfere with the assembly of the E3 ligase complex, but binds to a component of E3 ligase thus preventing complete activation of the ligase. This ultimately leads to suppression of IκB degradation, thus preventing the activation of NF-κB.

Conclusion

Mice infected with Δ*steA* showed lower survival as compared to those infected with the wt. The mice infected with Δ*steA* displayed symptoms of septic shock, an overwhelming immune response which seemed to be the cause of their lower survival. Further observations confirmed that SteA suppresses pro-inflammatory responses generated by macrophages in response to *S.* Typhimurium infection by inhibiting the ubiquitination of IκB, thus preventing the activation of NF-κB.

Table of Contents

List of figures

List of Tables

List of Illustrations

List of Abbreviations

PRR- Pattern Recognition Receptor

PAMP- Pathogen Associated Molecular Patterns

TLR- Toll-like Receptor

NLR- Nucleotide binding Leucine rich repeat containing Receptor

RLR- RIG-I like Receptors

CLR- C-type Lectin Receptor

IL- Interleukin

TNFα- Tumour Necrosis Factor α

NO- Nitric Oxide

LPS- Lipopolysaccharide

MyD88- Myeloid differentiation factor 88

IκB- Inhibitor of NF-κB

OMP- Outer Membrane Protein

T3SS- Type 3 secretion system

OmpU- Outer membrane protein U

VpOmpU- OmpU of *Vibrio parahaemolyticus*

wt-VpOmpU- OmpU isolated from the outer membrane of *Vibrio parahaemolyticus*

TDH- Thermostable direct haemolysin

TRH- TDH-related haemolysin

T6SS- Type 6 secretion system

LB- Luria Bertani broth

BMDM- Bone marrow derived macrophages

Tlr2$^{-/-}$ -TLR2 knockout mice

Myd88$^{-/-}$ -MyD88 knockout mice

M-CSF- Macrophage colony-stimulating factor

PBS- Phosphate buffer saline

SDS- Sodium dodecyl sulphate

CD- Circular Dichroism

ELISA- Enzyme linked immunosorbent assay

DTT- Dithiothreitol

SteA- *Salmonella* translocation effector A

SCV- *Salmonella* containing vacuole

SPI- *Salmonella* Pathogenicity Island

SIF- *Salmonella* induced filament

hpi- hours post infection

MOI- Multiplicity of Infection

PEI- Polyethylenimine

CFU- Colony forming units

HRP- Horseraddish peroxidase

IP- Immunoprecipitation

IB- Immunoblot

SCF- Skp-1, Cullin-1, F-box complex

Introduction

1. Immune system and its components

In a world of co-existence with various micro-organisms such as viruses, bacteria, fungi and parasites, the intrusion of our system by these micro-organisms is inevitable. To be able to endure this, our body is equipped with a defence system called the immune system. The human immune system comprises of the innate immune system and the adaptive immune system (1). The innate immune system with which we are born (as the name suggests), whereas, the immune system that is developed after birth is known as the adaptive immune system. The innate immune cells are capable of recognizing distinct patterns on the invading microbes and hence are the first responder to an invasion (2). They engulf and kill the invading pathogens and secrete various chemical messengers such as cytokines and chemokines to inform and recruit other cells at the site of infection and initiate inflammatory responses (1). The adaptive immune system, upon activation, induces a pathogen-specific response and clears the infection and generates memory (1).

Similar to RBCs, both the innate and the adaptive immune cells or WBCs are derived from haematopoietic stem cell. The immune cells originate from the myeloid or the lymphoid lineage of the haematopoietic stem cell. The innate immune cells such as monocytes and macrophages are derivatives of the myeloid lineage and the adaptive immune cells such as B-cells and T-cells are derived from the lymphoid lineage (1) (Illustration 1).

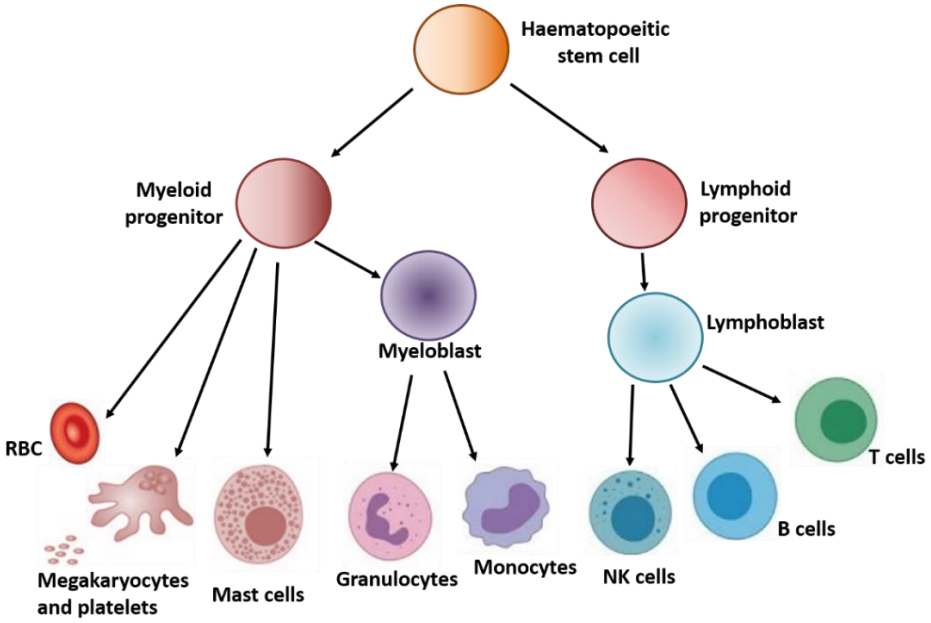

Illustration 1. Cells of the immune system
(parts of the illustration derived from https://www.ibiology.org/immunology/cells-immune-system/)
The haematopoetic stem cell differentiates to either the myeloid progenitor or the lymphoid progenitor. All the immune cells are derived from either the lymphoid or the myeloid progenitor.

1.1 The innate immune cells involved in bacterial infection

The innate immune cells are responsible for the surveillance in the body for any invading pathogen and are the first to respond to an infection. The macrophages, monocytes, neutrophils and dendritic cells are the major innate immune cells involved in the response to a bacterial infection (1).

Macrophages are the tissue-resident phagocytic cells. They are derived from monocytes and are named differently in different organs such as Kupffer cells in the liver, osteoclasts in bone and microglial cells in the brain. They recognize a pathogen and kill it by phagocytosis. They also phagocytose infected cells to avoid the spread of infection. They secrete cytokines like TNFα, IL-1β and IL-6 which lead to the generation of a pro-inflammatory response. Macrophages are also involved in adaptive immune responses by acting as antigen presenting cells.

Monocytes circulate in the bloodstream and migrate to the site of infection where they get differentiated to macrophages upon sensing of pathogens or cytokine signals from other immune cells. They secrete cytokines like TNFα, IL-1β and IL-6 which lead to the generation of a pro-inflammatory response.

Neutrophils are granulocytes and are proficient in killing the pathogens. They sense chemokines secreted at the site of infection and are the first to reach the site of infection from the blood.

Dendritic cells are highly proficient antigen-presenting cells and are responsible for the initiation of the adaptive immune response. These cells reside in immature state in the non-lymphoid tissues and take up the antigen in cases of infection. They process the antigens and present the antigens to the T-cells thereby activating the adaptive immune response.

Gamma delta T-cells are a distinct class of T cells carrying the γδ receptors instead of the conventional αβ receptors. In addition to the T cell receptors, they also have Toll-like receptors (TLR), scavenger receptors and Natural killer cell receptors. They have also been shown to interact with cells of the innate immune system like macrophages and dendritic cells and have been indicated to act as antigen presenting cells. They are known to produce the pro-inflammatory cytokine IL-17 thereby mediating the recruitment and movement of neutrophils to the site of infection. IL-17 also induces the activation of antimicrobial peptides thereby leading to the eradication of bacterial and fungal pathogens.

Complement system involves various proteins which help in chemotaxis, opsonisation and cytolysis of the pathogens. It involves a cascade of proteolytic reactions involving the C1, C2, C4 complexes which eventually cleave C3 and C5 which lead to the formation of membrane attack complex (MAC). MAC forms a transmembrane channel leading to osmotic lysis. The complement system also helps in the clearance of the immune complexes and apoptotic cells. It is known to help in the B-cell response and more recently has also been associated with the T-cell mediated immune response.

2. The process of inflammation

A pathogen when invades our body, it first encounters the physical and chemical barriers of the body like the mucosal layer on the gut epithelium, the hair in the nose, the lysozymes in the tears, gastric acid in the stomach etc (1). If the pathogen is able to breach these barriers, the macrophages residing in the tissue sense these pathogens. The macrophages then phagocytose the pathogen and kill it. Additionally, they secrete various cytokines and chemokines, which help in informing other immune cells of the intrusion. Neutrophils and monocytes, which are present in the bloodstream, then, reach the site of infection and further help in killing the pathogen. Further, the flow of the lymphatic system brings the activated antigen-presenting cells (such as dendritic cells) to the lymphoid organs, thus activating the adaptive immune system

(1). Altogether, the responses initiated by the chemokines and cytokines is called inflammation. Inflammation is characterized by four signs namely heat (calor), redness (rubor), pain (dolor) and swelling (tumor), which are a result of the following stages of inflammation (1):

1. Release of cytokines from macrophages: Upon recognition of the pathogen the tissue-resident macrophages secrete pro-inflammatory cytokines like TNFα and IL-6.
2. Vasodilation: It is the increase in diameter of the capillaries which is caused by various cytokines like TNFα. This results in increased blood flow at the site of infection, resulting in increased access to circulating immune cells to the site of infection. This also causes heat and redness at the infection site.
3. Increase in vascular permeability: Cytokines also increase the permeability of blood vessels, resulting in the rush of circulating immune cells such as neutrophils and monocytes to the site of infection. This is the cause of swelling at the infection site.

2.1 Pro-inflammatory cytokines and chemokines

Cytokines and chemokines play a central role in the process of inflammation (as described above). The following table describes various cytokines and chemokines and their roles in the process of inflammation (Table 1).

Table 1. Pro-inflammatory cytokines and chemokines

Cytokine	Main Source	Function
Cytokines		
TNFα	Macrophages, monocytes, Dendritic cells, NK cells, $CD4^+$ lymphocytes	Induction of cytokine production, proliferation, differentiation, cell death
IL-1β	Macrophages, Dendritic cells, Monocytes	Proliferation, differentiation, cell death
IL-6	Macrophages, Dendritic cells, Monocytes	Induction of cytokine production, differentiation, induction of acute phase protein synthesis
IL-8	Macrophages, epithelial cells, endothelial cells	Chemo-attractant of neutrophils
IL-12	Dendritic cells, macrophages, neutrophils	Cell differentiation, NK cell activation

IFN-γ	T-cells, NK cells	Anti-viral response
GM-CSF	T-cells, macrophages, fibroblasts	Stimulate production of dendritic cells from bone marrow precursors
Chemokines		
CXCL3 (MIP-1α)	Macrophages, mast cells, epithelial cells, neutrophils	Recruitment of immune cells to the site of infection
CCL4 (MIP-1β)	Macrophages, mast cells, epithelial cells, neutrophils	Regulation of pro-inflammation
CCL20	Macrophages, neutrophils	Movement of WBCs

3. How do innate immune cells recognize the pathogens?

The most crucial step in the process of inflammation, which marks the beginning of the immune response against any pathogen is the recognition of the invading pathogen (2). For this, the innate immune cells and the antigen-presenting cells are equipped with an array of receptors called pattern recognition receptors (PRRs). As their name suggests, PRRs are receptors capable of recognizing specific patterns on the pathogen called the pathogen-associated molecular patterns (PAMPs)(3). Upon recognition of a PAMP by the PRR, downstream signalling is elicited in the cells resulting in the generation of an immune response (4). Generally, four classes of PRRs have been established till date namely Toll-like receptors (TLRs), Nucleotide-binding Leucine-rich repeat containing receptors (NLRs), RIG-I like receptors (RLRs) and C-type lectin receptors (CLRs) (4).

3.1 Toll-like receptors (TLRs)

TLR is the best-characterized class of PRRs. These are present in the outer membrane and on the endosomes (4). About 13 TLRs are known till date, each recognizes a different PAMP which have been depicted in Illustration 2. Generally, surface TLRs include TLR1, TLR2, TLR4, TLR5, and TLR6. The endosomal TLRs include TLR3, TLR7, TLR8 and TLR9 (5). TLR4 was the first TLR discovered and was found to recognize lipopolysaccharide (LPS) (6). In addition to LPS, TLRs have also been found to recognize various outer membrane proteins of bacteria (7-9).

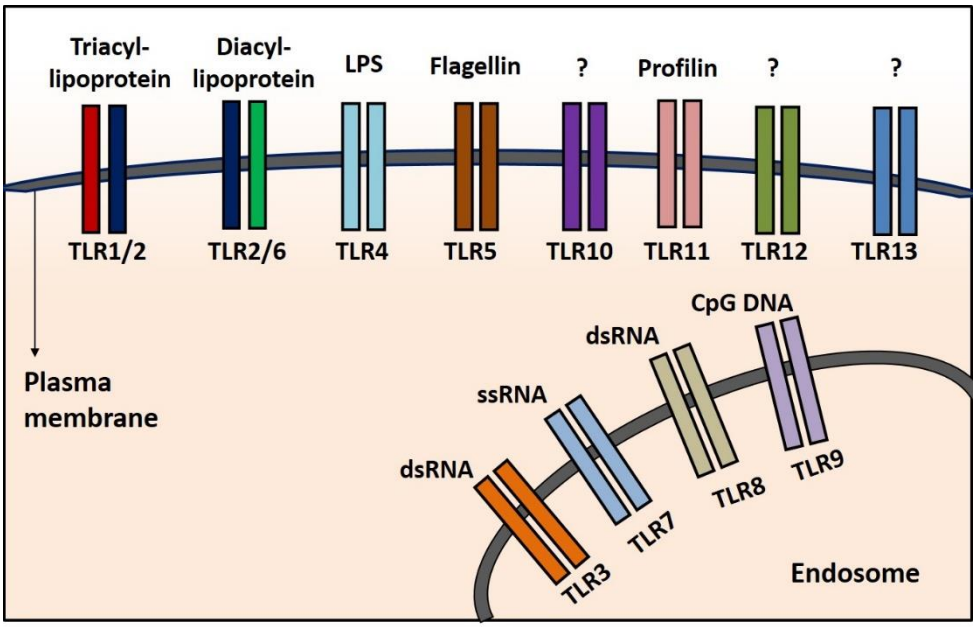

Illustration 2. TLRs and their ligands

TLRs are mainly present on the plasma membrane or on the endosomal membrane. The localization and the ligands of all the TLRs known till date have been depicted.

TLR generally consists of a Leucine-rich repeat (LRR) containing extracellular domain and a TLR/IL-1R homology (TIR) domain at the cytoplasmic side. Upon recognition of a PAMP by the extracellular domain, the downstream signalling is initiated by the TIR domain (10, 11).

3.2 TLR mediated pro-inflammatory response

The recognition of PAMPs by TLRs induces a signalling cascade leading to the activation of transcription factors and induction of a pro-inflammatory response (5). TLRs are known to form homo-dimers or hetero-dimers for ligand recognition followed by induction of the down-stream signalling (10). The down-stream signalling is either MyD88-dependent or independent manner depending on the recruitment of the adaptor protein-MyD88 or TRIF/TRAM to the cytosolic TIR domain (2, 3).

3.2.1 MyD88-dependent signalling

MyD88 or Myeloid differentiation factor 88 is an adaptor involved in the canonical TLR-mediated signalling (4). The recognition of the ligand by TLR induces the recruitment of MyD88 to the TIR domain which helps in the recruitment of the IL-1 receptor activated kinase (IRAK)-1 and IRAK-4 to the receptor complex leading to the phosphorylation of IRAK-1 by IRAK-4 (4). Phosphorylated IRAK-1 recruits and activates TRAF6 and activated TRAF6 then gets dissociated from the receptor complex and activates TGFβ-activating kinase-1 (TAK-1) with the

help of adaptor proteins TAK-1 binding protein 1 and 2 (TAB1 and TAB2). TRAF6, a ubiquitin ligase along with ubiquitin-conjugating enzyme 13 (UBC13) and Uev1A activates TAK-1 by adding a polyubiquitin chain at lysine 63 of TAK-1. TAK-1 then activates the MAP-kinase cascade or the IKK complex. The MAP-kinase cascade leads to the activation of the terminal MAP-kinases- p38, JNK and ERK (4). MAP-kinases then generally activate the transcription factor AP-1. On the other hand, the activated IKK complex phosphorylates IκB (inhibitor of NF-κB). IκB is bound to NF-κB in the cytoplasm in the inactive state. Upon activation, phosphorylation of IκB leads to its polyubiquitination and degradation. This renders NF-κB free to translocate to the nucleus. Both NF-κB and AP-1 are responsible for the transcription of genes for pro-inflammatory cytokines namely TNFα, IL-6 etc. (4). The pathway has been described in Illustration 3.

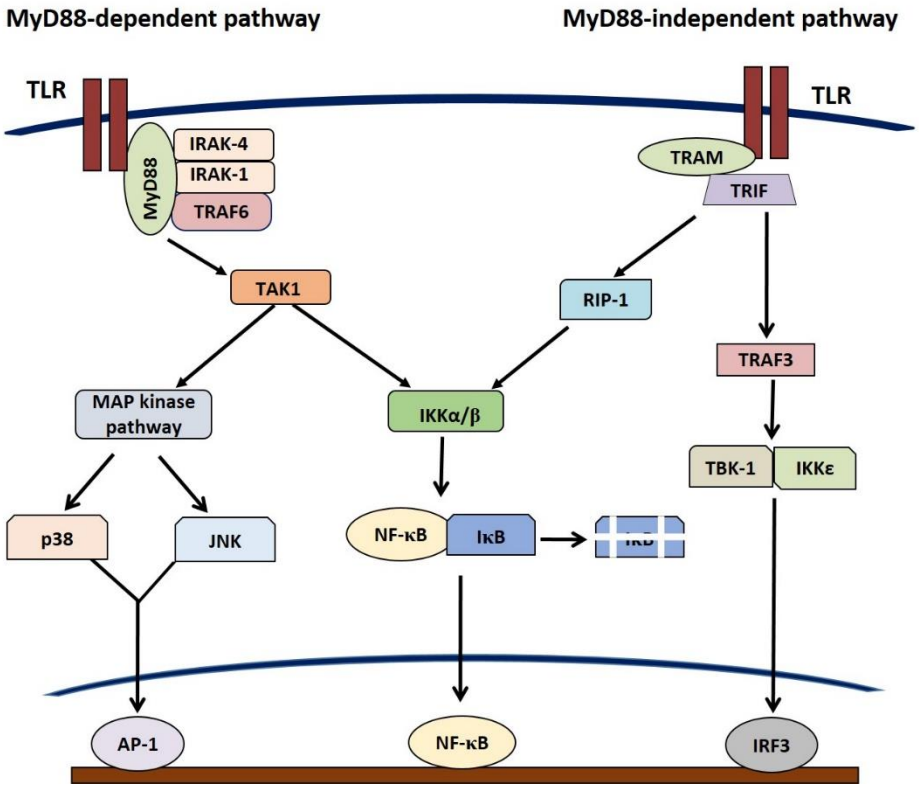

Illustration 3. TLR-mediated MyD88-dependent and -independent pathway

Upon recognition of the ligand by the TLR, it recruits an adaptor molecule- MyD88 or TRIF/TRAM. This recruitment leads to a signalling cascade leading to the activation of the transcription factors AP-1, NF-κB or IRF3.

3.2.2 MyD88-independent signalling

Apart from MyD88, some TLRs like TLR3 and TLR2 signal via the adaptor molecules- TRIF (4, 12). TLR4 can also mediate its signalling via TRIF, but it requires an additional protein

called TRAM (4). TRIF after being recruited to the TLR generally recruit Receptor inducing protein (RIP)-1 or TRAF3. RIP-1 binds to TRAF6 which then activates the IKK complex leading to the activation of NF-κB transcription factor. TRAF3, on the other hand, activates TBK-1 and IKKε which directly phosphorylates transcription factor IRF3 (4, 13) (Illustration 3).

4. The mechanisms of host-modulation by bacteria

Despite an elaborate mechanism to defend against pathogens, bacteria are able to establish an infection in the host as they have also evolved various mechanisms of modulating the host's immune responses for its own pathogenesis. The bacterial outer membrane consists of various components such as proteins, LPS etc. which are recognized by the host, resulting in a pro-inflammatory response (14). Some bacteria such as *Streptococcus pneumoniae, Haemophilia influenzae, Neisseria meningitides* etc. prevent this recognition by forming a capsule around their surface, helping them to move around in the host's system without being recognized and establish an infection (15). Gram-negative bacteria have LPS in their outer membranes, which is promptly recognized by TLR4 (16). To curb this recognition, various bacteria alter their LPS. LPS is made up of an oligosaccharide core or lipid A and polysaccharide side chain called the O-antigen. *Salmonella enterica,* upon infection, up-regulates the expression of PagL and PagP which increase the deacylation and palmitoylation of the lipid A, reducing its ability to be recognized by TLR4 (17, 18). *Porphyromonas gingivalis* has more than one type of LPS, which act as both agonist and antagonist for the TLRs, thus reducing the activation levels of TLR4-mediated pro-inflammatory responses (19, 20).

As previously described, phagocytosis of the pathogen is also an immune mechanism for clearing of the pathogen from the host's system, some bacteria such as *Salmonella, Mycobacterium, Listeria, Yersinia,* etc. have devised strategies to avoid phagocytosis (21). *Yersinia pestis* secretes effectors such as, YopH, YopE and YopT directly into the host cell via a type-three secretion system (T3SS) which modulate the actin-machinery of the host (22). Since actin is crucial for phagocytosis, these effectors affect the phagocytosis of the bacteria. Upon internalization of the bacteria by the phagocytes, a phagosome is formed, which then fuses with lysosomes forming the phagolysosomes, resulting in killing of the phagocytosed bacteria (1). Some bacteria avoid phagocytosis by escaping the phagosome. For example, *Listeria monocytogenes* secrete a toxin called Listeriolysin O, which forms pores in the phagosomal membrane, helping the bacteria to escape the phagosome (23). Some bacteria such as *Mycobacterium tuberculosis* suppresses the maturation of phagolysosomes, thus, making the phagolysosome favourable for

its replication (24). *Salmonella enterica* Typhimurium, does not prevent the maturation of phagolysosomes, but secretes effectors which help in forming a niche for the bacterial replication upon acidification of the phagolysosomes (25). *Coxiella burnetii* is a bacteria, which has adapted to the low pH of the phagolysosomes and replicates inside the acidified phagolysosome (26).

In addition to these strategies, bacteria also can subdue the pro-inflammatory responses generated against the bacteria. *S.* Typhimurium and *Shigella flexineri* secrete effectors via T3SS which suppress the pro-inflammatory responses. Interestingly, some bacteria induce pro-inflammatory responses to cause their pathogenesis. In some cases such as, in case of *Salmonella*, induction of pro-inflammatory responses helps in increasing the niche for their replication (27) and in bacterial infections involved in inflammatory diseases such as ulcerative colitis, pro-inflammation is essential for the pathogenesis (28).

4.1 Immune-modulation by bacterial outer membrane proteins

Outer membrane proteins (OMPs) from various bacteria namely *Neisseria* sp., *Helicobacter pylori*, *Haemophilus influenzae*, *Salmonella* sp. etc. have been shown to modulate host immune responses in different ways (14). They are capable of modulating both the innate and the adaptive immune responses of the host (Illustration 4). OmpS1 of *Salmonella enterica* Typhi, Hib of *Haemophilus influenzae* and Omp16 of *Brucella abortus* are outer membrane proteins which have been reported to induce pro-inflammatory responses in terms of production of TNFα, IL-6 or nitric oxide (NO) in innate immune cells such as macrophages and monocytes (29-31). OMPs from *N. gonorrhoeae*, *N. meningitides*, *S.* Typhimurium, *Klebsiella pneumoniae*, *Legionella pneumophila* etc. have been shown to activate the complement system, which also helps in the generation of pro-inflammatory responses (32-36).

In addition to inducing pro-inflammatory responses in the host's innate immune cells, some OMPs have been reported to activate the adaptive immune system as well (14). The activation of the adaptive immune system requires antigen presentation by dendritic cells and macrophages (1). Upon activation of the innate immune response, the expression of MHCs and the co-stimulatory molecules such as CD80, CD86, CD40 etc. increases on the antigen-presenting cells (APCs), which are required for the activation of T-cells (1). OMPs from *Shigella* sp., *Salmonella* sp., *N. meningitidis* have been reported to induce the expression of the co-stimulatory molecules on the dendritic cells (9, 30, 37-40). OMPs from *Shigella dysenteriae*, *S.* Typhimurium, *N. meningitidis* and *N. gonorrheae* have also been shown to induce the expression of

co-stimulatory molecules on B-cells and cause the generation of IgM responses in these cells (7, 41-45).

OmpU of *V. cholerae* has been shown to induce pro-inflammatory responses in monocytes and macrophages (46). *V. cholerae* OmpU also translocates to the mitochondria and induces a programmed cell death (47).

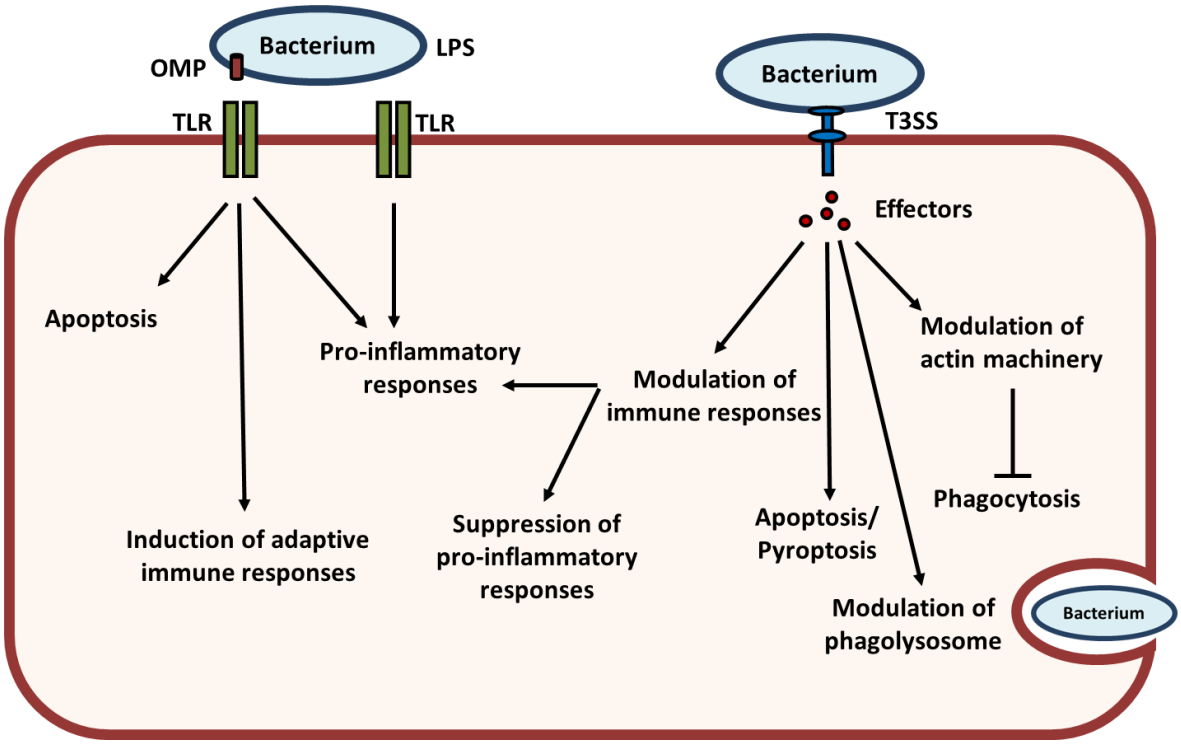

Illustration 4. Immunomodulation by Outer membrane proteins (OMPs) and T3SS effectors.

OMPs and T3SS effectors of various bacteria have been shown to modulate various host immune responses thereby helping the bacteria in causing their virulence.

4.2 Immune-modulation by effectors of the Type three secretion systems

The type three secretion system (T3SS) is a needle like complex which is assembled across the host and the bacterial membranes. This system secretes proteins directly from the cytoplasm of the bacterial cell to that of the host cell. Many bacteria namely *Shigella*, *Yersinia*, *Salmonella* etc. have been reported to utilize the T3SS to translocate various effectors into the host cell for their virulence. Some of these effectors have been shown to modulate host-immune responses (Illustration 4). For example, SopE of *Salmonella* is known to induce pro-inflammatory responses in the host (48). OspG and OspF which are T3SS effectors secreted by *Shigella* and

YopE and YopP/YopJ of *Yersinia* have been shown to suppress host's pro-inflammatory responses (22, 49-54). Some effectors of *Salmonella* namely SptP, GogB, AvrA etc. have also been shown to suppress the pro-inflammatory responses of the host (55-59).

Additionally, IpaB, an effector of *Shigella* is known to activate caspase-1 and induce a pro-inflammatory cell death called pyroptosis (60). On the other hand, YopE of *Yersinia* has been shown to suppress the activation of caspase-1 (61).

These complexities of pathogenesis processes underscores the need for the study of bacterial pathogenesis in great detail, with emphasis on how individual bacterial ligands modulate host's immune responses. This will further help us in designing specific vaccines against the diseases.

5. Objectives of the study

In this study, we have explored how an outer membrane protein, OmpU of *Vibrio parahaemolyticus* and a T3SS effector, SteA of *Salmonella enterica* Typhimurium modulate the immune responses of the host. Towards this, we have formulated the following aims:

Aim 1- To study the host immunomodulation by OmpU of *Vibrio parahaemolyticus.*

OmpU is an outer membrane protein present across *Vibrio* species and has been implicated in virulence of various *Vibrio* sp. However, OmpU of *V. parahaemolyticus* is yet to be characterized.

Aim 2- To study the host immunomodulation by SteA of *Salmonella enterica* Typhimurium *Salmonella enterica* Typhimurium secretes various effectors into the host cell via a type three secretion system. These effectors modulate host processes and help in the infection caused by the bacteria. SteA is such an effector, whose function has not been fully characterized.

Chapter 1:

To study the host-immunomodulation by OmpU of Vibrio parahaemolyticus

1. Introduction

1.1 *Vibrio parahaemolyticus* and its pathogenesis

Vibrio parahaemolyticus is a Gram-negative, non-invasive bacteria which was discovered in 1951 in Japan after a major outbreak affecting about 272 people and causing 20 deaths. Since then, many outbreaks have occurred in Japan, India, Europe, Africa, China and U.S.A. (62-67). Of the 802 outbreaks of foodborne illnesses in China, about 40 % have been reported to be due to *V. parahaemolyticus* infection (68, 69). Although *V. parahaemolyticus* is known to infect various marine species such as eels, shrimps, squids, lobsters, oysters, sardines, crabs etc., but the major cause of the gastroenteritis outbreaks was found to be raw or undercooked fish and shellfish (70). Upon consumption of raw or undercooked sea-food, the disease is almost inevitable. The patient develops symptoms such as acute diarrhoea, abdominal pain, fever, chills, vomiting and nausea. The watery stools of the patients are also mixed with mucus and blood. Additionally, wound infection by *V. parahaemolyticus* results in septicaemia and may lead to death (71).

The pathogenesis of *V. parahaemolyticus* has majorly been attributed to haemolysins namely thermostable-direct haemolysin (TDH), TDH-related haemolysin (TRH) and thermolabile haemolysin (TLH) (70). In addition to these, *V. parahaemolyticus* also utilizes the type three secretion systems (T3SS-1 & 2) and the type six secretion system (T6SS-1 & 2) to secrete certain proteins into the cytoplasm of the host cells (72). Of all these factors which have been attributed to the pathogenesis of *V. parahaemolyticus*, TDH has been found to be a major player and has been found in about 95 % of the clinical isolates (72).

1.1.1 Thermostable direct haemolysin (TDH) and TDH-related haemolysin (TRH)

TDH and TRH are both β-haemolysins and have been implicated as major virulence factors in *V. parahaemolyticus* infection (73). The pore forming ability of these toxins seems to be the major reason for their toxicity.

TDH is stable at 100 °C for 10 minutes, thus earned its name. In addition to haemolysis, TDH has been known to cause enterotoxicity, cytotoxicity and cardiotoxicity in the host (73). TDH forms a pore in the red blood cells (RBC) membrane causing its osmotic lysis. Due to RBC lysis by TDH, *V. parahaemolyticus* forms a special ring around the colony when grown on

Wagatsuma blood agar plates. This is called the 'Kanagawa phenomenon' (KP) (74, 75). In addition to RBC, TDH forms pore in the membrane of other host cells, thereby increasing the intracellular Ca^{2+} levels and also leading to Cl^- secretion out of the cells (76). This leads to the disturbance of the osmotic balance leading to cell expansion and thus cell death. Since TDH is prevalent in about 95 % of *V. parahaemolyticus* strains, pore-forming property has been used to detect *V. parahaemolyticus* (72). The genes encoding TDH (*tdh*) and TRH (*trh*) share about 70 % sequence similarity (73).

TRH was first identified from KP^- strain (77). TRH has been shown to be stable at 60 °C for 10 minutes (78). Similar to TDH, TRH also causes cell death by disturbing the osmotic balance of the cell by activating Cl^- channels leading to Cl^- efflux and Ca^{2+} influx (78).

Although TDH and TRH are major virulence factors, strains deficient in both *tdh* and *trh* genes also showed virulence indicating contribution by other factors in the virulence of *V. parahaemolyticus* (79, 80).

1.1.2 Thermolabile Haemolysin

Thermolabile haemolysin (TLH) is another toxin secreted by all the strains of *V. parahaemolyticus* (81). Like TDH and TRH, it also acts as a haemolysin (82, 83). In addition to its haemolytic activity, it acts as a lecithin-dependent phospholipase (70). Wang *et al.*, demonstrated that TLH is cytotoxic to epithelial cells (HeLa) and macrophages (RAW 264.7 cells) (71). Further, the expression of TLH is increased in conditions similar to the human intestine, indicating its role in the pathogenesis of *V. parahaemolyticus* (72).

1.1.3 Outer membrane proteins of *V. parahaemolyticus*

V. parahaemolyticus has a vast array of outer membrane proteins, many of which have been implicated in its virulence. Most of the OMPs help *V. parahaemolyticus* to survive in the gut of the host upon infection (84-86). Some OMPs also act as sensors of the host environment, thereby inducing the expression of virulence-related genes. The free iron levels are low in the host and it has been shown that the virulence of *V. parahaemolyticus* was enhanced in the iron limiting conditions (84). PsuA and PvuA are OMPs which are iron sensors and have been implicated in the enhanced virulence and increased expression of TDH (85, 86).

Antimicrobial peptides or defensins are present in the gut and are proficient in killing the bacteria (87). TolC, a transmembrane channel protein, has been found to be involved in providing

resistance to antimicrobial peptides as it is a part of the efflux pump system, which is also involved in antibiotic resistance (88). NorM, NhaD and VmrA are Na^+/drug antiporter, hence, help *V. parahaemolyticus* in acquiring resistance to various antimicrobial agents and drugs (89-91). Another OMP, Multivalent adhesion molecule 7 (MAM7) binds to fibronectin and phosphatidic acid, thus, helping in adhesion of *V. parahaemolyticus* to the host cell (92). Also, the enolase present on the cell membrane of *V. parahaemolyticus* binds to plasminogen of the host cell, thereby helping in adhesion (93). Adhesion of *V. parahaemolyticus* to the host cell is necessary for the formation of the T3SS and T6SS machineries, which are then able to secrete effectors involved in the pathogenesis of *V. parahaemolyticus*.

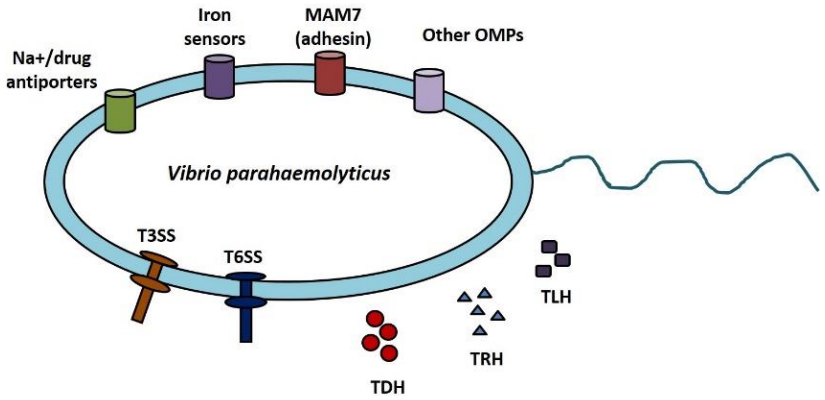

Illustration 5. Virulence factors of *V. parahaemolyticus*

Vibrio parahaemolyticus employs various virulence factors such as toxins namely TDH, TRH and TLH; outer membrane proteins which act as adhesins, iron sensors and antiporters; and it also secretes effectors via the type three and type six secretion systems.

Being majorly a non-invasive bacteria, outer membrane proteins (OMPs) of *V. parahaemolyticus* play an important role in manipulating host system. *Vibrio* outer protein (Vop) Q and VopS are type three secretion system (T3SS)-1 effectors, which have been implicated in the pathogenesis of *V. parahaemolyticus*. VopQ causes the deacidification of the lysosome, leading to lysosomal rupture and hence, host cell lysis (94, 95). VopS suppresses the actin-modulation of the host cells by acting on the GTPases, thereby affecting various functions of the host cell like phagocytosis (96-98). VopC, VopL, VopV are T3SS-2 effector proteins which are involved in actin modulations (99-102). VopA/P and VopZ are also T3SS-2 effectors which suppress the MAP-kinase activation (103, 104). VopZ also helps in the intestinal colonization and fluid accumulation by *V. parahaemolyticus* (105).

In addition to these, some OMPs have been found to be up-regulated in conditions mimicking the host environment, implicating their role in the virulence of *V. parahaemolyticus*. For example, OmpV has been found to be up-regulated in low salt conditions indicating its role in survival in the host environment and hence, in virulence of *V. parahaemolyticus* (106). Another OMP which may have a role in the virulence of *V. parahaemolyticus* is Outer membrane protein U (OmpU). It is controlled by the ToxRS regulon, which responds to environmental signals and regulates most of the virulence factors of *V. parahaemolyticus* namely TDH, TRH, T3SS-1, T3SS-2 implying the role of OmpU in its pathogenesis (107, 108).

1.1.3.1 Outer membrane proteins as vaccine candidates

OMPs have been shown to induce pro-inflammatory responses and also induce adaptive immune responses, thus, providing protection against the infection. Hence, OMPs have been widely tested for their use as vaccines or components of vaccines (14). PorB of *N. gonorrhoeae* induces Th1 responses in mice (109); OprF of *P. aeruginosa* induces the production of IgG1 and provides protection against pulmonary infection (110); OmpA of *Burkholderia pseudomallei* protects the mice against *B. pseudomallei* infection when injected intra-peritoneally (111); OmpS1, OmpS2 and OmpA of *S. typhi* have been shown to provide protection against *S. typhi* infection in mice (30, 112).

Various OMPs of *Vibrio* sp. have also been studied for their vaccine potential. OmpK of *V. harveyi*, *V. alginolyticus* and *V. parahaemolyticus* provides protection against infection of pathogenic *Vibrio* sp. when injected in the fish- *Epinephelus coioides* (113). OmpW of *V. alginolyticus* provides protection in *Larimichthys crocea* (114). Also, outer membrane vesicles (containing various OMPs) of *V. cholerae* have been shown to provide resistance against *V. cholerae* infection in mice (115, 116).

Several OMPs of *V. parahaemolyticus* such as PsuA, PvuA, OmpW, OmpK and OmpV have been shown to be immunogenic and provide protection in yellow croaker fish (*Pseudosciaena crocea*) (86, 117). Also, OmpK, OmpA, LptD, LamB, VP0802, VP1243 and VP0966 have been suggested to be immunogenic using an immunoproteomics approach (118).

In addition to these, OmpU of *V. alginolyticus* has been reported to provide protection in *Lutjanus erythropterus* (119). *V. parahaemolyticus* OmpU has also been found to be immunogenic

in the immunoproteomic screen and was found to be immunogenic in yellow croaker fish (117, 118).

1.1.3.2 Outer membrane protein U (OmpU)

OmpU is an outer membrane protein, which is present across various *Vibrio* sp. The *V. parahaemolyticus* OmpU (VpOmpU), has high similarity to OmpU from other *Vibrio* sp. In many of the *Vibrio* sp., it has been shown to be a porin and has also been indicated in their pathogenesis. In *V. alginolyticus,* OmpU helps the bacteria in acquiring antibiotic resistance (120). OmpU of *V. splendidus* helps the bacteria in bile and anti-microbial peptide resistance (121). In *V. vulnificus,* OmpU is reported to act as an adhesin (122). Further, in *V. splendidus,* OmpU has been reported to help in adhesion and invasion (123).

V. cholerae, V. parahaemolyticus and *V. vulnificus* are human pathogens. *V. cholerae* OmpU (VcOmpU) and VpOmpU share around 70 % homology between themselves. Further, the expression of VpOmpU is under the ToxRS regulon (107). Similarly, VcOmpU expression is regulated by ToxR, a homologue of ToxRS (108). Further, *V. cholerae* OmpU has been reported to help in resistance to bile and anti-microbial peptides, thus helping *V. cholerae* to survive in the intestine of the host (124, 125). Similarly, VpOmpU has been found to be up-regulated in the presence of bile, indicating the role of VpOmpU in the survival of the pathogen in the host intestine during pathogenesis (126). *V. cholerae* OmpU has been shown to modulate host responses (46, 47, 127, 128). VpOmpU was also found to be immunogenic in yellow croaker fish (117) and could act as a potential vaccine candidate. Our laboratory characterized the role of VcOmpU in host response modulation in great details (46, 47, 127, 128). However, the immunomodulatory role of VpOmpU is yet to be characterized.

2. Objectives of this study

In this study, we have characterized how *V. parahaemolyticus* OmpU (VpOmpU) modulates host-immune responses. Towards this, we have formulated the following objectives:

1) To purify OmpU from *Vibrio parahaemolyticus*

2) To check if OmpU modulates innate immune cells

3) To probe how OmpU is recognized by the innate immune cells

4) To understand the underlying signalling mechanism of innate-immunomodulation

3. Materials and Methods

3.1 Ethics statement

All animal experiments were carried out in accordance with the guidelines of Committee for the Purpose of Control and Supervision of Experiments on Animals (CPCSEA) (No. 1842/GO/ReBiBt/S/15/CPCSEA). All the protocols for animal handling were approved by the Institutional Animals Ethics Committee (IAEC) of Indian Institute of Science Education and Research, Mohali (Protocols for the knockout mice: IISERM/SAFE/PRT/2017-2018/ 001).

3.2 Bacterial strains and chemicals

The *V. parahaemolyticus* strain was obtained from the Microbial Type Culture Collection (MTCC) and Gene bank facility (MTCC Code 451) of the Institute of Microbial Technology, Chandigarh, India. All the DNA modifying enzymes were obtained from New England Biolabs (USA). Luria Bertani (LB) broth and antibiotics were from Himedia, Mumbai. Brain Heart Infusion (BHI) media was from Fluka, USA. Plasmid and DNA isolation kits were obtained from QIAGEN. Ni-NTA Agarose was obtained from QIAGEN. Most of the chemicals were obtained from Himedia, Mumbai unless otherwise mentioned.

3.3 Cell lines and culture conditions

RAW 264.7 (a murine macrophage cell line) and THP-1 (a human monocytic cell line) used in this study were obtained from the National Centre for Cell Science (NCCS), Pune, India. RAW 264.7 and THP-1 cells were maintained in RPMI 1640 supplemented with 10 % fetal bovine serum (FBS), 100 units/ml of penicillin and 100 µg/ml of streptomycin (Invitrogen, Life Technologies, USA) at 37 °C and 5 % CO_2. In all the experiments with VpOmpU, cells were pre-treated with 10 µg/ml of Polymixin B (Sigma Aldrich, USA) for 30 min to prevent any LPS contamination to interfere with the responses.

3.4 Differentiation of bone marrow cells to bone marrow-derived macrophages (BMDMs)

6-8 weeks old C57BL6 or *Tlr2*$^{-/-}$ or *Myd88*$^{-/-}$ mice were euthanized and their femur and tibia bones were extracted. The muscle tissue of the bones was then removed off and were then washed with ice-cold PBS. They were then dipped in 70 % alcohol for 2 min and were transferred to RPMI 1640 media. Then, using sterile scissors, the epiphyses of the bones were cut and the bone marrow cells were extracted by flushing the bones with RPMI 1640 media. These bone marrow cells were then differentiated to bone marrow-derived macrophages (BMDMs) using macrophage colony-stimulating factor (M-CSF). Briefly, cells were suspended in differentiation media (RPMI 1640 supplemented with 10 % FBS, 100 units/ml of Penicillin, 100 µg/ml of Streptomycin, 1 mM sodium pyruvate, 0.1 mM non-essential amino acids (NEAA), 1 % β-mercaptoethanol and 20 ng/ml of M-CSF) and plated in 24-well plates. They were incubated at 37 °C with 5 % CO_2. The media was changed every 2 days and fresh differentiation media was added. The adhered cells obtained at day 7 were BMDMs and were used for further experiments.

3.5 Cloning of VpOmpU

The full-length nucleotide sequence encoding the putative OmpU protein of *V. parahaemolyticus* (VpOmpU) was retrieved from the NCBI server (available online at http://www.ncbi.nlm.nih.gov/pubmed) (GenBank: HM042874.1). The N-terminal signal sequence of the VpOmpU protein was determined using SignalP (available online at http://www.cbs.dtu.dk/services/SignalP/). The nucleotide sequence encoding VpOmpU, omitting the N-terminal signal sequence, was amplified by polymerase chain reaction (PCR) using the *V. parahaemolyticus* (MTCC strain Code 451) genomic DNA as the template and the following primers:

Forward- 5’ TA**CATATG**GCTGAACTTTACAACCAAG 3’

Reverse 5’ CG**GGATCC**TTAGAAGTCGTAACGTAGAC 3’

The primer sequences were designed based on the VpOmpU nucleotide sequence (GenBank: HM042874.1), omitting the sequence for the N-terminal signal peptide.

The amplified PCR product was first cloned into the TA cloning vector (pTZ57R/T; Fermentas Life Sciences), and transformed into *E. coli* TOP10 cells (Invitrogen). Transformed cells were

screened for the positive plasmid harboring the cloned nucleotide sequence for VpOmpU gene by PCR, using the gene-specific primers mentioned above. The cloned sequence encoding VpOmpU was excised from the pTZ57R/T vector by restriction digestion with *Nde*I and *Bam*H1, re-cloned into the pET-14b bacterial expression vector (Novagen, Sigma-Aldrich), and the recombinant pET-14b vector (pET-14b/*VpOmpU*) was transformed into the *E. coli* TOP10 cells. The transformants were selected on ampicillin (50 μg/ml)-supplemented LB-agar plates. Bacterial colonies were screened for the recombinant pET-14b/*VpOmpU* plasmid by colony PCR using the gene-specific primers. Recombinant pET-14b/*VpOmpU* plasmid was purified, and the construct was verified by DNA sequencing of the cloned nucleotide segment for VpOmpU.

3.6 Over-expression and purification of VpOmpU

Recombinant pET-14b/*VpOmpU* plasmid was transformed into the *E. coli* Origami B cells (Merck-Millipore). A single colony of *E. coli* Origami B cells harboring the pET-14b/*VpOmpU* plasmid was inoculated into 20 ml LB media containing ampicillin (50 μg/ml), and the cells were grown at 37 ^{o}C for overnight. For large scale protein expression, 1 litre of the LB media, supplemented with 50 μg/ml ampicillin, was inoculated with 20 ml of the overnight-grown seed culture and was grown at 37 ^{o}C. The protein over-expression was induced by addition of 1 mM isopropylthiogalactoside (IPTG) when the OD_{600} of the culture media reached 0.4–0.6. After induction for 3 h at 37 ^{o}C, the cells were harvested by centrifugation at 3,220 g for 30 min. The cells were re-suspended in 10 ml of 20 mM sodium phosphate buffer (pH 7.0) containing bacterial protease inhibitor cocktail (Sigma Aldrich, USA). The cells were disrupted by sonication. Insoluble inclusion body was separated from the soluble fraction of the cell lysate by centrifugation at 18,500 g for 30 min. Presence of the majority of the recombinant VpOmpU protein in the insoluble inclusion body fraction was observed by SDS-PAGE/Coomassie staining. The crude inclusion body was washed twice with the 20 mM sodium phosphate buffer (pH 7.0) containing 150 mM sodium chloride (PBS). Subsequently, the inclusion body was solubilized in PBS, containing 8 M urea (10 ml of the urea-containing buffer was used to solubilize the inclusion body obtained from 1 litre culture), by constant stirring at 25 ^{o}C. Insoluble debris was separated by centrifugation at 18,500 g for 30 min at 4 ^{o}C. Recombinant VpOmpU protein was further purified from the crude urea-solubilized inclusion body fraction by passing through the Ni-NTA agarose affinity chromatography resins (QIAGEN) under denaturing condition in

presence of 8 M urea. The urea-solubilized inclusion body fraction was adjusted with 10 mM imidazole and was applied to the Ni-NTA agarose resin, pre-equilibrated with PBS containing 8 M urea (4 ml Ni-NTA agarose resin/10 ml of the solubilized inclusion body fraction). After washing with 10-volumes of PBS containing 8 M urea and 40 mM imidazole, the bound protein was eluted with PBS containing 8 M urea and 300 mM imidazole. The purity of the protein was examined by SDS–PAGE and Coomassie staining.

3.7 SDS-PAGE

The SDS-PAGE gel used contained a stacking gel and a resolving gel. Both the stacking and the resolving gels were prepared using the following solutions A, B and C (described below) in the proportions given in Table 2. The pH of the stacking gel was 6.8 and that of the resolving gel was 8.8. The resolving gel prepared was either of 10 % or 12.5 % acrylamide percentage.

Solution A: 29.2 % w/v Acrylamide, 0.8 % w/v bis-acrylamide in distilled water.

Solution B: 1.5 M Tris-Cl (pH 8.8), 0.4 % w/v SDS in distilled water

Solution C: 0.5 M Tris-Cl (pH 6.8), 0.4 % w/v SDS in distilled water

Table 2. Components of SDS-PAGE gel

Component	Stacking gel	10 % Resolving gel	12.5 % Resolving gel
Solution A	0.45 ml	3 ml	3.75 ml
Solution B	-	2.25 ml	2.25 ml
Solution C	0.75 ml	-	-
Water	1.8 ml	3.75 Ml	3 Ml

3.8 Refolding of the recombinant VpOmpU protein

Purified recombinant VpOmpU protein was subjected to refolding by using rapid dilution method. The purified protein in 8 M urea was diluted into the refolding buffer [PBS, containing 10 % glycerol, 0.5 % Lauryl dimethylamine N-oxide (LDAO) (Sigma Aldrich, USA)] at 25 ^{o}C with constant shaking for 10 min. Diluted protein was further incubated at 4 ^{o}C for overnight to allow optimal refolding of the protein. Thereafter, the refolding mixture was centrifuged at 18,500 g for 30 min at 4 ^{o}C to remove the insoluble aggregates formed during the refolding

process. The soluble fraction was immediately subjected to size-exclusion chromatography by passing through a Sephacryl S-200 column (1.6 x 60 cm; bed volume of 120 ml; flow rate used was 1 ml/min) (GE Healthcare) equilibrated with the 10 mM Tris-HCl buffer (pH 7.6), containing 10 mM NaCl and 0.5 % LDAO. Eluted Fractions containing the VpOmpU protein (eluted at around 40 ml of elution volume) was analyzed by SDS-PAGE/Coomassie staining, pooled, and concentrated by ultrafiltration using Millipore Ultra 10 kDa cut-off filters. Protein concentration was estimated using the Bradford reagent (Sigma Aldrich, USA), using BSA as the standard. The final soluble fraction of the purified form of the refolded recombinant VpOmpU protein was analyzed by SDS–PAGE/ Coomassie staining. The N-terminal 6X His-tag of the recombinant protein was removed by treatment with Thrombin (1 unit enzyme/ 300 µg of protein) for 2 h at 37 ^{o}C. The reaction was stopped with 2 mM PMSF.

3.9 Purification of wild type VpOmpU from the *V. parahaemolyticus* outer membrane fraction

V. parahaemolyticus was grown in 2 litres of BHI media till the OD_{600} of the culture reached 1.0. Bacterial culture was subsequently centrifuged at 2,050 g for 30 min. The bacterial cell pellet was re-suspended in 20 mM Tris-HCl (pH 7.6), containing protease inhibitor cocktail (Sigma Aldrich, USA), bacterial cells were lysed by sonication and were subjected to centrifugation at 18,500 g for 50 min. The supernatant was collected and was subjected to ultracentrifugation at 320,000 g for 20 min. The pellet, thus obtained, was re-suspended in PBS, and ultracentrifuged at 320,000 g for 20 min. The pellet was further subjected to treatment with 1 % N-sarkosyl in PBS for 30 min at 37 ^{o}C, and was ultracentrifuged at 105,000 g for 1 h. The pellet was washed twice with 20 mM Tris-HCl (pH 7.6) at 320,000 g for 20 min and was then subjected to treatment with 4 % Triton X-100 in 20 mM Tris-HCl (pH 8.0) for 20 min at 37 ^{o}C. The supernatant thus obtained contained the outer membrane proteins. The extracted protein fractions were incubated with 10 mM dithiothrietol (DTT) for 10 min at room temperature and were further diluted 5-times with 20 mM Tris-HCl buffer (pH 7.6), containing 0.1 % Triton X-100. The protein sample was loaded onto a DEAE-cellulose column, equilibrated with 20 mM Tris-HCl (pH 7.6) containing 0.1 % Triton X-100. Bound proteins were eluted with a gradient of 50-250 mM NaCl in Tris-HCl (pH 7.6) buffer at the flow-rate of 1 ml/min. The eluted fractions were subjected to SDS-PAGE/ Coomassie staining analysis for the detection

of the eluted proteins. The eluted fractions were collected, and selectively pooled, and subjected to size-exclusion chromatography on Sephacryl S-200 column (1.6 x 60 cm; bed volume of 120 ml; flow rate used was 1 ml/min) (GE Healthcare) equilibrated with 10 mM Tris-HCl (pH 7.6) buffer containing 10 mM sodium chloride and 0.5 % LDAO. The fractions eluted at around 36 ml contained the purified form of VpOmpU protein as analyzed by SDS-PAGE/ Coomassie staining.

3.10 Immunological relatedness between the wild type and the recombinant VpOmpU protein

Polyclonal antiserum was generated in rabbit using the purified refolded form of the recombinant His-tagged VpOmpU protein as the antigen. The antiserum was raised in New Zealand White rabbit using the 'polyclonal antibody production service' of Genei, India. The antisera recognized the wild type VpOmpU extracted from the *V. parahaemolyticus* outer membrane fraction in the immunoblot assay confirming the antigenic identity/immunological relatedness between the wild type and recombinant form of VpOmpU generated in our study.

3.11 Sequence alignment and Protein structural model

Amino acid sequence alignment was generated with CLUSTALW using the server available online (https://www.genome.jp/tools-bin/clustalw) and was visualized with ESPript (http://espript.ibcp.fr/ESPript/ESPript/).

VpOmpU polypeptide sequence was subjected to BLAST search in the NCBI server (http://blast.ncbi.nlm.nih.gov/Blast.cgi) against the protein sequences having experimentally determined three-dimension structure in the Protein Data Bank (PDB; http://www.rcsb.org/pdb/home/home.do). The most suitable template was found to be OmpU of *Vibrio cholerae* (PDB entry: 6EHB). Therefore, a homology-based structural model of VpOmpU was generated based on the structural coordinates of 6EHB using the SWISS-MODEL server (http://www.expasy.org/spdbv/). Protein structural models were visualized with PyMOL [DeLano WL, the PyMOL Molecular Graphics System (2002) found online (http://pymol.org)].

3.12 Far-UV circular dichroism (CD)

The far-UV CD spectra were collected on an Applied Photophysics Chirascan spectropolarimeter equipped with Peltier-based temperature control system, using a 5 mm path-length quartz cuvette. Far-UV CD spectra of the purified refolded recombinant VpOmpU and wild type VpOmpU (extracted from the *V. parahaemolyticus* outer membrane fraction) were recorded between 200-260 nm. Protein concentrations were adjusted at 1.5-3.0 µM in 10 mM Tris-HCl buffer (pH 7.6), containing 10 mM NaCl and 0.5 % LDAO. Resulting spectra were averaged (average of three spectra), and were corrected with the corresponding buffer spectra. All the spectra were recorded at 25 ^{o}C.

3.13 Liposome-swelling assay

Functional channel-forming activity of VpOmpU (wild type and the refolded recombinant proteins) in the membrane lipid bilayer was performed by the conventional liposome-swelling assay following the method described by Nikaido et al. (129), with slight modifications. Liposomes were prepared with egg yolk phosphatidylcholine (Sigma Aldrich, USA) and dicetylphosphate (Sigma Aldrich, USA) following the method described earlier, with modifications. Phosphatidylcholine (4.7 mg dissolved in 500 µl chloroform) and dicetylphosphate (0.10 mg dissolved in 1 ml of chloroform: methanol mixture, 1:1 volume ratio) were mixed together in a round-bottom flask, and the lipid film was allowed to generate by evaporating in a vacuum-desiccators for 4 h. To this completely dried and solvent-free lipid film, 1 ml of the VpOmpU protein solution [in 5 mM Tris-HCl buffer (pH 7.6)] was added. The refolded recombinant VpOmpU protein was used up to 25 µg/ml final concentration, and the wild type protein was used up to 30 µg/ml final concentration. Control liposomes were prepared by mixing the dried lipid film in 5 mM Tris-HCl buffer (pH 7.6), without the protein. Proteoliposomes and the control liposomes were subjected to ultracentrifugation at 350,000 g for 15 min at 4 ^{o}C, and washed thrice with 5 mM Tris-HCl buffer (pH 7.6). The pellets were dried under reduced pressure in a vacuum desiccator for overnight, and then re-suspended in 0.6 ml of the same buffer containing 15 % dextran-40,000 (Sigma Aldrich, USA) by incubating for 2 h at 25 ^{o}C. For the liposome-swelling assay, 20 µl of the proteoliposomes or the control liposomes were mixed rapidly in a cuvette with 580 µl of 30 mM sugar solutions (arabinose, glucose, sucrose and

raffinose (Sigma Aldrich, USA)) in 5 mM Tris-HCl buffer (pH 7.6), and the OD_{400} was continuously monitored for 10 min at an interval of 10 s. The assay was carried out at room temperature in triplicate sets.

3.14 Cell viability assay

1 x 10^5 cells were plated in 100 µl media in a 96-well plate and treated with different concentrations of VpOmpU for 24 h. The buffer (10 mM Tris-HCl with 0.5 % LDAO) was used as a negative control. The amount of buffer added to the cells was the same as that of the highest concentration of VpOmpU. The cell viability was quantified using MTT assay (EZ count kit, HiMedia Mumbai, India) by the manufacturer's protocol. Briefly, 10 µl of MTT reagent was added to each well. After 3-4 h, 100 µl of solubilization buffer was added to each well and was mixed well by pipetting. The OD was measured at 595 nm using a plate reader (Bio-Rad, USA).

3.15 Quantification of nitric oxide (NO)

RAW 264.7 and THP-1 cells were plated at a density of 1 x 10^6 /ml in a 6- well plate and were treated with VpOmpU. At different time points, the supernatant was collected for quantification of NO using Griess' Reagent (Sigma Aldrich, USA). Equal volumes of Griess' reagent and the supernatant was mixed and incubated in the dark for 15 min and the optical density was measured at 540 nm. The NO was quantified using a standard curve prepared with different concentrations of Sodium Nitrite (Sigma Aldrich, USA). 1 µg/ml of *E. coli* lipopolysaccharide (LPS) (Sigma Aldrich, USA) was used as a positive control in the experiments. Buffer (10 mM Tris-HCl with 0.5 % LDAO) was used as a negative control. For time-dependent analysis, the buffer was added in equal amount as VpOmpU, and for dose-dependent studies, amount of buffer added was equivalent to the highest dose of VpOmpU.

3.16 Quantification of TNFα and IL-6

Cells were plated at a density of 1 x 10^6 /ml in a 6-well plate and were treated with VpOmpU. At different time points, the supernatant was collected. TNFα and IL-6 were quantified by ELISA (BD Biosciences, USA, Table 3) by the manufacturer's protocol. 1 µg/ml of *E. coli* Lipopolysaccharide (LPS) (Sigma Aldrich, USA) was used as a positive control in the experiments. Buffer (10 mM Tris-HCl with 0.5 % LDAO) was used as a negative control. For time-

dependent analysis, buffer was added in equal amount as VpOmpU and for dose-dependent studies, amount of buffer added was equivalent to the highest dose of VpOmpU.

Table 3. ELISA kits used in this study

Cytokine	Catalogue no.	
	For mouse samples	**For human samples**
TNFα	Capture: 551225 Detection: 554415	Capture: 551220 Detection: 554511
IL-6	BD OptEIA, 555240	BD OptEIA, 555220

3.17 Gene-expression analysis

2 x 10^6 cells were plated in 2 ml media and were treated for different time with 5 µg/ml of VpOmpU. At all the time points, buffer (equivalent to the amount of VpOmpU being added) was used as a control. Cells were then harvested and RNA was isolated according to the manufacturer's protocol using Nucleopore RNA isolation Kit (Genetix). The cDNA was then synthesized using Verso-cDNA kit (Thermo-Fischer) (Table 4).

Table 4. Reaction for cDNA synthesis

Component	Volume
5X cDNA synthesis buffer	4 µl
dNTP mix	2 µl
RT enhancer	1 µl
RNA primer	1 µl
Vero enzyme mix	1 µl
Template RNA (100-1000 ng)	1-10 µl
Nuclease free water	Make up to 20 µl

The PCRs were done using Maxima SYBR Green qPCR master mix (Thermo Fischer) (Table 5) and the Eppendorf Realplex master cycler.

Table 5. Reaction for semi-quantitative PCR

Component	Volume
SYBR green master mix	5 µl
cDNA	1 µl
Primer mix (2.5 µM each)	1 µl
Molecular grade water	3 µl

Primers sequences were used from the primer bank (Table 6) and were synthesized by Integrated DNA technologies. The fold change of gene expression in VpOmpU-treated cells was calculated above the buffer-treated cells for each time point. Also, the C_t values of both the buffer-treated and VpOmpU-treated cells were normalized to the respective C_t values of the housekeeping genes.

Table 6. List of primers used for gene expression studies

Name of gene		Primer sequences	
		Mouse	Human
TLR1	Forward	TGAGGGTCCTGA-TAATGTCCTAC	CCACGTTCCTAAAGAC-CTATCCC
	Reverse	AGAGGTCCAAATGCTT-GAGGC	CCAAGTGCTT-GAGGTTCACAG
TLR2	Forward	GCAAAC-GCTGTTCTGCTCAG	CCTCTCGGTGTCG-GAATGTC
	Reverse	AGGCGTCTCCCTC-TATTGTATT	TCCCGCTCACTGTAA-GAAACA
TLR4	Forward	ATGGCATGGCTTACAC-CACC	AGAC-CTGTCCCTGAACCCTAT
	Reverse	GAGGCCAATTTT-GTCTCCACA	CGATGGACTTCTAAAC-CAGACCA
TLR6	Forward	TGAGCCAAGA-CAGAAAACCCA	TGAATGCAAAAACCCTTC ACC
	Reverse	GGGACATGAG-TAAGGTTCCTGTT	CCAAGTCGTTTC-TATGTGGTTGA

Myd88	Forward	AGGACAAACGCCG-GAACTTTT	GGCTGCTCTCAACATGCGA
	Reverse	GCCGA-TAGTCTGTCTGTTCTAGT	CTGTGTCCGCAC-GTTCAAGA
β-Actin	Forward	GGCTG-TATTCCCCTCCATCG	-
	Reverse	CCAGTTGG-TAACAATGCCATGT	-
GAPDH	Forward	TGGATTTGGACGCATT-GGTC	AAGGTGAAGGTCGGAG-TCAAC
	Reverse	TTTGCACTGGTACGTGTT-GAT	GGGGTCATTGATGG-CAACAATA
HPRT	Forward	TCAGTCAACGGGG-GACATAAA	CCTGGCGTCGTGATTAG-TGAT
	Reverse	GGGGCTGTACTGCTTAAC-CAG	AGACGTTCAG-TCCTGTCCATAA
RPL13	Forward	GGGCAGGTTCTGG-TATTGGAT	GCCATCGTGGCTAAACAG GTA
	Reverse	GGCTCGGAAATGG-TAGGGG	GTT-GGTGTTCATCCGCTTGC
RPL0	Forward	TGAGATTCGGGA-TATGCTGTTGG	AGAAACTGCTGCCTCATA-TCCG
	Reverse	CGGGTCCTAGACCAG-TGTTCT	CCCCTGGAGATTTTAG-TGGTGA

3.18 Analysis of surface expression of TLRs

1 x 10^6 cells were plated in a 6-well plate and treated with 5 μg/ml of VpOmpU for different time points. Buffer (10 mM Tris-HCl with 0.5 % LDAO)-treated cells were used as control. Cells were then harvested and washed twice with flow cytometry buffer (PBS supplemented with 1 % FBS and 0.05 % Sodium azide). RAW 264.7 cells were incubated with mouse Fc block for 15 min at 4 °C and in THP-1 cells, isotype controls were used. RAW 264.7 and THP-1 cells were then incubated with FITC-, PE- or APC- tagged anti-TLR antibody or the isotype control for 1 h at 4 °C. Cells were then washed twice with ice-cold flow cytometry buffer and

analyzed on a FACSCaliber flow cytometer (BD Biosciences, USA). The antibodies used for flow cytometry are listed in Table 7.

Table 7. Antibodies used for flow cytometry

Antibody	Company	Catalogue no.
PE tagged anti-mouse TLR1	eBiosciences	12901180
FITC-tagged anti-human TLR1	Abcam	AB59702
FITC-tagged anti-mouse/human TLR2	Biolegend	121805
APC- tagged anti-mouse TLR6	R&D Systems	FAB1533A
PE- tagged anti-human TLR6	Biologend	334707

3.19 Neutralization of TLRs

Cells were plated in a 96- well plate at a density of 1 x 10^6 cells/ml. Cells were pre-treated for 1 h with 5 µg/ml anti-TLR neutralizing antibodies or the isotype controls and then treated with 5 µg/ml of VpOmpU. Supernatants were collected after 4 h for THP-1 cells and after 24 h for RAW 264.7 cells. TNFα was then quantified using ELISA. Neutralizing antibodies against mouse/human TLR2 (cat# 121802) and its isotype was from Biolegend and neutralizing antibodies against human TLR1 (cat# mabg-htlr1), TLR6 (cat# mabg-htlr6) was from Invivogen.

3.20 Inhibitor studies

Cells were plated at a density of 1 x 10^6 cells/ml. Cells were then pre-treated for 1 h with different pharmacological inhibitors and then were treated with 5 µg/ml of VpOmpU for 24 h for RAW 264.7 cells and for 4 h for THP-1 cells. The supernatants were then collected and analyzed for TNFα by ELISA. The inhibitors used in this study are listed in Table 8.

Table 8. Inhibitors used in this study

Inhibitor	Company	Catalogue no.
MLN4924	R&D Systems, USA	1502
SP600125	Sigma-Aldrich, USA	57067
VX745	Santa Cruz Biotechnology, USA	sc-361401
JNK-IN8	Santa Cruz Biotechnology, USA	sc-364745
IRAK inhibitor	Sigma-Aldrich, USA	15409

MG132	Sigma-Aldrich, USA	M7449

3.21 siRNA knockdown

For THP-1, 7 x 10^4 cells were plated in a 24-well plate and were transfected using ONTARGET plus siRNA against human TLR2, human TLR6, or ONTARGET plus Non-targeted siRNA pool (Dharmacon, GE) using Dharmafect 1 according to the manufacturer's protocol. The knockdown was observed using flow cytometry at 48 h. After 48 h of transfection, cells were treated with 5 μg/ml of VpOmpU for 4 h, after which the supernatants were collected and analyzed for TNFα using ELISA. For RAW 264.7 cells, 2.5 x 10^5 cells were plated in a 24-well plate and were transfected with ONTARGET plus siRNA against mouse TLR1, mouse TLR6 or ONTARGET plus Non-targeted siRNA pool (Dharmacon, GE) using FuGENE HD (Promega, USA) at a ratio of 1:5 (RNA: FuGENE) for 24 h. After which, knockdown was analyzed by semi-quantitative PCR and cells were treated with 10 μg/ml of VpOmpU for 12 h. Supernatants were then collected and TNFα was quantified using ELISA.

3.22 Whole cell lysate preparation

RAW 264.7 and THP-1 cells (a confluent 100 mm petri-dish) were treated with 5 μg/ml of VpOmpU and incubated at 37 °C for different time points. Cells were harvested at 2,000 g and washed twice with PBS. The pellet was then resuspended in whole cell lysis buffer (50 mM Tris-Cl, 150 mM NaCl, 0.1 % SDS and 0.1 % TritonX-100, pH 8) with mammalian protease inhibitor cocktail (Sigma Aldrich, USA). This was then subjected to sonication at 10 A for 15s with 3 pulses of 5 s each. Then, it was centrifuged at 16,000 g for 30 min. The supernatant was collected as the whole cell lysate.

3.23 Nuclear lysate preparation

RAW 264.7 and THP-1 cells (a confluent 100 mm petri-dish) were treated with 5 μg/ml of VpOmpU and incubated at 37 °C for different time points. Cells were then then harvested at 2,000 g for 5 min and washed twice with sterile PBS. The pellet volume was measured and it was dissolved in 5 times the pellet volume in hypotonic buffer (10 mM HEPES pH 7.9 with 1.5 mM $MgCl_2$ and 10 mM KCl) and centrifuged at 1,850 g for 5 min at 4 °C. Then, the pellet was dissolved in hypotonic buffer with 0.5 M DTT and mammalian protease inhibitor and was

then incubated on ice for 15 min. This was then sonicated at 10 A for 15 s with 3 pulses of 5 s each and centrifuged at 3,300 g for 15 min at 4 °C. The pellet was then resuspended in 70 µl of low salt buffer (20 mM HEPES pH 7.9, 1.5 mM $MgCl_2$, 20 mM KCl, 0.2 mM EDTA and 25 % glycerol) with 0.5 M DTT and mammalian protease inhibitor. To this, 30 µl of high salt buffer (20 mM HEPES pH 7.9, 1.5 mM $MgCl_2$, 800 mM KCl, 0.2 mM EDTA and 25 % glycerol) was added dropwise and incubated on ice for 10 min before subjecting to sonication at 10 A for 15 s. Then, it was incubated on ice for 30 min with periodic shaking and centrifuged at 24,000 g for 30 min at 4 °C. The supernatant hence obtained contained the nuclear lysate.

3.24 Co-immunoprecipitation studies

Whole cell lysates were prepared (as previously described) and were incubated with 3 µg of anti-TLR1, anti-TLR2 or anti-TLR6 antibody for 3 to 4 h with continuous low speed shaking at 4 °C. Then, 20 µl of Protein A/G beads (# sc2003, Santa Cruz Biotechnologies, USA) was added and it was subjected to continuous low speed shaking at 4 °C for overnight. Then, the beads were washed thrice with whole cell lysis buffer by centrifugation at 6,000 g for 5 min at 4 °C. The beads were re-suspended in SDS-loading buffer and boiled for 10 min. The samples were then run on SDS-PAGE gel and subjected to immunoblotting.

3.25 Immunoblotting

The whole cell lysates or the nuclear lysates were run on SDS-PAGE gel and were transferred to PVDF membrane using wet transfer. After the transfer, the membrane was incubated with 5 % BSA for blocking. Then, it was incubated with various primary antibodies (incubated generally for 3 h for all the primary antibodies except for TLRs which were incubated for overnight) which were purchased from different companies. Then, the blot was washed four times with TBST (25mM Tris-HCl (pH 7.6, containing 137 mM NaCl and 0.1 % Tween 20). Further blot was incubated with HRP-tagged secondary antibody (Sigma-Aldrich, USA) for 1 h and washed four times with TBST following incubation. The immunoblots were then developed using Clarity™ ECL Substrate (Bio-Rad, USA) and detected using LAS 4000 (GE Healthcare Technologies, USA). The primary antibodies used in this study are listed in Table 9.

Table 9. List of antibodies used for immunoblotting under Aim 1

Antibody against	Company and Catalogue no.	Antibody against	Company and Catalogue no.
TLR1	Santa Cruz Biotechnologies, USA (# sc-514399)	**c-Fos**	Cell signalling technologies, USA (# 2250BC)
TLR2	Santa Cruz Biotechnologies, USA (# sc-21760)	**P65**	Santa Cruz Biotechnologies, USA (# sc-372)
TLR6	Cell signalling technologies, USA (# 12717S)	**Lamin B1**	Santa Cruz Biotechnologies, USA (# sc-20682)
MyD88	Santa Cruz Biotechnologies, USA (# sc-74532)	**CRel**	Santa Cruz Biotechnologies, USA (# sc-71)
p-p38	Cell signalling technologies, USA (# 4511BC)	**P38**	Cell signalling technologies, USA (# 8690BC)
p-JNK	Cell signalling technologies, USA (# 9251BC)	**JNK**	Cell signalling technologies, USA (# 9252BC)
p-IκB	SAB4504445	**IκB**	Santa Cruz Biotechnologies, USA (# sc-847)
c-Jun	Cell signalling technologies, USA (#9165BC)	**GAPDH**	Santa Cruz Biotechnologies, USA (# sc-25778)
Jun B	Cell signalling technologies, USA (#3753BC)	**β-actin**	Santa Cruz Biotechnologies, USA (# sc-81178)
Jun D	Santa Cruz Biotechnologies, USA (# sc-74)	**PCNA**	Biolegend, USA (# 307902)

3.26 Densitometric analysis

The densitometric analysis of the western blots was done using the Image J software (Rasband, W.S., ImageJ, U. S. National Institutes of Health, Bethesda, Maryland, USA, https://imagej.nih.gov/ij/, 1997-2018). The band intensities of IκB were normalized to the respective band intensities of the loading control GAPDH. For co-immunoprecipitation studies, the fold changes of the band intensities in the VpOmpU-treated cells were calculated above the band intensities in the buffer-treated cells. For analysis of the phosphorylation status of p38 and

JNK, the band intensities of p-p38 or p-JNK were calculated above the band intensities of p38 or JNK, respectively.

3.27 Statistical analysis

Data were expressed as mean ± SD or SEM. The statistical analysis was done using Student's two-sided t-test and the p values less than 0.05 were considered significant. The p values indicated are *p<0.05, **p< 0.01, ***p<0.001, ns p>0.05.

4. Results

4.1 Identification and analysis of putative OmpU from *Vibrio parahaemolyticus*

Analysis of the *V. parahaemolyticus* genome revealed the presence of a gene sequence encoding a putative OmpU protein (130), composed of 330 amino acid residues with a predicted molecular mass of 35.6 kDa. This putative OmpU of *V. parahaemolyticus* (VpOmpU) showed 60-90 % sequence similarity with the OmpU proteins of the related *Vibrio* species (Figure 1A). Homology-based structural modelling based on the crystal structure of *V. cholerae* OmpU (131) showed typical porin-like β-barrel architecture of VpOmpU (Figure 1B).

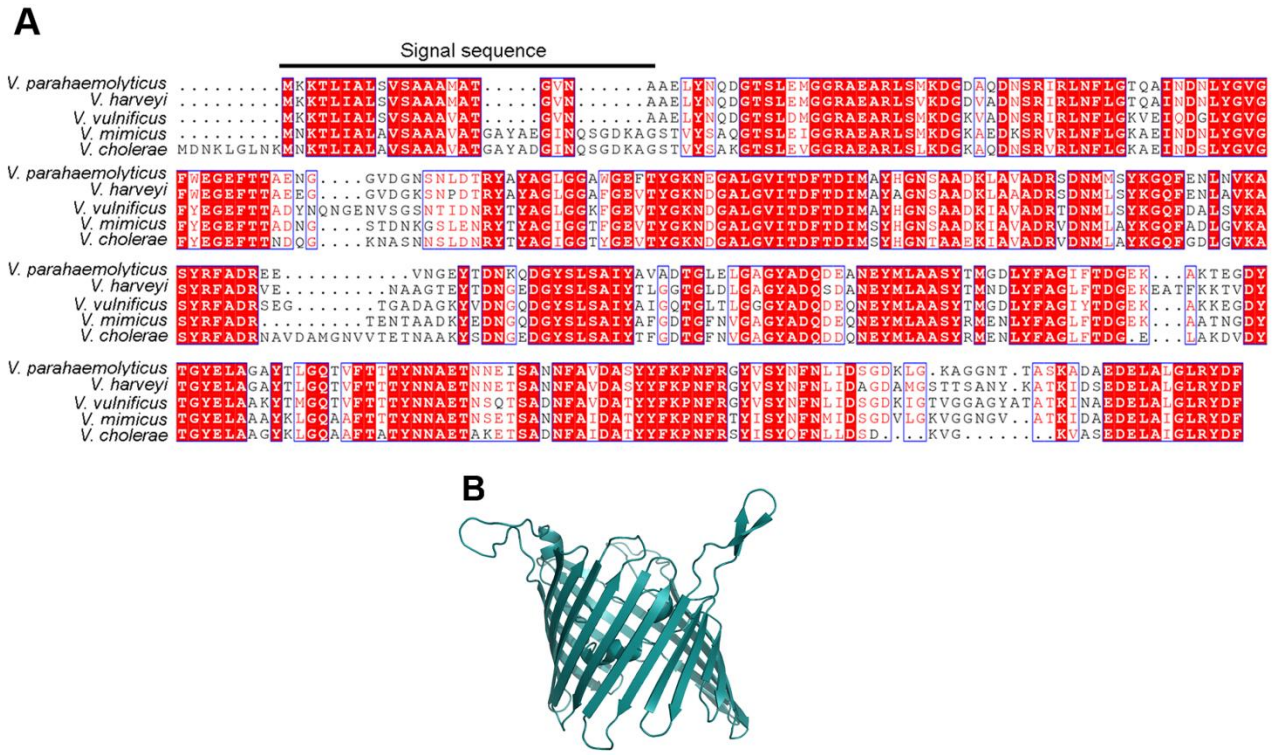

Figure 1. Amino acid sequence alignment and homology-based structural model of VpOmpU.

(A) Amino acid sequence alignment of VpOmpU and OmpU porins from related *Vibrio* species showed its homology with OmpU of other *Vibrio* sp.. The region corresponding to the signal sequence is marked. (B) Homology-based structural model of VpOmpU based on the

crystal structure of VcOmpU (PDB ID: 6EHB). Based on this analysis, this putative OmpU, which is probably a porin, was selected for purification and its functional characterization.

4.2 Purification of VpOmpU from the outer membrane of *Vibrio parahaemolyticus*

Wild type VpOmpU (wt-VpOmpU) was purified from the outer membrane fraction of the *V. parahaemolyticus*. Bacterial cells were grown in BHI broth, cells were lysed, and bacterial membrane fractions were harvested upon fractionation with 1 % N-sarkosyl. Subsequently, the outer membrane proteins were extracted via solubilisation with 4 % Triton X-100. VpOmpU was purified from the solubilized membrane fraction by anion-exchange chromatography on DEAE-cellulose in presence of 0.1 % Triton X-100, followed by size-exclusion chromatography on Sephacryl S-200 in presence of 0.5 % LDAO. Homogeneity of the purified wild type VpOmpU preparation was analyzed by SDS-PAGE and Coomassie staining (Figure 2).

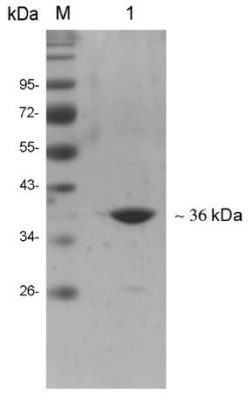

Figure 2. Purified VpOmpU from the outer membrane of *V. parahaemolyticus*.
SDS-PAGE/Coomassie staining analysis of the purified form of wtOmpU extracted from the *V. parahaemolyticus* outer membrane fraction.

4.3 Overexpression, purification and refolding of recombinant VpOmpU

The wild type VpOmpU thus obtained was limited in quantity for the functional characterization of VpOmpU. So, to obtain large quantity of the VpOmpU protein, and also to reduce the LPS contamination, we cloned and expressed VpOmpU in *E. coli*. The nucleotide sequence encoding VpOmpU without the N-terminal signal sequence was cloned into the bacterial expression vector pET14b, and was transformed into the *E. coli* Origami B cells. The pET14b vector allowed expression of the recombinant VpOmpU (r-VpOmpU) with an N-terminal 6X

His tag that would allow affinity purification of the recombinant protein using Ni-affinity chromatography. The N-terminal signal sequence (Figure 1A) was omitted from the cloned construct to avoid the possible incorporation of the recombinant protein into the bacterial membrane fractions.

Upon overexpression of the recombinant protein in the *E. coli* Origami B cells via IPTG induction, majority of the VpOmpU was found to be present in the form of insoluble inclusion bodies (Figure 3A). The recombinant form of His-tagged VpOmpU was solubilized from the insoluble inclusion bodies using 8 M urea, and was purified by Ni-NTA Agarose affinity chromatography under the denaturing condition in 8 M urea.

The denatured form of purified recombinant VpOmpU in 8 M urea was refolded by dilution in a buffer containing 0.5 % LDAO and 10 % glycerol. Upon refolding, the majority of VpOmpU remained in the soluble form, and was separated from the insoluble aggregated fractions of the protein via centrifugation (Figure 3B). Refolded VpOmpU was further purified by size-exclusion chromatography on Sephacryl S-200 (Figure 3B). Homogeneity of the purified form of the recombinant His-tagged VpOmpU preparation was analysed by SDS-PAGE and Coomassie staining (Figure 3B). The cloning and purification of recombinant VpOmpU was done by Dr. Ranjai Kumar.

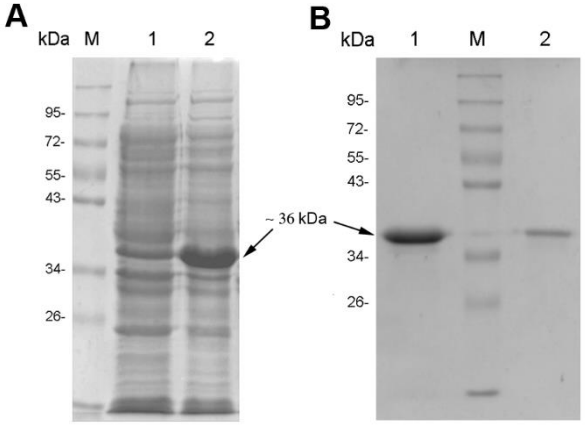

Figure 3. Purification of recombinant VpOmpU

(A) Overexpression of recombinant VpOmpU in *E. coli*. Protein overexpression was induced with 1 mM IPTG, cells were lysed, the soluble fraction of the cell lysate (lane 1) and insoluble inclusion body fraction (lane 2) were analysed by SDS-PAGE/Coomassie staining. The band corresponding to the recombinant VpOmpU is marked. The majority of the VpOmpU protein was found to be associated with the insoluble inclusion body fraction. Lane M, molecular weight markers. (B) Purification of refolded recombinant VpOmpU as analysed by SDS-PAGE/Coomassie staining. The recombinant form of VpOmpU was refolded by rapid dilution in a buffer containing 0.5 % LDAO (lane 1). Refolded VpOmpU was further purified

by size-exclusion chromatography on Sephacryl S-200 (lane 2). Lane M, molecular weight markers. Molecular weight markers are indicated.

Further, the His-tag was removed from recombinant VpOmpU by thrombin cleavage. The size of the recombinant VpOmpU without the His-tag was compared to the wild type VpOmpU as observed by western blotting using the antisera generated against the recombinant VpOmpU (Figure 4).

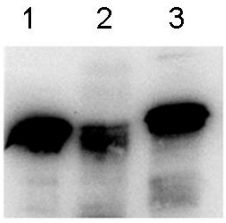

Figure 4. Immunoblot analysis of recombinant and wild type VpOmpU using anti-VpOmpU antisera

Lane 1, purified form of refolded recombinant His-tagged VpOmpU; lane 2, purified form of refolded recombinant VpOmpU after removal of the N-terminal His-tag; lane 3, wt-VpOmpU extracted from the *V. parahaemolyticus* outer membrane fraction.

4.4 Far-UV CD spectra of VpOmpU reveals its β-sheet rich structure

Consistent with their β-barrel structural assembly, Gram-negative bacterial porins display far-UV CD profiles showing typical signature of the β-sheet-rich architecture. In the same direction, we examined the structural characteristics of the VpOmpU protein by monitoring the far-UV CD profiles of the recombinant and the wild type form of the protein.

Wild type VpOmpU displayed a symmetric far-UV CD spectrum, with a sharp negative ellipticity minimum at 218 nm, suggesting a β-sheet-rich structural organization of the protein (Figure 5A). The far-UV CD profile of the refolded recombinant protein also showed an ellipticity minimum at 218 nm suggesting β-sheet-rich structure of recombinant VpOmpU (Fig 5B).

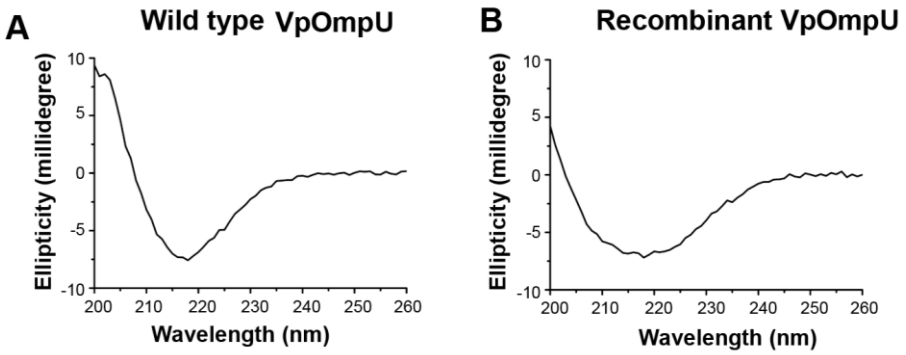

Figure 5. The recombinant VpOmpU and wt-VpOmpU have similar structures

(A-B) Far UV CD-spectra of wild type (A) and recombinant VpOmpU (B) showed negative ellipticity minima at around 218 nm for both the proteins indicating a β-sheet rich structures of both the wild type and the recombinant forms of VpOmpU.

The β-sheet-rich structure of the wt-VpOmpU and the r-VpOmpU were similar to those observed with the typical bacterial outer membrane porin proteins.

4.5 Liposome-swelling assay demonstrates porin-like channel-forming property of VpOmpU

Porins are typically characterized by their ability to form channels in the membrane lipid bi-layer, allowing free diffusion of small molecules up to a definite size limit as per the size constraint imposed by the corresponding pore diameter. Therefore, we wanted to explore whether the VpOmpU protein could show any such porin-like channel-forming ability in the membrane lipid bilayer of synthetic lipid vesicles or liposomes. Channel-forming property of VpOmpU was assayed using the conventional liposome-swelling assay. In this assay, liposomes incorporating the VpOmpU protein were subjected to treatment in presence of sugars of varying molecular sizes. Formation of VpOmpU channel in the liposome membranes would allow free diffusion of water into the lipid vesicles resulting into the swelling of the liposomes. The VpOmpU channel, however, would not allow the passage of the sugars/saccharides having molecular sizes larger than the pore diameter. Such saccharides would act as the osmoprotectants, and thus those would presumably suppress the liposome-swelling response. Based on such notion, both the wild type and the refolded recombinant form of the VpOmpU proteins, incorporated in the liposome membranes, were examined using the liposome-swelling assay (Figure 6A, 6B). It was observed in both the cases that in the presence of monosaccharides, such as arabinose and glucose, there was a steady increase in the liposome-swelling response. In the presence of disaccharide sucrose, liposome-swelling responses of wild type and recombinant

VpOmpU were prominently suppressed, while trisaccharide raffinose severely compromised the liposome-swelling on the proteoliposomes made up of the wild type and the recombinant proteins (Figure 6A, 6B). These results clearly suggested that the VpOmpU indeed displayed porin-like channel-forming property with a definite pore size, thus allowing free diffusion of solutes within the specific size limit. The VpOmpU channel allowed free diffusion of the monosaccharides, while the permeability efficiency decreased progressively in case of the disaccharides, and even further in case of the trisaccharides of larger molecular sizes. It is also important to note here that the refolded form of the recombinant VpOmpU showed similar trend in the channel-forming ability (i.e. monosaccharide>disaccharide>trisaccharide) as observed with the wild type protein, thus showing functional integrity of the recombinant protein generated in our study (Figure 6C).

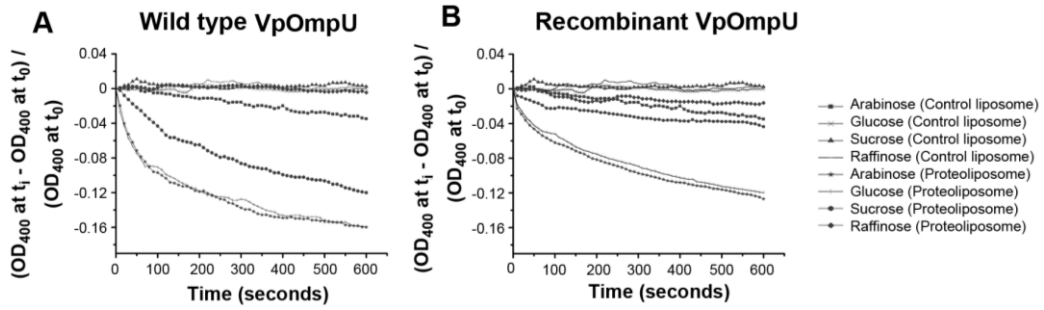

C Rate of liposome swelling (OD_{400} at t_i - OD_{400} at t_0)/ (OD_{400} at t_0))(per second)

	Arabinose	Glucose	Sucrose	Raffinose
r-VpOmpU	$8.5 \times 10^{-4} \pm 1.45 \times 10^{-4}$	$7.8 \times 10^{-4} \pm 1.12 \times 10^{-4}$	$2.7 \times 10^{-4} \pm 0.51 \times 10^{-4}$	$0.066 \times 10^{-4} \pm 0.156 \times 10^{-4}$
wt-VpOmpU	$14.2 \times 10^{-4} \pm 1.29 \times 10^{-4}$	$14.5 \times 10^{-4} \pm 1.64 \times 10^{-4}$	$4.6 \times 10^{-4} \pm 0.236 \times 10^{-4}$	$0.4 \times 10^{-4} \pm 0.11 \times 10^{-4}$

Figure 6. The recombinant VpOmpU and wt-VpOmpU show similar channel-forming ability

(A-C) The refolded recombinant form and the wild type VpOmpU protein showed nearly similar trend in the liposome-swelling response. Control liposomes, liposome preparation lacking VpOmpU; proteoliposomes, liposomes containing VpOmpU. (C) The initial rates of the liposome swelling response (calculated from the slope of the linear fitting of the data over the initial period of 50 seconds) are shown in the table (r-VpOmpU: for recombinant VpOmpU; wt-VpOmpU: for wild type VpOmpU).

Based on these observations it could be concluded that the recombinant VpOmpU was structurally and functionally similar to the native wild type OmpU of *V. parahaemolyticus*.

4.6 VpOmpU induces pro-inflammatory responses in monocytes and macrophages

As a part of the functional characterization we explored the host-immunomodulatory role of VpOmpU. Generally, bacterial ligands, known as PAMPs (pathogen associated molecular pattern) are recognized by PRRs (pattern-recognition receptors) of the innate-immune cells such as macrophages and monocytes leading to their activation that results in the production of various pro-inflammatory molecules, such as nitric oxide (NO) (132, 133), TNFα and IL-6 (4). Therefore, to probe whether VpOmpU acts as a PAMP, RAW 264.7 cells (a murine macrophage cell line) and THP-1 cells (a human monocytic cell line) were treated with 10 μg/ml of recombinant VpOmpU. At different time points, supernatants were analysed for TNFα and IL-6 by ELISA. A time-dependent analysis of TNFα and IL-6 in response to 10 μg/ml of VpOmpU showed a maximum production of both the cytokines at 24 h in RAW 264.7 cells (Figure 7A, 7C). However, in THP-1 cells, maximum TNFα production was observed at 4 h (Figure 7B) and maximum IL-6 production was observed at 8 h (Figure 7D).

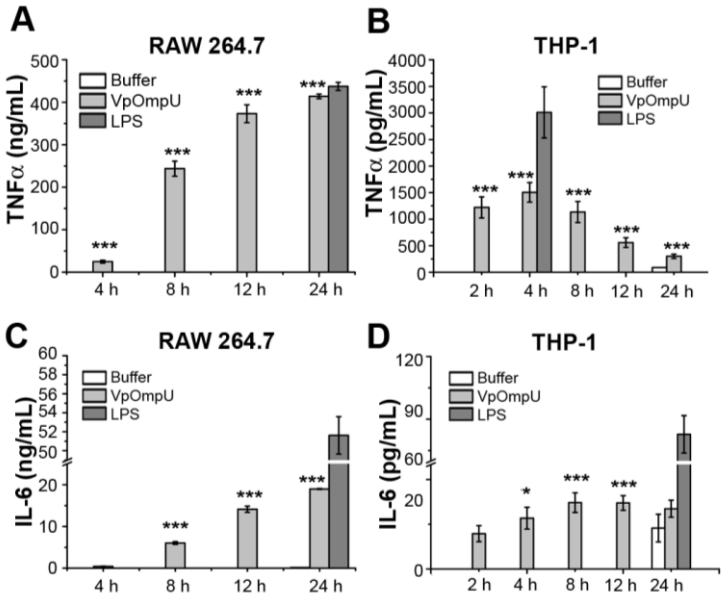

Figure 7. VpOmpU induces pro-inflammatory responses in THP-1 monocyte and RAW 264.7 macrophage

(A-B) Maximum production of TNFα was observed at 24 h in RAW 264.7 cells (A), and at 4 h in THP-1 cells (B), in response to VpOmpU. (C-D) Maximum production of IL-6 was observed at 24 h in RAW 264.7 cells (B), and at 8 h in THP-1 cells (D), in response to VpOmpU. RAW 264.7 and THP-1 cells were treated with 10 μg/ml of recombinant VpOmpU for different time points and supernatants were analysed for TNFα (A) and IL-6 (B) production by ELISA. (A-D) LPS (1 μg/ml) was used as a positive control for all the

experiments. Bar graphs are expressed as mean ± SEM from three to four independent experiments (*p<0.05, **p< 0.01, ***p<0.001, ns p>0.05 versus buffer-treated cells).

A similar time-dependent analysis of NO production in RAW 264.7 cells treated with 10 μg/ml of VpOmpU showed a maximum NO production at 24 h. (Figure 8A). THP-1 cells did not produce NO in response to VpOmpU as observed by a time-dependent analysis of VpOmpU treated cells (Figure 8B).

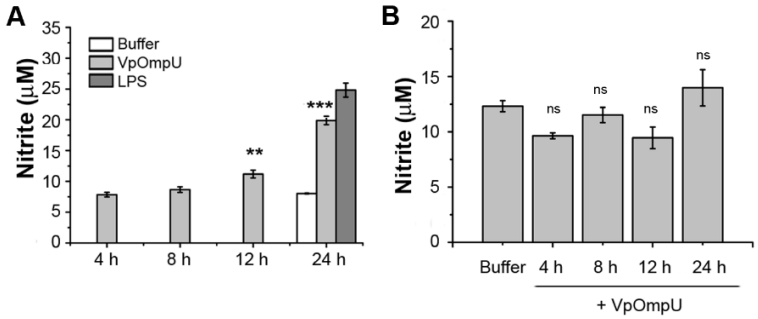

Figure 8. RAW 264.7 macrophages produce Nitric oxide in response to VpOmpU
(A-B) Nitric oxide (NO) production was observed in VpOmpU-treated RAW 264.7 cells (A) but not in THP-1 cells (B). RAW 264.7 cells and THP-1 cells were treated with 10 μg/ml of recombinant VpOmpU and incubated for different time points. Supernatants were analyzed for NO (in terms of nitrite). Bar graphs are expressed as mean ± SEM from three to four independent experiments (*p<0.05, **p< 0.01, ***p<0.001, ns p>0.05 versus buffer-treated cells).

Further, RAW 264.7 cells and THP-1 cells were treated with different concentrations of recombinant VpOmpU. Supernatants were analysed for TNFα and IL-6 by ELISA at the time point where maximum cytokine production has been observed. A dose-dependent increase in TNFα (Figure 9A) and IL-6 (Figure 9B) were observed in both the cell types. A similar dose-dependent analysis of NO production was quantified in the supernatant of RAW 264.7 at 24 h post-treatment. RAW 264.7 cells produced comparable amounts of NO in response to different concentrations of VpOmpU ranging from 3 μg/ml to 10 μg/ml (Figure 9C).

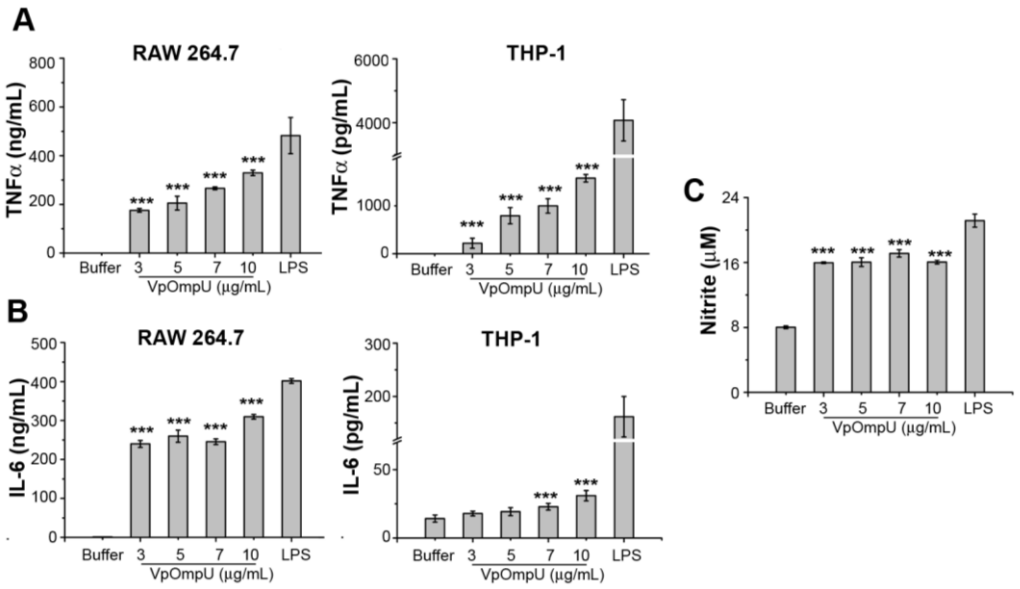

Figure 9. Pro-inflammatory cytokines TNFα and IL-6 are produced in response to VpOmpU in a dose-dependent manner

(A-B) A dose-dependent increase in TNFα (A) and IL-6 (B) production is noticed in both RAW 264.7 and THP-1 cells in response to different doses of VpOmpU. Cells were incubated with different doses of recombinant VpOmpU, and following incubation supernatants were collected and analysed for TNFα and IL-6 production. RAW 264.7 cells and THP-1 cells incubated with VpOmpU for 24 h and 4 h, respectively, for TNFα production (A), and for 24 h and 8 h, respectively, for IL-6 production (B). (C) Similar extent of NO production was observed when RAW 264.7 cells were treated with different doses of recombinant VpOmpU and incubated for 24 h. (A-C) LPS (1 μg/ml) was used as a positive control for all the experiments. Bar graphs are expressed as mean ± SEM from three to four independent experiments (*$p<0.05$, **$p< 0.01$, ***$p<0.001$, ns $p>0.05$ versus buffer-treated cells).

Further, we have done MTT assay to examine cell mortality rate in response to different doses of recombinant VpOmpU following 24 h of incubation. The cell mortality in response to VpOmpU was comparable at doses upto 10 μg/ml and it is in the range of 30-40 % in case of RAW 264.7 cells and about 5-15 % in case of THP-1 cells (Figure 10).

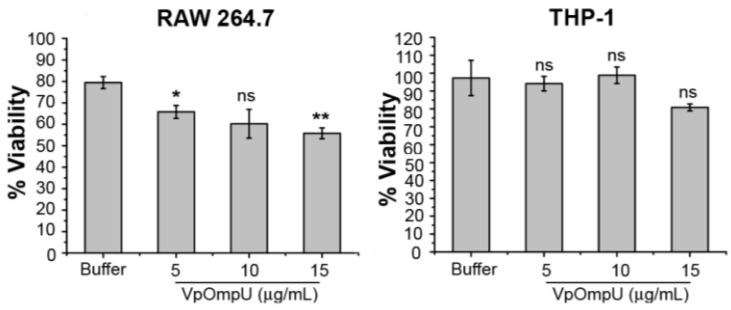

Figure 10. Cell viability was minimally affected in response to different doses of VpOmpU in both RAW 264.7 and THP-1 cells

RAW 264.7 and THP-1 cells were treated with different doses of VpOmpU for 24 h and then, the viability was measured using MTT assay. Bar graphs are expressed as mean ± SEM from three to four independent experiments (*$p<0.05$, **$p< 0.01$, ***$p<0.001$, ns $p>0.05$ versus buffer-treated cells).

These results show that VpOmpU can activate macrophages and monocytes to induce pro-inflammatory responses.

4.7 Wild type (wt)-VpOmpU and recombinant (r)-VpOmpU induce similar pro-inflammatory responses in macrophages and monocytes

We next wanted to compare the pro-inflammatory responses generated by the cells upon treatment with wild type and recombinant VpOmpU. For this, we treated both RAW 264.7 and THP-1 cells with equal amount (5 µg/ml) of each of the proteins, and analysed the supernatants for TNFα and IL-6 at the time point, where maximum amount of the respective cytokine was observed in the time-dependent analysis (Figure 3A-B). We observed that comparable amount of TNFα (Figure 11A) and IL-6 (Figure 11B) were being produced in response to wild type and recombinant VpOmpU in both RAW 264.7 and THP-1 cells.

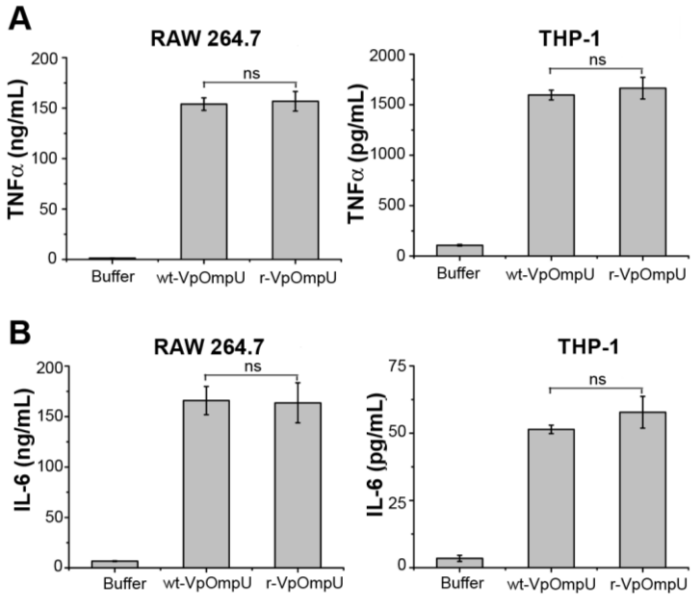

Figure 11. Comparable production of TNFα and IL-6 in response to wt-VpOmpU and r-VpOmpU.

Comparable production of TNFα and IL-6 was observed in both RAW 264.7 and THP-1 cells in response to similar doses of purified wild type VpOmpU (wt-VpOmpU) and recombinant VpOmpU (r-VpOmpU). (A-B) RAW 264.7 and THP-1 cells were treated with 5 μg/ml of wt-VpOmpU or r-VpOmpU, and incubated for 24 h and 4 h respectively, for TNFα (A), and for 24 h and 8 h, respectively, for IL-6 measurements (B). Bar graphs are expressed as mean ± SEM from three independent experiments (*p<0.05, **p< 0.01, ***p<0.001, ns p>0.05 versus wt-VpOmpU-treated cells).

Based on this result, recombinant form of VpOmpU was used in all the subsequent experiments.

4.8 VpOmpU elicits the pro-inflammatory responses via TLR-signalling pathway

The observation that VpOmpU induces a pro-inflammatory response in monocytes and macrophages reflected upon the possibility that VpOmpU may be recognized as a PAMP by PRRs on the host cells. One of the major classes of PRRs which recognize bacterial PAMPs is the Toll-like receptors (TLRs) (4). Since *V. parahaemolyticus* are non-invasive bacteria, VpOmpU will be most likely recognized as a PAMP by the surface TLRs present on the cells. Therefore, a time-course analysis of gene-expression of surface TLRs was done in VpOmpU-treated RAW

264.7 and THP-1 cells. An increase in gene-expression of TLR2, TLR1 and TLR6 was observed in RAW 264.7 cells, whereas, an up-regulation of TLR2 and TLR1 was observed in THP-1 cells (Figure 12).

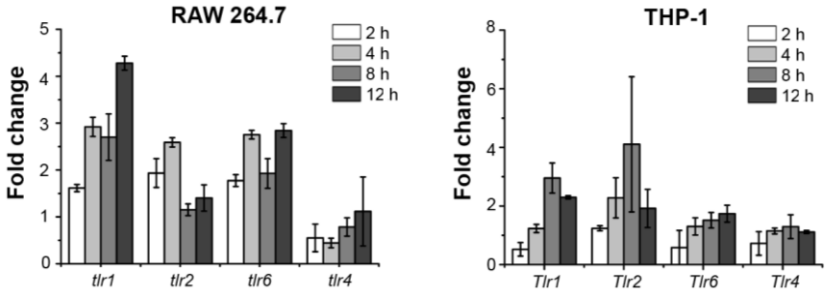

Figure 12. Up-regulation in gene-expressions of TLR1, TLR2 and TLR6 in response to VpOmpU

Up-regulation in gene-expressions of TLR1, TLR2 and TLR6 at different time points in response to VpOmpU in RAW 264.7 and of TLR1 and TLR2 in THP-1 cells. Following treatment with VpOmpU, cells were harvested to isolate total RNA. Further, cDNA was generated, and subjected to RT-PCR. The Ct values obtained were normalized to the respective Ct values of the house-keeping genes. Fold change is calculated above buffer treated cells and bar graphs are expressed as mean ± SD from three independent experiments.

Further, we checked the surface expression of TLR1, TLR2 and TLR6 in both RAW 264.7 and THP-1 cells. In accordance with the gene-expression analysis, we observed an increase in the surface expression of TLR1, TLR2 and TLR6 in RAW 264.7 cells, while in THP-1 cells, an increase in surface expression of TLR1 and TLR2 was observed (Figure 13A, 13B).

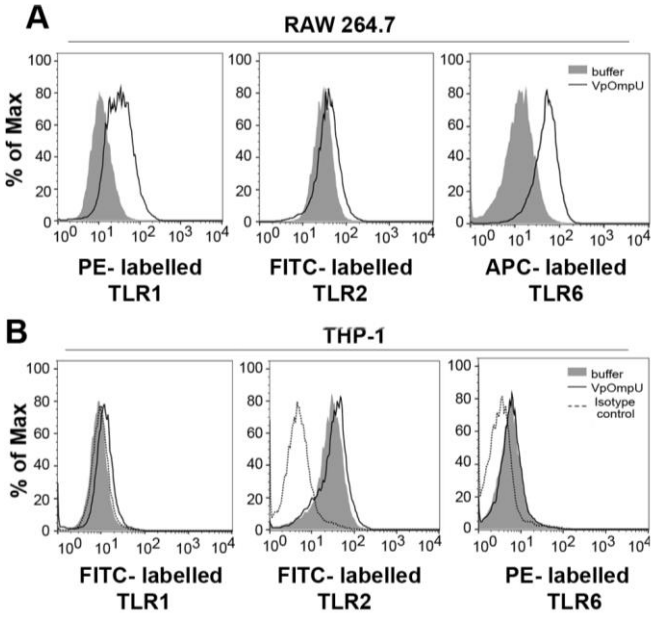

Figure 13. Surface expression analysis of TLR1, 2 & 6 in RAW 264.7 and THP-1 cells
(A-B) Increase in surface expression of TLR1, TLR2 and TLR6 in RAW 264.7 (A), and TLR1 and TLR2 in THP-1 cells (B) in response to VpOmpU. RAW 264.7 (A) and THP-1 (B) cells were treated with VpOmpU and analysed for surface expression of TLRs by flow cytometry.

The above data indicated that TLR1 and TLR2 could be involved in recognition of VpOmpU in THP-1 cells, whereas, in RAW 264.7, TLR1, TLR2 and TLR6 could be involved in recognition of VpOmpU.

To confirm the involvement of TLR2, we used neutralizing antibody. Upon neutralizing TLR2, we observed a significant decrease in the pro-inflammatory cytokine production in both THP-1 and RAW 264.7 cells compared to the control-treated cells, in response to VpOmpU (Figure 14). This result confirmed that TLR2 is probably involved in recognition of VpOmpU in both monocytes and macrophages.

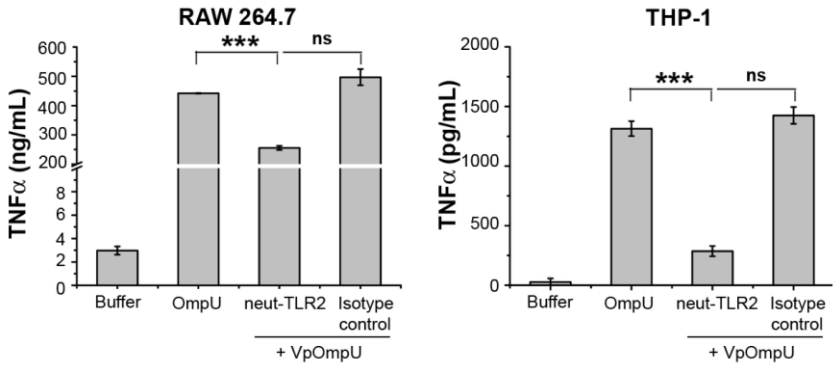

Figure 14. TLR2 seems to be involved in VpOmpU-mediated signalling

Decrease in TNFα-production upon TLR2-neutralization in VpOmpU-treated RAW 264.7 and THP-1 cells compared to the isotype pre-treated VpOmpU-treated cells and only VpOmpU-treated cells. Cells were pre-treated with neutralizing antibody and the isotype for 1 h, followed by VpOmpU treatment for 24 h in RAW 264.7 and for 4 h in THP-1 cells. Supernatants were analysed for TNFα by ELISA. Bar graphs are expressed as mean ± SEM from three independent experiments (*p<0.05, **p< 0.01, ***p<0.001, ns p>0.05 versus cells treated with VpOmpU only).

To further confirm the involvement of TLR2 in monocytes, we performed siRNA-mediated knock-down of TLR2 in THP-1 cells (Figure 15A), and observed a decrease in cytokine production upon treatment of TLR2 knocked-down cells with VpOmpU (Figure 15B).

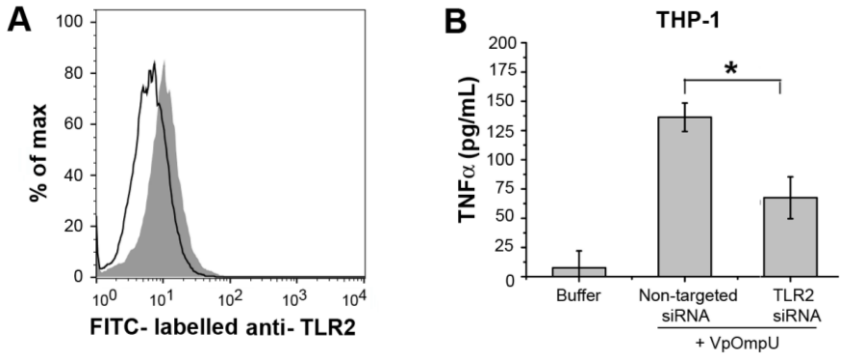

Figure 15. TLR2 is involved in VpOmpU-mediated response in THP-1 cells

(A) TLR2 was knocked down in THP-1 cells. THP-1 cells were transfected with siRNA for TLR2 and the knockdown was confirmed by flow cytometry after 48 h. (B) Decrease in TNFα production in response to VpOmpU upon knock-down of TLR2 by siRNA in VpOmpU-treated THP-1 cells compared to the non-targeted siRNA-treated VpOmpU-treated cells. Following siRNA knockdown, cells were treated with VpOmpU for 4 h and supernatant was

analysed for TNFα by ELISA. Bar graphs are expressed as mean ± SEM from three independent experiments (*p<0.05, **p< 0.01, ***p<0.001, ns p>0.05 versus non-targeted siRNA-transfected VpOmpU-treated cells).

To confirm the involvement of TLR2 in macrophages, we used bone marrow-derived macrophages (BMDMs) from *Tlr2*$^{-/-}$ mice and wild type mice. We treated the BMDMs with VpOmpU, and compared the cytokine production following 24 h incubation. We observed significantly less production of TNFα and IL-6 in *Tlr2*$^{-/-}$ BMDMs as compared to the wild type BMDMs (Figure 16).

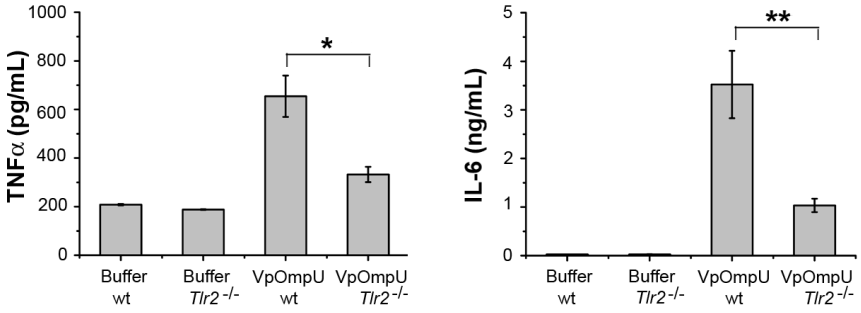

Figure 16. TLR2 is involved in VpOmpU-mediated response in macrophages

Decrease in TNFα and IL-6 production by VpOmpU–treated BMDMs differentiated from *Tlr2*$^{-/-}$ mice compared to the wild type control. Bar graphs are expressed as mean ± SEM from three independent experiments (*p<0.05, **p< 0.01, ***p<0.001, ns p>0.05 versus VpOmpU-treated cells from wild type mice).

Altogether, these data confirmed that TLR2 is involved in recognition of VpOmpU in both monocytes and macrophages.

In response to a PAMP, TLRs are known to dimerize and activate the downstream signalling, and TLR2 is known to make hetero-dimers with TLR1 or TLR6, gene expression profile (Figure 12) and surface expression profile (Figure 13) suggested that in RAW 264.7 cells, VpOmpU could be recognized by both TLR1/2 and TLR2/6 hetero-dimers, while in THP-1 cells, VpOmpU could be recognized by TLR1/2 hetero-dimer only.

Therefore, to find out the hetero-dimerizing partner of TLR2, we pulled-down the VpOmpU-treated cell lysates with anti-TLR2 antibody, and observed that both TLR1 and TLR6 co-immunoprecipitated with TLR2 in RAW 264.7 cells (Figure 17A). To further confirm this result, we immunoprecipitated VpOmpU-treated RAW 264.7 cell lysates with anti-TLR1 and anti-

TLR6 antibodies, and observed co-immunoprecipitation of TLR2 along with both TLR1 (Figure 17B) and TLR6 (Figure 17C). VpOmpU also co-immunoprecipitated with TLR2, TLR1, and TLR6 (Figure 17A-C).

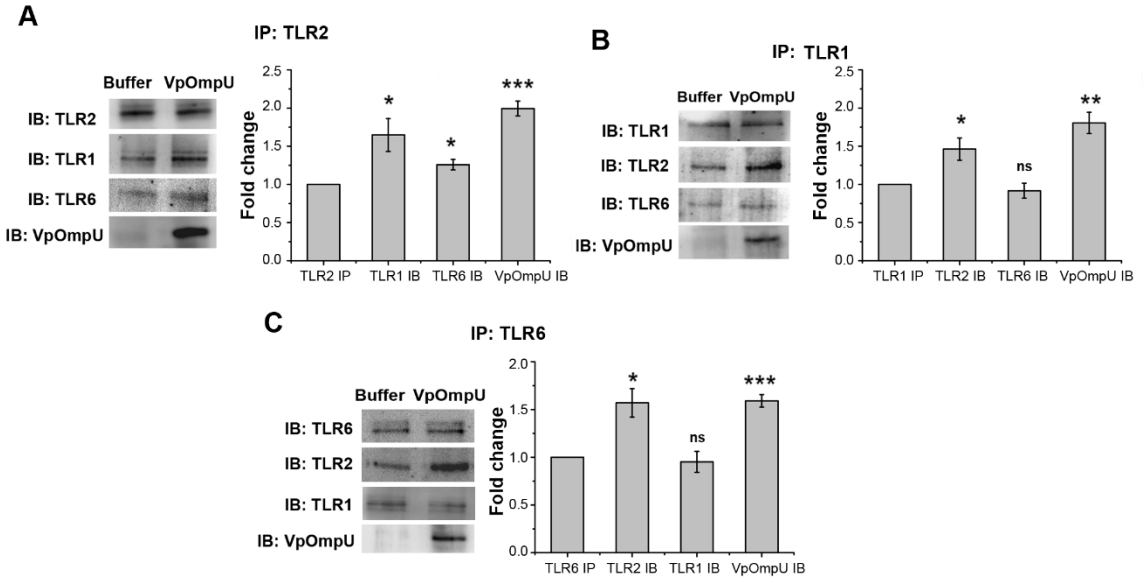

Figure 17. VpOmpU is recognized by both TLR1/2 and TLR2/6 in macrophages

(A-C) In RAW 264.7 cells, VpOmpU associates with TLR2, TLR1 and TLR6 as evidenced in co-immunoprecipitation (co-IP) and reverse co-IP studies using anti-TLR2, anti-TLR1 and anti-TLR6 antibodies. (A) TLR1 and TLR6 were co-immunoprecipitated with TLR2 in VpOmpU-treated RAW 264.7 cells as observed by immunoblotting and densitometric analysis of the bands. (B) TLR2 was co-immunoprecipitated with TLR1 in VpOmpU-treated RAW 264.7 cells as observed by immunoblotting and densitometric analysis of the bands. (C) TLR2 was co-immunoprecipitated with TLR6 in VpOmpU-treated RAW 264.7 cells as observed by immunoblotting and densitometric analysis of the bands. (A-C) Cell lysates were prepared after 15 min of VpOmpU treatment and were immunoprecipitated with anti-TLR1 or anti-TLR2 or anti-TLR6 antibody, and the IP lysates were further analysed for TLRs co-immonoprecipitated together to find out the receptor complex. For the densitometric analysis, the band intensities of TLR1, TLR2, TLR6 or VpOmpU in the VpOmpU-treated samples were estimated above the respective band intensities in the buffer-treated samples. Bar graphs are expressed as mean ± SEM from three independent experiments (*$p<0.05$, **$p< 0.01$, ***$p<0.001$, ns $p>0.05$ versus band intensities in the buffer-treated cells).

These data indicated that TLR2 is probably hetero-dimerizing with both TLR1 and TLR6 in response to VpOmpU in RAW 264.7 macrophages. In case of THP-1 cells we observed that TLR1, but not TLR6 co-immunoprecipitated with TLR2 in response to VpOmpU treatment (Figure 18A). To further confirm this result, we did reverse co-IP of VpOmpU-treated THP-1

cell lysates with anti-TLR1 and anti-TLR6 antibodies, and observed co-immunoprecipitation of TLR2 along with TLR1 (Figure 18B), but not with TLR6 (Figure 18C). Consistent with this VpOmpU co-immunoprecipitated with only TLR2 and TLR1, but not with TLR6 (Figure 18A-C). These data indicated that in THP-1 cells TLR2 is probably hetero-dimerizing with TLR1 but not TLR6 in response to VpOmpU.

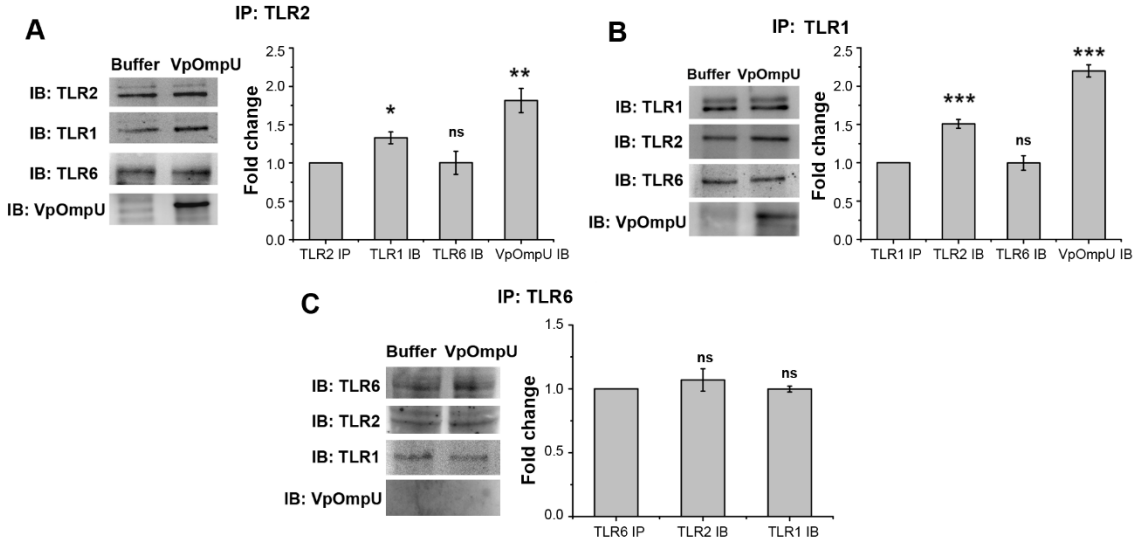

Figure 18. VpOmpU is recognized by TLR1/2 and not by TLR2/6 hetero-dimers in THP-1 cells

(A-C) VpOmpU associates with TLR1 and TLR2 in THP-1 cells as observed by co-IP and reverse co-IP using anti-TLR2, anti-TLR1 and anti-TLR6 antibodies. (A) TLR1 was co-immunoprecipitated with TLR2 in VpOmpU-treated THP-1 cells as observed by immunoblotting and densitometric analysis of the bands. (B) TLR2 co-immunoprecipitated with TLR1 in VpOmpU-treated THP-1 cells as observed by immunoblotting and densitometric analysis of the bands. (C) TLR2 did not co-immunoprecipitate with TLR6 in VpOmpU-treated THP-1 cells as observed by immunoblotting and densitometric analysis. (A-C) Cell lysates were prepared after 15 min of VpOmpU treatment and were immunoprecipitated with anti-TLR1 or anti-TLR2 or anti-TLR6 antibody, and the IP lysates were further analysed for TLRs co-immonoprecipitated together to find out the receptor complex. For the densitometric analysis, the band intensities of TLR1, TLR2, TLR6 or VpOmpU in the VpOmpU-treated samples were estimated above the respective band intensities in the buffer-treated samples. Bar graphs are expressed as mean ± SEM from three independent experiments (*$p<0.05$, **$p< 0.01$, ***$p<0.001$, ns $p>0.05$ versus band intensities in the buffer-treated cells).

The co-immunoprecipitation data suggested the involvement of both the TLR1/2 and TLR2/6 hetero-dimers in recognizing VpOmpU in RAW 264.7 cells, unlike only the TLR1/2 hetero-dimers in THP-1 cells.

Further, to confirm the above results we used neutralizing antibodies against TLR1 and TLR6 in THP-1 cells followed by treatment with VpOmpU. We observed reduced production of TNFα in cells pre-treated with TLR1 but not with TLR6 neutralizing antibodies, confirming the involvement of TLR1/2 hetero-dimer, and not TLR2/6 hetero-dimer in VpOmpU-mediated pro-inflammatory responses in THP-1 cells (Figure 19A). Also, no decrease was observed in TNFα after siRNA knock-down of TLR6 in THP-1 cells (Figure 19B and Figure 19C).

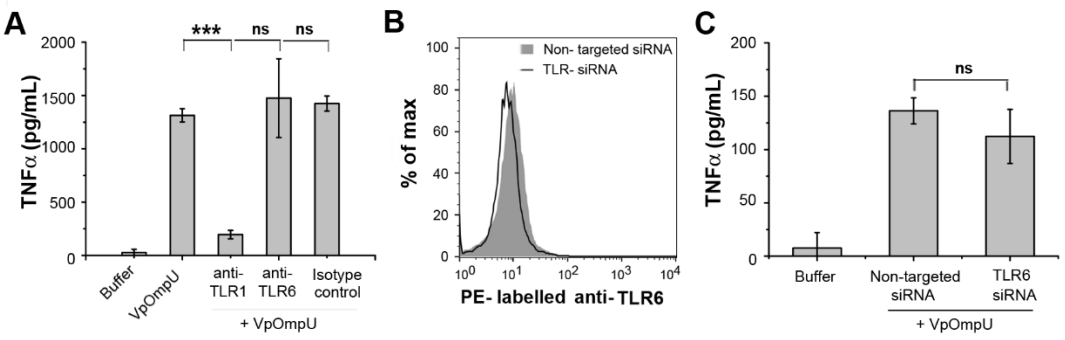

Figure 19. TLR6 is not involved in VpOmpU-mediated pro-inflammatory response in THP-1 cells

(A) Decrease in TNFα production with anti-TLR1, but not with anti-TLR6 neutralizing antibody in VpOmpU-treated THP-1 cells compared to isotype pre-treated VpOmpU-treated and only VpOmpU-treated cells. Bar graphs are expressed as mean ± SEM from three independent experiments (*p< 0.05, **p< 0.01, ***p< 0.001, ns p> 0.05 versus cells treated with VpOmpU only). (B) TLR6 was knocked down in THP-1 cells. THP-1 cells were transfected with siRNA against TLR6 and the knockdown was confirmed by flow cytometry after 48 h. (C) No decrease in TNFα production in THP-1 cells with knockdown of TLR6 by siRNA compared to the non-targeted siRNA-transfected control, in response to VpOmpU. Following siRNA knockdown, cells were treated with VpOmpU for 4 h and supernatant was analysed for TNFα by ELISA. Bar graphs are expressed as mean ± SEM from three independent experiments (*p<0.05, **p< 0.01, ***p<0.001, ns p>0.05 versus non-targeted siRNA-transfected VpOmpU-treated cells).

Altogether, these results confirmed the involvement of TLR1/2 dimer in VpOmpU-mediated pro-inflammatory response in THP-1 cells.

Further, to confirm the TLR hetero-dimers involved in recognition of VpOmpU in macrophages, we knocked down TLR1 and TLR6 using siRNA in RAW 264.7 cells (Figure 20A). Upon TLR6 knock down, a decrease in TNFα production was observed (Figure 20B). However, when TLR1 was knocked down, there was no significant decrease in TNFα production (Figure 20B).

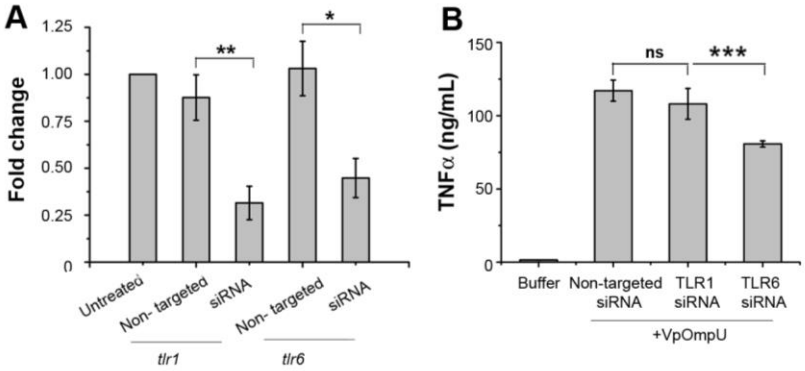

Figure 20. TLR6 is the major player in VpOmpU-mediated pro-inflammatory response in RAW 264.7 cells

(A) TLR1 and TLR6 was knocked down in RAW 264.7 cells. RAW 264.7 cells were transfected with siRNA against TLR1 and TLR6 and the knockdown was confirmed by gene-expression analysis after 24 h. (B) Decrease in TNFα production with siRNA-mediated knockdown of TLR6 but not with TLR1 compared to non-targeted siRNA-transfected control in RAW 264.7 cells in response to VpOmpU. (H-I) Bar graphs are expressed as mean ± SEM from three independent experiments (*$p<0.05$, **$p< 0.01$, ***$p<0.001$, ns $p>0.05$ versus VpOmpU-treated cells transfected with non-targeted siRNA).

Although, by co-immunoprecipitation studies both TLR1/2 and TLR2/6 hetero-dimers seemed to be involved (Figure 17), but the siRNA knock-down (Figure 20B) implied that TLR6 is the major player for the recognition of VpOmpU in RAW 264.7 cells.

4.9 MyD88 and IRAK-1 are involved in TLR-mediated signalling by VpOmpU

TLR activation signal can be mediated through MyD88-dependent or -independent pathway (16). If MyD88 is recruited to the receptor complex as a result of TLR activation, it most certainly recruits IRAK-1 to the receptor complex (16). Gene-expression analysis showed an up-regulation of MyD88 in VpOmpU-treated THP-1 and RAW 264.7 cells indicating its involvement in VpOmpU-mediated TLR-signalling (Figure 21A, 21B).

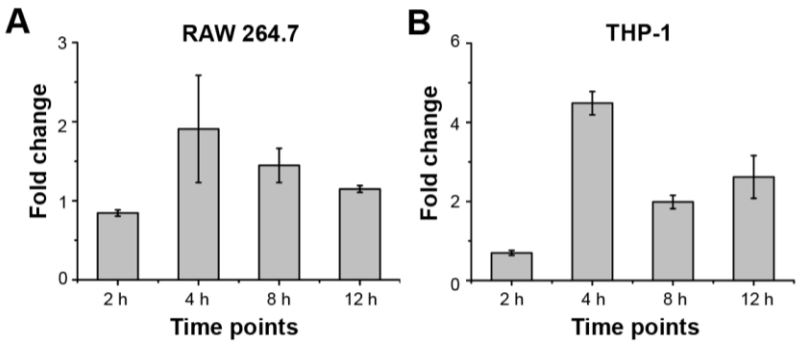

Figure 21. MyD88 could be involved in VpOmpU-mediated signalling

Increase in gene-expression of MyD88 in VpOmpU-treated RAW 264.7 and THP-1 cells at different time points. Fold change is calculated above buffer-treated cells and bar graphs are expressed as mean ± SD from three independent experiments.

Further, we observed that MyD88 co-immunoprecipitated along with TLR2 when lysates of VpOmpU-treated RAW 264.7 (Figure 22A) and THP-1 cells (Figure 22B) were pulled-down using anti-TLR2 antibody.

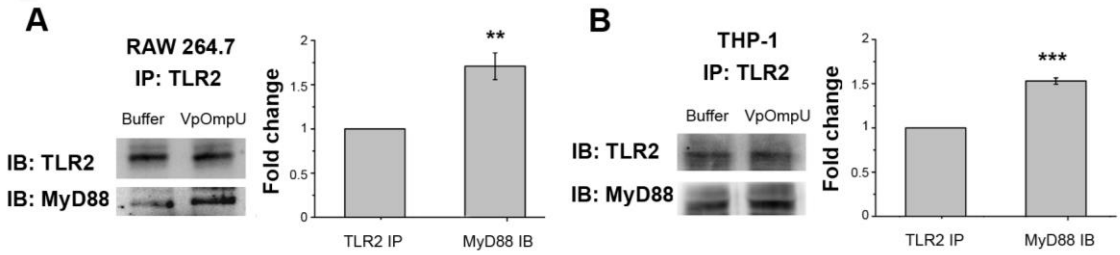

Figure 22. MyD88 is recruited to the TLR complex in response to VpOmpU

(A-B) MyD88 co-immunoprecipitated with TLR2 upon VpOmpU treatment in RAW 264.7 cells (A) and THP-1 cells (B) as evidenced by immunoblotting and densitometric analysis of the bands. Bar graphs are expressed as mean ± SEM from three independent experiments (*p<0.05, **p<0.01, ***p<0.001, ns p>0.05 versus band intensities in the buffer-treated cells).

These data suggested that VpOmpU-mediated TLR signalling involved MyD88. Further, we have confirmed the involvement of MyD88 by using MyD88-deficient (*Myd88*$^{-/-}$) transgenic mice, wherein the TNFα and IL-6 production in response to VpOmpU by the BMDMs from the *Myd88*$^{-/-}$ mice was significantly lower than that from the wild type mice (Figure 23).

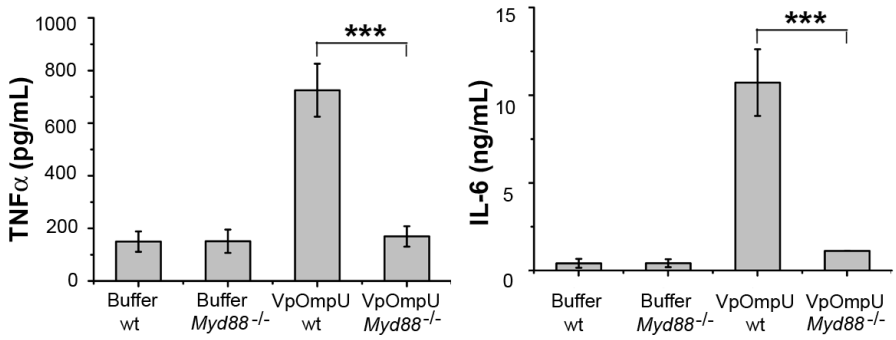

Figure 23. MyD88 is involved in VpOmpU-mediated responses

Decrease in TNFα and IL-6 production in VpOmpU-treated BMDMs differentiated from *Myd88*$^{-/-}$ mice compared to the wild type control. Bar graphs are expressed as mean ± SEM from three independent experiments (*p<0.05, **p< 0.01, ***p<0.001, ns p>0.05 versus VpOmpU-treated BMDMs from wild type mice).

Further, to check whether, IRAK-1 is involved in VpOmpU-mediated signalling, we used a pharmacological inhibitor of IRAK-1. We observed a considerable decrease in the pro-inflammatory cytokine production in the VpOmpU-treated cells with the use of IRAK-1 inhibitor in both RAW 264.7 and THP-1 cells (Figure 24).

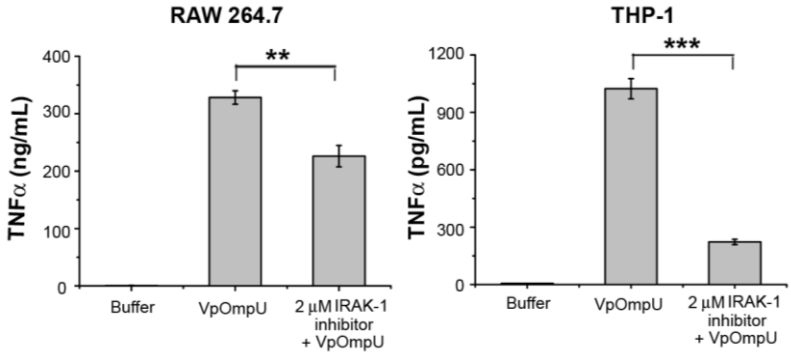

Figure 24. IRAK-1 is involved in VpOmpU-mediated responses

Decrease in TNFα production with use of IRAK-1 inhibitor in response to VpOmpU treatment in RAW 264.7 and THP-1 cells. Bar graphs are expressed as mean ± SEM from three independent experiments (*p<0.05, **p< 0.01, ***p<0.001, ns p>0.05 versus cells treated with VpOmpU only).

These observations confirmed that in macrophages and monocytes the pro-inflammatory responses generated on recognition of VpOmpU by the TLRs involve MyD88 and IRAK-1.

4.10 NF-κB transcription factor is involved in TLR-mediated signalling of VpOmpU

In general, TLR activation ultimately leads to the activation of transcription factor NF-κB (4). Upon pre-treatment of the cells with NF-κB inhibitor (MLN4924) followed by VpOmpU stimulation, a decrease in the production of TNFα was observed in both RAW 264.7 cells and THP-1 cells compared to VpOmpU-treated cells (Figure 25). These data indicated that NF-κB might be involved in VpOmpU-mediated pro-inflammatory responses.

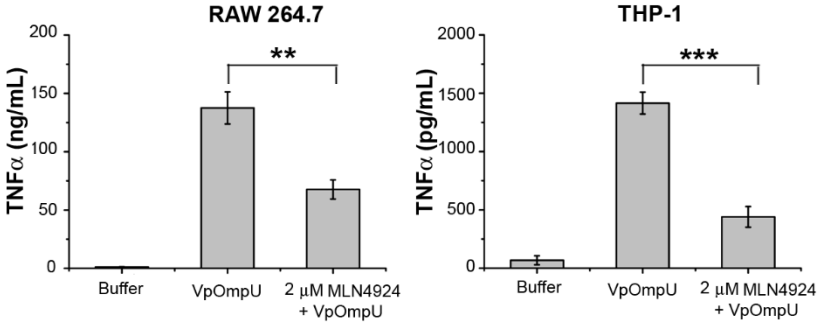

Figure 25. NF-κB seems to be involved in VpOmpU-mediated pro- inflammatory response
Decrease in production of TNFα in response to VpOmpU with the use of inhibitor of NF-κB (MLN4924) in both RAW 264.7 and THP-1 cells. Bar graphs are expressed as mean ± SEM from three independent experiments (*p<0.05, **p< 0.01, ***p<0.001, ns p>0.05 versus cells treated with VpOmpU only).

In an unstimulated cell, NF-κB remains bound to its inhibitor IκB and are present in the cytoplasm. Activation of the IRAK-1/4 complex results in the activation of signalling cascades that leads to the phosphorylation and degradation of IκB rendering NF-κB free to translocate to the nucleus and transcribe the genes for pro-inflammatory cytokines. There are five members in the NF-κB subfamily. They either hetero-dimerize or homo-dimerize and depending on the subunits and their nature of dimerization the cell exerts pro- or anti-inflammatory responses (134). Majorly, p65 and/or c-Rel are the members of the NF-κB family which dimerize with p50 to transcribe pro-inflammatory genes. Therefore, phosphorylation and degradation of IκB is crucial for activation of NF-κB (134). In VpOmpU-treated RAW 264.7 and THP-1 cells, we observed phosphorylation and degradation of IκB indicating the probable activation of NF-κB (Figure 26A). Further, we also observed nuclear translocation of c-Rel in RAW 264.7 cells and p65 in THP-1 cells (Figure 26B).

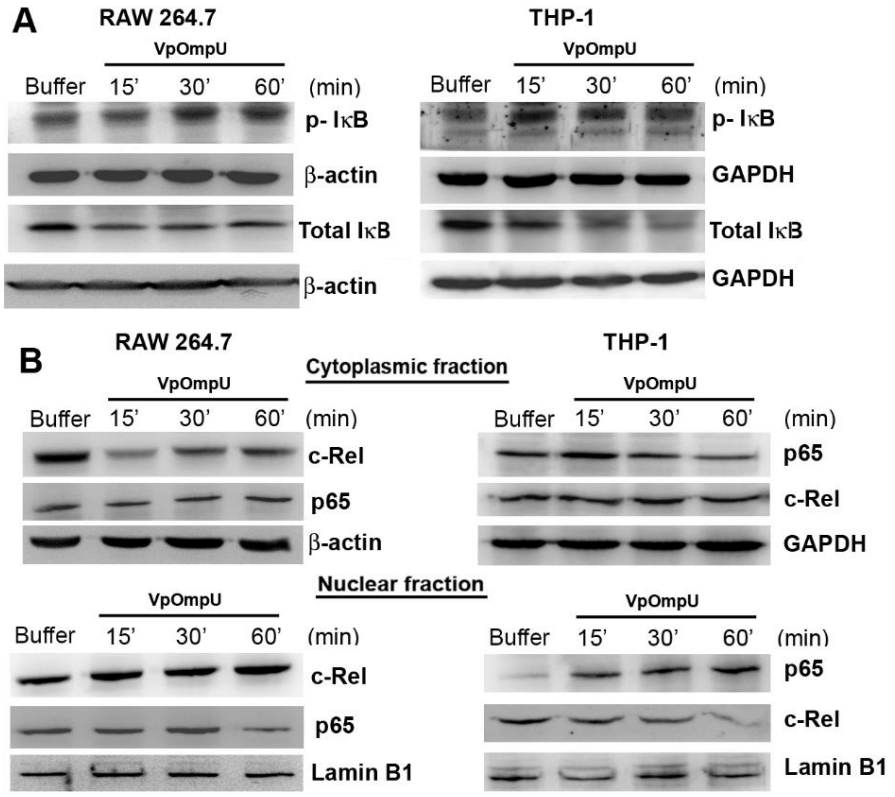

Figure 26. VpOmpU induces the phosphorylation and degradation of IκB leading to NF-κB translocation to the nucleus

(A) Increase in phosphorylated IκB and decrease in total IκB in response to VpOmpU with increase in time in both RAW 264.7 and THP-1 cells. Cells were treated with VpOmpU and incubated for different time points. Whole cell lysates were prepared and analysed by western blotting for phosphorylated- and total IκB. β–actin and GAPDH were used as loading controls for the whole cell lysates. (B) Translocation of NF-κB subunits namely c-Rel in RAW 264.7 and p65 in THP-1 from the cytoplasm to the nucleus in response to VpOmpU. Lamin B1 was used as a loading control for nuclear lysates and β–actin and GAPDH were used as loading controls for the cytoplasmic lysates.

Altogether these experiments confirmed that NF-κB is involved in VpOmpU-mediated pro-inflammatory responses.

4.11 AP-1 transcription factor is involved in VpOmpU-mediated signalling

Apart from NF-κB, another transcription factor namely, AP-1 is also known to be involved in pro-inflammatory responses (16). To probe, whether, AP-1 has a role in VpOmpU-mediated pro-inflammatory response, we first used a chemical inhibitor against AP-1 (SP600125). We observed a decrease in the production of TNFα in VpOmpU-treated RAW 264.7 and THP-1

cells in presence of the inhibitor (Figure 27), indicating a role of AP-1 transcription in VpOmpU-mediated pro-inflammatory response.

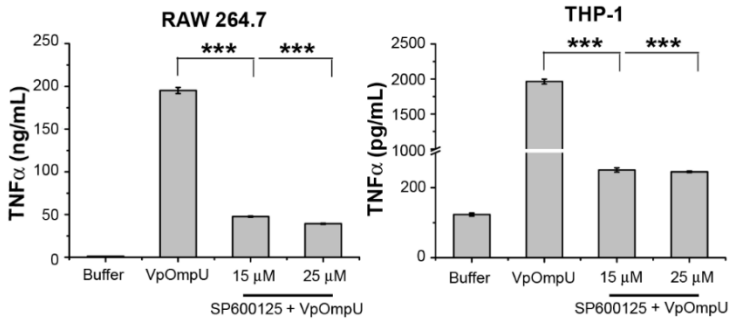

Figure 27. AP-1 transcription factor could be involved in VpOmpU-mediated responses

Decrease in the production of TNFα in response to VpOmpU in the presence of AP-1 inhibitor (SP600125) in both RAW 264.7 and THP-1 cells. Bar graphs are expressed as mean ± SEM from three independent experiments (*p<0.05, **p< 0.01, ***p<0.001, ns p>0.05 versus cells treated with VpOmpU only).

The sub-units of AP-1 transcription factor are divided majorly into two families- Fos and Jun. The members of Fos and Jun families generally hetero-dimerize and form AP-1 to function as a transcription factor (135). Further, nuclear fractions of VpOmpU-treated RAW 264.7 and THP-1 cells were analyzed for the involvement of AP-1 sub-units in VpOmpU-mediated pro-inflammatory processes. By looking at the AP-1 sub-unit levels in the nuclear lysates, we came to the conclusion that in VpOmpU-treated RAW 264.7 cells, AP-1 subunits such as, JunB, c-Jun and c-Fos and in THP-1 cells, AP-1 subunits such as, JunB, JunD, c-Jun and c-Fos could be involved (Figure 28).

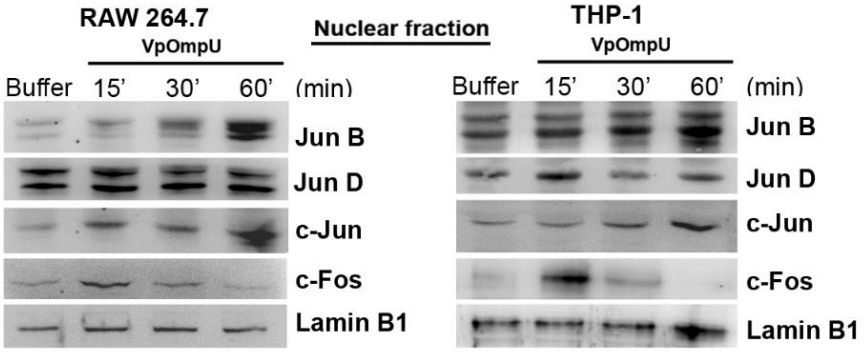

Figure 28. AP-1 family members increase in the nucleus in response to VpOmpU

Increase in AP-1 family members in the nuclear lysates of VpOmpU-treated cells, namely JunB, c-Jun, c-Fos in RAW 264.7 and JunB, c-Jun, c-Fos and JunD in THP-1 cells. Lamin B1 was used as a loading control for nuclear lysates.

4.12 VpOmpU leads to the activation of MAP-kinases

Generally, MAP kinase activation leads to the activation of AP-1 (16). To probe whether MAP kinases are involved in VpOmpU-mediated pro-inflammatory responses in RAW 264.7 and THP-1 cells, we checked the phosphorylation level of both JNK and P38. We observed phosphorylation (indicative of activation status) of both P38 and JNK in RAW 264.7 (Figure 29A) and THP-1 cells (Figure 29B).

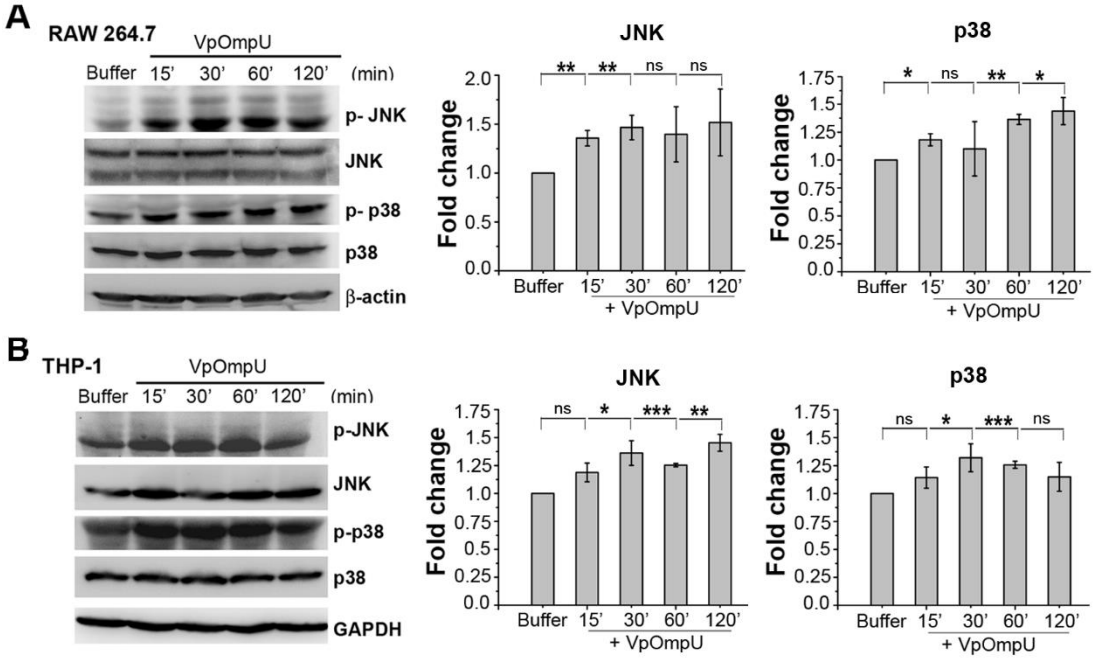

Figure 29. P38 and JNK MAP-kinases are activated in response to VpOmpU

(A-B) Increased phosphorylation of p38 and JNK in RAW 264.7 (A) and THP-1 cells (B) in response to VpOmpU as evidenced by immunoblot and densitometric analysis of the bands. Whole cell lysates were analysed for the phosphorylation of p38 and JNK at different time points following VpOmpU treatment. Total p38 and JNK in the cells were also probed. Densitometric analysis of the immunoblots confirmed increased phosphorylation of p38 and JNK in RAW 264.7 cells in response to VpOmpU. For the densitometric analysis, the band intensities of p-p38 or p-JNK in the samples were calculated above the band intensities of p38 or JNK, respectively, and fold changes upon VpOmpU treatments were estimated with respect to the buffer-treated cells. Bar graphs are expressed as mean± SEM from three independent experiments (*p<0.05, **p< 0.01, ***p<0.001, ns p>0.05 versus band intensities in the buffer-treated cells).

Further, we observed decrease in cytokine production in VpOmpU-treated cells, pre-treated with chemical inhibitors against JNK and P38 (Figure 30).

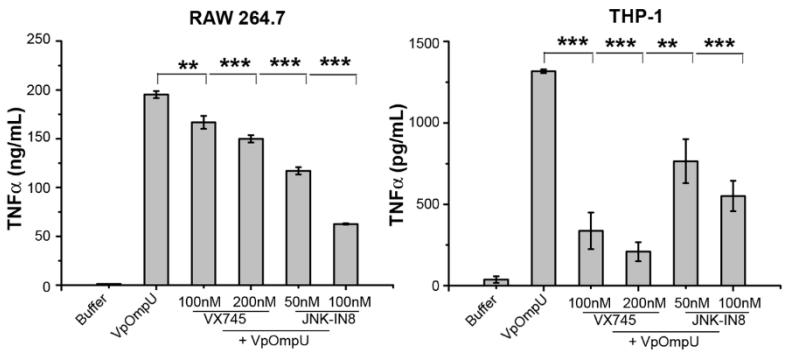

Figure 30. P38 and JNK are involved in VpOmpU-mediated pro-inflammatory response
Decrease in TNFα in response to VpOmpU upon pre-treatment with inhibitors of the MAP-kinases p38 (VX745) and JNK (JNK-IN8) in RAW 264.7 and THP-1 cells. Bar graphs are expressed as mean ± SEM from three independent experiments (*p<0.05, **p< 0.01, ***p<0.001, ns p>0.05 versus cells treated with VpOmpU only).

Altogether, these results showed that P38 and JNK MAP kinases are involved in VpOmpU-mediated pro-inflammatory responses.

4.13 TLR2 activation by VpOmpU leads to the MAP-kinase activation

A recent report showed that OmpU of *V. cholerae*, which is about 70 % similar to VpOmpU induced the activation of P38 by a TLR2-mediated pathway, but, the activation of JNK in macrophages was found to be dependent on its recognition by the scavenger receptor CD36 (128). So, to probe whether the activation of MAP-kinases in response to VpOmpU was TLR2-mediated, we investigated the phosphorylation levels of P38 and JNK in BMDMs from *Tlr2*$^{-/-}$ mice. We found that in the absence of TLR2, MAP-kinases (p38 and JNK) were not activated in response to VpOmpU (Figure 31).

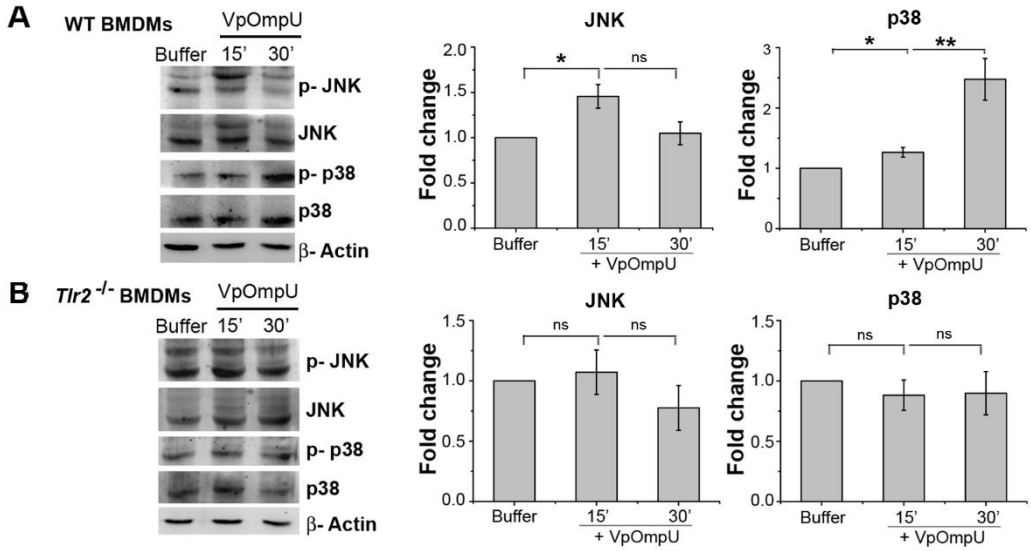

Figure 31. MAP-kinase activation in response to VpOmpU is TLR2-dependent

(A-B) Increased phosphorylation of p38 and JNK in VpOmpU-treated BMDMs from wild type mice (WT), while no change in phosphorylation status of p38 and JNK in the VpOmpU-treated BMDM obtained from the *Tlr2*$^{-/-}$ mice. Densitometric analysis of the immunoblots show increased phosphorylation of JNK at 15 min, and of p38 at both 15 min and 30 min in the wild type BMDMs, and no change in phosphorylation status of JNK and p38 in the *Tlr2*$^{-/-}$ BMDMs in response to VpOmpU. For the densitometric analysis, the band intensities of p-p38 or p-JNK in the samples were calculated above the band intensities of p38 or JNK, respectively, and fold changes upon VpOmpU treatments were estimated with respect to the buffer-treated cells. Bar graphs are expressed as mean ± SEM from three independent experiments (*$p<0.05$, **$p< 0.01$, ***$p<0.001$, ns $p>0.05$ versus band intensities in buffer-treated cells). β–actin and GAPDH were used as the loading controls in the immunoblots of the whole cell lysates.

5. Conclusions and Discussion

OmpU is a major outer membrane protein which is present across the *Vibrio* species. In most of the *Vibrio* species it plays a role in pathogenesis and modulation of host immune function. In *V. alginolyticus* and in *V. harveyi*, OmpU has been considered as a vaccine candidate (119, 136). OmpU of *V. parahaemolyticus* (VpOmpU) has also been reported to be immunogenic in yellow croaker fish (117), though it has not been well elucidated.

Many porins such as PorB of *Neisseria meningitides* (137), OmpS1 and OmpS2 of *Salmonella typhi* (30) have been found to induce pro-inflammatory responses. In this study, we have char-

acterized the role of VpOmpU in modulating host's innate immune responses. We have observed that VpOmpU activates macrophages and monocytes in terms of production of pro-inflammatory mediators, such as, TNFα and IL-6 in both macrophages and monocytes (Figure 7) and nitric oxide (NO) in macrophages (Figure 8). Further, to identify the pattern recognition receptor (PRR) which recognizes VpOmpU, we started with the cue that, since VpOmpU is present on the outer membrane of *V. parahaemolyticus* which is a non-invasive bacteria, it could be recognized by the surface PRRs of the cell. Of the surface PRRs, TLRs are mostly involved in the recognition of bacterial ligands (4). TLR1, TLR2, TLR4, TLR5, and TLR6 are the common surface TLRs (5). Generally, upon activation, TLRs form homo- or hetero-dimers, such as TLR2 forms hetero-dimer either with TLR1 or TLR6, whereas, TLR4 forms homo-dimer (138). Various other outer membrane proteins like PorB of *Neisseria meningitidis* (8) and OspA of *Borrelia spirochetes* (139) have been shown to be recognized by TLR1/2 hetero-dimers. Also, OmpA, an outer membrane protein of *Shigella flexneri* (140) and OmpS2 of *S. typhi* (30) are known to be recognized by TLR2/6 heterodimers. We observed that VpOmpU mediates its pro-inflammatory response through TLR2 in both monocytes and macrophages (Figure 14, 15, 16). Further, towards finding the binding partner of TLR2, we observed that TLR1 co-immunoprecipitated with TLR2 in VpOmpU-treated THP-1 monocyte (Figure 18), whereas, in macrophage both TLR1 and TLR6 co-immunoprecipitated with TLR2 (Figure 17). Even reverse co-immunoprecipitation with anti-TLR1 and anti-TLR6 antibodies confirmed the result (Figure 17, 18). This result is particularly intriguing since, to the best of our knowledge, this is the first report where a natural PAMP (VpOmpU) is being recognized by both TLR1/2 and TLR2/6 heterodimers. As mentioned earlier, while TLR1/2 and TLR2/6 heterodimers have been known to recognize discrete ligands, a previous report indicated the recognition of a synthetic lipoprotein (Pam_2CSK_4 which is a diacylated lipoprotein) by both the TLR1/2 and TLR2/6 heterodimers (141, 142). Buwitt et al. (141) also showed that recognition of a ligand by TLR6 does not completely depend on the acylation of the ligand, but also on the peptide sequence and the overall structure of the protein ligand. However, Farhat et al. (142) showed that this difference in ligand recognition did not alter the downstream signalling elicited by the dimers. They also speculated that this difference in ligand recognition was necessary to increase the array of ligands recognized by the cells. Further, our study showed that, though VpOmpU is recognized by both TLR1/2 and TLR2/6 in macrophages, TLR2/6 is the preferred dimer for the induction of downstream signalling cascades (Figure 20).

Bacterial porins of *S. enterica* Typhimurium (143), PorB of *N. meningitidis* (137), OmpA of *S. flexineri* (140), P2 porin of *Haemophilus influenzae* (144) and OmpU of *V. cholerae* (127) have previously been reported to induce NF-κB or AP-1 mediated pro-inflammatory responses. In the present study, we have shown that VpOmpU-mediated activation of the TLR- signalling leads to the activation of the transcription factors NF-κB and AP-1 in both THP-1 monocytes and RAW 264.7 macrophages (Figures 25-28). AP-1 is activated by upstream MAP kinases (4). Furthermore, in this study, we have also shown that the activation of MAP kinases (P38 and JNK) is TLR2-dependent (Figure 31). These data suggested that a difference in the recognition of VpOmpU by the TLR1/2 or TLR2/6 heterodimer does not affect the downstream signalling elicited by it.

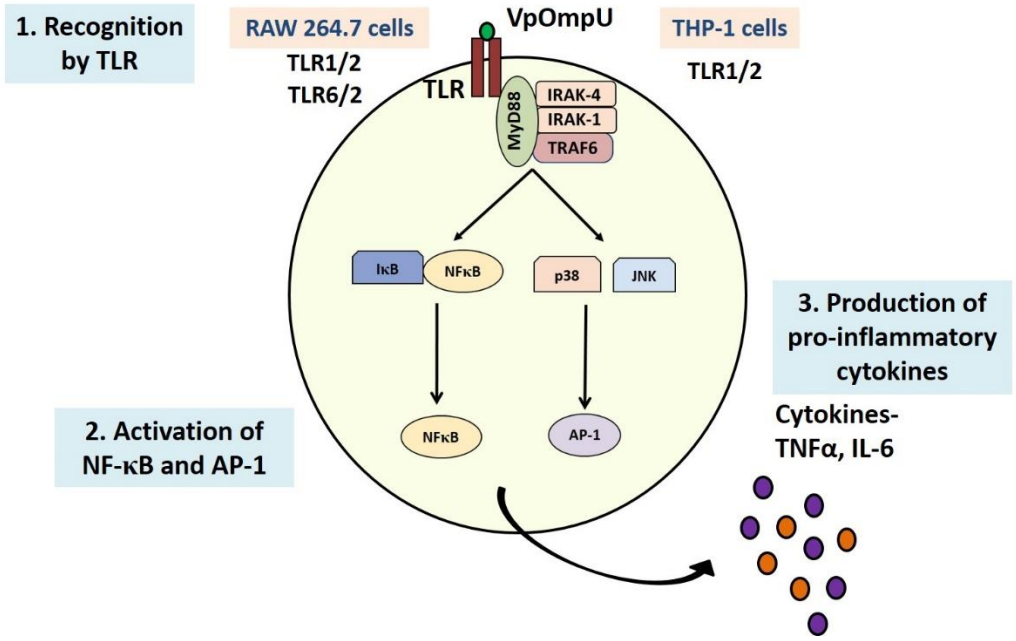

Illustration 6. Immunomodulation by VpOmpU

VpOmpU is recognized by TLR1/2 in THP-1 monocytes and by TLR1/2 and TLR2/6 in RAW 264.7 macrophages. This further results in a MyD88-dependent signalling leading to the activation of NF-κB and AP-1 transcription factors thereby leading to the production of a pro-inflammatory response.

As mentioned earlier, VpOmpU shares about 70 % sequence identity with *V. cholerae* OmpU (VcOmpU). Similar to VcOmpU, VpOmpU is also porin in nature (Figure 6). As previously mentioned extensive studies from our laboratory characterized the host immunomodulation by VcOmpU (46, 47, 127, 128). In this study we have attempted to characterize the VpOmpU and we have noticed certain similarities and dissimilarities in the host-immunomodulatory nature

of these two porins. Work from our laboratory has shown that VcOmpU is recognized only by TLR1/2 in both monocytes and macrophages (127), whereas, in this study we have shown that VpOmpU can be recognized by TLR1/2 in monocytes but in macrophages both TLR1/2 and TLR2/6 recognize VpOmpU, with TLR2/6 being favourable for the induction of pro-inflammatory responses (Figure 20). Further, in case of VpOmpU, the activation of both the MAP kinases (P38 and JNK) are mainly TLR-dependent (Figure 31) but in case of VcOmpU, only P38 MAP kinase activation is dependent on TLR-mediated signalling in macrophages (128).

Altogether, our study showed that VpOmpU elicits pro-inflammatory responses via TLR1/2 in monocytes and TLR2/6 in macrophages. Recognition of VpOmpU by the TLR hetero-dimer leads to MyD88-IRAK-1-dependent activation of NF-κB and AP-1 transcription factors towards the generation of pro-inflammatory response.

Since, VpOmpU was capable of activating the immune system and generating a pro-inflammatory response. Hence, it may prove to be a potential adjuvant for the vaccine against *Vibrio* infections.

Chapter 2:

To study the host-immunomodulation by SteA of Salmonella enterica Typhimurium

1. Introduction

1.1 *Salmonella enterica* types and disease

Salmonella is a genus of Gram-negative bacterium belonging to the Enterobacteriaceae family. *S. enterica* consists of about 2500 serovars and serotypes, most of which can infect humans (145). It is caused by the consumption of contaminated meat, poultry, milk, eggs or even fruits and vegetables. Disease caused by *S. enterica* can be divided into two types namely, gastroenteritis (local disease) and typhoid (systemic disease) (145). The gastro-enteric disease caused by non-typhoidal *Salmonella* is called salmonellosis. Salmonellosis is majorly caused by *S. enterica* Enteritidis and *S. enterica* Typhimurium (*S*. Typhimurium) and may be lethal for immune-compromised individuals (145). According to WHO, *Salmonella* is one of the four leading causes of all diarrheal diseases and non-typhoidal Salmonellosis (NTS) has claimed about 600,000 deaths worldwide. Invasive NTS is the emerging cause of death in the sub-Saharan areas where the fatality rate is about 20-47 % (www.who.int/news-room/fact-sheets/detail/salmonella-(non-typhoidal)). Further, the emergence of multi-drug resistant *Salmonella* has worsened the situation. Typhoid is a systemic infection which is characterized by high fever, nausea, headache and diarrhoea. *S. enterica* Typhi and *S. enterica* Paratyphi majorly cause typhoid in humans. According to a recent WHO report, annually about 11 to 20 million cases of typhoid are reported worldwide. Of these, typhoid causes about 128,000 to 160,000 deaths every year (https://www.who.int/features/qa/typhoid-fever/en/). In addition to this, *Salmonella* infections have also been linked to some cancers like gall bladder cancer (146). *S. enterica* Typhi is about 85 % similar to *S. enterica* Typhimurium or *S. typhimurium* which causes a typhoid-like systemic disease in mice and thus, has been widely used as model strain to study salmonellosis.

1.2 Infection of *S.* Typhimurium

S. Typhimurium enters the host through oral route, survives the gastric acidity and comes in contact with the intestinal epithelium. In response to the bacteria, an inflammatory response is elicited by the intestinal cells which leads to the production of tetrathionate. Tetrathionate provides *Salmonella* with an advantage to thrive over gut bacteria which are unable to survive in such an environment (147). *Salmonella* uses the microfold cells or M-cells of the intestinal epithelium to breach the mucosal barrier of the gut (148). Further they are engulfed by the macrophages and dendritic cells in the intestine. *Salmonella* is able to hijack these immune

cells and the epithelial cells for its survival and replication. Upon invasion of these cells, *Salmonella* forms a *Salmonella* containing vacuole (SCV) and resides protected in these vacuoles. It replicates in the SCV and disseminates to other organs or cells of the host (145). To be able to survive and multiply in the immune cells, which are otherwise fatal for the pathogen, *Salmonella* is equipped with two T3SSs which secrete a repertoire of effectors involved in modulating various functions of the host cells (149, 150) (Illustration 6). The *Salmonella* genome encodes about five major *Salmonella* pathogenicity islands (SPI) which encode various genes. Of these, the majority of effectors and the T3SS are either encoded or regulated by the SPI-1 and SPI-2 (151, 152).

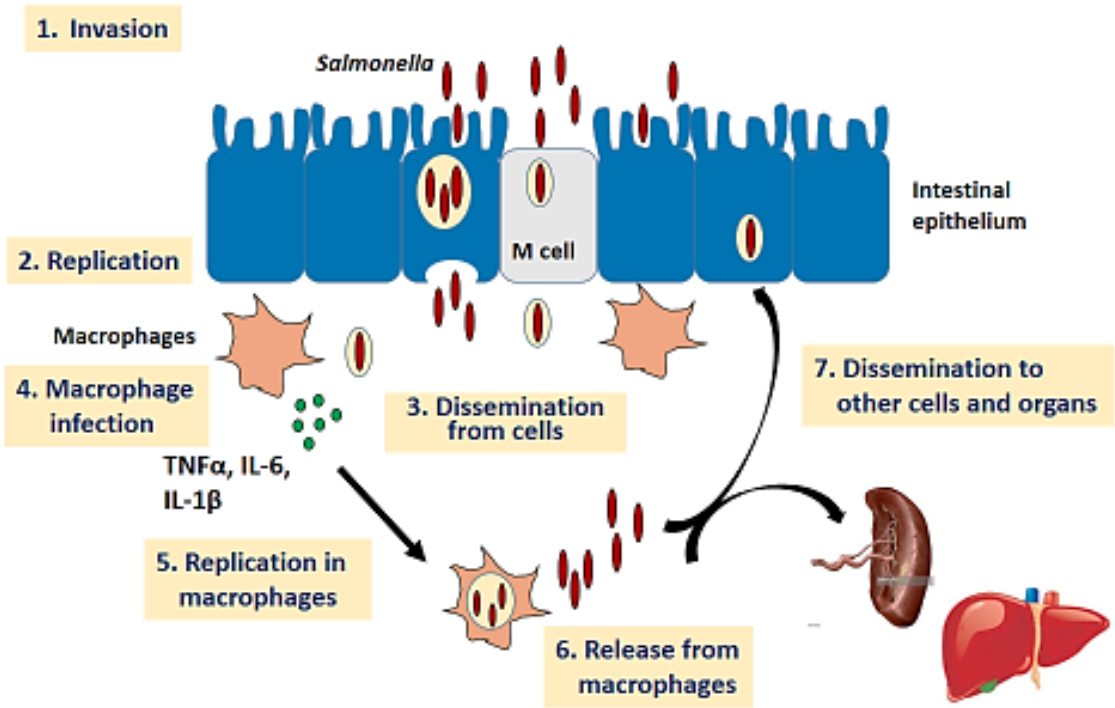

Illustration 7. The infection cycle of *Salmonella* upon its encounter with the gut epithelium of the host.

Upon ingestion of contaminated food, *Salmonella* encounters and invades the intestinal epithelium where it replicates and disseminates from the basolateral side of the epithelium. *Salmonella* infects the macrophages present at the basolateral side of the epithelium leading to generation of pro-inflammatory responses. *Salmonella* form a niche in the macrophages and disseminate to other organs and cells of the host.

1.3 Type three secretion systems (T3SS) of *Salmonella* Typhimurium

It is a needle-like complex which connects the bacterial and the host cytoplasm. Many proteins called effectors are translocated via T3SS from the bacterial cytoplasm directly to the host

cytoplasm. These effectors modulate host functions to help the bacteria to thrive in the cell. The T3SS of *Salmonella* was first visualized using Transmission electron microscopy (TEM) in 1998, which revealed that it consisted of two outer rings, 2 inner rings and a long needle like stem (149). Later, the complete repertoire of proteins involved in forming the apparatus were discovered using high throughput cryo-EM (153) (Illustration 7). *Salmonella* uses the T3SS twice during its lifecycle in a cell which secrete different effectors depending on the stage of infection i.e. T3SS-1 secretes effectors which help in the early phases of infection and T3SS-2 is used at the later stages of infection (154).

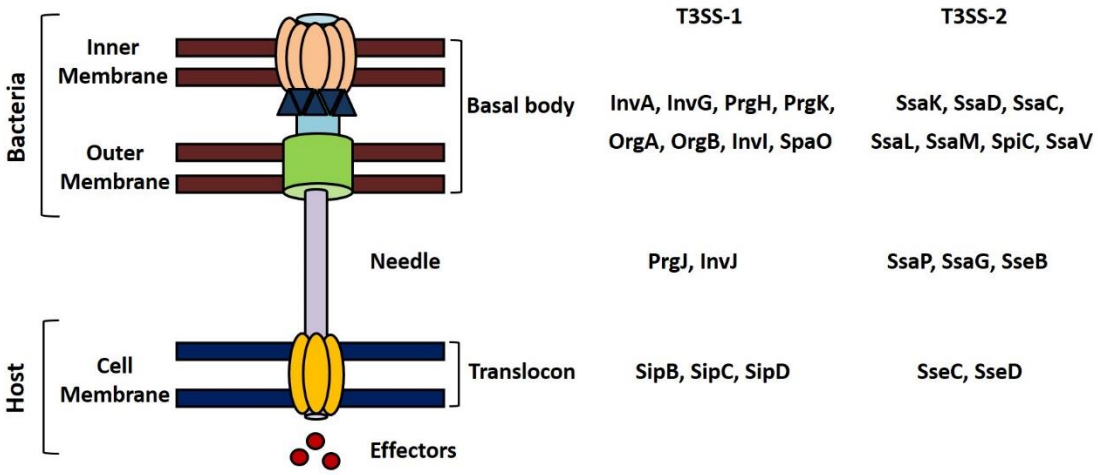

Illustration 8. The type three secretion system apparatus

Salmonella utilizes two type three secretion systems (T3SS) namely T3SS-1 and T3SS-2. It assembles the T3SS consisting of a basal body, a needle complex and a translocon using various proteins.

1.3.1 T3SS-1 and the effectors secreted by it

The T3SS-1 is formed first and secretes effectors which help the bacteria for functions related to invasion and formation of SCV such as actin modulation, suppression of immune responses etc. Most of the genes involved in T3SS-1 apparatus formation (Illustration 7) and regulation of T3SS-1 effector proteins are present in a gene cluster called the *Salmonella* pathogenicity island 1 (SPI-1) (155, 156). The gut environment is sensed by the bacteria leading to the expression of the SPI-1 genes. The process of invasion begins with the induction of membrane ruffling, which is caused by the effector SopB (157). In addition to membrane ruffling, various other actin modulations are caused by the effectors such as SopE, SopE2, SipA and SipC which are also required for its invasion (158, 159). Upon internalization of the bacteria, the effector

SptP restores the architecture of the cell by subduing the activations induced by SopB, SopE and SopE2 (160). SopB and SptP are also involved in the formation of early SCV (161, 162). After the formation of the early SCV, it moves towards the nucleus. The juxta-nuclear positioning of SCV is necessary for nutrient uptake and intra-vacuolar replication. SipA and SopB, in addition to the T3SS-2 effectors (SifA, SseF and SseG) help in the positioning of the SCV. As previously described, induction of inflammation is also necessary for the infection of *Salmonella*, some effectors including SopE, SopE2, SopB induce a pro-inflammatory response leading to loosening of tight junctions of the intestinal epithelium, thus, enhancing trans-epithelial migration of *Salmonella* (158). SptP, which subdues the actin rearrangements induced by these effectors, also suppresses the inflammation induced by them (55). After entering the cells, it is necessary to suppress its immune responses for the survival of *Salmonella* inside the host. Some effectors like AvrA are known to suppress the immune responses of the cell generated against *Salmonella* (57, 58, 163). Also, apoptosis may be induced in the cells, if the infection is irreparable. Interestingly, AvrA and SopB also suppress apoptosis in epithelial cells, helping the bacteria to survive in the host (58, 164). Another form of programmed cell death called pyroptosis has been found to be induced by SipB, PrgJ and flagellin (165-168). Pyroptosis is an inflammatory cell death majorly induced in macrophages and dendritic cells which helps in increasing the inflammation and in dissemination of the bacteria to other organs.

1.3.2 T3SS-2 and the effectors secreted by it

The T3SS-2 (Illustration 7) is formed across the SCV membrane and translocates effectors from the cytoplasm of *Salmonella* to cytoplasm of the host's cell. It secretes effectors which majorly help in the maturation of SCV, maintenance of SCV and the dissemination of bacteria to other cells. The genes related to T3SS-2 are either expressed or controlled by those present in the gene cluster, SPI-2 (169). The environment of the SCV leads to the expression of the SPI-2 genes. As previously mentioned, the effectors namely SifA, SseF and SseG help in the positioning of the SCV close to the nucleus (170-172). SifA, SseJ, SseF, SseG and SopD2 are involved in the formation of filaments called *Salmonella* induced filaments (SIFs) (170-174). SIFs are required for nutrient acquisition which is necessary for the replication of the *Salmonella* inside the vacuole. Upon maturation of SCV, an F-actin meshwork is formed around the SCV in many cell types including epithelial cells and macrophages (175). This meshwork has been thought to be involved in protecting the SCV. SteC has been found to be responsible for

the formation of this meshwork (176). SspH2 also associates to the F-actin meshwork (173). It has been shown that SrfH is involved in increasing the motility of macrophages thereby helping in the dissemination of the bacteria (177). Some T3SS-2 effectors like SpvB and SseL also induce apoptosis in epithelial cells or macrophages respectively (178, 179). SpvB, SspH1, and SseL are also known to suppress the immune signalling of the cell (180-182). Other effectors like SopD2, SseF and SseG have been shown to suppress the antigen presentation on dendritic cells and also, T-cell proliferation, thereby suppressing the host's immune response against *Salmonella* (183).

1.3.3 Effectors secreted by both T3SS

In addition to effectors which are secreted by T3SS-1 or T3SS-2, some effectors are secreted by both the secretion systems and may have different roles in both the conditions. SopD, SlrP, SspH1, GtgE, SpvD, SpvC, PipB2, SteE, SteA, GogB are the effectors discovered till date to be secreted by both the T3SSs (145). SopD has been shown to be involved in the induction of inflammation and fluid accumulation in the *Salmonella*-infected intestines (184). Additionally, in association with the T3SS-1 effector SopB, it has been shown to be involved in invasion of *Salmonella* into epithelial cells (157). SopD has also been implicated in intra-macrophage replication and the systemic spread of the disease (184, 185). GtgE helps in the maintenance of the SCV (186) and PipB2, along with other T3SS-2 effectors, has been found to help in SIF formation (187). Some of the effectors have also been implicated in host immune-modulation. SlrP and SspH1 are E3-ubiquitin ligases which cause host cell's death and suppress pro-inflammatory responses respectively (180, 188). SpvC and SpvD also suppress pro-inflammatory responses by acting on the MAP-kinase and the NF-κB pathway respectively (189, 190). Although, some of the roles of these effectors have been discovered, many others are yet to be deciphered. In this study, we have explored the role of SteA, which is also secreted by both the T3SSs.

1.4 SteA

SteA or *Salmonella* translocation effector A is secreted by both the T3SSs (191). SteA has been implicated to have a role in virulence and has been found to localize to the trans-golgi network (191). SteA is also present in typhoid causing strains namely *S. enterica* Typhi and *S. enterica* Paratyphi, which share more than 90 % sequence similarity with each other, indicating that it may also be necessary for human infections. It has been shown that the deletion of *steA* (Δ*steA*)

does not affect the invasion or the replication of *Salmonella* in the macrophages (192). A microarray-based study indicated that SteA might have a role in extracellular matrix organization, cell proliferation and may also be involved in the suppression of immune responses of the host (193). A recent study showed that lesser SIF formation and abnormal SCV (one SCV with more than one bacterium) were observed in the absence of SteA. They further hypothesized that SteA may be involved in membrane fission after the replication of bacteria in the SCV (194). SteA was also observed to be localized on the SCV membrane. Another study showed that SteA binds to phosphatidylinositol 4-phosphate (PI4P), which is involved in membrane trafficking in the Golgi (195). The role of SteA in the control of membrane dynamics was shown to be due to its secretion via T3SS-2 (194). However, the role of SteA in the early phases of infection remained to be elucidated.

2. Objectives of this study

In this study, we have probed the role of SteA in the early phases of infection i.e. upon its secretion via T3SS-1. Towards this, we formulated the following objectives:

1) To probe if SteA has a role in virulence of *S.* Typhimurium

2) To probe how SteA affects the immune responses

3) To probe the mechanism underlying the SteA-mediated effect on immune responses

3. Materials and Methods

5.1 Ethics statement

All animal experiments were carried out in accordance with the guidelines of Committee for the Purpose of Control and Supervision of Experiments on Animals (CPCSEA) (No. 1842/GO/ReBiBt/S/15/CPCSEA). All the protocols for animal handling were approved by the Institutional Animals Ethics Committee (IAEC) of Indian Institute of Science Education and Research, Mohali (IISERM/SAFE/PRT/2016-2018/004, 010, 015).

5.2 Bacterial strains and chemicals

Salmonella enterica Typhimurium SL1344 strain was a kind gift from Dr. Mahak Sharma (IISER Mohali). The Δ*spi2 S. typhimurium* 14028 strain was a kind gift from Dr. Francisco Ramos-Morales (University of Seville, Spain) (196). The P22 phage transduction method was

used to construct Δ*spi2* SL1344 and Δ*spi2*Δ*steA* SL1344 strains. The strains and plasmids used in this study are listed in Table 10. All the DNA modifying enzymes were obtained from New England Biolabs (USA). Luria Bertani (LB) broth and antibiotics were from Himedia, Mumbai. Plasmid and DNA isolation kits were obtained from QIAGEN. Most of the chemicals were obtained from Himedia, Mumbai unless otherwise mentioned.

Table 10. Strains and plasmids used in this study

Strains	**Genotype or description**	**Reference**
E. coli		
TOP10	Strain used for cloning	Invitrogen
Origami B	Strain used for expression of gene	Merck-Millipore
Dam$^-$	Strain used for cloning, where methylation interferes with digestion	Kind gift from Dr. Ram K. Yadav
***S.* Typhimurium**		
Wt	Wild type SL1344	A kind gift from Dr. Mahak Sharma
Δ*steA*	*steA*::Km^R	This study
Compl	*steA*::Km^R, pACYC177-*steA* (with native promoter)	This study
compl-H	*steA*::Km^R, pACYC177-*steA*-His (with native promoter)	This study
14028 Δ*spi2*	*spi2*::Cm^R	A kind gift from Dr. Francisco Ramos-Morales
SL1344 Δ*spi2*	*spi2*::Cm^R	This study
Δ*spi2*Δ*steA*	*spi2*::Cm^R, *steA*::Km^R	This study
Plasmids	**Description**	**Reference**
pKD13	Template used for amplifying Kanamycin Cassette	A kind gift from Dr. Rachna Chaba
pKD46	Plasmid expressing λ-red recombinase	A kind gift from Dr. Rachna Chaba

pACYC177	Bacterial expression plasmid used for complementation	A kind gift from Dr. Rachna Chaba
pACYC177-*steA*	*steA* with its native promoter cloned in pACYC177	This study
pACYC177-*steA*-His	His-tagged *steA* with its native promoter cloned in pACYC177	This study
pGEX4T3	Plasmid expressing GST	A kind gift from Dr. Mahak Sharma
pGEX4T3-*steA*	Plasmid expressing GST-tagged SteA	This study
pcDNA3.1(+)	Mammalian expression plasmid	A kind gift from Dr. Kausik Chattopadhyay
pcDNA3.1(+)*steA*	Mammalian expression plasmid expressing HA-tagged SteA	This study
pGL4.32	NF-κB promoter reporter plasmid	Promega, USA (cat# 8491)
pRL	Plasmid expressing Renilla luciferase	A kind gift from Dr. Rajesh Ramachandran
pGADC1	Yeast expression plasmid with activation domain (AD)	A kind gift from Dr. Shravan Mishra
pGADC1-*IκB*	Yeast expression plasmid with activation domain (AD) fused with IκB	This study
pGADC1-*Rbx1*	Yeast expression plasmid with activation domain (AD) fused with Rbx-1	This study
pGADC1-*Skp1*	Yeast expression plasmid with activation domain (AD) fused with Skp-1	This study
pGADT7	Yeast expression plasmid with activation domain (AD)	A kind gift from Dr. Ram K. Yadav
pGADT7-*Cullin1*	Yeast expression plasmid with activation domain (AD) fused with Cullin-1	This study
pGBDUC1	Yeast expression plasmid with binding domain (BD)	A kind gift from Dr. Shravan K. Mishra
pGBDUC1-*steA*	Yeast expression plasmid with binding domain (BD) fused with SteA	This study

5.3 Cell lines and culture conditions

RAW 264.7 (a murine macrophage cell line) was obtained from the National Centre for Cell Science (NCCS), Pune, India and HEK 293 (a human kidney epithelial cells line) was obtained from American Type Culture Collection (ATCC). The RAW 264.7 cells were maintained in RPMI 1640 supplemented with 10 % fetal bovine serum (FBS), 100 units/ml of penicillin and 100 µg/ml of streptomycin (Invitrogen, Life Technologies, USA) at 37 °C and 5 % CO_2. HEK 293 cells were maintained in DMEM supplemented with 10 % fetal bovine serum (FBS), 100 units/ml of penicillin and 100 µg/ml of streptomycin (Invitrogen, Life Technologies, USA) at 37 °C and 5 % CO_2.

5.4 Differentiation of bone marrow cells to bone marrow-derived macrophages (BMDMs)

6-8 weeks old Balb/c mice were euthanized and their femur and tibia bones were extracted. The muscle tissue of the bones was then removed off and were then washed with ice-cold PBS. They were then dipped in 70 % alcohol for 2 min and were transferred to RPMI 1640 media. Then, using sterile scissors, the epiphyses of the bones were cut and the bone marrow cells were extracted by flushing the bones with RPMI 1640 media. These bone marrow cells were then differentiated to bone marrow-derived macrophages (BMDMs) using macrophage colony-stimulating factor (M-CSF). Briefly, cells were suspended in differentiation media (RPMI 1640 supplemented with 10 % FBS, 100 units/ml of Penicillin, 100 µg/ml of Streptomycin, 1 mM sodium pyruvate, 0.1 mM non-essential amino acids (NEAA), 1 % β-mercaptoethanol and 20 ng/ml of M-CSF) and plated in 24-well plates. They were incubated at 37 °C with 5 % CO_2. The media was changed every 2 days and fresh differentiation media was added. The adhered cells obtained at day 7 were BMDMs and were used for further experiments.

5.5 Deletion of *steA* gene from the genome of *S.* Typhimurium

SteA in the genome of *S.* Typhimurium was replaced with a Kanamycin cassette by one-step inactivation method following the protocol by Datsenko and Warner (197). Briefly, Kanamycin cassette was amplified from the plasmid pKD13 using primers- SteA H1P2 and SteA H2P1 (Table 11). The amplified Kanamycin cassette with flanking regions corresponding to the flanking regions of the *steA* gene in the *S.* Typhimurium genome was digested with Dpn1, gel extracted and transformed into *S.* Typhimurium expressing the λ-red recombinase via the

helper plasmid pKD46 by electroporation. The colonies were selected on Kanamycin plates and screened by colony PCR. The deletion mutant of Δ*steA* was then transduced to a clean background (*S.* Typhimurium SL1344) using P22 phage. For complementation, *steA* gene of *S.* Typhimurium (www.ncbi.nlm.gov.in) was cloned in pACYC177 (a kind gift from Dr. Rachna Chaba, IISER Mohali) using restriction cloning and was transformed in the deletion mutant of SteA (Δ*steA*) background. The primers used in this study are listed in Table 11.

Table 11. Primers used in this study

Name of primer		**Sequence 5'-3'**
SteA H1P2		AGTCTGATTTCTAACAAAACTGGCTAAACATAAAC-GCTTTATTCCGGGGATCCGTCGACC
SteA H2P1		GACATATAAAGCTATTGAGCAAAATTTGAAGGAG-TAGGATATGTGTAGGCTGGAGCTGCTTCG
SteA	Forward	GCGC**CATATG**ATGCCATATACATCAGTTTC
	Reverse	CGCG**GGATCC**TTAATAATTGTCCAAATAGT
SteA-GST	Forward	ATTGTT**GGATCC**CCATATACATCAGTTTCTAC
	Reverse	GTTATT**CTCGAG**TTAATAATTGTCCAAATAGTTATG
SteA-HA	Forward	CCATATT**GGATCC**CCACCATGCCATATACATCAG-TTTCTACC
	Reverse	AAGCTAT**CTCGAG**TTAAGCGTAATCTGGAACATCG-TATGGGTAATAATTGTCCAAATAGTTATGG-TAGCGAG
SteA compl	Forward	ACCT**GGATCC**AAGCAGCATAAGATCAGGCCG
	Reverse	CGT**GACGTC**TTAATAATTGTCCAAATAGTTATGG
SteA compl-H	Forward	ACCT**GGATCC**AAGCAGCATAAGATCAGGCCG
	Reverse	CGT**GACGTC**TTAGTGATGATGATGATGATGA-TAATTGTCCAAATAGTTATGG
TNFα	Forward	CCCTCACACTCAGATCATCTTCT
	Reverse	GCTACGACGTGGGCTACAG
IL-6	Forward	TAGTCCTTCCTACCCCAATTTCC
	Reverse	TTGGTCCTTAGCCACTCCTTC

IκB	Forward	TTACT**GGATCC**ATGTTTCAGCCAGCTGGGCAC
	Reverse	TCGGTC**GTCGAC**TTATAATGTCAGACGCTGGCC
Rbx-1	Forward	TTACT**GGATCC**ATGGCGGCGGCGATGGATGT
	Reverse	TCGGTC**GTCGAC**CTAATGCCCATACTTCTGGAA
Skp-1	Forward	TTACT**GGATCC**ATGCCTACGATAAAGTTGCAG
	Reverse	TCGGTC**GTCGAC**TCACTTCTCTTCACACCATT
Cullin-1	Forward	CACCATGTCATCAAACAGGAGTCAGAAT
	Reverse	TCGGTC**GTCGAC**TTAAGCCAAGTAACTGTAGGT
SteA Y2H	Forward	ATTGTT**GGATCC**CCATATACATCAGTTTCTAC
	Reverse	GTTATT**GTCGAC**TTAATAATTGTCCAAATAGTTATG
P1		GTGTAGGCTGGAGCTGCTTC
P2		GGTCGACGGATCCCCGGAAT
K1		GAGGCTATTCGGCTATGACTG
K2		TTCCATCCGAGTACGTGCTC

5.5.1 Electro-competent cell preparation

An overnight bacterial culture was used to inoculate 50 ml of Super-optimal broth (SOB; 2 % Tryptone, 0.5 % Yeast extract, 8.56 mM NaCl, 2.5 mM KCl, 10 mM $MgCl_2$, pH 7). At an OD_{600} of 0.1, 10 mM of arabinose (Sigma-Aldrich, USA) was added to the culture. Then, at an OD_{600} of 0.4-0.5, the bacteria were pelleted at 4 °C by centrifugation at 3,300 g for 15 min. The supernatant was discarded and the pellet was washed with 50 ml of ice-cold sterile 10 % glycerol. Then, the bacteria were pelleted at 4 °C by centrifugation at 3,300 g for 15 min. A total of four such washes were done using 50 ml, 25 ml and 2 washes with 12 ml of sterile 10 % glycerol. The pellet obtained after the last wash was resuspended in the residual 10 % glycerol (i.e. the glycerol left after discarding supernatant- about 300 µl). This was then aliquotted in autoclaved micro-centrifuge tubes (MCT) with 50 µl in each MCT and stored at -80 °C.

5.5.2 Transformation using electroporation

The DNA (20 ng to 500 ng) to be transformed was added to the electro-competent cell and incubated for 10 min on ice. Parallelly, the 1 mm electro-cuvettes (cat# 1652089, Bio-Rad)

were kept on ice. Then, the electro-competent cells and DNA mixture was added to the electro-cuvettes without forming bubbles. Then, using an electroporator, a 1.8 V pulse of 1 s was passed through the electro-cuvette. To this, 1 ml of SOC media (SOB with 20 mM Glucose) was added immediately and transferred to an autoclaved MCT. That was then incubated at 37 °C (for *Salmonella* competent cells) or at 30 °C (for *Salmonella* containing pKD46 competent cells) for 1 to 1.5 h with shaking. The bacteria were pelleted at 6,000 g for 3 min and 900 µl of supernatant was discarded. The bacteria were then resuspended in rest of the media and plated on LB agar (LA) plates containing required antibiotics. For transformation of the linear kanamycin cassette, the final concentration of 30 µg/ml of kanamycin was used in the LA plates. The transformants were checked for deletion using kanamycin specific primers (i.e. P1, P2, K1 and K2) and gene-specific primers (Table 11).

5.5.3 P22 Phage transduction

One ml of an overnight culture of the donor strain was incubated with 4 ml of the P22 phage broth for 9 h at 37 °C. Then, this was subjected to centrifugation at 6,500 g for 5 min. The supernatant was then transferred to a fresh, autoclaved glass tube and chloroform was added to it at a ratio of 100 µl chloroform per 1 ml of supernatant. This was then vortexed for 2 min and left undisturbed till the chloroform settles at the bottom of the tube. The upper layer contained the phage lysate, which was transferred to a fresh tube and stored at 4 °C after sealing with parafilm. For the transduction of the recipient strain, the phage lysate was diluted 1:1000 to 1:10000 in LB and was mixed with the overnight culture of the recipient strain in 1:1 ratio i.e. 100 µl of culture was mixed with 100 µl of diluted phage lysate. After 30 min of incubation at 37 °C, this mixture was plated on LA plates containing antibiotics and 10 mM of EGTA and incubated at 37 °C for overnight. The transductants were then streaked on green plates (2 g Bacto-tryptone, 0.25 g Yeast extract, 1.25 g NaCl, 1.9 g Dextrose, 3.75 g Agar, 16.5 mg Methyl blue, 0.16 g Alizarin yellow dissolved in 222.5 ml of distilled water). Then, the phage free light green or white colonies were picked from the streaked green plates. This step was repeated 3-4 times for phage clearing. To remove lysogens from this screen, a streak of phage broth (about 30- 50 µl) was made across the middle of a green plate. The colonies to be checked for lysogens were streaked across the green plate perpendicularly to the phage broth streak and incubated at 37 °C for 12 to 16 h. the colonies which appeared to be light green or white before coming in

contact with the phage broth streak and turned green after the contact were selected as the lysogen free transductants (Illustration 8). These were then used for further experiments.

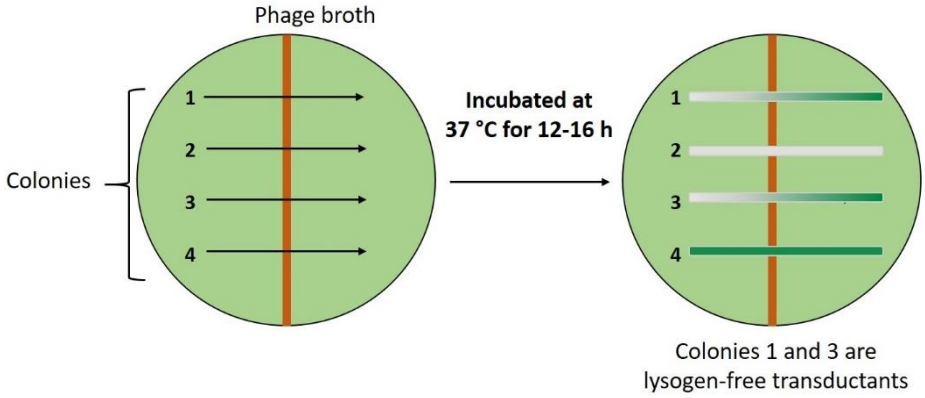

Illustration 9. Selection for lysogens on green plates

A streak of phage broth was placed at the centre of a green plate (depicted by red line), then, the colonies were streaked across the phage broth and incubated for 12 to 16 h at 37 °C. The colonies which appeared white prior to their contact with the phage broth and green after contact were taken as the lysogen-free transductants.

5.6 *In vivo* (mice) experiments

5.6.1 Mice infection and scoring

Bacteria grown overnight in LB medium supplemented with 50 µg/ml of streptomycin were sub-cultured and grown till log-phase at 37 °C. 6 to 8 weeks old Balb/c mice were infected intra-peritoneally with 5 x 10^5 or 5 x 10^7 log-phase bacteria and the survival of mice was monitored for 24 h and 96 h respectively. For the mice infected with 5 x 10^5 bacteria we have started monitoring the phenotypic changes in the mice 36 h post-infection (h. p. i.). The infected mice were scored for their response to stimuli, the extent of decrease in activity, the extent of eye closure and the pilorected fur on a scale of 1 to 4 as compared to the uninfected age matched mice following the method as described by Shrum *et al*. (198). Briefly, each infected mice was scored at 36 h.p.i. on a scale of 1 to 4 for the features described above. Then, the average of the scores was calculated.

5.6.2 Colonization and splenic lysate preparation

6 to 8 weeks old Balb/c mice were infected intra-peritoneally with 5 x 10^5 log-phase bacteria. At 36 h. p .i., spleens were isolated and homogenized in PBS using a sterile pestle.

For colonization, the homogenate was subjected to lysis with 0.1 % Triton-X-100 at 37 °C for 30 min. The bacteria were enumerated after serial dilution on LB-agar (LA) plates supplemented with 50 µg/ml of streptomycin.

For splenic lysate preparation, the homogenate was pelleted by centrifugation at 2,000 g for 5 min and washed twice with PBS. Then, the pellet was treated with 500 µl of ACK lysis buffer (154.95 mM NH_4Cl, 10 mM $KHCO_3$ and 0.1 mM EDTA; pH 7.2) at room temperature for 5 min. To stop the reaction, 100 µl of FBS was added to it and was centrifuged at 2,000 g for 5 min and washed twice with PBS. The pellet was then re-suspended in 70 µl of RIPA buffer (50 mM Tris-Cl (pH 8), 150 mM NaCl, 5 mM EDTA, 1 % NP-40, 0.5 % sodium deoxycholate and 0.1 % sodium dodecylsulphate) containing 1X mammalian protease inhibitor cocktail (Sigma-Aldrich, USA) and sonicated at 10 A for three pulses of 5 s each. This was then centrifuged at 24,000 g for 30 min. The supernatant thus obtained was the splenic lysate.

5.6.3 TNFα and IL-6 gene expression in spleen

6 to 8 weeks old Balb/c mice were infected intra-peritoneally with 5 x 10^5 log-phase bacteria. At 36 h. p .i., spleens were isolated and were subjected to ballooning with 10 % Collagenase D in HBSS and incubated at 37 °C for 25 min. To stop the reaction, 100 µl of 0.5 M EDTA was added and incubated at 37 °C for 5 min. This was then passed through a 40 µm strainer and 5 ml of ice-cold RPMI 1640 media supplemented with 10 % FBS was added to it. The cells were then harvested at 2,000 g for 5 min and washed with PBS. The pellet was re-suspended in 3 ml of 30 % Bovine Serum Albumin (Sigma-Aldrich, USA). To this, 1 ml of PBS was added slowly along the wall of the conical tube to form a layer and was subjected to density gradient centrifugation (with zero acceleration or deceleration) at 2,200 g for 30 min at 12 °C. The interface of the two layers contained the mononuclear cells, which were then harvested and RNA was isolated according to the manufacturer's protocol using the Nucleopore RNA isolation Kit (Genetix, India). The cDNA was then synthesized using Verso-cDNA kit (Thermo-Fischer, USA) using the reaction in Table 4 (in chapter 1).

The PCRs were done using Maxima SYBR green qPCR master mix (Thermo-Fischer, USA) (Table 5 chapter 1) and the Eppendorf Realplex master cycler. Primer sequences were used from the Harvard primer bank (Table 5 in chapter 1) and were synthesized by Integrated DNA Technologies, USA.

5.7 Cell based assays

5.7.1 Infection of cells

For inducing SPI-1 conditions, as described previously by Cardenal-Munoz *et al.* (199), bacteria were grown till stationary phase in LB broth supplemented with 0.3 M NaCl and appropriate antibiotics. Cells were plated in 24-well or 6-well plates at a density of 1 x 10^6 cells/ml for overnight and infected with the stationary phase bacteria at a multiplicity of infection (MOI) of 10:1 (for BMDMs) or 20:1 (for RAW 264.7 and HEK 293 cells) for 30 min. The media containing the bacteria was removed and fresh media supplemented with 100 μg/ml of gentamicin was added to the wells. After 1 h, this media was replaced with fresh media supplemented with 20 μg/ml of gentamicin for different time points depending on the assay. In all the experiments, the invasion was checked after 2 h of infection by enumerating the bacteria after the cells were lysed with 0.1 % Triton-X-100 (Himedia, India) in phosphate buffer saline or PBS.

5.7.2 Quantification of TNFα and IL-6

RAW 264.7 and BMDMs were plated at a density of 1 x 10^6 cells/ml and infected with wt, Δ*steA* or compl strains at an MOI of 20:1 or 10:1 respectively. The supernatant was collected after 8 h of infection and TNFα was quantified using ELISA (BD Biosciences, USA, Table 3 in chapter 1) as per the manufacturer's protocol. Further, to confirm equal invasion in all the experiments, cells were lysed after 2 h of infection with 0.1 % Triton-X-100 at 37 °C for 30 min and bacteria were enumerated on LA plates. The sets with unequal invasion were not analysed for TNFα.

5.7.3 Transfection of HEK 293 cells

7 x 10^6 HEK 293 (a human kidney epithelial cell line) cells were plated in DMEM in a 90 mm Petri-dish for whole cell lysate preparation and 2.5 x 10^4 HEK 293 cells were seeded on coverslips in a 24-well plate for co-localization studies. Cells were then transfected with 3 μg (for whole cell lysates) or 1 μg (for co-localization experiment) of pCDNA3.1(+) or pCDNA3.1(+)*steA* (Table 3) using Polyethyleneimine (PEI) at a ratio of 1:3 (DNA: PEI). The media was changed after 8 h of transfection. Then, after 24 h or 36 h of transfection, the cells

were stimulated with 10 ng/ml of TNFα for 15 or 30 min and whole cell lysates were prepared or subjected to co-localization studies.

5.7.4 Whole cell lysate preparation

For infection:

Cells were plated at a density of 1.5 x 10^6/ml in a 6-well plate for overnight. 4.5 x 10^6 cells (3 wells of 1.5 x 10^6/ml) were infected with wt, Δ*steA* or compl for 30 min. Then, the bacteria were removed and RPMI 1640 media containing 100 µg/ml of gentamicin was added to each well for 30 min. The cells were then washed twice with sterile PBS and were then harvested at 2,000 g for 5 min. The pellet was then re-suspended in 70 to 100 µl of whole cell lysis buffer (50 mM Tris-Cl, 150 mM NaCl, 0.1 % SDS and 0.1 % Triton-X-100, pH 8) with mammalian protease inhibitor cocktail (Sigma-Aldrich, USA) and subjected to sonication at 10 A for 15 s with a pulse of 5 s each. Then, it was centrifuged at 16,000 g for 30 min at 4 °C. The supernatant thus obtained was the whole cell lysate. Additionally, the invasion was also checked by C.F.U. counting for all the experiments.

For transfections:

After 24 h of transfection in HEK 293 cells (as described previously), cells were washed twice with PBS and were harvested by centrifugation at 2,000 g for 5 min. The pellet was then re-suspended in 150 to 200 µl of whole cell lysis buffer supplemented with mammalian protease inhibitor cocktail. This was then subjected to sonication at 10 A for 15 s with a pulse of 5 s each. Then, it was centrifuged at 16,000 g for 30 min at 4 °C and the supernatant obtained was collected as whole cell lysate.

5.7.5 Nuclear lysate preparation

For infection with S. Typhimurium

4.5 x 10^6 cells (3 wells of 1.5 x 10^6/ml) of RAW 264.7 were plated in a 6-well plate overnight for each sample and then, infected with wt, Δ*steA* or compl for 30 min. Then, the bacteria were removed and RPMI 1640 media containing 100 µg/ml of gentamicin was added to each well for 30 min. Cells were then washed twice with sterile PBS and were then harvested at 2,000 g for 5 min. The pellet volume was measured and it was dissolved in 5 times of the pellet volume

in hypotonic buffer (10 mM HEPES pH 7.9 with 1.5 mM $MgCl_2$ and 10 mM KCl) and centrifuged at 1,850 g for 5 min at 4 °C. Then, the pellet was dissolved in hypotonic buffer with 0.5 M DTT and mammalian protease inhibitor and was then incubated on ice for 15 min. This was then sonicated at 10 A for 15 s with 3 pulses of 5 s each and centrifuged at 3,300 g for 15 min at 4 °C. The pellet was then resuspended in 70 µl of low salt buffer (20 mM HEPES pH 7.9, 1.5 mM $MgCl_2$, 20 mM KCl, 0.2 mM EDTA and 25 % glycerol) with 0.5 M DTT and mammalian protease inhibitor. To this, 30 µl of high salt buffer (20 mM HEPES pH 7.9, 1.5 mM $MgCl_2$, 800 mM KCl, 0.2 mM EDTA and 25 % glycerol) was added dropwise and incubated on ice for 10 min before subjecting to sonication at 10 A for 15 s. Then, it was incubated on ice for 30 min with periodic shaking and centrifuged at 24,000 g for 30 min at 4 °C. The supernatant hence obtained contained the nuclear lysate.

5.7.6 Co-immunoprecipitation studies

Whole cell lysates were prepared (as previously described) and were incubated with 1-2 µg of anti-HA, anti-His, anti-Cullin-1, anti-β-TrCP or anti-IκB antibody for 3 to 4 h with continuous low speed shaking at 4 °C. Then, 20 µl of Protein A/G beads (# sc2003, Santa Cruz Biotechnologies, USA) was added and it was subjected to continuous low speed shaking at 4 °C for overnight. Then, the beads were washed thrice with whole cell lysis buffer by centrifugation at 6,000 g for 5 min at 4 °C. The beads were re-suspended in SDS-loading buffer and boiled for 10 min. The samples were then run on SDS-PAGE gel and subjected to immunoblotting.

For IκB pull-down

HEK 293 cells were transfected with 3 µg of pcDNA3.1(+) or pcDNA3.1(+)*steA* (as described previously). After 24 h of transfection, cells were treated with 20 nM of proteasomal inhibitor, MG132 (Sigma-Aldrich, USA) for 3 hours. The cells were then stimulated with 10 ng/ml of TNFα for 20 min and whole cell lysates were prepared. The whole cell lysates were then subjected to co-immunoprecipitation with 2 µg of the anti-IκB antibody as described above.

5.7.7 Immunoblotting

The whole cell lysates or the nuclear lysates were run on SDS-PAGE gel and were transferred to PVDF membrane using wet transfer. After the transfer, the membrane was incubated with 5 % BSA for blocking. Then, it was incubated with various primary antibodies purchased from

different companies. Then, the blot was washed four times with TBST (25mM Tris-HCl (pH 7.6, containing 137 mM NaCl and 0.1 % Tween 20). Afterwhich, it was incubated with HRP-tagged secondary antibody (Sigma-Aldrich, USA) and washed four times with TBST. The immunoblots were then developed using Clarity^{TM} ECL Substrate (Bio-Rad, USA) and detected using LAS 4000 (GE Healthcare Technologies, USA). The primary antibodies used in this study are listed in Table 12.

Table 12. List of antibodies used for immunoblotting under Aim 2

Antibody against	**Company and Catalogue no.**	**Antibody against**	**Company and Catalogue no.**
IκB	Santa Cruz Biotechnologies, USA (# sc-847)	**HA**	Biolegend, USA (# 901501)
GAPDH	Santa Cruz Biotechnologies, USA (# sc-25778)	**p-IKKα/β**	Cell signalling technologies, USA (# 2697S)
PCNA	Biolegend, USA (# 307902)	**Ubiquitin**	Cell signalling technologies, USA (# 3933S)
His	Biolegend, USA (# 652502)	**β-TrCP**	Cell signalling technologies, USA (# 11984S)
p-p38	Cell signalling technologies, USA (# 4511BC)	**Cullin-1**	Cell signalling technologies, USA (# 4995S)
p-JNK	Cell signalling technologies, USA (# 9251BC)	**Rbx-1**	Cell signalling technologies, USA (#BC)
p-IκB	SAB4504445	**Skp-1**	Cell signalling technologies, USA (# 2156T)
P38	Cell signalling technologies, USA (# 8690BC)	**Nedd8-Cullin**	Abcam (# ab81264)
JNK	Cell signalling technologies, USA (# 9252BC)	**Cand-1**	Cell signalling technologies, USA (# 8759S)
P65	Santa Cruz Biotechnologies, USA (# sc-372)	**Lamin B1**	Santa Cruz Biotechnologies, USA (# sc-20682)
GST	Sigma-Aldrich, USA (# 16-209)	**cRel**	Santa Cruz Biotechnologies, USA (# sc-71)

5.7.8 Luciferase reporter assay

2.5 x 10^4 HEK 293 cells were plated in 100 µl of DMEM in a 96-well plate and were transfected with 0.1 µg each of NF-κB reporter plasmid pGL4.32 (Promega, USA) and renilla luciferase plasmid (pRL) (Table 10) using Lipofectamine 3000 (Promega, USA) as per the manufacturer's protocol. Additionally, in assays for studying the effect of endogenous expression of SteA on NF-κB activation, cells were also transfected with pcDNA3.1(+) or pcDNA3.1(+)*steA* in addition to pGL4.1 and pRL. After 18 h of transfection, the cells were either infected with wt, Δ*steA* and compl or stimulated with 10 ng/ml of TNFα for 6 h and 8 h respectively. The dual luciferase assay kit (cat# E2920, Promega, USA) was used according to the manufactures' protocol to analyse the luminescence corresponding to NF-κB activation (firefly luciferase) and the renilla luciferase. The luminescence was detected using a plate reader (BMG Biotech, Germany). The luminescence corresponding to NF-κB activation was normalized to that of renilla luciferase (corresponding to the transfection efficiency). In infection based experiments, the luminescence was also normalized to the invasion.

5.7.9 Co-localization studies

After 24 h of transfection in HEK 293 cells and TNFα stimulation for 30 min (as described previously), cells were washed twice with PBS and were then fixed with 2.5 % of Paraformaldehyde (PFA) for 30 min at RT. Cells were then washed twice with PBS and incubated with anti-IκB (1:750), anti-HA (1:250), anti-Cullin-1 (1:250) or anti-Cand-1 (1:500) antibodies for 45 min at room temperature (Table 12). Then, cells were washed thrice with PBS and incubated with Alexa 488 conjugated anti-rabbit IgG secondary antibody (1:500) (# A11034, Life Technologies, USA) and Alexa 568 conjugated anti-mouse IgG secondary antibody (1:500) (# A11004, Life Technologies, USA) for 30 min at RT. All the antibody dilutions were prepared in 0.2 % Saponin dissolved in PBS. The cells were washed thrice with PBS and were mounted on glass slides using Fluoromount (Sigma-Aldrich, USA). The imaging was done using a Zeiss Confocal microscope (for co-localization of IκB or Cullin-1 with SteA-HA) or Leica Confocal microscope (for co-localization of Cand-1 with SteA-HA).

5.8 GST pull-down assay

The *steA* gene was cloned in the plasmid pGEX4T3 (Table 10) using restriction cloning. The empty pGEX4T3 and pGEX4T3-*steA* were each transformed to *E. coli* Origami B1 cells

(Merck, Germany) by chemical transformation method. Then, using these transformants, GST and GST-tagged SteA were overexpressed using 0.1 mM IPTG at 18 °C for 24 h. The bacteria were pelleted at 2,050 g for 30 min at 4 °C. The pellet was re-suspended in PBS containing bacterial protease inhibitor cocktail (Sigma-Aldrich, USA) and was subjected to sonication at 25 A for 15 min. Then, this was centrifuged at 18,500 g for 50 min at 4 °C and analysed by SDS-PAGE. Both GST and GST-tagged SteA were found to be present in the soluble fractions. Parallelly, the glutathione beads (Qiagen, USA) were washed twice with lysis buffer (50 mM Tris-Cl, 150 mM NaCl, 0.05 % NP-40, pH 7.5). Then, to 10 ml of the soluble fraction containing GST or GST-tagged SteA, 300 µl of washed glutathione beads were added and incubated at 4 °C with shaking. After 2 h of incubation, the beads were pelleted at 1,800 g for 5 min and washed four times with lysis buffer. Then, the beads were incubated with 500 µl of 5 % BSA in PBS for 90 min. Then, the beads were pelleted and washed 4 times with lysis buffer. To this, whole cell lysate of un-stimulated RAW 264.7 cells was added and incubated at 4 °C for 3 to 4 h with shaking. Then, the beads were pelleted and washed 4 times with lysis buffer and re-suspended in 40 µl of SDS-loading buffer. This was then boiled for 5 min and subjected to SDS-PAGE and immunoblotting.

5.9 Yeast two-hybrid assay

The coding sequences of IκB, Skp-1, Rbx-1 and Cullin-1 from *Mus musculus* were taken from www.ncbi.nlm.gov.in. A cDNA library was prepared according to the manufacturer's protocol (Invitrogen, Life Technologies, U.S.A.) using RNA isolated (according to the manufacturer's protocol; Genetix, India) from untreated RAW 264.7 cells. IκB, Skp-1 and Rbx-1 were amplified from the cDNA library and cloned in pGADC1 (Table 10) plasmid by restriction cloning. Cullin-1 was amplified and cloned in pGADT7 (Table 10) by gateway cloning method according to manufacturer's protocol (Thermo-Fischer, USA). The *steA* gene was amplified from the *S.* Typhimurium genome and cloned in pGBDC1 plasmid (Table 10) by restriction cloning. The cloned AD and the BD plasmids were co-transformed in yeast (PJ697a) and plated on synthetic complete media deficient in leucine and uracil (SC-Leu, -Ura). The colonies thus obtained were then spotted on plates with media deficient in leucine, uracil and histidine (SC-Leu, -Ura, -His).

5.10 Densitometric analysis

The densitometric analysis of the western blots was done using the Image J software (Rasband, W.S., ImageJ, U. S. National Institutes of Health, Bethesda, Maryland, USA, https://imagej.nih.gov/ij/, 1997-2018). The band intensities of IκB, IKKα/β, p65 or c-Rel were normalized to the respective band intensities of the loading controls i.e. GAPDH for whole cell lysates and PCNA for nuclear lysates. For co-immunoprecipitation studies, the fold changes of the band intensities in the VpOmpU-treated cells were calculated above the band intensities in the buffer-treated cells. For analysis of the phosphorylation status of p38 and JNK, the band intensities of p-p38 or p-JNK were calculated above the band intensities of p38 or JNK, respectively.

5.11 Statistical analysis

Data were expressed as mean ± SD or SEM. The statistical analysis was done using Student's two-sided t-test and the p values less than 0.05 were considered significant. The p values indicated are *$p<0.05$, **$p< 0.01$, ***$p<0.001$, ns $p>0.05$.

6. Results

6.1 Deletion of *steA* from the genome of *S.* Typhimurium

SteA, being an effector which is translocated to the host cytoplasm via the T3SS during an infection, its role would be best studied in an infection scenario. To be able to understand the role of SteA in the infection of *S.* Typhimurium, we first deleted *steA* gene from the genome of *S.* Typhimurium. We used the one-step inactivation method (197) wherein we replaced the *steA* gene with a kanamycin cassette. To check the deletion, we used a combination of PCRs using primers against the priming sites of kanamycin cassette (P1 and P2), internal regions in kanamycin cassette (K1 and K2) and the gene-specific primers. The PCR with P1-P2, K1-K2, P1-K2 and P2-K1 were found to be positive for the two deletion mutants (labelled as 1 and 2) and negative for the wild type *S.* Typhimurium (labelled as C) (Figure 32). The PCR using gene-specific primers of *steA* gene was positive for wild type *S.* Typhimurium but negative for the deletion mutants of *steA* (Δ*steA*) (Figure 32). Altogether, this indicated that SteA was replaced with the kanamycin cassette in Δ*steA* mutants.

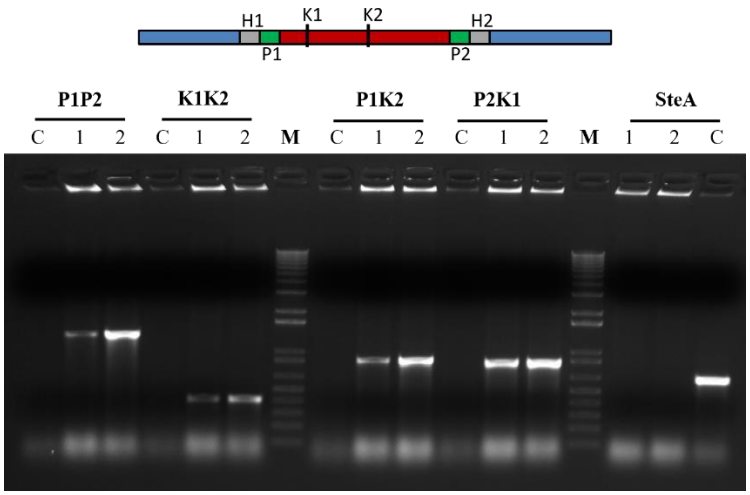

Figure 32. SteA was deleted from *S.* Typhimurium

Agarose gel confirming the deletion of *steA* and its replacement with the kanamycin cassette. C denotes the wild type *S.* Typhimurium, 1 & 2 are the deletion mutants and M denotes the 1 kb molecular weight marker. The deletion mutants 1 and 2 show amplicon of P1P2 (1300 bp), K1K2 (400 bp), P1K2 (876 bp), P2K1 (824 bp) and show no amplification for gene specific primers (623 bp).

6.2 Effect of *steA* deletion on the virulence of *S.* Typhimurium in mice

To be able to understand whether SteA has a role in the virulence of *S.* Typhimurium, we infected Balb/c mice intra-peritoneally with wild type *S.* Typhimurium (wt), Δ*steA* and Δ*steA*-complemented with a plasmid expressing *steA* (compl). We found that the mice infected with Δ*steA* had lower survival than the wt- or the compl-infected mice (Figure 33A, 33B). Also, mice infected with Δ*steA* had pilorected fur, decreased activity, decrease in response to stimuli and closed eyes, which are symptoms of a heightened immune response (198). We scored these symptoms and found them higher in case of Δ*steA* than wt or compl-infected mice (Figure 33C).

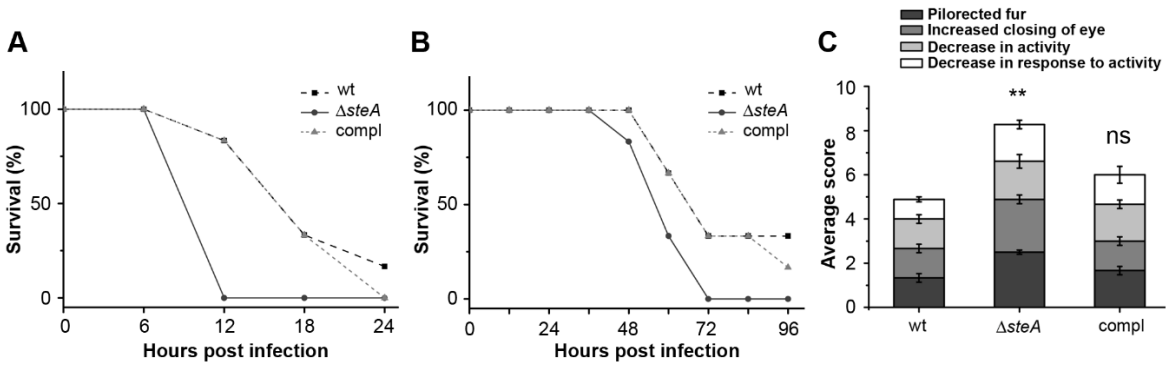

Figure 33. Mice infected with Δ*steA* have a lower survival and show symptoms of heightened immune response

(A-B) Mice infected with Δ*steA* showed lower survival than the wt or compl-infected mice. 6-8 weeks old Balb/c mice were injected intra-peritoneally with 5 x 10^7 (A) or 5 x 10^5 (B) bacteria (wt, Δ*steA* or compl) and were monitored at every 6 h (A) or 12 h (B) post infection (h.p.i.) for 24 h or 96 h respectively. The survival percentage was calculated as [(No. of surviving mice/total no. of mice infected) x 100]. The graph shown represents the cumulated data (n=6) from three independent sets with three mice (n=3) in each set. (B) Mice infected with Δ*steA* showed higher symptoms of heightened immune response than wt- or compl-infected mice. 6-8 weeks old Balb/c mice were injected intra-peritoneally with 5 x 10^5 bacteria and were scored at 36 h.p.i. for septic shock symptoms namely pilorected fur, extent of decrease in activity, extent of decrease in response to stimuli and the extent of closing the eye on a scale of 1 to 4. Each mice was scored independently and the total score was averaged over the total mice in the group. The graph represents mean ± SEM from three independent sets. ***$p \leq 0.001$, **$p \leq 0.01$, *$p \leq 0.05$, ns $p > 0.05$ versus wt infected mice.

To further investigate whether a higher immune response was being generated in mice infected with Δ*steA*, we checked the levels of TNFα, IL-6, IL-1β, IFNγ, IL-12 and IL-10 in the serum of infected mice at 24 h.p.i. and 36 h.p.i. We found a higher TNFα, IL-6, IFNγ, IL-12 and IL-10 in mice infected with Δ*steA* than the controls (Fig. 34A-F). Further, we isolated spleens from the infected mice and probed the gene-expression levels of TNFα and IL-6 in the mononuclear cells of the spleen. We observed that TNFα and IL-6 gene expression levels were higher in Δ*steA*-infected mice than wt- or compl-infected ones (Fig 34G). We further wanted to check whether this difference in expression of TNFα and IL-6 was due to lesser bacterial load in the spleens of the infected mice. Towards this, we checked the bacterial load in spleens of mice

infected with wt or Δ*steA* and found no significant difference (Fig 34H). Altogether, this indicated that SteA was involved in immune suppression during infection.

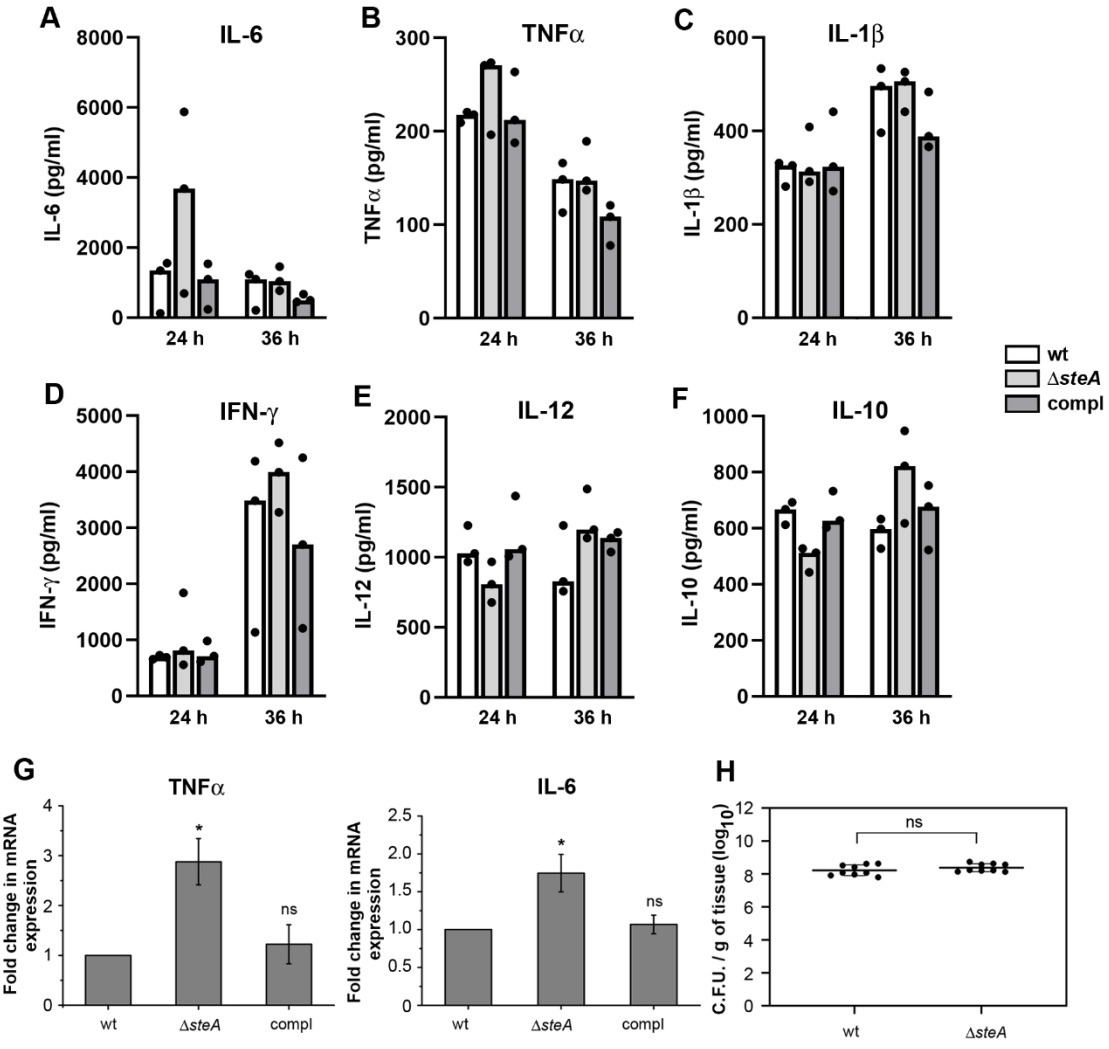

Figure 34. Mice infected with Δ*steA* showed higher immune response

(A-F) The levels of IL-6 (A), TNFα (B), IFNγ (D), IL-12 (E) and IL-10 (F) were higher in the serum of mice infected with Δ*steA* than the wt- and compl-infected mice. 6-8 weeks old mice were infected with 5 x 10^5 wt, Δ*steA* and compl strains. At 24 h.p.i. and 36 h.p.i., blood was drawn from the infected mice and the serum was probed for various cytokines using ELISA. Bar graph represents median from three mice (n=3), each represented as a dot (•). (G) TNFα and IL-6 gene expression was higher in splenic mononuclear cells of mice infected with Δ*steA* than the wt- or compl-infected mice. The mononuclear cells were isolated from the spleens of infected mice using density gradient centrifugation and then, RNA was isolated from these cells. The cDNA was prepared from this RNA and gene expressions of TNFα and IL-6 were calculated using semi-quantitative RT-PCR. Bar graph

represents mean ± SEM from three independent experiments. (H) No difference in the colonization of wt or Δ*steA* in spleens of the infected mice. The bacteria were enumerated in the spleen of the infected mice on LA plates and were normalized to the weight of the tissue. The graph represents data from 9 mice (n=9) with each mice represented as a dot (•). (A-B) 6-8 weeks old Balb/c mice were injected intra-peritoneally with 5 x 10^5 wt or Δ*steA* strains and spleens were isolated at 36 h.p.i. ***$p \leq 0.001$, **$p \leq 0.01$, *$p \leq 0.05$, ns $p > 0.05$ versus wt-infected mice.

6.3 SteA suppresses immune responses

S. Typhimurium is known to infect macrophages, which are immune cells (145). To further confirm the role of SteA in immune suppression, we infected RAW 264.7 murine macrophages and bone-marrow derived macrophages (BMDM) with wt, Δ*steA* and compl and checked the production of TNFα. We observed that cells infected with Δ*steA* produced more TNFα than wt- or compl-infected cells in both RAW 264.7 macrophages and BMDMs (Figure 35). This confirmed that in the absence of SteA there is a heightened production of pro-inflammatory cytokines indicating that SteA suppresses pro-inflammatory responses during *S.* Typhimurium infection.

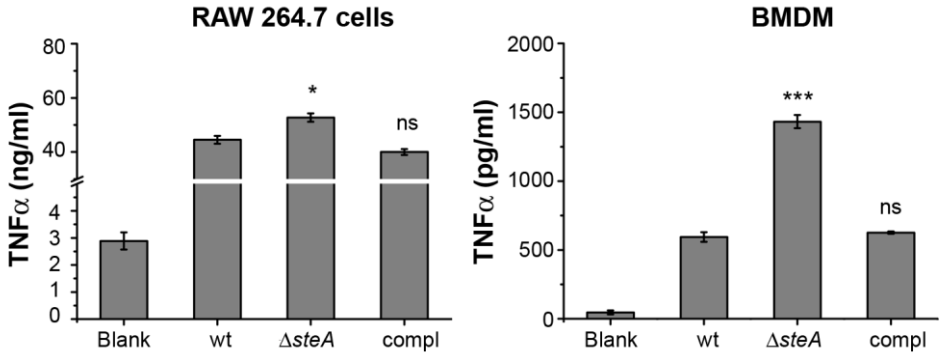

Figure 35. A higher pro-inflammatory response is generated in RAW 264.7 macrophages and BMDMs in response to Δ*steA* than wt or compl-infected cells

RAW 264.7 cells or BMDMs were infected with wt, Δ*steA* or compl at an MOI of 20:1 (for RAW 264.7 cells) and 10:1 (for BMDMs). Supernatants were collected after 8 h and analysed for TNFα using ELISA. Bar graphs represent mean ± SEM from three independent sets. ***$p \leq 0.001$, **$p \leq 0.01$, *$p \leq 0.05$, ns $p > 0.05$ versus wt infected cells.

6.4 SteA does not act on the MAP-kinase pathway

A pro-inflammatory response may be dependent on the activation of the MAP-kinase pathway (as described on page no. 17). The activation of the MAP-kinase pathway leads to the phosphorylation of the terminal MAP-kinases namely p38 and JNK (4). So, to be able to decipher how SteA suppresses the pro-inflammatory responses, we checked the activation levels of p38 and JNK in RAW 264.7 cells infected with wt, Δ*steA* or compl and found no difference in their activation levels (Figure 36A, 36B) indicating that SteA was not acting on the MAP-kinase activation cascade to suppress the pro-inflammatory response.

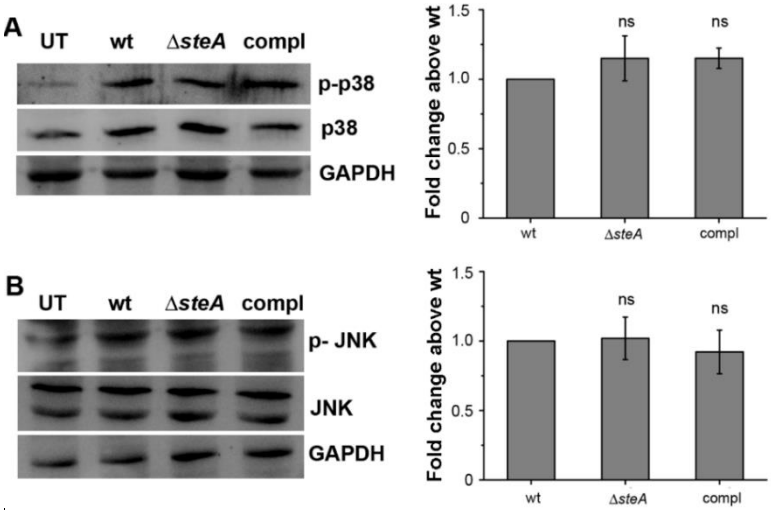

Figure 36. SteA does not act on the MAP-kinase pathway

(A-B) SteA does not act on p38 (A) or JNK (B) activation pathway. RAW 264.7 cells were infected with wt, Δ*steA* or compl at an MOI of 20:1. After 30 min of infection, whole cell lysates were prepared and analysed for the activation of p38 (p-p38) and JNK (p-JNK) using western blotting. GAPDH was used a loading control. Fold change in the densitometric values of p38 and JNK were calculated above those in wt infected cells. Bar graphs represent mean ± SEM from three independent sets. ***$p \leq 0.001$, **$p \leq 0.01$, *$p \leq 0.05$, ns $p > 0.05$ versus wt-infected cells.

6.5 SteA suppresses IκB degradation

In addition to the MAP-kinase pathway, the pro-inflammatory responses may also be NF-κB mediated (4). For the activation of NF-κB, a signalling cascade leads to the degradation of IκB, the inhibitor of NF-κB. This allows NF-κB to translocate to the nucleus and transcribe genes

related to inflammation (4). Since SteA does not seem to interfere with the MAP-kinase activation (Figure 36), we further checked the levels of total IκB in macrophages infected with wt, Δ*steA* and compl. We found the IκB levels to be lower in both RAW 264.7 and BMDMs infected with Δ*steA* than wt- or compl-infected cells (Figure 37A, 37B).

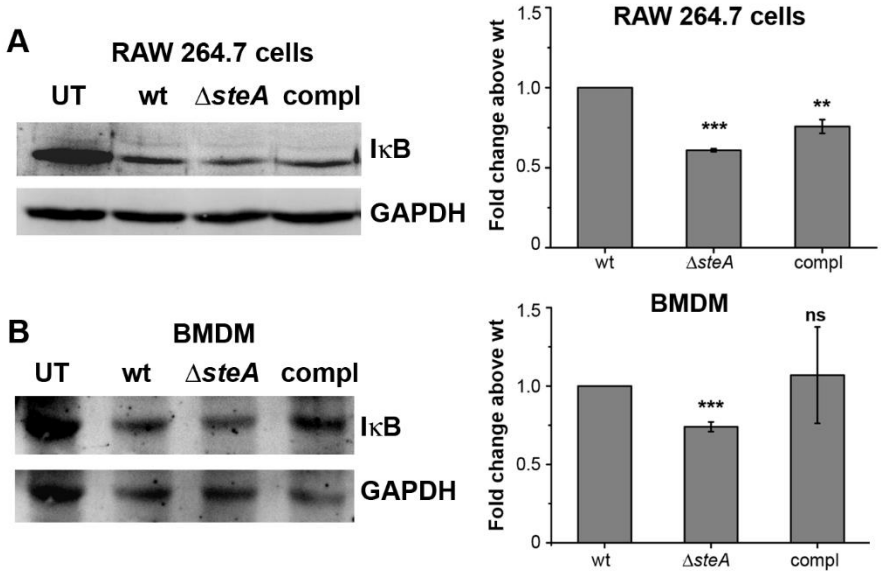

Figure 37. SteA suppresses the degradation of IκB in macrophages

(A-B) IκB degradation was higher in RAW 264.7 cells (A) and BMDMs (B) infected with Δ*steA* than wt- or compl-infected cells. RAW 264.7 cells or BMDMs were infected with wt, Δ*steA* or compl at an MOI of 20:1 (for RAW 264.7 cells) and 10:1 (for BMDMs). Whole cell lysates were prepared after 30 min and analysed for IκB levels by western blotting and densitometry. GAPDH was used as a loading control. Fold change in the densitometric values of IκB were calculated above those in wt-infected cells. Bar graphs represent mean ± SEM from three independent sets. ***$p \leq 0.001$, **$p \leq 0.01$, *$p \leq 0.05$, ns $p > 0.05$ versus wt-infected cells.

Further, to probe whether SteA affected the IκB levels in mice, we isolated spleen from mice infected with wt, Δ*steA* and compl and checked the IκB levels in the splenic lysates. We observed more IκB degradation in the splenic lysates of mice infected with Δ*steA* than the controls (Figure 38).

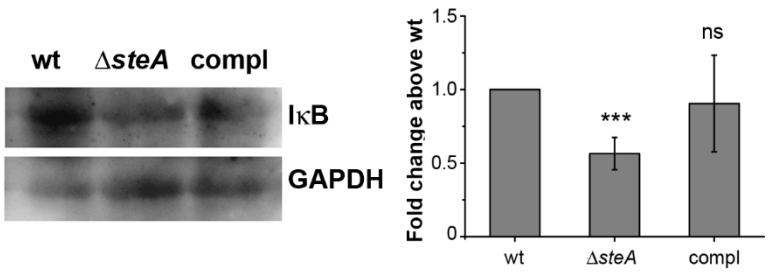

Figure 38. SteA suppresses IκB degradation *in vivo*

IκB degradation was more in mice infected with Δ*steA* than wt- or compl-infected mice. 6-8 weeks old Balb/c mice were infected with 5 x 10^5 bacteria. The spleen was isolated at 36 h.p.i. and splenic lysates were analysed for IκB by western blotting and densitometry. GAPDH was used as a loading control. Fold change in the densitometric values of IκB were calculated above those in wt-infected mice. Bar graphs represent mean ± SEM from three independent sets. ***$p \leq 0.001$, **$p \leq 0.01$, *$p \leq 0.05$, ns $p > 0.05$ versus wt infected mice.

We further wanted to probe whether SteA alone could suppress IκB degradation. Towards this, we endogenously expressed SteA in HEK 293 cells using a plasmid containing *steA* (pcDNA3.1(+)*steA*) and checked the degradation of IκB after stimulation with TNFα (this part of the work was done by Ms. Rhythm Shukla, MS final year student under my supervision). We observed that IκB degradation was grossly affected in cells expressing SteA as compared to the empty plasmid transfected cells (Fig 39).

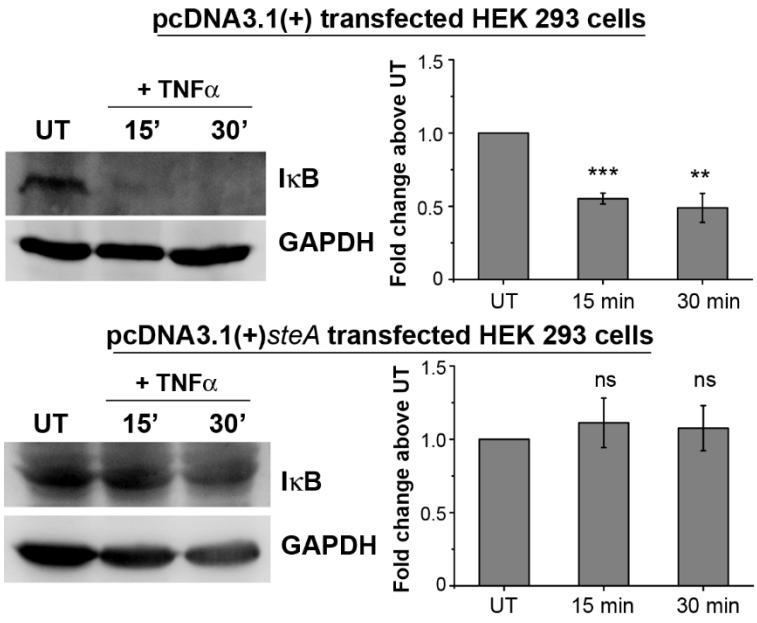

Figure 39. IκB degradation is suppressed in HEK 293 cells expressing SteA

HEK 293 cells were transfected with pcDNA3.1(+) or pcDNA3.1(+)*steA* and stimulated with TNFα for 15 and 30 min. Whole cell lysates were then prepared and probed for IκB using western blotting and densitometry. GAPDH was used as a loading control. Fold change in the densitometric values of IκB were calculated above those in the untreated cells. Bar graphs represent mean ± SEM from three independent sets. ***$p \leq 0.001$, **$p \leq 0.01$, *$p \leq 0.05$, ns $p > 0.05$ versus untreated cells.

Altogether, these results showed that IκB degradation was affected in presence of SteA.

6.6 SteA suppresses the NF-κB activation

In the inactive state, IκB binds to the NF-κB, restricting it in the cytosol. IκB degradation leads to the translocation of NF-κB to the nucleus, leading to the transcription of various pro-inflammatory genes (as previously described). The NF-κB family consists of five members namely RelA (or p65), RelB, c-Rel, p50 and p52 which form homo- or hetero-dimers and form a functional NF-κB leading to a pro-inflammatory or anti-inflammatory response. Of these, p65 and c-Rel are involved in the pro-inflammatory responses (134). So, we next wanted to check the translocation of p65 and c-Rel to the nucleus, upon infection with wt, Δ*steA* and compl. Towards this, we checked the levels of p65 and c-Rel in the nuclear lysates of RAW 264.7 macrophages after infection with wt, Δ*steA* and compl and found them to be higher in cells infected with Δ*steA* than the controls (Figure 40).

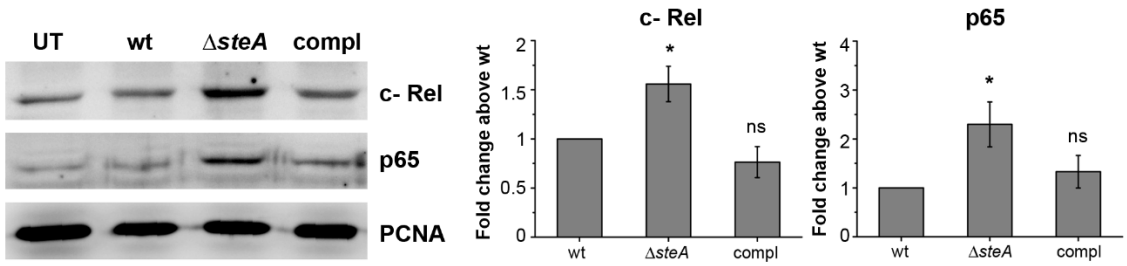

Figure 40. Nuclear translocation of NF-κB subunits is higher in cells infected with Δ*steA*

RAW 264.7 cells were infected with wt, Δ*steA* or compl at an MOI of 20:1. After 30 min, nuclear lysates were prepared and p65 and c-Rel (NF-κB family members) were analysed by western blotting and densitometry. PCNA was used as a nuclear marker. Fold change in the densitometric values of p65 or c-Rel were calculated above those in wt-infected mice. Bar graphs represent mean ± SEM from three independent sets. ***p ≤ 0.001, **p ≤ 0.01, *p ≤ 0.05, ns p > 0.05 versus wt infected cells.

Further, to confirm that SteA suppresses the NF-κB pathway, we transfected HEK 293 cells with a NF-κB reporter plasmid and checked the activation levels of NF-κB upon infection with wt, Δ*steA* and compl (this part of the study was done by Ms. Rhythm Shukla). We found higher NF-κB activation in cells infected with Δ*steA* than the wt- or compl-infected cells (Fig 41A). Furthermore, we checked the NF-κB reporter activity in HEK 293 cells expressing SteA, upon TNFα stimulation (this part of the study was also done by Ms. Rhythm Shukla). We found NF-κB activity to be much lower as compared to the empty plasmid transfected cells upon stimulation with TNFα (Fig 41B).

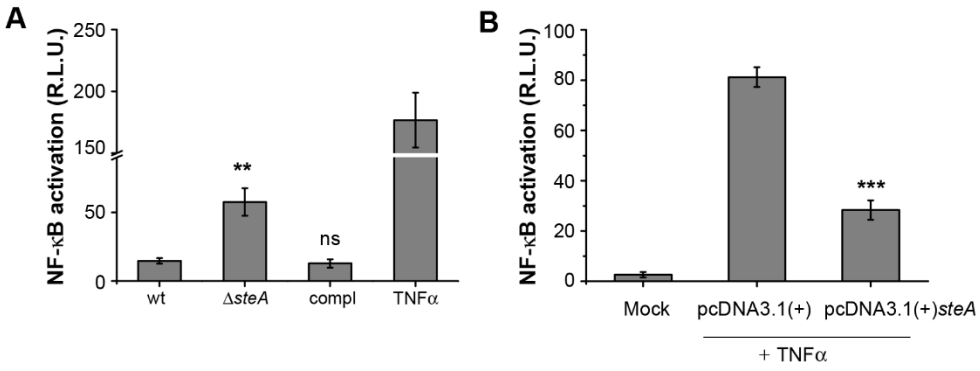

Figure 41. SteA suppresses the NF-κB activation

(A) NF-κB activation was higher in Δ*steA*-infected HEK 293 cells than the wt- or compl-infected cells. HEK 293 cells were transfected with NF-κB luciferase reporter plasmid and the renilla luciferase plasmid (pRL). After 18 h of transfection, cells were infected with wt, Δ*steA* or compl at an MOI of 20:1. The NF-κB reporter activity was measured 8 h.p.i.; TNFα

was used as a positive control. (B) Endogenous expression of SteA suppresses NF-κB activation. HEK 293 cells were transfected with NF-κB luciferase reporter plasmid and pRL along with pcDNA3.1(+) or pcDNA3.1(+)*steA* for 24 h. cells were then stimulated with TNFα and the NF-κB reporter activity was measured after 8 h. (A-B) Bar graphs represent mean ± SEM from three independent sets. ***$p \leq 0.001$, **$p \leq 0.01$, *$p \leq 0.05$, ns $p > 0.05$ versus wt infected cells (A) or pcDNA3.1(+) transfected cells (B).

Altogether, these results confirmed that SteA was suppressing the NF-κB pathway to subdue the pro-inflammatory responses.

6.7 SteA affects the ubiquitination of IκB

The degradation of IκB is dependent on its ubiquitination, which is initiated by the phosphorylation of IκB. The upstream signalling leads to the phosphorylation of the IκB kinase (IKKα/β) which then phosphorylates IκB (5). Therefore, we wanted to probe whether the observed difference in the total IκB levels (Figure 37) was due to the lesser activation of IKK. Towards this, we infected RAW 264.7 macrophages and BMDMs with wt, Δ*steA* and compl and checked the levels of phosphorylated IKKα/β in the whole cell lysates. We observed no difference in the activation levels of IKKα/β in the presence or absence of SteA (Figure 42A), indicating that SteA doesn't act on the upstream signalling, which leads to the activation of IKKα/β. As previously described, the activated IKK phosphorylates IκB, which results in its ubiquitination. Therefore, next we wanted to check if the ubiquitination of IκB was affected in the presence of SteA. Towards that we transfected HEK 293 cells with pcDNA3.1(+)*steA* or pcDNA3.1(+) empty plasmid and checked the ubiquitination of IκB upon TNFα stimulation in the presence or absence of MG132. MG132 is a proteasomal inhibitor which prevents the degradation of ubiquitinated proteins. To check the ubiquitination level of IκB, we immunoprecipitated IκB with anti-IκB antibody and checked the ubiquitination levels of IκB by immunoblotting. If SteA interferes with the ubiquitination of IκB, the levels of ubiquitinated IκB in the presence of MG132 will be lesser in cells expressing SteA than the empty-plasmid transfected cells. In accordance with this, we observed that the ubiquitination levels of IκB were lower in the presence of SteA as compared to the control (Figure 42B). This indicated that SteA was somehow interfering with the ubiquitination of IκB and was not acting on the upstream signalling pathway.

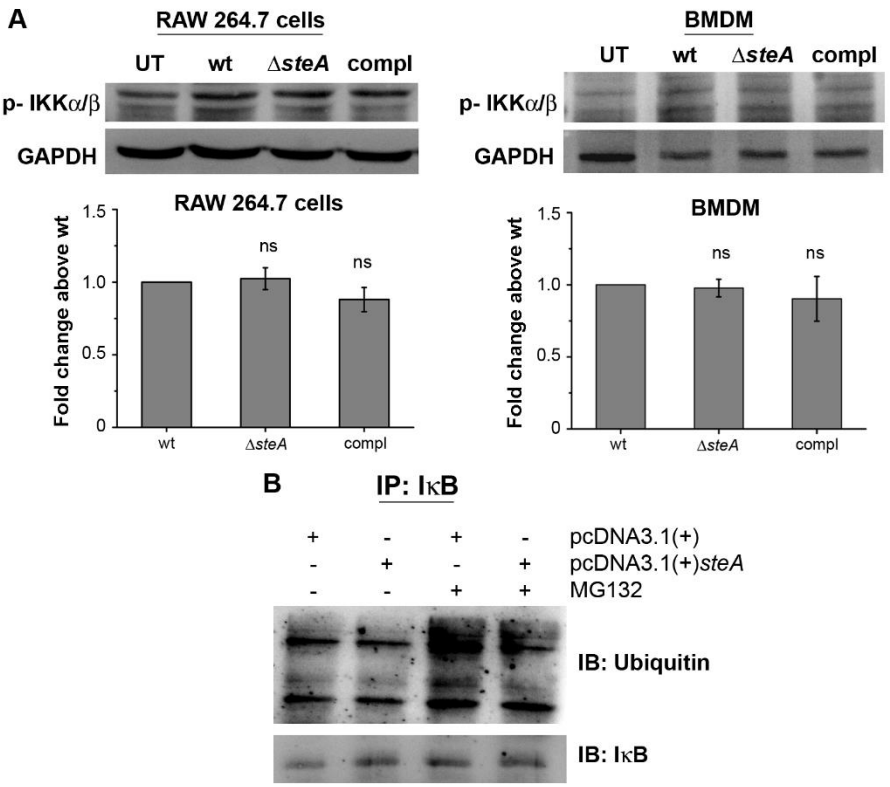

Figure 42. SteA affects the ubiquitination of IκB

(A) SteA doesn't affect the activation of IKKα/β which is the upstream kinase of IκB. RAW 264.7 macrophages and BMDMs were infected with wt, Δ*steA* or compl at an MOI of 20:1 or 10:1 respectively. After 30 min, whole cells lysates were prepared and analysed for phosphorylated IKKα/β by western blotting and densitometry. GAPDH was used a loading control. Fold change in the densitometric values of p-IKKα/β was calculated above those in wt-infected mice. Bar graphs represent mean ± SEM from three independent sets. ***p ≤ 0.001, **p ≤ 0.01, *p ≤ 0.05, ns p > 0.05 versus wt infected cells. (B) Endogenous expression of SteA suppresses IκB ubiquitination. HEK 293 cells were transfected with pcDNA3.1(+) or pcDNA3.1(+)*steA* for 18 h. The cells were then pre-treated with the proteasomal inhibitor (MG132) for 3 h and stimulated with TNFα for 20 min. Whole-cell lysates were prepared and immunoprecipitated with anti-IκB antibody. IκB and ubiquitin were probed by western blotting.

6.8 SteA does not interfere with the assembly of the E3-ligase on IκB

The ubiquitination of IκB is a sequential reaction wherein the ubiquitin is first activated by the ubiquitin activating enzyme (E1) and then is transferred to the ubiquitin-conjugating enzyme (E2). The ubiquitin from the E2 is then transferred to the substrate (IκB in this case) by the E3 ligase complex which recognizes the substrate. The E3 ligase responsible for the ubiquitination

of IκB consists of Skp-1, Cullin-1 and an F-box protein (SCF-E3 ligase complex) (200, 201). The F-box protein called beta transducing repeat containing protein (β-TrCP) recognizes phosphorylated IκB. Skp-1 is an adaptor protein, which binds the Cullin-1 to β-TrCP. Cullin-1 is bound to Rbx-1, which is the adaptor for the E2 complex.

First, we wanted to check whether SteA affects the assembly of the E3 ligase complex to phosphorylated IκB. Therefore, we infected RAW 264.7 cells with wt or Δ*steA* and immunoprecipitated using anti-β-TrCP antibody and probed for the SCF complex and phosphorylated IκB. We observed that the assembly of SCF E3-ligase complex at IκB was similar in the presence or absence of SteA (Figure 43).

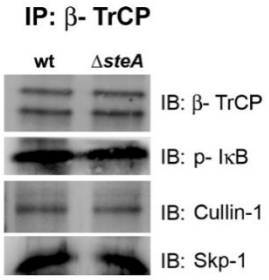

Figure 43. SteA does not affect the assembly of SCF-E3 ligase on IκB

RAW 264.7 cells were infected with wt or Δ*steA* at an MOI of 20:1. Whole cell lysates were prepared after 30 min and immunoprecipitated with anti-β-TrCP antibody. SCF-E3 ligase components and phosphorylated IκB were probed using western blotting.

Further, we have observed that SteA was co-localizing with IκB in HEK 293 cells expressing SteA upon stimulation with TNFα (Ms. Rhythm Shukla, Figure 44) indicating that SteA might itself be associated to IκB or the E3 ligase complex.

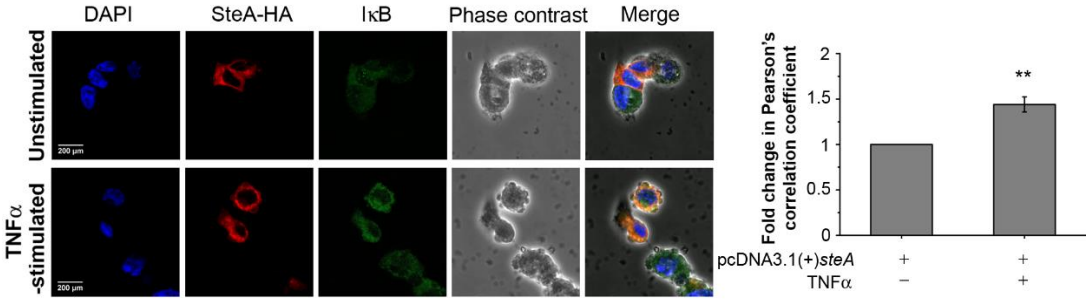

Figure 44. SteA and IκB colocalize upon TNFα stimulation in SteA expressing HEK 293 cells

HEK 293 cells were transfected with pcDNA3.1(+)*steA* for 18 h and stimulated with TNFα for 30 min. Cells were then fixed and stained with anti-IκB, anti-HA (for SteA) primary

antibodies and then, stained with Alexa 488-tagged and Alexa 568-tagged secondary antibodies respectively. DAPI was used to stain the nucleus. Co-localization was quantified using Pearson's correlation coefficient for 8-10 fields per experiment. Bar graphs represent mean ± SEM from three independent experiments. ***$p \leq 0.001$, **$p \leq 0.01$, *$p \leq 0.05$, ns $p > 0.05$ versus unstimulated cells.

Next we wanted to check whether SteA itself was associated to this complex. For this, we infected RAW 264.7 cells with Δ*steA* and Δ*steA*-complemented with his-tagged SteA (compl-H) and checked its association to the SCF E3-complex by immunoprecipitation with anti-His antibody. Interestingly, components of the SCF E3 complex and IκB were co-immunoprecipitated with SteA (Figure 45A). Further, we also expressed HA-tagged SteA in HEK 293 cells and immunoprecipitated using anti-HA antibody. We observed the components of the SCF E3 ligase and IκB to be co-immunoprecipitated with HA-tagged SteA also (Fig 45B).

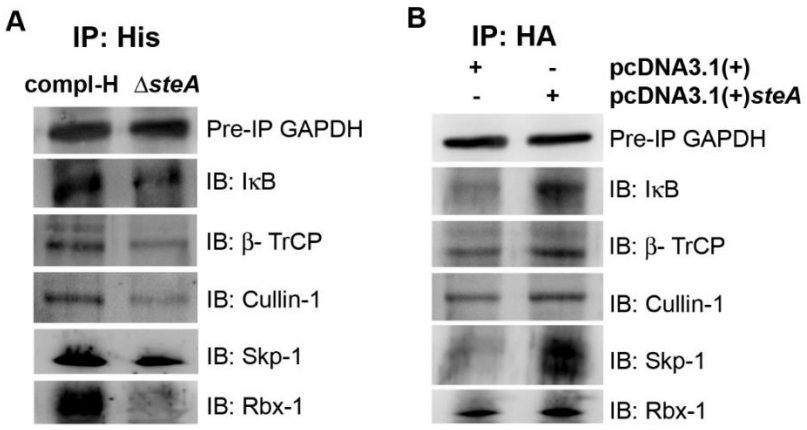

Figure 45. SteA seems to localize to the SCF E3 ligase complex assembled on IκB

(A) SCF E3 ligase components and IκB co-immunoprecipitate with SteA upon infection in RAW 264.7 cells. RAW 264.7 cells were infected with Δ*steA* and Δ*steA* complemented with His-tagged *steA* (compl-H) at an MOI of 20:1 for 30 min. Whole-cell lysates were prepared and immunoprecipitated with anti-His antibody. (B) The components of SCF-E3 ligase and IκB co-immunoprecipitate with SteA upon TNFα-stimulation in HEK 293 cells expressing HA-tagged SteA. HEK 293 cells were transfected with pcDNA3.1(+) or pcDNA3.1(+)*steA* (expressing HA-tagged SteA) for 18 h and stimulated with TNFα for 30 min. Whole-cell lysates were prepared and immunoprecipitated with anti-HA antibody. (A-B) The components of SCF E3 ligase and IκB were analysed by western blotting. GAPDH was used as loading control and was checked prior to immunoprecipitation (pre-IP).

Altogether, these results showed that SteA does not affect the assembly of the SCF E3 ligase complex to IκB, but also itself associate with it.

6.9 SteA binds to Cullin-1 of the SCF E3 ligase complex

Since, SteA seems associated with the SCF E3 ligase complex, it must be binding to one of the components of the SCF complex or to IκB itself. To probe this, we performed a yeast two-hybrid screen for the association of SteA with IκB, Cullin-1, Rbx-1 or Skp-1 and found SteA to bind to Cullin-1 (Figure 46).

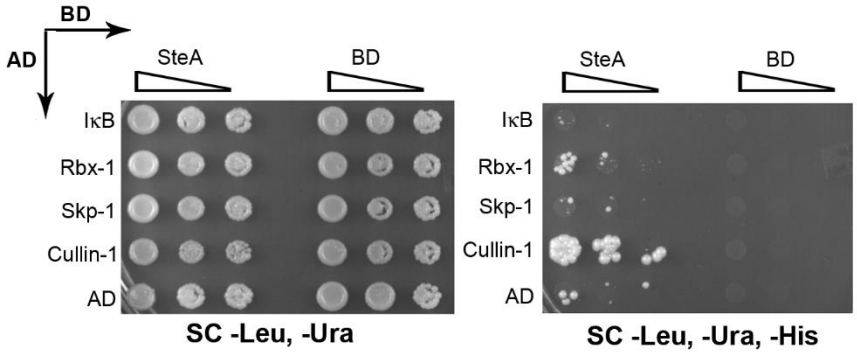

Figure 46. SteA interacts with Cullin-1 of the SCF E3 ligase complex

The components of the SCF E3 ligase complex and IκB were cloned in a vector containing activation domain (AD) and *steA* was cloned in a vector expressing the binding domain (BD) for the yeast two-hybrid screen. The AD and the BD vectors were co-transformed in yeast and plated on synthetic complete (SC) medium without leucine and uracil (SC -Leu, -Ura). The transformants were then serially diluted and spotted on SC -Leu, -Ura and SC without leucine, uracil and histidine (SC -Leu, -Ura, -His). The plates were incubated at 30 °C for 2 days. The growth on SC -Leu, -Ura, -His plates corresponding to the co-transformation of AD vector containing Cullin-1 and BD vector containing SteA showed the interaction of Cullin-1 and SteA.

Further, it had been observed in our lab (by Ms. Rhythm Shukla) that SteA and Cullin-1 co-localized in unstimulated condition and their co-localization did not change upon stimulation (Figure 47A). This indicated that SteA binds to Cullin-1 even in the absence of stimulation. To further confirm this, we did a GST-pull-down assay using GST-tagged SteA in unstimulated RAW 264.7 cells. We found that Cullin-1 was associating with GST-tagged SteA (Figure 47B).

Further, we immunoprecipitated HEK 293 cells expressing SteA-HA using anti-Cullin-1 antibody upon stimulation and found SteA to co-immunoprecipitate with Cullin-1 (Figure 47C).

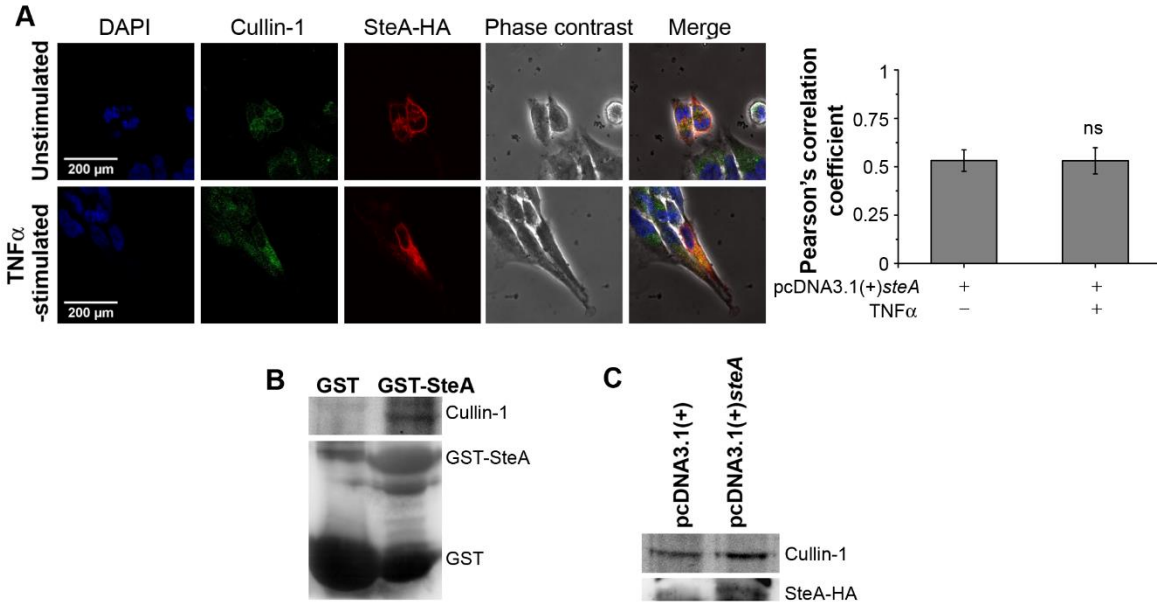

Figure 47. SteA interacts with Cullin-1 in the presence or absence of stimulation

(A) SteA co-localizes with Cullin-1 in unstimulated and stimulated HEK 293 cells expressing SteA. HEK 293 cells expressing HA-tagged SteA were stimulated with TNFα for 30 min. Cells were then fixed and stained with anti-Cullin-1 and anti-HA primary antibodies and then, stained with Alexa 488-tagged and Alexa 568-tagged secondary antibodies respectively. DAPI was used to stain the nucleus. Co-localization was quantified using Pearson's correlation coefficient for 8-10 fields per experiment. Bar graphs represent mean ± SEM from three independent experiments. ***$p \leq 0.001$, **$p \leq 0.01$, *$p \leq 0.05$, ns $p > 0.05$ versus unstimulated cells. (B) Cullin-1 co-immunoprecipitated with GST-tagged SteA in unstimulated RAW 264.7 cells. GST pull-down assay was done by using GST-tagged SteA and GST alone with unstimulated RAW 264.7 cells and analysed with anti-Cullin-1 and anti-GST antibodies by western blotting. (C) SteA co-immunoprecipitates with Cullin-1 upon stimulation in HEK 293 cells expressing SteA. HEK 293 cells were transfected with pcDNA3.1(+) or pcDNA3.1(+)*steA* (expressing HA-tagged SteA) for 36 h and stimulated with TNFα for 30 min. Whole-cell lysates were prepared and immunprecipitated with anti-Cullin-1 antibody. SteA was analysed by western blotting using anti-HA antibody.

Altogether these results showed that SteA binds to Cullin-1 of the SCF complex even in the absence of stimulation.

6.10 SteA suppresses the neddylation of Cullin-1 and dissociation of Cand-1

Since, SteA was binding to Cullin-1, thereby, suppressing the IκB degradation, we next wanted to check how SteA and Cullin-1 association was affecting the ubiquitination of IκB. The activation of the E3 ligase complex requires another crucial step i.e. the neddylation (addition of Nedd8 moiety) of Cullin-1. The neddylation of Cullin-1 causes a conformational change of the E3 ligase which brings the ubiquitin and the substrate in close proximity, resulting in the transfer of ubiquitin to the substrate (202). So, we first checked if SteA was affecting the neddylation of Cullin-1 in HEK 293 cells expressing SteA. We found that, upon TNFα stimulation, the neddylated Cullin-1 was less in cells expressing SteA than the empty plasmid transfected cells (Figure 48A).

Cullin-1 remains bound to Cand-1 in the inactive state. Upon activation, Cullin-1 gets dissociates from Cand-1and gets neddylated. The observation that upon stimulation, Cullin-1 (as part of the SCF complex) was associated with IκB (Fig) lead us to check if Cand-1 dissociation from IκB was hampered in the presence of SteA. Therefore, we treated HEK 293 cells endogenously expressing SteA with the proteasomal inhibitor, MG132 and immunoprecipitated using anti-IκB antibody upon TNFα-stimulation. We found more Cand-1 to be co-immunoprecipitated with IκB in cells expressing SteA than empty plasmid transfected cells (Figure 48B).

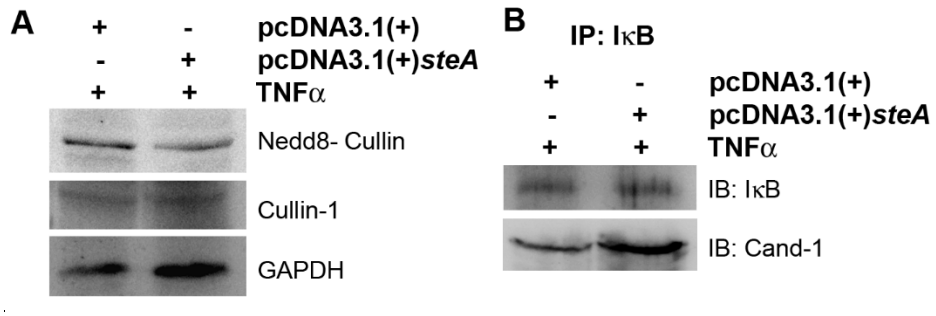

Figure 48. SteA suppresses neddylation of Cullin-1 and Cand-1 dissociation

(A) Cullin-1 neddylation is suppressed in HEK 293 cells expressing SteA. HEK 293 cells were transfected with pcDNA3.1(+) or pcDNA3.1(+)*steA* for 24 h. Whole cell lysates were prepared upon stimulation with TNFα for 30 min and analysed for Nedd8-Cullin-1 by western blotting. Total Cullin-1 in the cells was also analysed and GAPDH was used as a loading control. (B) SteA suppresses the Cand-1 dissociation from the SCF E3 ligase complex on IκB. HEK 293 cells expressing SteA were stimulated with TNFα for 20 min upon pre-treatment with MG132 (proteasomal inhibitor). Then, whole cell lysates were prepared and immunoprecipitated with anti-IκB antibody. Cand-1 was analysed by western blotting.

Since, Cullin-1 is bound to Cand-1 in the unstimulated state and we had previously observed that SteA associates with Cullin-1 in the absence of stimulation. Therefore, we wanted to check whether SteA was associating with Cand-1 as well in the absence of stimulation. Towards this, we checked the association of SteA with Cand-1 in a GST-pull-down assay using GST-tagged SteA in unstimulated RAW 264.7 cells. We found Cand-1 bound to GST-SteA (Figure 49).

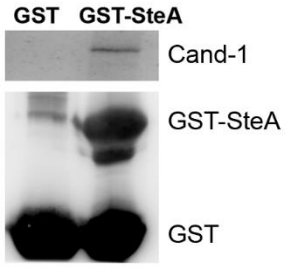

Figure 49. SteA binds to Cand-1 in unstimulated RAW 264.7 cells

Whole-cell lysates of untreated RAW 264.7 cells were subjected to a GST pull-down assay with GST tagged SteA and Cand-1 was analysed by western blotting.

Further, we also checked the co-localization of SteA and Cand-1 in HEK 293 cells expressing SteA in the presence or absence of TNFα-stimulation (this work was done by Ms. Rhythm Shukla). We found SteA to co-localize with Cand-1 in both unstimulated and stimulated state (Figure 50).

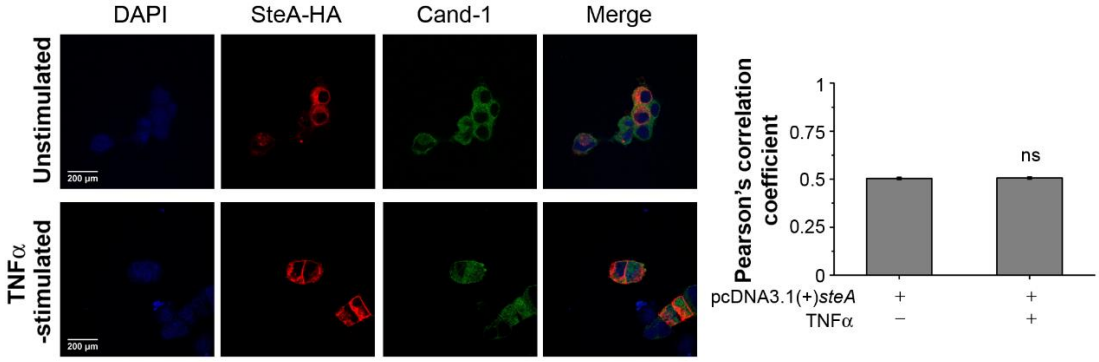

Figure 50. SteA co-localizes with Cand-1 in the presence or absence of stimulation

HEK 293 cells expressing HA-tagged SteA were stimulated with TNFα for 30 min. Cells were then fixed and stained with anti-Cand-1 and anti-HA primary antibodies, then with Alexa 488-tagged and Alexa 568-tagged secondary antibodies respectively. DAPI was used to stain the nucleus. Co-localization was quantified using Pearson's correlation coefficient

for 8-10 fields per experiment. Bar graphs represent mean ± SEM from three independent experiments. ***p ≤ 0.001, **p ≤ 0.01, *p ≤ 0.05, ns p > 0.05 versus unstimulated cells.

We had earlier observed similar co-localization of SteA and Cullin-1 as well, indicating that SteA binds to the Cullin-1/Cand-1 complex in both stimulated and unstimulated state thus preventing the dissociation of Cand-1 from Cullin-1.

6.11 SteA-mediated suppression of the pro-inflammatory responses is a T3SS-1-dependent phenomenon

As previously described, SteA is an effector which is secreted by both the T3SS-1 and T3SS-2 (48, 199). Therefore, we wanted to probe whether the suppression of pro-inflammatory responses by SteA is dependent on its secretion via T3SS-1 or T3SS-2. Since, the functions like invasion and SCV formation are affected by T3SS-1/SPI-1 and use of T3SS-1/SPI-1 deletion mutant can mask the SteA-mediated effect, therefore, we used a mutant deficient in SPI-2 (Δ*spi2*) i.e. it was incapable of forming the T3SS-2 injectisome. This would ensure that SteA was not being secreted by T3SS-2 and the effect on the pro-inflammatory responses hence observed would solely be dependent on its secretion via T3SS-1. We infected RAW 264.7 macrophages and BMDMs with Δ*spi2* and a double deletion mutant of Δ*steA* in Δ*spi2* background (Δ*spi2*Δ*steA*) and then checked the production of TNFα. We found that TNFα production was higher in the absence of SteA even in the Δ*spi2* background (Figure 51). This was similar to the TNFα production in the wt background.

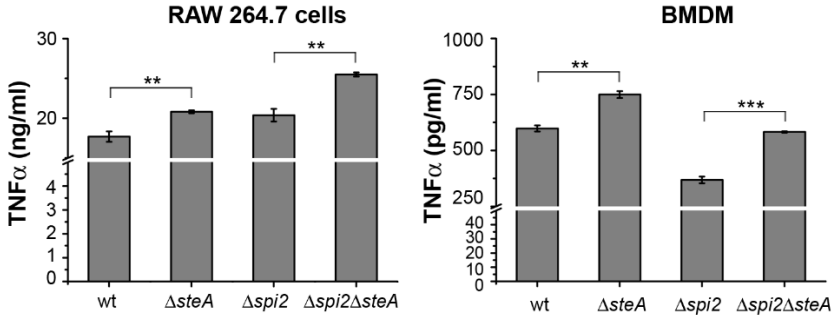

Figure 51. The suppression of pro-inflammatory responses by SteA is mediated by its translocation via T3SS-1

RAW 264.7 macrophages and BMDMs were infected with wt, Δ*steA*, deletion mutant of Δ*spi2* (spi2) and Δ*steA* in Δ*spi2* background (Δ*spi2*Δ*steA*) at an MOI of 20:1 (for RAW 264.7 cells) and 10:1 (for BMDMs). After 8 h, supernatants were collected and analysed for

TNFα using ELISA. Bar graphs represent mean ± SEM from three independent experiments. ***p ≤ 0.001, **p ≤ 0.01, *p ≤ 0.05, ns p > 0.05 versus unstimulated cells.

Since, in the absence of T3SS-2, the effect of SteA on the pro-inflammatory responses remained unaltered, it confirmed that the suppression of pro-inflammatory responses by SteA is a T3SS-1 mediated effect.

7. Conclusions and Discussion

S. Typhimurium secretes various effectors into the host cytoplasm via its T3SS-1 and -2 (150, 151, 169). These effectors modulate various host functions for the *S.* Typhimurium to survive and replicate inside the host, thereby establishing an infection in the host. SteA is an effector which is secreted by both the T3SSs (191, 199). It has been shown to be involved in the membrane dynamics of SCV when being secreted by T3SS-2 (194). In this study, we have explored the role of SteA in the early phases of infection i.e. when it is secreted by the T3SS-1. Towards this, we first checked the survival of mice upon infection with wt, Δ*steA* and compl. We observed that the mice infected with Δ*steA* had a lower survival than the wt or the compl-infected mice (Figure 33). Further, we observed that the mice infected with Δ*steA* showed symptoms of a heightened immune response which indicated that SteA might have a role in suppression of host's immune responses (Figure 33). Upon bacterial infection, the immune system of the host elicits a pro-inflammatory response, which helps in clearing of the bacteria from the host (203). *S.* Typhimurium is known to suppress the pro-inflammatory responses for its benefit. Various effectors like AvrA, GogA, GogB, SpvD etc. are secreted by *S.* Typhimurium which are known to suppress the pro-inflammatory responses (56, 57, 190, 204). To confirm, whether SteA could suppress pro-inflammatory responses of the host, we infected RAW 264.7 macrophages as well as bone marrow-derived macrophages (BMDMs) with wt, Δ*steA* and compl. We observed higher TNFα production when cells were infected with Δ*steA* than the wt-or compl-infected cells (Figure 35). Further, we observed higher expression of TNFα and IL-6 genes in mononuclear cells obtained from the spleens of mice infected with Δ*steA* than the wt or compl-infected mice (Figure 34). These findings led us to believe that SteA was involved in immune suppression during infection.

Generally, a pro-inflammatory response is generated in a cell via the activation of the transcription factors NF-κB or AP-1 (16). AP-1 activation is mediated by the MAP-kinase signalling cascade. The terminal MAP kinases P38 and JNK are activated in response to a stimulus, which in turn activate AP-1 (16). Some effectors namely SpvC, SptP and AvrA are known to act on the MAP-kinases to suppress pro-inflammatory responses (55, 58, 189). To probe if SteA was suppressing the immune responses by acting on the MAP kinase pathway, we checked the activation of P38 and JNK in RAW 264.7 macrophages and found them to be unaffected in the presence or absence of SteA (Figure 36), suggesting MAP kinases, hence AP-1 pathway is not affected by SteA. As mentioned previously, activation of NF-κB could also elicit pro-inflammatory responses. NF-κB remains bound to its inhibitor IκB in the inactive state. Upon activation, IκB is degraded and NF-κB translocates to the nucleus to transcribe pro-inflammatory genes (4). Therefore, we checked the IκB levels in RAW 264.7 macrophages, as well as, BMDMs infected with wt, Δ*steA* or compl and observed that more IκB was being degraded in Δ*steA*-infected cells than the controls (Figure 37). Further, we observed similar effect on IκB in splenic lysates of mice infected with wt, Δ*steA* and compl (Figure 38). Further, the degradation of IκB was inhibited in HEK 293 cells expressing SteA, upon stimulation with TNFα (Figure 39). This indicated that SteA probably acts on the NF-κB pathway to suppress pro-inflammatory responses. To further confirm that SteA was acting on the NF-κB pathway, we transfected HEK 293 cells with a NF-κB reporter plasmid and checked the NF-κB reporter activity upon infection with wt, Δ*steA* and compl. We observed higher NF-κB reporter activity in cells infected with Δ*steA* than wt or compl infected cells (Figure 41). Further, we also checked the NF-κB reporter activity in HEK 293 cells expressing SteA upon TNFα stimulation and found the NF-κB activation to be lower than the empty plasmid transfected cells (Figure 41). Altogether, these observations confirmed that SteA was acting on the NF-κB pathway to suppress the pro-inflammatory responses.

Further, our observation that higher IκB was being degraded in cells infected with *ΔsteA*, suggested that SteA probably acts on the upstream signalling pathway leading to IκB degradation. Therefore, we checked the activation levels of the upstream kinases, IKK which phosphorylates IκB, a crucial step for IκB degradation and found no difference in the activation levels of IKK in cells infected with wt, Δ*steA* or compl (Figure 42). IKK phosphorylates IκB, which then is ubiquitinated and degraded (4). Therefore, further we checked, whether SteA was affecting the ubiquitination of IκB and found that the ubiquitination of IκB was affected in the presence of SteA (Figure 42).

The ubiquitination of IκB is a multi-step process resulting in the Skp-1, Cullin-1, F-box (SCF) E3 ligase complex adding ubiquitin to IκB (201). The F-box protein which recognizes phosphorylated IκB is β-TrCP (201). Upon immunoprecipitation of lysates prepared from RAW 264.7 cells infected with wt or Δ*steA* using anti-β-TrCP antibody, we observed no difference in the assembly SCF E3 ligase complex at IκB in presence or absence of SteA (Figure 43). Further, using confocal microscopy and immunoprecipitation studies, we observed that upon activation (TNFα stimulation) SteA localizes with IκB in HEK 293 cells endogenously expressing SteA (Figure 44, 45). This indicated that, SteA associates with the SCF E3 ligase complex on IκB upon stimulation. To further study the direct interaction of SteA with the components of SCF E3 ligase complex or IκB, using yeast two-hybrid screen we found that SteA directly interacts with Cullin-1 (Figure 46). Further, by using confocal microscopy also, we observed that SteA co-localizes with Cullin-1 in HEK 293 cells endogenously expressing SteA (Figure 47). Interestingly, we observed SteA and Cullin-1 co-localization in both stimulated and unstimulated HEK 293-SteA cells (Figure 47). These results showed that binding of SteA to Cullin-1 probably suppresses IκB ubiquitination.

After assembly of the SCF E3 ligase complex on IκB, the neddylation of Cullin-1 is an essential step (202). So, we checked the levels of Cullin neddylation in HEK 293 cells expressing SteA and found them to be lesser in cells expressing SteA than empty plasmid transfected cells (Figure 48). In an inactive state, Cullin-1 remains bound to Cand-1 and upon activation, neddylation of Cullin-1 causes the dissociation of Cand-1 from Cullin-1 (205). Therefore, next to check whether SteA interferes with the dissociation of Cand-1 from Cullin-1 in the SCF complex on IκB in stimulated HEK 293 cells expressing SteA, we did immunoprecipitation using anti-IκB antibody. We observed that Cand-1 dissociation was lesser in cells expressing SteA than empty plasmid transfected cells (Figure 48) suggesting SteA inhibits the dissociation of Cand-1 from Cullin-1, thus affecting neddylation and ubiquitination of IκB. Further, we also found that SteA co-localizes with Cand-1 in HEK 293 cells in both the stimulated and unstimulated cells (Figure 50) suggesting SteA interacts with Cullin-1 and Cand-1 complex and inhibits their dissociation.

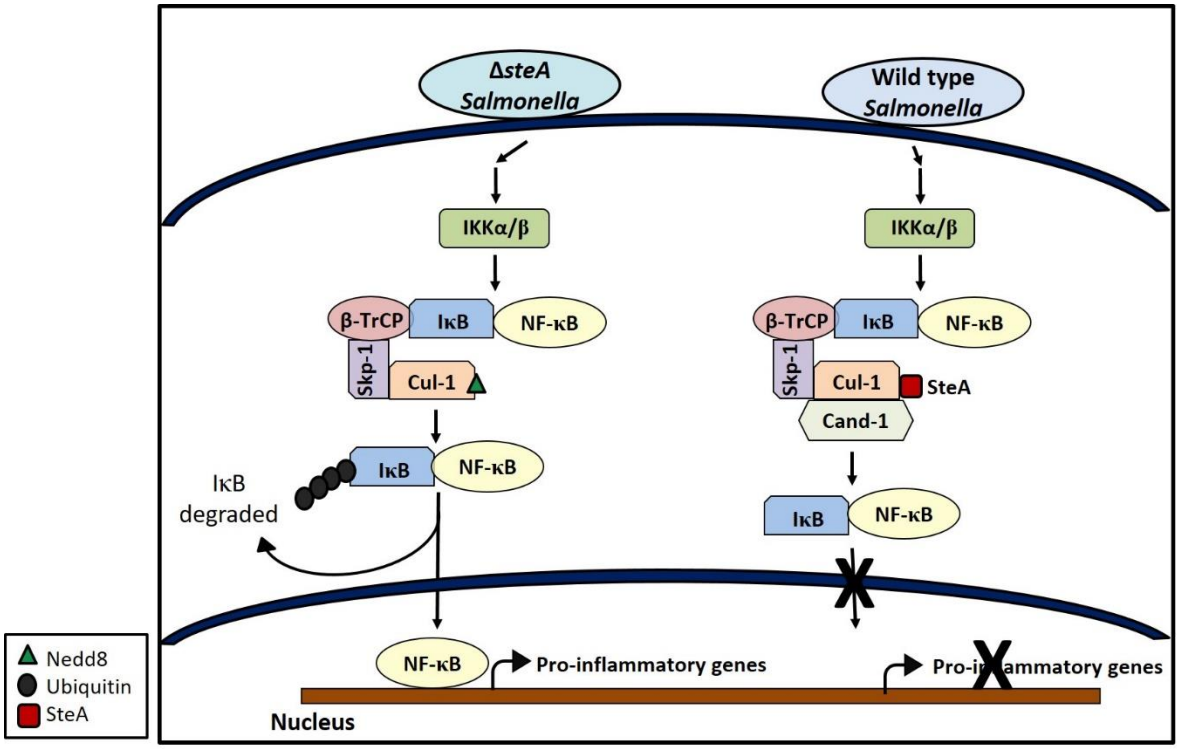

Illustration 10. SteA-mediated suppression of the NF-κB pathway

Upon infection with Δ*steA Salmonella*, a signalling cascade leads to the activation of IKKα/β which then phosphorylates IκB. Phosphorylated IκB is recognized by the SCF (Skp-1, Cullin-1 and F-box protein, β-TrCP). Cullin-1 of SCF complex is then neddylated leading to the activation of the E3 ligase thereby ubiquitinating IκB which is then degraded rendering NF-κB free to translocate to the nucleus leading to a pro-inflammatory response. However, in the presence of SteA, Cullin-1 neddylation is inhibited thereby suppressing the activation of the E3 ligase, hence, suppressing the pro-inflammatory response.

Altogether, this study shows that SteA binds to the Cullin-1/Cand-1 complex, thereby preventing the neddylation and Cand-1 dissociation from Cullin-1 resulting in lesser ubiquitination and degradation of IκB (Illustration 9). Since, SteA suppresses the degradation of IκB, it results in reduced activation of the transcription factor NF-κB leading to a reduced pro-inflammatory response by the host against *S.* Typhimurium.

Upon infection of the host by *S.* Typhimurium, an array of pro-inflammatory responses are induced in the host. These immune responses help in the eradication of the infecting pathogen. *S. typhimurium* is known to secrete various effectors like AvrA, GogB, SpvD, PipA, GogA etc. to suppress these pro-inflammatory responses (56-59, 190, 204). This host-modulation by the bacteria plays a very important role in helping the bacteria to survive and thereby replicate in

the host. This study shows that SteA is another effector which helps in the suppression of the host-immune responses which is a very crucial step in the pathogenesis of the *S.* Typhimurium.

Discussion

Infectious diseases are one of the leading causes of death worldwide and have claimed about 17 million deaths since 1995, according to WHO. Of these, about half of the deaths were caused by bacterial infections (https://www.who.int/whr/1996/media_centre/press_release/en/index1.html). Diarrheal diseases alone accounted for about 3.1 million deaths since 1995 (https://www.who.int/whr/1996/media_centre/press_release/en/index1.html). The major causes of diarrheal diseases include stomach flu, gastroenteritis and celiac diseases. *Salmonella* sp., *Shigella* sp., *Vibrio* sp., *Campylobacter* sp. and some strains of *E. coli* majorly cause bacterial gastroenteric diseases.

The interaction of pathogenic bacteria and the host immune system is a continuous tussle i.e. the host's immune cells recognize pathogenic bacteria and activate various immune processes which lead to clearing of the invading pathogen. The pathogenic bacteria, on the other hand, employ different strategies to modulate the host immune responses and establish an infection. The immune cells are equipped with specialized receptors called PRRs which recognize distinct patterns on the invading pathogen and thus, induce an inflammatory response against the pathogen (3). A common strategy employed by the bacteria is to hide from the host's immune system either by infecting and dividing in an inaccessible area of the body or by modulating its surface to portray as 'self' to the immune system. For example, *Neisseria meningitides* and *Haemophilus influenzae* form capsule around its surface to hide from the host's immune system (15). *Salmonella enterica* Typhimurium secretes enzymes which modify the lipid A on its surface thereby reducing its recognition by the immune cells (17). Also, some bacteria like *Staphylococcus aureus* and *Streptococcus pyrogenes* express Protein A and Protein G respectively, which bind to the Fc regions of the antibody, thereby making them ineffective against the bacteria. Some bacteria like *Shigella* sp. also induce pro-inflammatory responses in the intestine of the host to disrupt the epithelial barrier (206).

In this thesis work, we have studied how OmpU, an outer membrane protein of *Vibrio parahaemolyticus* and SteA, an effector of *Salmonella enterica* Typhimurium modulate host immune responses. Both *V. parahaemolyticus* and *S.* Typhimurium are Gram-negative bacteria which cause gastroenteritis in humans and may also be fatal to the host if left unchecked. *V. parahaemolyticus* may also cause septicaemia upon wound infections or in individuals with compromised immune systems. *S.* Typhimurium is highly similar to *S.* Typhi which causes typhoid in humans.

With the emergence of multi-drug resistant bacteria, newer vaccines and drugs need to be formulated to fight off these infections. Various outer membrane proteins are being tested for their vaccine potential. Some outer membrane proteins like OmpS1 of *S.* Typhi, OprA of *Pseudomonas aeruginosa* and OmpA of *Burkholderia pseudomallei* have been found to provide protection to mice against their respective infections (30, 110-112). Interestingly, OmpU of *V. parahaemolyticus* (VpOmpU) has also been found to be immunogenic in yellow croaker fish (117). However, a detailed immunological characterization was required to understand the vaccine potential of VpOmpU.

We found that VpOmpU induces a pro-inflammatory response in macrophages and monocytes. A pro-inflammatory response is characterized by the production of cytokines like TNFα and IL-6 (Figure 7). Outer membrane proteins of bacteria such as *S.* Typhi, *Haemophilus influenzae* and other *Vibrio* species like *V. cholerae* also induce pro-inflammatory responses in the host (29, 30, 46, 112). The generation of a pro-inflammatory response is a result of the recognition of the ligand by the PRRs present on the innate immune cells. Most of the bacterial ligands are recognized by toll-like receptors (TLRs). TLRs form homo- or hetero-dimers to recognize a PAMP and induce downstream signalling. For example, PorB of *Neisseria meningitidis* is recognized by TLR1/2 heterodimers (8) and OmpA of *Shigella flexineri* is recognized by TLR2/6 heterodimers (140). OmpU of *V. cholerae*, which shares about 70 % of sequence identity with VpOmpU has been shown to be recognized by TLR1/2 heterodimers in both monocytes and macrophages (127). Interestingly, VpOmpU was found to be recognized differently in monocytes and macrophages i.e. it was being recognized by TLR1/2 heterodimers in THP-1 monocytes (Figure 18) and by both TLR1/2 and TLR2/6 heterodimers in RAW 264.7 macrophages (Figure 17). This was the first report wherein a natural ligand was being recognized by different TLR-heterodimers. Previously, Pam_2CSK_4, a synthetic lipoprotein had been reported to be recognized by different TLR-heterodimers (141).

Upon probing the downstream signalling activated in response to VpOmpU, we found that MAP-kinases (p38 and JNK) (Figure 29) and transcription factors NF-κB and AP-1 were being activated in both the cell types (Figure 25-28). Porins of other bacteria namely *S.* Typhimurium, *Shigella flexineri*, *Haemophilus inflenzae*, etc. also induce NF-κB and AP-1 mediated activation of pro-inflammatory responses (140, 143, 144).

In addition to outer membrane proteins, an upcoming class of proteins which are being studied for their vaccine potential are the translocation effectors (207). Some bacteria like *Yersinia*,

Shigella and *Salmonella* are known to translocate effectors to the host cytoplasm via the type three secretion system (T3SS). These effectors modulate the host processes and help the pathogen in infection of the host cells. Since many of these effectors suppress host-immune responses, they are also being considered to be used as immune-therapeutics for various inflammatory disorders (207). However, a detailed characterization of these effectors and their roles in immune modulation needs to be carried out.

S. Typhimurium also secretes various effectors via the T3SS to modulate the host cells for its benefit. SteA is also a translocation effector and it has previously been shown to control the membrane dynamics of the *Salmonella* containing vacuole (SCV) (194), which the bacteria forms inside the cell to protect itself from the cell's environment and replicate. In this study, we have found that SteA suppresses the pro-inflammatory responses of the host by acting on the NF-κB activation pathway (Figure 35, 40, 41). Suppression of the pro-inflammatory responses is a common strategy used by various bacteria. *Yersinia* and *Shigella* also secrete effectors via T3SS to subdue host's pro-inflammatory responses. YopP/J of *Yersinia* suppresses both the MAP-kinase and the NF-κB pathway to suppress the pro-inflammatory response (52, 53). *Shigella flexineri* T3SS effector IpaH4.5 has also been shown to suppress the NF-κB mediated pro-inflammation (208). Other effectors of *S.* Typhimurium like PipA and SpvD have also been shown to act on NF-κB by cleaving RelA, an NF-κB family member and acting on the recycling of NF-κB respectively (190, 204) thereby suppressing the pro-inflammatory responses.

We further found that SteA acts on the IκB degradation pathway for this suppression (Figure 37-39). IκB is the inhibitor of NF-κB, which upon activation of the upstream signalling, is ubiquitinated and degraded by the proteasomal degradation system (4). Effectors of various bacteria have been shown to utilize ubiquitination or deubiquitination to modulate the host functions. IpaH9.8 of *Shigella flexineri* promotes ubiquitination and degradation of NEMO, which is involved in the activation of the NF-κB pathway, thereby suppressing NF-κB mediated pro-inflammation (209). YopJ of *Yersinia* sp. has been found to act on IκB as a deubiquitinase, thus preventing the nuclear translocation of NF-κB (51, 54). Some effectors of *S.* Typhimurium namely AvrA and SseL are also known to suppress the degradation and ubiquitination of IκB (59, 181).

The ubiquitination of a substrate like IκB involves a series of reactions involving E1 ubiquitin activating enzyme, E2 ubiquitin-conjugating enzyme and E3-ubiquitin ligase. The SCF (Skp-

1, Cullin-1, F-box protein)-E3 ubiquitin ligase is responsible for the ubiquitination of IκB (201). Some of the bacterial effectors like OspG of *Shigella* act on the E2 ubiquitin ligase which is involved in the ubiquitination of IκB, thereby suppressing the NF-κB mediated pro-inflammatory responses (49). Another *S.* Typhimurium effector, GogB binds to Skp-1 of the SCF-E3 ligase complex to suppress the pro-inflammatory responses (56). *Lactobacillus casei* is also known to down-regulate the transcription of Rbx-1, a component of the E3-ligase complex to suppress IκB degradation (210). In this study, we found that SteA binds to Cullin-1 of the SCF-E3 ubiquitin ligase and suppresses its neddylation to suppress the ubiquitination of IκB (Figure 46, 47). Interestingly, suppression of Cullin neddylation has been used as a mechanism to prevent immune activation by the commensal bacteria (211). This shows that *S.* Typhimurium seems to mimic the commensal bacterial mechanism to establish an infection in the host.

Altogether, this study on how ligands of two different bacteria modulate host immune responses sheds light on the diversity of strategies employed by the bacteria to establish an infection in the host. This further highlights the importance of understanding the mechanisms underlying these strategies, to be able to design vaccines or therapies using such bacterial ligands.

References

1. Murphy K, Weaver C. 2017. Janeway's immunobiology.
2. Janeway CA, Jr., Medzhitov R. 2002. Innate immune recognition. Annu Rev Immunol 20:197-216.
3. Mogensen TH. 2009. Pathogen recognition and inflammatory signaling in innate immune defenses. Clin Microbiol Rev 22:240-73, Table of Contents.
4. Akira S, Uematsu S, Takeuchi O. 2006. Pathogen recognition and innate immunity. Cell 124:783-801.
5. Kawasaki T, Kawai T. 2014. Toll-like receptor signaling pathways. Front Immunol 5:461.
6. Poltorak A, He X, Smirnova I, Liu MY, Van Huffel C, Du X, Birdwell D, Alejos E, Silva M, Galanos C, Freudenberg M, Ricciardi-Castagnoli P, Layton B, Beutler B. 1998. Defective LPS signaling in C3H/HeJ and C57BL/10ScCr mice: mutations in Tlr4 gene. Science 282:2085-8.
7. Cervantes-Barragan L, Gil-Cruz C, Pastelin-Palacios R, Lang KS, Isibasi A, Ludewig B, Lopez-Macias C. 2009. TLR2 and TLR4 signaling shapes specific antibody responses to Salmonella typhi antigens. Eur J Immunol 39:126-35.
8. Massari P, Visintin A, Gunawardana J, Halmen KA, King CA, Golenbock DT, Wetzler LM. 2006. Meningococcal porin PorB binds to TLR2 and requires TLR1 for signaling. J Immunol 176:2373-80.
9. Pore D, Mahata N, Chakrabarti MK. 2012. Outer membrane protein A (OmpA) of Shigella flexneri 2a links innate and adaptive immunity in a TLR2-dependent manner and involvement of IL-12 and nitric oxide. J Biol Chem 287:12589-601.
10. Medzhitov R. 2001. Toll-like receptors and innate immunity. Nat Rev Immunol 1:135-45.
11. Akira S, Takeda K, Kaisho T. 2001. Toll-like receptors: critical proteins linking innate and acquired immunity. Nat Immunol 2:675-80.
12. Yamamoto M, Sato S, Mori K, Hoshino K, Takeuchi O, Takeda K, Akira S. 2002. Cutting edge: a novel Toll/IL-1 receptor domain-containing adapter that preferentially activates the IFN-beta promoter in the Toll-like receptor signaling. J Immunol 169:6668-72.
13. Takeuchi O, Akira S. 2010. Pattern recognition receptors and inflammation. Cell 140:805-20.

14. Sakharwade SC, Prasad GV, Mukhopadhaya A. 2015. Immuno-modulatory role of porins: host immune responses, signaling mechanisms and vaccine potential. Adv Exp Med Biol 842:79-108.
15. Finlay BB, McFadden G. 2006. Anti-immunology: evasion of the host immune system by bacterial and viral pathogens. Cell 124:767-82.
16. Kawai T, Akira S. 2010. The role of pattern-recognition receptors in innate immunity: update on Toll-like receptors. Nat Immunol 11:373-84.
17. Kawasaki K, Ernst RK, Miller SI. 2005. Inhibition of Salmonella enterica serovar Typhimurium lipopolysaccharide deacylation by aminoarabinose membrane modification. J Bacteriol 187:2448-57.
18. Reynolds CM, Ribeiro AA, McGrath SC, Cotter RJ, Raetz CR, Trent MS. 2006. An outer membrane enzyme encoded by Salmonella typhimurium lpxR that removes the 3'-acyloxyacyl moiety of lipid A. J Biol Chem 281:21974-87.
19. Sawada N, Ogawa T, Asai Y, Makimura Y, Sugiyama A. 2007. Toll-like receptor 4-dependent recognition of structurally different forms of chemically synthesized lipid As of Porphyromonas gingivalis. Clin Exp Immunol 148:529-36.
20. Darveau RP, Pham TT, Lemley K, Reife RA, Bainbridge BW, Coats SR, Howald WN, Way SS, Hajjar AM. 2004. Porphyromonas gingivalis lipopolysaccharide contains multiple lipid A species that functionally interact with both toll-like receptors 2 and 4. Infect Immun 72:5041-51.
21. Celli J, Finlay BB. 2002. Bacterial avoidance of phagocytosis. Trends Microbiol 10:232-7.
22. Aepfelbacher M, Heesemann J. 2001. Modulation of Rho GTPases and the actin cytoskeleton by Yersinia outer proteins (Yops). Int J Med Microbiol 291:269-76.
23. Joseph B, Goebel W. 2007. Life of Listeria monocytogenes in the host cells' cytosol. Microbes Infect 9:1188-95.
24. Rohde KH, Abramovitch RB, Russell DG. 2007. Mycobacterium tuberculosis invasion of macrophages: linking bacterial gene expression to environmental cues. Cell Host Microbe 2:352-64.
25. Anderson CJ, Kendall MM. 2017. Salmonella enterica Serovar Typhimurium Strategies for Host Adaptation. Front Microbiol 8:1983.

26. Maurin M, Benoliel AM, Bongrand P, Raoult D. 1992. Phagolysosomes of Coxiella burnetii-infected cell lines maintain an acidic pH during persistent infection. Infect Immun 60:5013-6.
27. Woolard MD, Frelinger JA. 2008. Outsmarting the host: bacteria modulating the immune response. Immunol Res 41:188-202.
28. Ohkusa T, Yoshida T, Sato N, Watanabe S, Tajiri H, Okayasu I. 2009. Commensal bacteria can enter colonic epithelial cells and induce proinflammatory cytokine secretion: a possible pathogenic mechanism of ulcerative colitis. J Med Microbiol 58:535-45.
29. Galdiero M, Galdiero M, Finamore E, Rossano F, Gambuzza M, Catania MR, Teti G, Midiri A, Mancuso G. 2004. Haemophilus influenzae porin induces Toll-like receptor 2-mediated cytokine production in human monocytes and mouse macrophages. Infect Immun 72:1204-9.
30. Moreno-Eutimio MA, Tenorio-Calvo A, Pastelin-Palacios R, Perez-Shibayama C, Gil-Cruz C, Lopez-Santiago R, Baeza I, Fernandez-Mora M, Bonifaz L, Isibasi A, Calva E, Lopez-Macias C. 2013. Salmonella Typhi OmpS1 and OmpS2 porins are potent protective immunogens with adjuvant properties. Immunology 139:459-71.
31. Pasquevich KA, Garcia Samartino C, Coria LM, Estein SM, Zwerdling A, Ibanez AE, Barrionuevo P, Oliveira FS, Carvalho NB, Borkowski J, Oliveira SC, Warzecha H, Giambartolomei GH, Cassataro J. 2010. The protein moiety of Brucella abortus outer membrane protein 16 is a new bacterial pathogen-associated molecular pattern that activates dendritic cells in vivo, induces a Th1 immune response, and is a promising self-adjuvanting vaccine against systemic and oral acquired brucellosis. J Immunol 184:5200-12.
32. Alberti S, Marques G, Camprubi S, Merino S, Tomas JM, Vivanco F, Benedi VJ. 1993. C1q binding and activation of the complement classical pathway by Klebsiella pneumoniae outer membrane proteins. Infect Immun 61:852-60.
33. Bjerre A, Brusletto B, Mollnes TE, Fritzsonn E, Rosenqvist E, Wedege E, Namork E, Kierulf P, Brandtzaeg P. 2002. Complement activation induced by purified Neisseria meningitidis lipopolysaccharide (LPS), outer membrane vesicles, whole bacteria, and an LPS-free mutant. J Infect Dis 185:220-8.

34. Alberti S, Alvarez D, Merino S, Casado MT, Vivanco F, Tomas JM, Benedi VJ. 1996. Analysis of complement C3 deposition and degradation on Klebsiella pneumoniae. Infect Immun 64:4726-32.
35. Lewis LA, Ram S, Prasad A, Gulati S, Getzlaff S, Blom AM, Vogel U, Rice PA. 2008. Defining targets for complement components C4b and C3b on the pathogenic neisseriae. Infect Immun 76:339-50.
36. Bellinger-Kawahara C, Horwitz MA. 1990. Complement component C3 fixes selectively to the major outer membrane protein (MOMP) of Legionella pneumophila and mediates phagocytosis of liposome-MOMP complexes by human monocytes. J Exp Med 172:1201-10.
37. Cervantes-Barragan L, Kalinke U, Zust R, Konig M, Reizis B, Lopez-Macias C, Thiel V, Ludewig B. 2009. Type I IFN-mediated protection of macrophages and dendritic cells secures control of murine coronavirus infection. J Immunol 182:1099-106.
38. Elena G, Giovanna D, Brunella P, De Anna F, Alessandro M, Antonietta TM. 2009. Proinflammatory signal transduction pathway induced by Shigella flexneri porins in caco-2 cells. Braz J Microbiol 40:701-13.
39. Al-Bader T, Jolley KA, Humphries HE, Holloway J, Heckels JE, Semper AE, Friedmann PS, Christodoulides M. 2004. Activation of human dendritic cells by the PorA protein of Neisseria meningitidis. Cell Microbiol 6:651-62.
40. Singleton TE, Massari P, Wetzler LM. 2005. Neisserial porin-induced dendritic cell activation is MyD88 and TLR2 dependent. J Immunol 174:3545-50.
41. Galdiero M, Pisciotta MG, Galdiero E, Carratelli CR. 2003. Porins and lipopolysaccharide from Salmonella typhimurium regulate the expression of CD80 and CD86 molecules on B cells and macrophages but not CD28 and CD152 on T cells. Clin Microbiol Infect 9:1104-11.
42. Ray A, Biswas T. 2005. Porin of Shigella dysenteriae enhances Toll-like receptors 2 and 6 of mouse peritoneal B-2 cells and induces the expression of immunoglobulin M, immunoglobulin G2a and immunoglobulin A. Immunology 114:94-100.
43. Ray PG, Kelkar SD. 2004. Measurement of antirotavirus IgM/IgA/IgG responses in the serum samples of Indian children following rotavirus diarrhoea and their mothers. J Med Virol 72:416-23.

44. Snapper CM, Rosas FR, Kehry MR, Mond JJ, Wetzler LM. 1997. Neisserial porins may provide critical second signals to polysaccharide-activated murine B cells for induction of immunoglobulin secretion. Infect Immun 65:3203-8.
45. Wetzler LM, Ho Y, Reiser H. 1996. Neisserial porins induce B lymphocytes to express costimulatory B7-2 molecules and to proliferate. J Exp Med 183:1151-9.
46. Sakharwade SC, Sharma PK, Mukhopadhaya A. 2013. Vibrio cholerae porin OmpU induces pro-inflammatory responses, but down-regulates LPS-mediated effects in RAW 264.7, THP-1 and human PBMCs. PLoS One 8:e76583.
47. Gupta S, Prasad GV, Mukhopadhaya A. 2015. Vibrio cholerae Porin OmpU Induces Caspase-independent Programmed Cell Death upon Translocation to the Host Cell Mitochondria. J Biol Chem 290:31051-68.
48. Bruno VM, Hannemann S, Lara-Tejero M, Flavell RA, Kleinstein SH, Galan JE. 2009. Salmonella Typhimurium type III secretion effectors stimulate innate immune responses in cultured epithelial cells. PLoS Pathog 5:e1000538.
49. Kim DW, Lenzen G, Page AL, Legrain P, Sansonetti PJ, Parsot C. 2005. The Shigella flexneri effector OspG interferes with innate immune responses by targeting ubiquitin-conjugating enzymes. Proc Natl Acad Sci U S A 102:14046-51.
50. Ashida H, Sasakawa C. 2014. Shigella hacks host immune responses by reprogramming the host epigenome. EMBO J 33:2598-600.
51. Orth K, Xu Z, Mudgett MB, Bao ZQ, Palmer LE, Bliska JB, Mangel WF, Staskawicz B, Dixon JE. 2000. Disruption of signaling by Yersinia effector YopJ, a ubiquitin-like protein protease. Science 290:1594-7.
52. Palmer LE, Pancetti AR, Greenberg S, Bliska JB. 1999. YopJ of Yersinia spp. is sufficient to cause downregulation of multiple mitogen-activated protein kinases in eukaryotic cells. Infect Immun 67:708-16.
53. Thiefes A, Wolf A, Doerrie A, Grassl GA, Matsumoto K, Autenrieth I, Bohn E, Sakurai H, Niedenthal R, Resch K, Kracht M. 2006. The Yersinia enterocolitica effector YopP inhibits host cell signalling by inactivating the protein kinase TAK1 in the IL-1 signalling pathway. EMBO Rep 7:838-44.
54. Zhou H, Monack DM, Kayagaki N, Wertz I, Yin J, Wolf B, Dixit VM. 2005. Yersinia virulence factor YopJ acts as a deubiquitinase to inhibit NF-kappa B activation. J Exp Med 202:1327-32.

55. Lin SL, Le TX, Cowen DS. 2003. SptP, a Salmonella typhimurium type III-secreted protein, inhibits the mitogen-activated protein kinase pathway by inhibiting Raf activation. Cell Microbiol 5:267-75.
56. Pilar AV, Reid-Yu SA, Cooper CA, Mulder DT, Coombes BK. 2012. GogB is an anti-inflammatory effector that limits tissue damage during Salmonella infection through interaction with human FBXO22 and Skp1. PLoS Pathog 8:e1002773.
57. Collier-Hyams LS, Zeng H, Sun J, Tomlinson AD, Bao ZQ, Chen H, Madara JL, Orth K, Neish AS. 2002. Cutting edge: Salmonella AvrA effector inhibits the key proinflammatory, anti-apoptotic NF-kappa B pathway. J Immunol 169:2846-50.
58. Jones RM, Wu H, Wentworth C, Luo L, Collier-Hyams L, Neish AS. 2008. Salmonella AvrA Coordinates Suppression of Host Immune and Apoptotic Defenses via JNK Pathway Blockade. Cell Host Microbe 3:233-44.
59. Ye Z, Petrof EO, Boone D, Claud EC, Sun J. 2007. Salmonella effector AvrA regulation of colonic epithelial cell inflammation by deubiquitination. Am J Pathol 171:882-92.
60. Hilbi H, Moss JE, Hersh D, Chen Y, Arondel J, Banerjee S, Flavell RA, Yuan J, Sansonetti PJ, Zychlinsky A. 1998. Shigella-induced apoptosis is dependent on caspase-1 which binds to IpaB. J Biol Chem 273:32895-900.
61. Schotte P, Denecker G, Van Den Broeke A, Vandenabeele P, Cornelis GR, Beyaert R. 2004. Targeting Rac1 by the Yersinia effector protein YopE inhibits caspase-1-mediated maturation and release of interleukin-1beta. J Biol Chem 279:25134-42.
62. DePaola A, Kaysner CA, Bowers J, Cook DW. 2000. Environmental investigations of Vibrio parahaemolyticus in oysters after outbreaks in Washington, Texas, and New York (1997 and 1998). Appl Environ Microbiol 66:4649-54.
63. Alam MJ, Tomochika KI, Miyoshi SI, Shinoda S. 2002. Environmental investigation of potentially pathogenic Vibrio parahaemolyticus in the Seto-Inland Sea, Japan. FEMS Microbiol Lett 208:83-7.
64. Lozano-Leon A, Torres J, Osorio CR, Martinez-Urtaza J. 2003. Identification of tdh-positive Vibrio parahaemolyticus from an outbreak associated with raw oyster consumption in Spain. FEMS Microbiol Lett 226:281-4.
65. Martinez-Urtaza J, Simental L, Velasco D, DePaola A, Ishibashi M, Nakaguchi Y, Nishibuchi M, Carrera-Flores D, Rey-Alvarez C, Pousa A. 2005. Pandemic Vibrio parahaemolyticus O3:K6, Europe. Emerg Infect Dis 11:1319-20.

66. Chao G, Jiao X, Zhou X, Yang Z, Pan Z, Huang J, Zhou L, Qian X. 2009. Systematic functional pandemic strain-specific genes, three genomic islands, two T3SSs in foodborne, and clinical Vibrio parahaemolyticus isolates in China. Foodborne Pathog Dis 6:689-98.
67. Su YC, Liu C. 2007. Vibrio parahaemolyticus: a concern of seafood safety. Food Microbiol 24:549-58.
68. Chao G, Jiao X, Zhou X, Wang F, Yang Z, Huang J, Pan Z, Zhou L, Qian X. 2010. Distribution of genes encoding four pathogenicity islands (VPaIs), T6SS, biofilm, and type I pilus in food and clinical strains of Vibrio parahaemolyticus in China. Foodborne Pathog Dis 7:649-58.
69. Liu XM, Chen Y, Fan YX, Wang MQ. 2006. [Foodborne diseases occurred in 2003--report of the National Foodborne Diseases Surveillance System, China]. Wei Sheng Yan Jiu 35:201-4.
70. Broberg CA, Calder TJ, Orth K. 2011. Vibrio parahaemolyticus cell biology and pathogenicity determinants. Microbes Infect 13:992-1001.
71. Wang R, Fang S, Wu D, Lian J, Fan J, Zhang Y, Wang S, Lin W. 2012. Screening for a single-chain variable-fragment antibody that can effectively neutralize the cytotoxicity of the Vibrio parahaemolyticus thermolabile hemolysin. Appl Environ Microbiol 78:4967-75.
72. Wang R, Zhong Y, Gu X, Yuan J, Saeed AF, Wang S. 2015. The pathogenesis, detection, and prevention of Vibrio parahaemolyticus. Front Microbiol 6:144.
73. Raghunath P. 2014. Roles of thermostable direct hemolysin (TDH) and TDH-related hemolysin (TRH) in Vibrio parahaemolyticus. Front Microbiol 5:805.
74. Nishibuchi M, Fasano A, Russell RG, Kaper JB. 1992. Enterotoxigenicity of Vibrio parahaemolyticus with and without genes encoding thermostable direct hemolysin. Infect Immun 60:3539-45.
75. Nishibuchi M, Kumagai K, Kaper JB. 1991. Contribution of the tdh1 gene of Kanagawa phenomenon-positive Vibrio parahaemolyticus to production of extracellular thermostable direct hemolysin. Microb Pathog 11:453-60.
76. Matsuda S, Kodama T, Okada N, Okayama K, Honda T, Iida T. 2010. Association of Vibrio parahaemolyticus thermostable direct hemolysin with lipid rafts is essential for cytotoxicity but not hemolytic activity. Infect Immun 78:603-10.

77. Qadri F, Chowdhury NR, Takeda Y, Nair GB. 2005. Vibrio parahaemolyticus—Seafood Safety and Associations with Higher Organisms, p 277-295. *In* Belkin S, Colwell RR (ed), Oceans and Health: Pathogens in the Marine Environment doi:10.1007/0-387-23709-7_11. Springer US, Boston, MA.
78. Takahashi A, Kenjyo N, Imura K, Myonsun Y, Honda T. 2000. Cl(-) secretion in colonic epithelial cells induced by the vibrio parahaemolyticus hemolytic toxin related to thermostable direct hemolysin. Infect Immun 68:5435-8.
79. Xu M, Yamamoto K, Honda T, Ming X. 1994. Construction and characterization of an isogenic mutant of Vibrio parahaemolyticus having a deletion in the thermostable direct hemolysin-related hemolysin gene (trh). J Bacteriol 176:4757-60.
80. Park KS, Ono T, Rokuda M, Jang MH, Okada K, Iida T, Honda T. 2004. Functional characterization of two type III secretion systems of Vibrio parahaemolyticus. Infect Immun 72:6659-65.
81. Bej AK, Patterson DP, Brasher CW, Vickery MC, Jones DD, Kaysner CA. 1999. Detection of total and hemolysin-producing Vibrio parahaemolyticus in shellfish using multiplex PCR amplification of tl, tdh and trh. J Microbiol Methods 36:215-25.
82. Wang L, Shi L, Su J, Ye Y, Zhong Q. 2013. Detection of Vibrio parahaemolyticus in food samples using in situ loop-mediated isothermal amplification method. Gene 515:421-5.
83. McCarthy SA, DePaola A, Cook DW, Kaysner CA, Hill WE. 1999. Evaluation of alkaline phosphatase- and digoxigenin-labelled probes for detection of the thermolabile hemolysin (tlh) gene of Vibrio parahaemolyticus. Lett Appl Microbiol 28:66-70.
84. Dai JH, Lee YS, Wong HC. 1992. Effects of iron limitation on production of a siderophore, outer membrane proteins, and hemolysin and on hydrophobicity, cell adherence, and lethality for mice of Vibrio parahaemolyticus. Infect Immun 60:2952-6.
85. Funahashi T, Moriya K, Uemura S, Miyoshi S, Shinoda S, Narimatsu S, Yamamoto S. 2002. Identification and characterization of pvuA, a gene encoding the ferric vibrioferrin receptor protein in Vibrio parahaemolyticus. J Bacteriol 184:936-46.
86. Mao Z, Yu L, You Z, Wei Y, Liu Y. 2007. Expression and immunogenicity analysis of two iron-regulated outer membrane proteins of Vibrio parahaemolyticus. Acta Biochim Biophys Sin (Shanghai) 39:763-9.

87. Ganz T. 2003. Defensins: antimicrobial peptides of innate immunity. Nat Rev Immunol 3:710-20.
88. Shen CJ, Kuo TY, Lin CC, Chow LP, Chen WJ. 2010. Proteomic identification of membrane proteins regulating antimicrobial peptide resistance in Vibrio parahaemolyticus. J Appl Microbiol 108:1398-407.
89. Morita Y, Kodama K, Shiota S, Mine T, Kataoka A, Mizushima T, Tsuchiya T. 1998. NorM, a putative multidrug efflux protein, of Vibrio parahaemolyticus and its homolog in Escherichia coli. Antimicrob Agents Chemother 42:1778-82.
90. Nozaki K, Kuroda T, Mizushima T, Tsuchiya T. 1998. A new Na+/H+ antiporter, NhaD, of Vibrio parahaemolyticus. Biochim Biophys Acta 1369:213-20.
91. Chen J, Morita Y, Huda MN, Kuroda T, Mizushima T, Tsuchiya T. 2002. VmrA, a member of a novel class of Na(+)-coupled multidrug efflux pumps from Vibrio parahaemolyticus. J Bacteriol 184:572-6.
92. Krachler AM, Ham H, Orth K. 2011. Outer membrane adhesion factor multivalent adhesion molecule 7 initiates host cell binding during infection by gram-negative pathogens. Proc Natl Acad Sci U S A 108:11614-9.
93. Jiang W, Han X, Wang Q, Li X, Yi L, Liu Y, Ding C. 2014. Vibrio parahaemolyticus enolase is an adhesion-related factor that binds plasminogen and functions as a protective antigen. Appl Microbiol Biotechnol 98:4937-48.
94. Sreelatha A, Bennett TL, Zheng H, Jiang QX, Orth K, Starai VJ. 2013. Vibrio effector protein, VopQ, forms a lysosomal gated channel that disrupts host ion homeostasis and autophagic flux. Proc Natl Acad Sci U S A 110:11559-64.
95. Matsuda S, Okada N, Kodama T, Honda T, Iida T. 2012. A cytotoxic type III secretion effector of Vibrio parahaemolyticus targets vacuolar H+-ATPase subunit c and ruptures host cell lysosomes. PLoS Pathog 8:e1002803.
96. Casselli T, Lynch T, Southward CM, Jones BW, DeVinney R. 2008. Vibrio parahaemolyticus inhibition of Rho family GTPase activation requires a functional chromosome I type III secretion system. Infect Immun 76:2202-11.
97. Yarbrough ML, Li Y, Kinch LN, Grishin NV, Ball HL, Orth K. 2009. AMPylation of Rho GTPases by Vibrio VopS disrupts effector binding and downstream signaling. Science 323:269-72.

98. Luong P, Kinch LN, Brautigam CA, Grishin NV, Tomchick DR, Orth K. 2010. Kinetic and structural insights into the mechanism of AMPylation by VopS Fic domain. J Biol Chem 285:20155-63.
99. Liverman AD, Cheng HC, Trosky JE, Leung DW, Yarbrough ML, Burdette DL, Rosen MK, Orth K. 2007. Arp2/3-independent assembly of actin by Vibrio type III effector VopL. Proc Natl Acad Sci U S A 104:17117-22.
100. Zhang L, Krachler AM, Broberg CA, Li Y, Mirzaei H, Gilpin CJ, Orth K. 2012. Type III effector VopC mediates invasion for Vibrio species. Cell Rep 1:453-60.
101. Haglund CM, Welch MD. 2011. Pathogens and polymers: microbe-host interactions illuminate the cytoskeleton. J Cell Biol 195:7-17.
102. Hiyoshi H, Kodama T, Saito K, Gotoh K, Matsuda S, Akeda Y, Honda T, Iida T. 2011. VopV, an F-actin-binding type III secretion effector, is required for Vibrio parahaemolyticus-induced enterotoxicity. Cell Host Microbe 10:401-9.
103. Trosky JE, Mukherjee S, Burdette DL, Roberts M, McCarter L, Siegel RM, Orth K. 2004. Inhibition of MAPK signaling pathways by VopA from Vibrio parahaemolyticus. J Biol Chem 279:51953-7.
104. Kajino-Sakamoto R, Omori E, Nighot PK, Blikslager AT, Matsumoto K, Ninomiya-Tsuji J. 2010. TGF-beta-activated kinase 1 signaling maintains intestinal integrity by preventing accumulation of reactive oxygen species in the intestinal epithelium. J Immunol 185:4729-37.
105. Zhou X, Gewurz BE, Ritchie JM, Takasaki K, Greenfeld H, Kieff E, Davis BM, Waldor MK. 2013. A Vibrio parahaemolyticus T3SS effector mediates pathogenesis by independently enabling intestinal colonization and inhibiting TAK1 activation. Cell Rep 3:1690-702.
106. Xu C, Ren H, Wang S, Peng X. 2004. Proteomic analysis of salt-sensitive outer membrane proteins of Vibrio parahaemolyticus. Res Microbiol 155:835-42.
107. Whitaker WB, Parent MA, Boyd A, Richards GP, Boyd EF. 2012. The Vibrio parahaemolyticus ToxRS regulator is required for stress tolerance and colonization in a novel orogastric streptomycin-induced adult murine model. Infect Immun 80:1834-45.
108. Lin Z, Kumagai K, Baba K, Mekalanos JJ, Nishibuchi M. 1993. Vibrio parahaemolyticus has a homolog of the Vibrio cholerae toxRS operon that mediates

environmentally induced regulation of the thermostable direct hemolysin gene. J Bacteriol 175:3844-55.

109. Zhu W, Thomas CE, Sparling PF. 2004. DNA immunization of mice with a plasmid encoding Neisseria gonorrhea PorB protein by intramuscular injection and epidermal particle bombardment. Vaccine 22:660-9.

110. von Specht BU, Knapp B, Muth G, Broker M, Hungerer KD, Diehl KD, Massarrat K, Seemann A, Domdey H. 1995. Protection of immunocompromised mice against lethal infection with Pseudomonas aeruginosa by active or passive immunization with recombinant P. aeruginosa outer membrane protein F and outer membrane protein I fusion proteins. Infect Immun 63:1855-62.

111. Hara Y, Mohamed R, Nathan S. 2009. Immunogenic Burkholderia pseudomallei outer membrane proteins as potential candidate vaccine targets. PLoS One 4:e6496.

112. Isibasi A, Ortiz V, Vargas M, Paniagua J, Gonzalez C, Moreno J, Kumate J. 1988. Protection against Salmonella typhi infection in mice after immunization with outer membrane proteins isolated from Salmonella typhi 9,12,d, Vi. Infect Immun 56:2953-9.

113. Li N, Yang Z, Bai J, Fu X, Liu L, Shi C, Wu S. 2010. A shared antigen among Vibrio species: outer membrane protein-OmpK as a versatile Vibriosis vaccine candidate in Orange-spotted grouper (Epinephelus coioides). Fish Shellfish Immunol 28:952-6.

114. Qian R, Chu W, Mao Z, Zhang C, Wei Y, Yu L. 2007. Expression, characterization and immunogenicity of a major outer membrane protein from Vibrio alginolyticus. Acta Biochim Biophys Sin (Shanghai) 39:194-200.

115. Leitner DR, Feichter S, Schild-Prufert K, Rechberger GN, Reidl J, Schild S. 2013. Lipopolysaccharide modifications of a cholera vaccine candidate based on outer membrane vesicles reduce endotoxicity and reveal the major protective antigen. Infect Immun 81:2379-93.

116. Schild S, Nelson EJ, Camilli A. 2008. Immunization with Vibrio cholerae outer membrane vesicles induces protective immunity in mice. Infect Immun 76:4554-63.

117. Mao Z, Yu L, You Z, Wei Y, Liu Y. 2007. Cloning, expression and immunogenicty analysis of five outer membrane proteins of Vibrio parahaemolyticus zj2003. Fish Shellfish Immunol 23:567-75.

118. Li C, Ye Z, Wen L, Chen R, Tian L, Zhao F, Pan J. 2014. Identification of a novel vaccine candidate by immunogenic screening of Vibrio parahaemolyticus outer membrane proteins. Vaccine 32:6115-21.
119. Cai SH, Lu YS, Wu ZH, Jian JC. 2013. Cloning, expression of Vibrio alginolyticus outer membrane protein-OmpU gene and its potential application as vaccine in crimson snapper, Lutjanus erythropterus Bloch. J Fish Dis 36:695-702.
120. Xiong XP, Zhang BW, Yang MJ, Ye MZ, Peng XX, Li H. 2010. Identification of vaccine candidates from differentially expressed outer membrane proteins of Vibrio alginolyticus in response to NaCl and iron limitation. Fish Shellfish Immunol 29:810-6.
121. Duperthuy M, Binesse J, Le Roux F, Romestand B, Caro A, Got P, Givaudan A, Mazel D, Bachere E, Destoumieux-Garzon D. 2010. The major outer membrane protein OmpU of Vibrio splendidus contributes to host antimicrobial peptide resistance and is required for virulence in the oyster Crassostrea gigas. Environ Microbiol 12:951-63.
122. Goo SY, Lee HJ, Kim WH, Han KL, Park DK, Lee HJ, Kim SM, Kim KS, Lee KH, Park SJ. 2006. Identification of OmpU of Vibrio vulnificus as a fibronectin-binding protein and its role in bacterial pathogenesis. Infect Immun 74:5586-94.
123. Duperthuy M, Schmitt P, Garzon E, Caro A, Rosa RD, Le Roux F, Lautredou-Audouy N, Got P, Romestand B, de Lorgeril J, Kieffer-Jaquinod S, Bachere E, Destoumieux-Garzon D. 2011. Use of OmpU porins for attachment and invasion of Crassostrea gigas immune cells by the oyster pathogen Vibrio splendidus. Proc Natl Acad Sci U S A 108:2993-8.
124. Mathur J, Waldor MK. 2004. The Vibrio cholerae ToxR-regulated porin OmpU confers resistance to antimicrobial peptides. Infect Immun 72:3577-83.
125. Provenzano D, Schuhmacher DA, Barker JL, Klose KE. 2000. The virulence regulatory protein ToxR mediates enhanced bile resistance in Vibrio cholerae and other pathogenic Vibrio species. Infect Immun 68:1491-7.
126. Wibbenmeyer JA, Provenzano D, Landry CF, Klose KE, Delcour AH. 2002. Vibrio cholerae OmpU and OmpT porins are differentially affected by bile. Infect Immun 70:121-6.
127. Khan J, Sharma PK, Mukhopadhaya A. 2015. Vibrio cholerae porin OmpU mediates M1-polarization of macrophages/monocytes via TLR1/TLR2 activation. Immunobiology doi:10.1016/j.imbio.2015.06.009.

128. Prasad G, Dhar V, Mukhopadhaya A. 2019. Vibrio cholerae OmpU Mediates CD36-Dependent Reactive Oxygen Species Generation Triggering an Additional Pathway of MAPK Activation in Macrophages. J Immunol 202:2431-2450.
129. Nikaido H, Rosenberg EY. 1983. Porin channels in Escherichia coli: studies with liposomes reconstituted from purified proteins. J Bacteriol 153:241-52.
130. Makino K, Oshima K, Kurokawa K, Yokoyama K, Uda T, Tagomori K, Iijima Y, Najima M, Nakano M, Yamashita A, Kubota Y, Kimura S, Yasunaga T, Honda T, Shinagawa H, Hattori M, Iida T. 2003. Genome sequence of Vibrio parahaemolyticus: a pathogenic mechanism distinct from that of V cholerae. Lancet 361:743-9.
131. Pathania M, Acosta-Gutierrez S, Bhamidimarri SP, Basle A, Winterhalter M, Ceccarelli M, van den Berg B. 2018. Unusual Constriction Zones in the Major Porins OmpU and OmpT from Vibrio cholerae. Structure 26:708-721 e4.
132. Bogdan C. 2001. Nitric oxide and the immune response. Nat Immunol 2:907-16.
133. MacMicking J, Xie QW, Nathan C. 1997. Nitric oxide and macrophage function. Annu Rev Immunol 15:323-50.
134. Oeckinghaus A, Ghosh S. 2009. The NF-kappaB family of transcription factors and its regulation. Cold Spring Harb Perspect Biol 1:a000034.
135. Zenz R, Eferl R, Scheinecker C, Redlich K, Smolen J, Schonthaler HB, Kenner L, Tschachler E, Wagner EF. 2008. Activator protein 1 (Fos/Jun) functions in inflammatory bone and skin disease. Arthritis Res Ther 10:201.
136. Wang Q, Chen J, Liu R, Jia J. 2011. Identification and evaluation of an outer membrane protein OmpU from a pathogenic Vibrio harveyi isolate as vaccine candidate in turbot (Scophthalmus maximus). Lett Appl Microbiol 53:22-9.
137. Massari P, Henneke P, Ho Y, Latz E, Golenbock DT, Wetzler LM. 2002. Cutting edge: Immune stimulation by neisserial porins is toll-like receptor 2 and MyD88 dependent. J Immunol 168:1533-7.
138. Botos I, Segal DM, Davies DR. 2011. The structural biology of Toll-like receptors. Structure 19:447-59.
139. Oosting M, Ter Hofstede H, Sturm P, Adema GJ, Kullberg BJ, van der Meer JW, Netea MG, Joosten LA. 2011. TLR1/TLR2 heterodimers play an important role in the recognition of Borrelia spirochetes. PLoS One 6:e25998.

140. Bhowmick R, Pore D, Chakrabarti MK. 2014. Outer membrane protein A (OmpA) of Shigella flexneri 2a induces TLR2-mediated activation of B cells: involvement of protein tyrosine kinase, ERK and NF-kappaB. PLoS One 9:e109107.
141. Buwitt-Beckmann U, Heine H, Wiesmuller KH, Jung G, Brock R, Akira S, Ulmer AJ. 2005. Toll-like receptor 6-independent signaling by diacylated lipopeptides. Eur J Immunol 35:282-9.
142. Farhat K, Riekenberg S, Heine H, Debarry J, Lang R, Mages J, Buwitt-Beckmann U, Roschmann K, Jung G, Wiesmuller KH, Ulmer AJ. 2008. Heterodimerization of TLR2 with TLR1 or TLR6 expands the ligand spectrum but does not lead to differential signaling. J Leukoc Biol 83:692-701.
143. Galdiero M, Vitiello M, Sanzari E, D'Isanto M, Tortora A, Longanella A, Galdiero S. 2002. Porins from Salmonella enterica serovar Typhimurium activate the transcription factors activating protein 1 and NF-kappaB through the Raf-1-mitogen-activated protein kinase cascade. Infect Immun 70:558-68.
144. Galdiero S, Capasso D, Vitiello M, D'Isanto M, Pedone C, Galdiero M. 2003. Role of surface-exposed loops of Haemophilus influenzae protein P2 in the mitogen-activated protein kinase cascade. Infect Immun 71:2798-809.
145. LaRock DL, Chaudhary A, Miller SI. 2015. Salmonellae interactions with host processes. Nat Rev Microbiol 13:191-205.
146. Scanu T, Spaapen RM, Bakker JM, Pratap CB, Wu LE, Hofland I, Broeks A, Shukla VK, Kumar M, Janssen H, Song JY, Neefjes-Borst EA, te Riele H, Holden DW, Nath G, Neefjes J. 2015. Salmonella Manipulation of Host Signaling Pathways Provokes Cellular Transformation Associated with Gallbladder Carcinoma. Cell Host Microbe 17:763-74.
147. Winter SE, Thiennimitr P, Winter MG, Butler BP, Huseby DL, Crawford RW, Russell JM, Bevins CL, Adams LG, Tsolis RM, Roth JR, Baumler AJ. 2010. Gut inflammation provides a respiratory electron acceptor for Salmonella. Nature 467:426-9.
148. Jones BD, Ghori N, Falkow S. 1994. Salmonella typhimurium initiates murine infection by penetrating and destroying the specialized epithelial M cells of the Peyer's patches. J Exp Med 180:15-23.
149. Kubori T, Matsushima Y, Nakamura D, Uralil J, Lara-Tejero M, Sukhan A, Galan JE, Aizawa SI. 1998. Supramolecular structure of the Salmonella typhimurium type III protein secretion system. Science 280:602-5.

150. Galan JE. 1999. Interaction of Salmonella with host cells through the centisome 63 type III secretion system. Curr Opin Microbiol 2:46-50.
151. Galan JE. 1996. Molecular genetic bases of Salmonella entry into host cells. Mol Microbiol 20:263-71.
152. Ochman H, Soncini FC, Solomon F, Groisman EA. 1996. Identification of a pathogenicity island required for Salmonella survival in host cells. Proc Natl Acad Sci U S A 93:7800-4.
153. Hu B, Lara-Tejero M, Kong Q, Galan JE, Liu J. 2017. In Situ Molecular Architecture of the Salmonella Type III Secretion Machine. Cell 168:1065-1074 e10.
154. McGhie EJ, Brawn LC, Hume PJ, Humphreys D, Koronakis V. 2009. Salmonella takes control: effector-driven manipulation of the host. Curr Opin Microbiol 12:117-24.
155. Shea JE, Hensel M, Gleeson C, Holden DW. 1996. Identification of a virulence locus encoding a second type III secretion system in Salmonella typhimurium. Proc Natl Acad Sci U S A 93:2593-7.
156. Eichelberg K, Galan JE. 1999. Differential regulation of Salmonella typhimurium type III secreted proteins by pathogenicity island 1 (SPI-1)-encoded transcriptional activators InvF and hilA. Infect Immun 67:4099-105.
157. Bakowski MA, Braun V, Lam GY, Yeung T, Heo WD, Meyer T, Finlay BB, Grinstein S, Brumell JH. 2010. The phosphoinositide phosphatase SopB manipulates membrane surface charge and trafficking of the Salmonella-containing vacuole. Cell Host Microbe 7:453-62.
158. Hapfelmeier S, Ehrbar K, Stecher B, Barthel M, Kremer M, Hardt WD. 2004. Role of the Salmonella pathogenicity island 1 effector proteins SipA, SopB, SopE, and SopE2 in Salmonella enterica subspecies 1 serovar Typhimurium colitis in streptomycin-pretreated mice. Infect Immun 72:795-809.
159. Myeni SK, Zhou D. 2010. The C terminus of SipC binds and bundles F-actin to promote Salmonella invasion. J Biol Chem 285:13357-63.
160. Murli S, Watson RO, Galan JE. 2001. Role of tyrosine kinases and the tyrosine phosphatase SptP in the interaction of Salmonella with host cells. Cell Microbiol 3:795-810.
161. Mallo GV, Espina M, Smith AC, Terebiznik MR, Aleman A, Finlay BB, Rameh LE, Grinstein S, Brumell JH. 2008. SopB promotes phosphatidylinositol 3-phosphate

formation on Salmonella vacuoles by recruiting Rab5 and Vps34. J Cell Biol 182:741-52.

162. Humphreys D, Hume PJ, Koronakis V. 2009. The Salmonella effector SptP dephosphorylates host AAA+ ATPase VCP to promote development of its intracellular replicative niche. Cell Host Microbe 5:225-33.

163. Du F, Galan JE. 2009. Selective inhibition of type III secretion activated signaling by the Salmonella effector AvrA. PLoS Pathog 5:e1000595.

164. Knodler LA, Finlay BB, Steele-Mortimer O. 2005. The Salmonella effector protein SopB protects epithelial cells from apoptosis by sustained activation of Akt. J Biol Chem 280:9058-64.

165. Hersh D, Monack DM, Smith MR, Ghori N, Falkow S, Zychlinsky A. 1999. The Salmonella invasin SipB induces macrophage apoptosis by binding to caspase-1. Proc Natl Acad Sci U S A 96:2396-401.

166. Miao EA, Alpuche-Aranda CM, Dors M, Clark AE, Bader MW, Miller SI, Aderem A. 2006. Cytoplasmic flagellin activates caspase-1 and secretion of interleukin 1beta via Ipaf. Nat Immunol 7:569-75.

167. Miao EA, Andersen-Nissen E, Warren SE, Aderem A. 2007. TLR5 and Ipaf: dual sensors of bacterial flagellin in the innate immune system. Semin Immunopathol 29:275-88.

168. Miao EA, Mao DP, Yudkovsky N, Bonneau R, Lorang CG, Warren SE, Leaf IA, Aderem A. 2010. Innate immune detection of the type III secretion apparatus through the NLRC4 inflammasome. Proc Natl Acad Sci U S A 107:3076-80.

169. Hensel M, Shea JE, Waterman SR, Mundy R, Nikolaus T, Banks G, Vazquez-Torres A, Gleeson C, Fang FC, Holden DW. 1998. Genes encoding putative effector proteins of the type III secretion system of Salmonella pathogenicity island 2 are required for bacterial virulence and proliferation in macrophages. Mol Microbiol 30:163-74.

170. Brumell JH, Goosney DL, Finlay BB. 2002. SifA, a type III secreted effector of Salmonella typhimurium, directs Salmonella-induced filament (Sif) formation along microtubules. Traffic 3:407-15.

171. Ohlson MB, Huang Z, Alto NM, Blanc MP, Dixon JE, Chai J, Miller SI. 2008. Structure and function of Salmonella SifA indicate that its interactions with SKIP, SseJ, and RhoA family GTPases induce endosomal tubulation. Cell Host Microbe 4:434-46.

172. Ruiz-Albert J, Yu XJ, Beuzon CR, Blakey AN, Galyov EE, Holden DW. 2002. Complementary activities of SseJ and SifA regulate dynamics of the Salmonella typhimurium vacuolar membrane. Mol Microbiol 44:645-61.

173. Miao EA, Brittnacher M, Haraga A, Jeng RL, Welch MD, Miller SI. 2003. Salmonella effectors translocated across the vacuolar membrane interact with the actin cytoskeleton. Mol Microbiol 48:401-15.

174. Kuhle V, Hensel M. 2002. SseF and SseG are translocated effectors of the type III secretion system of Salmonella pathogenicity island 2 that modulate aggregation of endosomal compartments. Cell Microbiol 4:813-24.

175. Meresse S, Unsworth KE, Habermann A, Griffiths G, Fang F, Martinez-Lorenzo MJ, Waterman SR, Gorvel JP, Holden DW. 2001. Remodelling of the actin cytoskeleton is essential for replication of intravacuolar Salmonella. Cell Microbiol 3:567-77.

176. Poh J, Odendall C, Spanos A, Boyle C, Liu M, Freemont P, Holden DW. 2008. SteC is a Salmonella kinase required for SPI-2-dependent F-actin remodelling. Cell Microbiol 10:20-30.

177. Worley MJ, Nieman GS, Geddes K, Heffron F. 2006. Salmonella typhimurium disseminates within its host by manipulating the motility of infected cells. Proc Natl Acad Sci U S A 103:17915-20.

178. Lesnick ML, Reiner NE, Fierer J, Guiney DG. 2001. The Salmonella spvB virulence gene encodes an enzyme that ADP-ribosylates actin and destabilizes the cytoskeleton of eukaryotic cells. Mol Microbiol 39:1464-70.

179. Rytkonen A, Poh J, Garmendia J, Boyle C, Thompson A, Liu M, Freemont P, Hinton JC, Holden DW. 2007. SseL, a Salmonella deubiquitinase required for macrophage killing and virulence. Proc Natl Acad Sci U S A 104:3502-7.

180. Haraga A, Miller SI. 2006. A Salmonella type III secretion effector interacts with the mammalian serine/threonine protein kinase PKN1. Cell Microbiol 8:837-46.

181. Le Negrate G, Faustin B, Welsh K, Loeffler M, Krajewska M, Hasegawa P, Mukherjee S, Orth K, Krajewski S, Godzik A, Guiney DG, Reed JC. 2008. Salmonella secreted factor L deubiquitinase of Salmonella typhimurium inhibits NF-kappaB, suppresses IkappaBalpha ubiquitination and modulates innate immune responses. J Immunol 180:5045-56.

182. Chu Y, Gao S, Wang T, Yan J, Xu G, Li Y, Niu H, Huang R, Wu S. 2016. A novel contribution of spvB to pathogenesis of Salmonella Typhimurium by inhibiting autophagy in host cells. Oncotarget 7:8295-309.
183. Halici S, Zenk SF, Jantsch J, Hensel M. 2008. Functional analysis of the Salmonella pathogenicity island 2-mediated inhibition of antigen presentation in dendritic cells. Infect Immun 76:4924-33.
184. Jiang X, Rossanese OW, Brown NF, Kujat-Choy S, Galan JE, Finlay BB, Brumell JH. 2004. The related effector proteins SopD and SopD2 from Salmonella enterica serovar Typhimurium contribute to virulence during systemic infection of mice. Mol Microbiol 54:1186-98.
185. Lawley TD, Chan K, Thompson LJ, Kim CC, Govoni GR, Monack DM. 2006. Genome-wide screen for Salmonella genes required for long-term systemic infection of the mouse. PLoS Pathog 2:e11.
186. Wachtel R, Brauning B, Mader SL, Ecker F, Kaila VRI, Groll M, Itzen A. 2018. The protease GtgE from Salmonella exclusively targets inactive Rab GTPases. Nat Commun 9:44.
187. Knodler LA, Steele-Mortimer O. 2005. The Salmonella effector PipB2 affects late endosome/lysosome distribution to mediate Sif extension. Mol Biol Cell 16:4108-23.
188. Bernal-Bayard J, Ramos-Morales F. 2009. Salmonella type III secretion effector SlrP is an E3 ubiquitin ligase for mammalian thioredoxin. J Biol Chem 284:27587-95.
189. Mazurkiewicz P, Thomas J, Thompson JA, Liu M, Arbibe L, Sansonetti P, Holden DW. 2008. SpvC is a Salmonella effector with phosphothreonine lyase activity on host mitogen-activated protein kinases. Mol Microbiol 67:1371-83.
190. Rolhion N, Furniss RC, Grabe G, Ryan A, Liu M, Matthews SA, Holden DW. 2016. Inhibition of Nuclear Transport of NF-kB p65 by the Salmonella Type III Secretion System Effector SpvD. PLoS Pathog 12:e1005653.
191. Geddes K, Worley M, Niemann G, Heffron F. 2005. Identification of new secreted effectors in Salmonella enterica serovar Typhimurium. Infect Immun 73:6260-71.
192. Figueira R, Watson KG, Holden DW, Helaine S. 2013. Identification of salmonella pathogenicity island-2 type III secretion system effectors involved in intramacrophage replication of S. enterica serovar typhimurium: implications for rational vaccine design. MBio 4:e00065.

193. Cardenal-Munoz E, Gutierrez G, Ramos-Morales F. 2014. Global impact of Salmonella type III secretion effector SteA on host cells. Biochem Biophys Res Commun 449:419-24.
194. Domingues L, Holden DW, Mota LJ. 2014. The Salmonella effector SteA contributes to the control of membrane dynamics of Salmonella-containing vacuoles. Infect Immun 82:2923-34.
195. Domingues L, Ismail A, Charro N, Rodriguez-Escudero I, Holden DW, Molina M, Cid VJ, Mota LJ. 2016. The Salmonella effector SteA binds phosphatidylinositol 4-phosphate for subcellular targeting within host cells. Cell Microbiol 18:949-69.
196. Baison-Olmo F, Cardenal-Munoz E, Ramos-Morales F. 2012. PipB2 is a substrate of the Salmonella pathogenicity island 1-encoded type III secretion system. Biochem Biophys Res Commun 423:240-6.
197. Datsenko KA, Wanner BL. 2000. One-step inactivation of chromosomal genes in Escherichia coli K-12 using PCR products. Proc Natl Acad Sci U S A 97:6640-5.
198. Shrum B, Anantha RV, Xu SX, Donnelly M, Haeryfar SM, McCormick JK, Mele T. 2014. A robust scoring system to evaluate sepsis severity in an animal model. BMC Res Notes 7:233.
199. Cardenal-Munoz E, Ramos-Morales F. 2011. Analysis of the expression, secretion and translocation of the Salmonella enterica type III secretion system effector SteA. PLoS One 6:e26930.
200. Deshaies RJ. 1999. SCF and Cullin/Ring H2-based ubiquitin ligases. Annu Rev Cell Dev Biol 15:435-67.
201. Kanarek N, London N, Schueler-Furman O, Ben-Neriah Y. 2010. Ubiquitination and degradation of the inhibitors of NF-kappaB. Cold Spring Harb Perspect Biol 2:a000166.
202. Petroski MD, Deshaies RJ. 2005. Function and regulation of cullin-RING ubiquitin ligases. Nat Rev Mol Cell Biol 6:9-20.
203. Murphy K, Weaver C. 2016. Janeway's Immunobiology. CRC Press.
204. Sun H, Kamanova J, Lara-Tejero M, Galan JE. 2016. A Family of Salmonella Type III Secretion Effector Proteins Selectively Targets the NF-kappaB Signaling Pathway to Preserve Host Homeostasis. PLoS Pathog 12:e1005484.

205. Goldenberg SJ, Cascio TC, Shumway SD, Garbutt KC, Liu J, Xiong Y, Zheng N. 2004. Structure of the Cand1-Cul1-Roc1 complex reveals regulatory mechanisms for the assembly of the multisubunit cullin-dependent ubiquitin ligases. Cell 119:517-28.
206. Girardin SE, Boneca IG, Viala J, Chamaillard M, Labigne A, Thomas G, Philpott DJ, Sansonetti PJ. 2003. Nod2 is a general sensor of peptidoglycan through muramyl dipeptide (MDP) detection. J Biol Chem 278:8869-72.
207. Ruter C, Hardwidge PR. 2014. 'Drugs from bugs': bacterial effector proteins as promising biological (immune-) therapeutics. FEMS Microbiol Lett 351:126-32.
208. Wang F, Jiang Z, Li Y, He X, Zhao J, Yang X, Zhu L, Yin Z, Li X, Wang X, Liu W, Shang W, Yang Z, Wang S, Zhen Q, Zhang Z, Yu Y, Zhong H, Ye Q, Huang L, Yuan J. 2013. Shigella flexneri T3SS effector IpaH4.5 modulates the host inflammatory response via interaction with NF-kappaB p65 protein. Cell Microbiol 15:474-85.
209. Seyedarabi A, Sullivan JA, Sasakawa C, Pickersgill RW. 2010. A disulfide driven domain swap switches off the activity of Shigella IpaH9.8 E3 ligase. FEBS Lett 584:4163-8.
210. Tien MT, Girardin SE, Regnault B, Le Bourhis L, Dillies MA, Coppee JY, Bourdet-Sicard R, Sansonetti PJ, Pedron T. 2006. Anti-inflammatory effect of Lactobacillus casei on Shigella-infected human intestinal epithelial cells. J Immunol 176:1228-37.
211. Collier-Hyams LS, Sloane V, Batten BC, Neish AS. 2005. Cutting edge: bacterial modulation of epithelial signaling via changes in neddylation of cullin-1. J Immunol 175:4194-8.

List of Publications

1. **Gulati A**., Kumar R. and Mukhopadhaya A. (2019) Differential recognition of *Vibrio parahaemolyticus* OmpU by TLRs in monocytes and macrophages for the induction of pro-inflammatory responses. Infection and Immunity, May 2019, Volume 87, DOI: 10.1128/IAI.00809-18

2. **Gulati A.**, Shukla R. and Mukhopadhaya A. (2019) *Salmonella* effector SteA suppresses pro-inflammatory responses of the host by interfering with IκB degradation. Frontiers in Immunology, December 2019, DOI: 10.3389/fimmu.2019.02822

3. **Gulati A.**, Kaur D., Krishna Prasad G.V.R., Mukhopadhaya A., (2018) PRR Function of Innate Immune Receptors in Recognition of Bacteria or Bacterial Ligands. Biochemical and Biophysical Roles of Eukaryotic Cell Surface Macromolecules (Part of the Advances in Experimental Medicine and Biology book series), Springer, 2018, DOI: 10.1007/978-981-13-3065-0_18

4. Joshi M., Verma I., **Gulati A.**, Bhalla A., Garg P., Mukhopadhaya A. and Choudhury A. R. (2019) Natural acid salts of Ofloxacin with enhanced physical and biological properties. Manuscript submitted.

5. Joshi M., Verma I., **Gulati A.**, Rani S., Budhwar C., Raza K., Mukhopadhaya A. and Choudhury A. R. (2020) In-vivo and in-vitro biological activity, structural and physiochemical studies on novel salts of Levofloxacin. Manuscript submitted.

Publications

AMERICAN SOCIETY FOR MICROBIOLOGY | Infection and Immunity®

HOST RESPONSE AND INFLAMMATION

Differential Recognition of *Vibrio parahaemolyticus* OmpU by Toll-Like Receptors in Monocytes and Macrophages for the Induction of Proinflammatory Responses

Aakanksha Gulati,[a] Ranjai Kumar,[a] Arunika Mukhopadhaya[a]

[a]Department of Biological Sciences, Indian Institute of Science Education and Research Mohali, Manauli, Punjab, India

ABSTRACT *Vibrio parahaemolyticus* is a human pathogen, and it is a major cause of severe gastroenteritis in coastal areas. OmpU is one of the major outer membrane porins of *V. parahaemolyticus*. Host-immunomodulatory effects of *V. parahaemolyticus* OmpU (VpOmpU) have not been elucidated yet. In this study, in an effort towards characterizing the effect of VpOmpU on innate immune responses of the host, we observed that VpOmpU is recognized by the Toll-like receptor 1/2 (TLR1/2) heterodimer in THP-1 monocytes but by both TLR1/2 and TLR2/6 heterodimers in RAW 264.7 macrophages. To the best of our knowledge, this is the first report of a natural pathogen-associated molecular pattern (PAMP) recognized by both TLR1/2 and TLR2/6 heterodimers; so far, mainly the synthetic ligand Pam_2CSK4 has been known to be recognized by both the TLR1/2 and TLR2/6 heterodimers. We also have shown that VpOmpU can activate monocytes and macrophages, leading to the generation of proinflammatory responses as indicated by tumor necrosis factor alpha (TNF-α), interleukin-6 (IL-6), and NO production in macrophages and TNF-α and IL-6 production in monocytes. VpOmpU-mediated proinflammatory responses involve MyD88-IRAK-1 leading to the activation of mitogen-activated protein (MAP) kinases (p38 and Jun N-terminal protein kinase [JNK]) and transcription factors NF-κB and AP-1. Further, we have shown that for the activation of macrophages leading to the proinflammatory responses, the TLR2/6 heterodimer is preferred over the TLR1/2 heterodimer. We have also shown that MAP kinase activation is TLR2 mediated.

KEYWORDS OmpU, TLR, *Vibrio parahaemolyticus*, innate immunity, proinflammatory responses

Vibrio parahaemolyticus is one of the human pathogens belonging to the genus *Vibrio*. It is a Gram-negative, motile, marine bacterium which has been a major cause of gastroenteritis worldwide. In addition to severe gastroenteritis, it can also cause septicemia and eventually death in cases of wound infection. *V. parahaemolyticus* infection occurs upon consumption of raw or undercooked seafood; hence, it is more prevalent in coastal areas.

The virulence property of *V. parahaemolyticus* has been attributed mainly to thermostable direct hemolysin (TDH) (1, 2) and TDH-related hemolysin (TRH) (3), but the observation that TDH and TRH deletion strains retain some virulence indicates the need for more research exploring other antigens of the bacterium for their contribution to its pathogenesis (4, 5).

One such potential antigen is *Vibrio parahaemolyticus* OmpU (VpOmpU), which is a major outer membrane protein of *V. parahaemolyticus*. OmpU is porin in nature, and it is present in all of the *Vibrio* species. In addition to its porin function, in various species of *Vibrio*, OmpU plays crucial roles in modulation of host cellular responses and

Citation Gulati A, Kumar R, Mukhopadhaya A. 2019. Differential recognition of *Vibrio parahaemolyticus* OmpU by Toll-like receptors in monocytes and macrophages for the induction of proinflammatory responses. Infect Immun 87:e00809-18. https://doi.org/10.1128/IAI.00809-18.

Editor Shelley M. Payne, The University of Texas at Austin

Address correspondence to Arunika Mukhopadhaya, arunika@iisermohali.ac.in.

Received 2 November 2018
Returned for modification 2 December 2018
Accepted 15 February 2019

Accepted manuscript posted online 25 February 2019
Published 23 April 2019

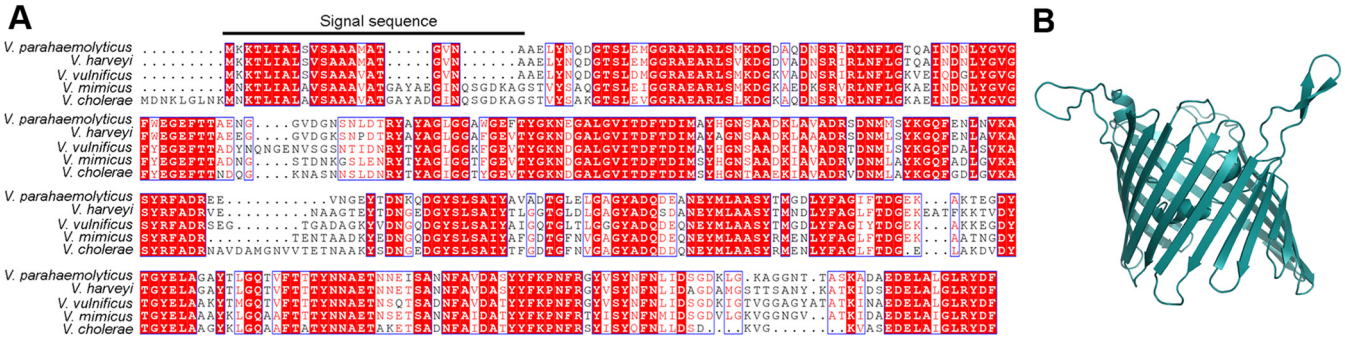

FIG 1 Amino acid sequence alignment and homology-based structural model of VpOmpU. (A) Amino acid sequence alignment of VpOmpU and OmpU porins from related *Vibrio* species. The region corresponding to the signal sequence is marked. (B) Homology-based structural model of VpOmpU based on the crystal structure of VcOmpU (PDB entry 6EHB).

bacterial pathogenesis. For example, the OmpU proteins of *V. cholerae* and *V. splendidus* help the bacteria in bile and antimicrobial peptide resistance (6, 7). In *V. vulnificus*, OmpU is reported to act as an adhesin (8), and in *V. alginolyticus*, OmpU has been reported to help the bacteria in acquiring antibiotic resistance (9). In *V. splendidus*, OmpU has been reported to help in adhesion and invasion (10). *V. cholerae* OmpU has been reported to cause programmed cell death (11). Further, the unique amino acid sequence of *V. cholerae* OmpU and its highly conserved nature distinguish epidemic strains from less pathogenic strains (12). This suggests that OmpU plays a critical role in *V. cholerae* pathogenesis.

OmpU proteins from various *Vibrio* spp. were also tested for their ability to modulate host immune responses and as potential vaccine candidates. OmpU has been developed as a vaccine candidate against *V. alginolyticus*, a fish pathogen (13), and against *V. splendidus*, an oyster pathogen (14). Antibodies against OmpU of *V. cholerae* in patient samples have also been reported (15). Though *V. cholerae* OmpU is one of the favorite candidates for development of vaccines against the disease cholera, reports from our lab challenge the candidacy, as they suggested that although *V. cholerae* OmpU can activate the innate immune response (16), it can also translocate to host cell mitochondria, thus inducing host cell death (11).

So far, no vaccine against *V. parahaemolyticus* has been reported. A report in 2007 indicated the production of antibody against *V. parahaemolyticus* OmpU (VpOmpU) when it was injected into yellow croaker fish (17). This suggests that VpOmpU could also be explored for its vaccine potential. For this, a detailed immunological characterization of VpOmpU to better understand its role in host immunomodulation and pathogenesis is required.

In this study, we have purified VpOmpU from wild-type and recombinant sources and further examined how VpOmpU modulates the innate immune response *in vitro*. We found that it generates a proinflammatory response in monocytes and macrophages via a Toll-like receptor (TLR)-mediated signaling pathway. Our study also shows the involvement of mitogen-activated protein (MAP) kinases and both NF-κB and AP-1 transcription factors in induction of the VpOmpU-mediated proinflammatory response.

RESULTS

Identification and analysis of putative OmpU from *Vibrio parahaemolyticus*. Analysis of the *V. parahaemolyticus* genome revealed the presence of a gene sequence encoding a putative OmpU protein (18) composed of 330 amino acid residues with a predicted molecular mass of 35.6 kDa. This putative OmpU of *V. parahaemolyticus* (VpOmpU) showed 60 to 90% sequence similarity with the OmpU proteins of the related *Vibrio* species (Fig. 1A). Homology-based structural modeling based on the crystal structure of *V. cholerae* OmpU (19) showed a typical porin-like β-barrel architecture of VpOmpU (Fig. 1B).

Based on this analysis, this putative OmpU, which is probably a porin, was selected for purification from the outer membrane of *V. parahaemolyticus*. An attempt was also made to express and purify the recombinant form of the protein by employing the heterologous expression system in *Escherichia coli*. Wild-type and recombinant forms of VpOmpU were also subjected to functional characterization.

Purification of VpOmpU from the outer membrane of *Vibrio parahaemolyticus*. Wild-type VpOmpU (wt-VpOmpU) was purified from the outer membrane fraction of *V. parahaemolyticus*. Bacterial cells were grown in brain heart infusion (BHI) broth, the cells were lysed, and bacterial membrane fractions were harvested upon fractionation with 1% *N*-Sarkosyl. Subsequently, the outer membrane proteins were extracted via solubilization with 4% Triton X-100. VpOmpU was purified from the solubilized membrane fraction by anion-exchange chromatography on DEAE-cellulose in the presence of 0.1% Triton X-100, followed by size exclusion chromatography on Sephacryl S-200 in the presence of 0.5% lauryldimethylamine *N*-oxide (LDAO). Homogeneity of the purified wild-type VpOmpU preparation was analyzed by SDS-PAGE and Coomassie blue staining (Fig. 2A).

Overexpression, purification, and refolding of r-VpOmpU. To obtain a large quantity of the VpOmpU protein and also to reduce lipopolysaccharide (LPS) contamination, we cloned and expressed VpOmpU in *Escherichia coli*. The nucleotide sequence encoding VpOmpU without the N-terminal signal sequence was cloned into the bacterial expression vector pET14b and was transformed into the *E. coli* Origami B cells. The pET14b vector allowed expression of the recombinant VpOmpU (r-VpOmpU) with an N-terminal 6×His tag that would allow affinity purification of the recombinant protein using Ni affinity chromatography. The N-terminal signal sequence (Fig. 1A) was omitted from the cloned construct to avoid possible incorporation of the recombinant protein into the bacterial membrane.

Upon overexpression of the recombinant protein in the *E. coli* Origami B cells via IPTG (isopropyl-β-D-thiogalactopyranoside) induction, the majority of the VpOmpU was found to be present in the form of insoluble inclusion bodies (Fig. 2B). The recombinant form of His-tagged VpOmpU was solubilized from the insoluble inclusion bodies using 8 M urea and was purified by Ni-nitrilotriacetic acid (NTA) agarose affinity chromatography under denaturing conditions in 8 M urea.

The denatured form of purified recombinant VpOmpU in 8 M urea was refolded by dilution in a buffer containing 0.5% LDAO and 10% glycerol. Upon refolding, the majority of VpOmpU remained in the soluble form and was separated from the insoluble aggregated fractions of the protein via centrifugation (Fig. 2C). Refolded VpOmpU was further purified by size exclusion chromatography on Sephacryl S-200 (Fig. 2C). Homogeneity of the purified form of the recombinant His-tagged VpOmpU preparation was analyzed by SDS-PAGE and Coomassie blue staining (Fig. 2C). Further, the His tag was removed from recombinant VpOmpU by thrombin cleavage. The size of the recombinant VpOmpU without the His tag was compared to that of wild-type VpOmpU by Western blotting using antiserum generated against the recombinant VpOmpU (Fig. 2D).

The far-UV CD spectrum of VpOmpU reveals its β-sheet-rich structure. Consistent with their β-barrel structural assembly, Gram-negative bacterial porins display far-UV circular dichroism (CD) profiles showing a typical signature of β-sheet-rich architecture. We examined the structural characteristics of the VpOmpU protein by monitoring the far-UV CD profiles of the recombinant and wild-type forms of the protein.

Wild-type VpOmpU displayed a symmetric far-UV CD spectrum, with a sharp negative ellipticity minimum at 218 nm, suggesting a β-sheet-rich structural organization of the protein (Fig. 2E). The far-UV CD profile of the refolded recombinant protein also showed an ellipticity minimum at 218 nm, suggesting a β-sheet-rich structure of recombinant VpOmpU. The β-sheet-rich structures of the wt-OmpU and the

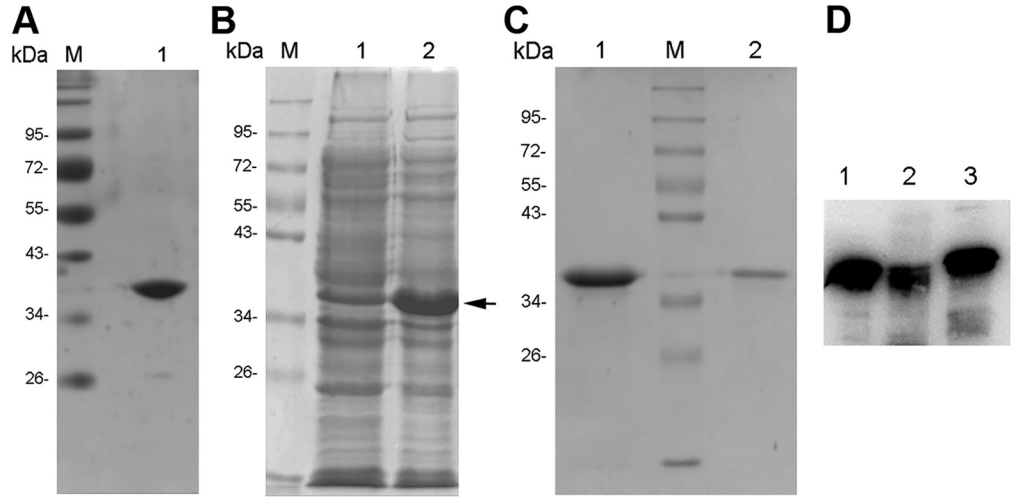

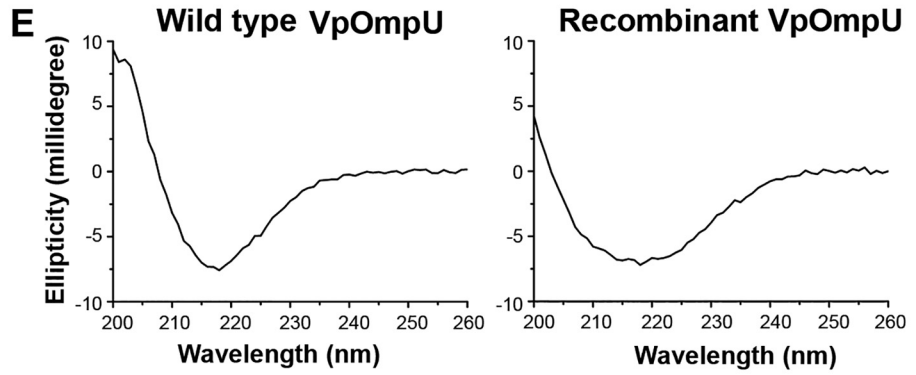

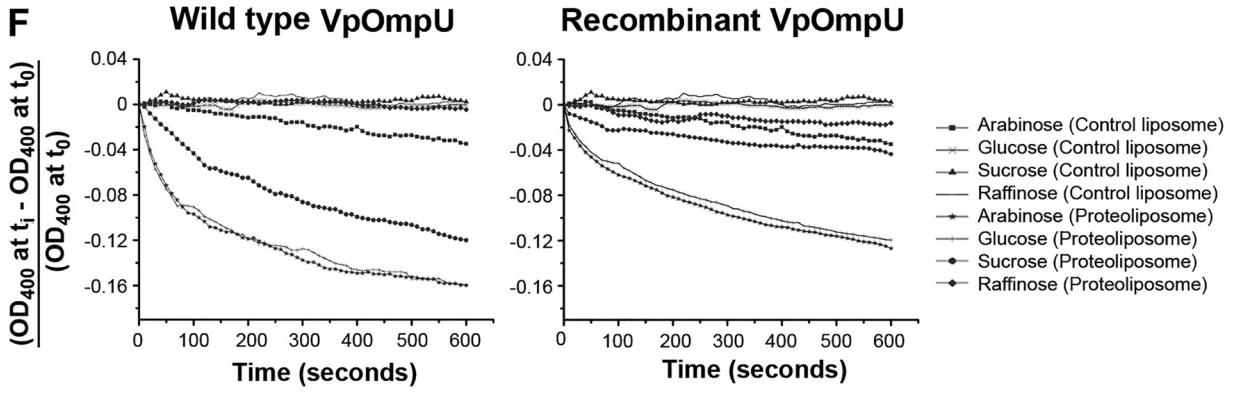

Rate of liposome swelling (per second)

	Arabinose	Glucose	Sucrose	Raffinose
r-VpOmpU	$8.5 \times 10^{-4} \pm 1.45 \times 10^{-4}$	$7.8 \times 10^{-4} \pm 1.12 \times 10^{-4}$	$2.7 \times 10^{-4} \pm 0.51 \times 10^{-4}$	$0.066 \times 10^{-4} \pm 0.156 \times 10^{-4}$
wt-VpOmpU	$14.2 \times 10^{-4} \pm 1.29 \times 10^{-4}$	$14.5 \times 10^{-4} \pm 1.64 \times 10^{-4}$	$4.6 \times 10^{-4} \pm 0.236 \times 10^{-4}$	$0.4 \times 10^{-4} \pm 0.11 \times 10^{-4}$

FIG 2 Characterization of OmpU from *Vibrio parahaemolyticus*. (A) Lane 1, SDS-PAGE/Coomassie blue staining analysis of the purified form of wt-OmpU extracted from the *V. parahaemolyticus* outer membrane fraction. Lane M, molecular weight markers. (B) Overexpression of recombinant VpOmpU in *E. coli*. Protein overexpression was induced with 1 mM IPTG, cells were lysed, and the soluble fraction of the cell lysate (lane 1) and the insoluble inclusion body fraction (lane 2) were analyzed by SDS-PAGE and Coomassie blue staining. The band corresponding to the recombinant VpOmpU is marked. The majority of the VpOmpU protein was found to be associated with the insoluble inclusion body fraction. Lane M, molecular weight markers. (C) Purification of refolded recombinant VpOmpU as analyzed by SDS-PAGE and Coomassie blue staining. The recombinant form of VpOmpU was refolded by rapid dilution in a buffer containing 0.5% LDAO (lane 1). Refolded VpOmpU was further purified

(Continued on next page)

r-VpOmpU were similar to those observed with typical bacterial outer membrane porin proteins.

Liposome-swelling assay demonstrates a porin-like channel-forming property of VpOmpU. Porins are typically characterized by their ability to form channels in the membrane lipid bilayer, allowing free diffusion of small molecules up to a definite size limit as per the size constraint imposed by the corresponding pore diameter. Therefore, we wanted to explore whether the VpOmpU protein could show any such porin-like channel-forming ability in the membrane lipid bilayer of synthetic lipid vesicles or liposomes. The channel-forming property of VpOmpU was assayed using the conventional liposome-swelling assay. In this assay, liposomes incorporating the VpOmpU protein were subjected to treatment in the presence of sugars of various molecular sizes. Formation of VpOmpU channels in the liposome membranes would allow free diffusion of water into the lipid vesicles, resulting in swelling of the liposomes. The VpOmpU channel, however, would not allow the passage of sugars/saccharides having molecular sizes larger than the pore diameter. Such saccharides would act as the osmoprotectants and thus would presumably suppress the liposome-swelling response. Based on this notion, both the wild-type and refolded recombinant forms of the VpOmpU proteins, incorporated in the liposome membranes, were examined using the liposome-swelling assay (Fig. 2F). It was observed in both cases that in the presence of monosaccharides, such as arabinose and glucose, there was a steady increase in the liposome-swelling response (Fig. 2F). In the presence of the disaccharide sucrose, the liposome-swelling responses of wild-type and recombinant VpOmpU were prominently suppressed, while the trisaccharide raffinose severely compromised the liposome swelling on proteoliposomes made up of the wild-type and the recombinant proteins (Fig. 2F). These results clearly suggested that VpOmpU indeed displayed a porin-like channel-forming property with a definite pore size, thus allowing free diffusion of solutes within the specific size limit. The VpOmpU channel allowed free diffusion of the monosaccharides, while the permeability efficiency decreased progressively in the case of the disaccharides and even further in the case of the trisaccharides of larger molecular size. It is also important to note here that the refolded form of the recombinant VpOmpU showed a trend in channel-forming ability (i.e., monosaccharide $>$ disaccharide $>$ trisaccharide) similar to that observed with the wild-type protein, thus showing functional integrity of the recombinant protein generated in our study (Fig. 2F). Based on these observations, it could be concluded that the recombinant VpOmpU was structurally and functionally similar to the native wild-type OmpU of *V. parahaemolyticus*.

VpOmpU induces proinflammatory responses in monocytes and macrophages. As a part of the functional characterization, we explored the host-immunomodulatory role of VpOmpU. Generally, bacterial ligands known as pathogen-associated molecular patterns (PAMPs) are recognized by pattern recognition receptors (PRRs) of the innate immune cells such as macrophages and monocytes, leading to their activation, which results in the production of various proinflammatory molecules, such as nitric oxide (NO) (20, 21) and tumor necrosis factor alpha (TNF-α) and interleukin-6 (IL-6) (22).

Therefore, to probe whether VpOmpU acts as a PAMP, RAW 264.7 cells (a murine macrophage cell line) and THP-1 cells (a human monocytic cell line) were treated with 10 μg/ml of recombinant VpOmpU. At different time points, supernatants were analyzed for TNF-α and IL-6 by enzyme-linked immunosorbent assay (ELISA). A time

FIG 2 Legend (Continued)
by size exclusion chromatography on Sephacryl S-200 (lane 2). Lane M, molecular weight markers. (D) Immunoblot analysis of recombinant and wild-type VpOmpU using anti-VpOmpU antiserum. Lane 1, purified form of refolded recombinant His-tagged VpOmpU; lane 2, purified form of refolded recombinant VpOmpU after removal of the N-terminal His tag; lane 3, wt-OmpU extracted from the *V. parahaemolyticus* outer membrane fraction. (E) Far-UV CD spectra of wild-type and recombinant VpOmpU show negative ellipticity minima at around 218 nm for both proteins. (F) The refolded recombinant form and the wild-type VpOmpU protein show nearly identical trends in the liposome-swelling response. Control liposome, liposome preparation lacking VpOmpU; proteoliposome, liposomes containing VpOmpU. The initial rates of the liposome-swelling response (calculated from the slope of the linear fit of the data over the initial period of 50 s) are shown in the table (r-VpOmpU, recombinant VpOmpU; wt-VpOmpU, wild-type VpOmpU).

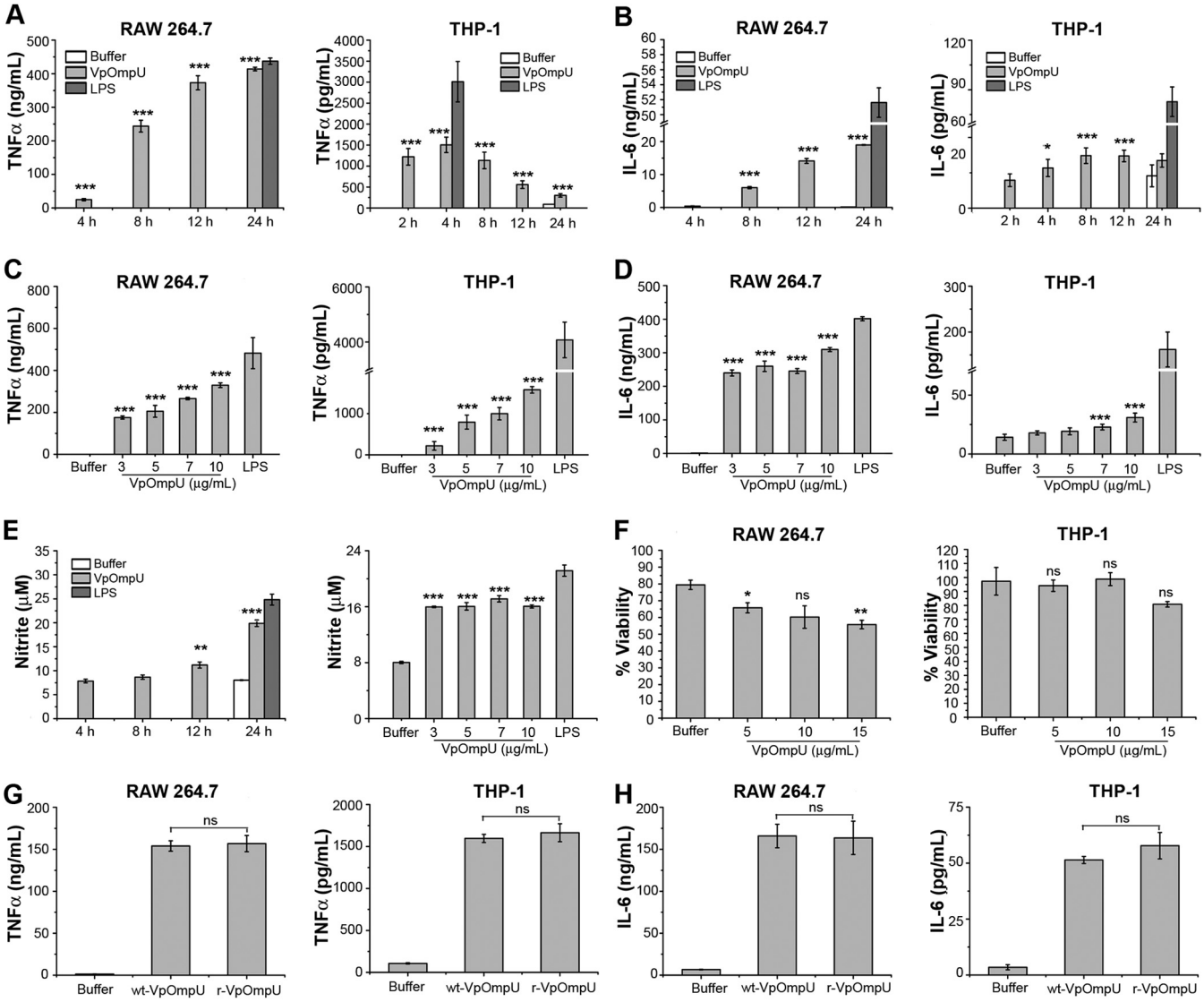

FIG 3 VpOmpU induces proinflammatory responses in THP-1 monocytes and RAW 264.7 macrophages. (A and B) Maximum production of TNF-α (A) and IL-6 (B) was observed at 24 h in RAW 264.7 cells and at 4 h and 8 h, respectively, in THP-1 cells in response to VpOmpU. RAW 264.7 and THP-1 cells were treated with 10 μg/ml of recombinant VpOmpU for different times, and supernatants were analyzed for TNF-α (A) and IL-6 (B) production by ELISA. (C and D) A dose-dependent increase in TNF-α (C) and IL-6 (D) production is seen in both RAW 264.7 and THP-1 cells in response to different doses of VpOmpU. Cells were incubated with different doses of recombinant VpOmpU, and following incubation, supernatants were collected and analyzed for TNF-α and IL-6 production. RAW 264.7 cells and THP-1 cells were incubated with VpOmpU for 24 h and 4 h, respectively, for TNF-α production (C) and for 24 h and 8 h, respectively, for IL-6 production (D). (E) Nitric oxide (NO) production was observed in VpOmpU-treated RAW 264.7 cells. RAW 264.7 cells were treated with 10 μg/ml of recombinant VpOmpU and incubated for different times. Supernatants were analyzed for NO (in terms of nitrite), and significant production of NO was observed at 24 h. Similar extents of NO production were observed when RAW 264.7 cells were treated with different doses of recombinant VpOmpU and incubated for 24 h. For panels A to E, LPS (1 μg/ml) was used as a positive control for all of the experiments. (F) Cell viability in response to different doses of VpOmpU was minimally affected in both RAW 264.7 and THP-1 cells. For panels A to F, results are expressed as mean $\pm$ SEM from three or four independent experiments (*, $P < 0.05$; **, $P < 0.01$; ***, $P < 0.001$; ns, $P > 0.05$ [versus buffer-treated cells]). (G and H) Comparable production of TNF-α and IL-6 was observed in both RAW 264.7 and THP-1 cells in response to similar doses of purified wild-type VpOmpU (wt-VpOmpU) and recombinant VpOmpU (r-VpOmpU). RAW 264.7 and THP-1 cells were treated with 5 μg/ml of wt-VpOmpU or r-VpOmpU and incubated for 24 h and 4 h, respectively, for TNF-α (G) and for 24 h and 8 h, respectively, for IL-6 (H). Results are expressed as mean $\pm$ SEM from three independent experiments (*, $P < 0.05$; **, $P < 0.01$; ***, $P < 0.001$; ns, $P > 0.05$ [versus wt-VpOmpU-treated cells]).

dependency analysis of TNF-α and IL-6 in response to 10 μg/ml of VpOmpU showed a maximum production of both cytokines at 24 h in RAW 264.7 cells (Fig. 3A and B). However, in THP-1 cells, maximum TNF-α production was observed at 4 h (Fig. 3A) and maximum IL-6 production was observed at 8 h (Fig. 3B). A similar time dependency analysis of NO production in RAW 264.7 cells treated with 10 μg/ml of VpOmpU showed a maximum NO production at 24 h (Fig. 3E). THP-1 cells did not produce NO in

response to VpOmpU as observed by a time dependency analysis of VpOmpU-treated cells (see Fig. S1 in the supplemental material).

Further, RAW 264.7 cells and THP-1 cells were treated with different concentrations of recombinant VpOmpU. Supernatants were analyzed for TNF-α and IL-6 by ELISA at the time point where maximum cytokine production had been observed. A dose-dependent increase in TNF-α (Fig. 3C) and IL-6 (Fig. 3D) was observed in both cell types. A similar dose dependency analysis of NO production was done with the supernatant of RAW 264.7 cells at 24 h posttreatment. RAW 264.7 cells produced comparable amounts of NO in response to different concentrations of VpOmpU ranging from 3 μg/ml to 10 μg/ml (Fig. 3E).

We also performed a 3-(4,5-dimethyl-2-thiazolyl)-2,5-diphenyl-2H-tetrazolium bromide (MTT) assay to examine the cell mortality rate in response to different doses of recombinant VpOmpU following 24 h of incubation. The cell mortality in response to VpOmpU was comparable at doses up to 10 μg/ml and was in the range of 30 to 40% for RAW 264.7 cells and about 5 to 15% for THP-1 cells (Fig. 3F).

These results show that VpOmpU can activate macrophages and monocytes to induce proinflammatory responses.

Further, we wanted to compare the proinflammatory responses generated by the cells upon treatment with wild-type and recombinant VpOmpU. For this, we treated both RAW 264.7 and THP-1 cells with an equal amount (5 μg/ml) of each of the proteins and analyzed the supernatants for TNF-α and IL-6 at the time point where the maximum amount of the respective cytokine was observed in the time dependency analysis (Fig. 3A and B). We observed that comparable amounts of TNF-α (Fig. 3G) and IL-6 (Fig. 3H) were produced in response to wild-type and recombinant VpOmpU in both RAW 264.7 and THP-1 cells.

Based on these results, the recombinant form of VpOmpU was used in all subsequent experiments.

VpOmpU elicits the proinflammatory responses via a TLR signaling pathway. The observation that VpOmpU induces a proinflammatory response in monocytes and macrophages reflected the possibility that VpOmpU may be recognized as a PAMP by PRRs on the host cells. One of the major classes of PRRs that recognize bacterial PAMPs is the Toll-like receptors (TLRs) (22). Since *V. parahaemolyticus* is a noninvasive bacterium, VpOmpU will be most likely recognized as a PAMP by the surface TLRs present on the cells. Therefore, a time course analysis of gene expression of surface TLRs was done in VpOmpU-treated RAW 264.7 and THP-1 cells. An increase in gene expression of TLR2, TLR1, and TLR6 was observed in RAW 264.7 cells, whereas an upregulation of TLR2 and TLR1 was observed in THP-1 cells (Fig. 4A). In accordance with this, we observed an increase in the surface expression of TLR1, TLR2, and TLR6 in RAW 264.7 cells, while in THP-1 cells, an increase in surface expression of TLR1 and TLR2 was observed (Fig. 4B).

The above data indicate that TLR1 and TLR2 could be involved in recognition of VpOmpU in THP-1 cells, whereas in RAW 264.7 cells, TLR1, TLR2, and TLR6 could be involved in recognition of VpOmpU.

To confirm the involvement of TLR2, we used a neutralizing antibody. Upon neutralizing TLR2, we observed a significant decrease in the proinflammatory cytokine production in both THP-1 and RAW 264.7 cells, compared to that in isotype-treated cells, in response to VpOmpU (Fig. 4C). This result confirms that TLR2 is probably involved in recognition of VpOmpU in both monocytes and macrophages. To further confirm the involvement of TLR2 in monocytes, we performed small interfering RNA (siRNA)-mediated knockdown of TLR2 in THP-1 cells (see Fig. S2A in the supplemental material) and observed a decrease in cytokine production upon treatment of TLR2-knocked-down cells with VpOmpU (Fig. 4D). To confirm the involvement of TLR2 in macrophages, we used bone marrow-derived macrophages (BMDMs) from TLR2$^{-/-}$ mice and wild-type mice. We treated the BMDMs with VpOmpU and compared the cytokine production following 24 h of incubation. We observed significantly less production of TNF-α and IL-6 in TLR2$^{-/-}$ BMDMs than in wild-type BMDMs (Fig. 4E).

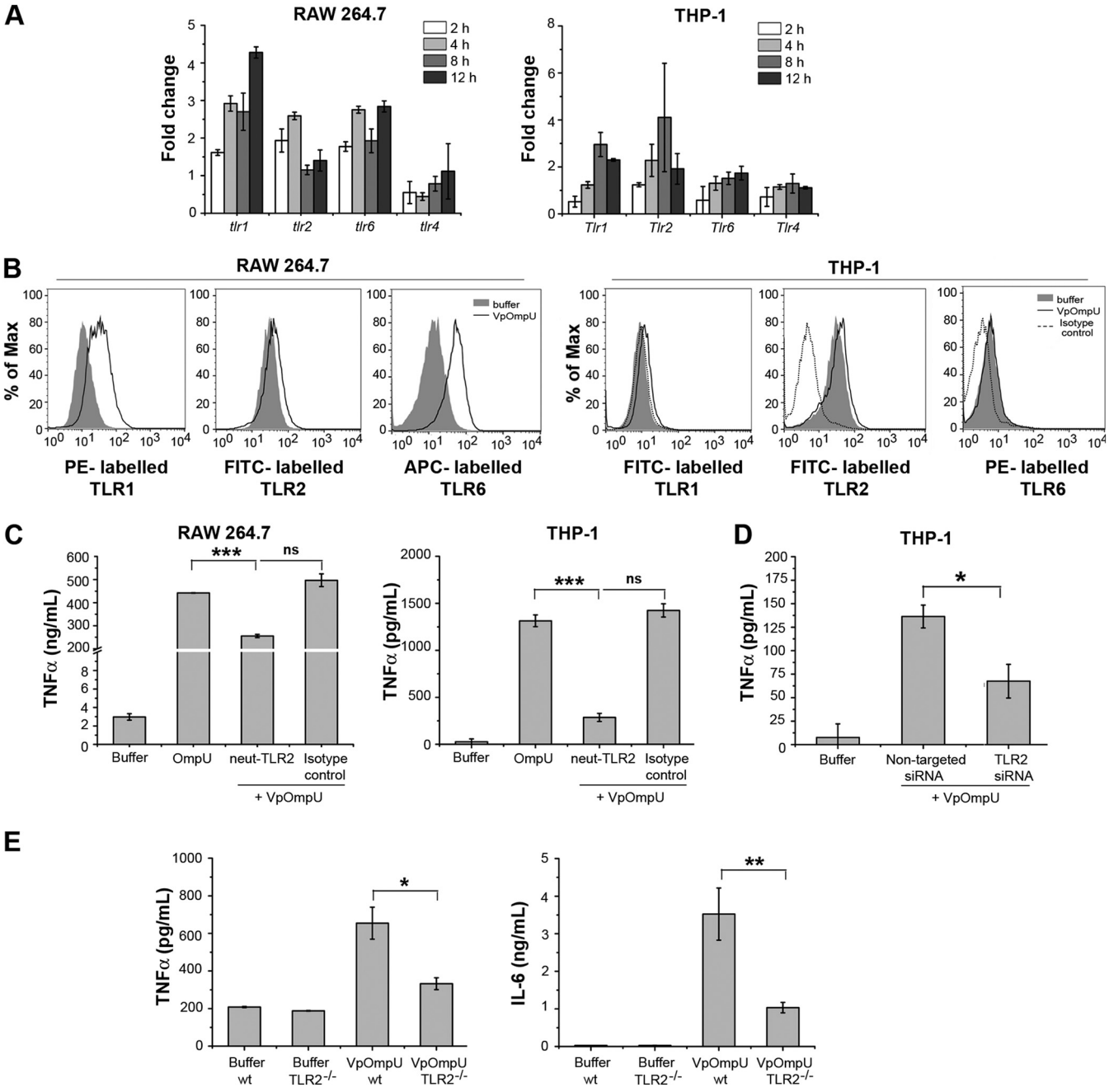

FIG 4 The VpOmpU-mediated proinflammatory response is TLR2 dependent. (A) Upregulation of gene expression of TLR1, TLR2, and TLR6 at different time points in response to VpOmpU in RAW 264.7 cells and of TLR1 and TLR2 in THP-1 cells. Following treatment with VpOmpU, cells were harvested to isolate total RNA. cDNA was generated and subjected to RT-PCR. The C_T values obtained were normalized to the respective C_T values of the housekeeping genes. Fold change was calculated above buffer-treated cells, and results are expressed as mean ± SD from three independent experiments. (B) Increase in surface expression of TLR1, TLR2, and TLR6 in RAW 264.7 cells and of TLR1 and TLR2 in THP-1 cells in response to VpOmpU compared to the buffer-treated cells. Cells were treated with VpOmpU and analyzed for surface expression of TLRs by flow cytometry. (C) Decrease in TNF-α production upon TLR2 neutralization in VpOmpU-treated RAW 264.7 and THP-1 cells compared to the isotype-pretreated VpOmpU-treated cells and cells treated with only VpOmpU. Cells were pretreated with neutralizing antibody and the isotype for 1 h, followed by VpOmpU treatment for 24 h in RAW 264.7 cells and for 4 h in THP-1 cells. Supernatants were analyzed for TNF-α by ELISA. Results are expressed as mean ± SEM from three independent experiments (*, $P < 0.05$; **, $P < 0.01$; ***, $P < 0.001$; ns, $P > 0.05$ [versus cells treated with VpOmpU only]). (D) Decrease in TNF-α production in response to VpOmpU upon knockdown of TLR2 by siRNA in VpOmpU-treated THP-1 cells compared to the nontargeted siRNA-treated VpOmpU-treated cells. Following siRNA knockdown, cells were treated with VpOmpU for 4 h, and supernatant was analyzed for TNF-α by ELISA. Results are expressed as mean ± SEM from three independent experiments (*, $P < 0.05$; **, $P < 0.01$; ***, $P < 0.001$; ns, $P > 0.05$ [versus nontargeted siRNA-transfected VpOmpU-treated cells]). (E) Decrease in TNF-α and IL-6 production by VpOmpU-treated BMDMs differentiated from TLR2$^{-/-}$ mice compared to the wild-type control. Results are expressed as mean ± SEM from three independent experiments (*, $P < 0.05$; **, $P < 0.01$; ***, $P < 0.001$; ns, $P > 0.05$ [versus VpOmpU-treated cells from wild-type mice]).

These data confirmed that TLR2 is involved in recognition of VpOmpU in both monocytes and macrophages.

In response to a PAMP, TLRs are known to dimerize and activate the downstream signaling, and TLR2 is known to make heterodimers with TLR1 or TLR6. The gene expression profile (Fig. 4A) and surface expression profile (Fig. 4B) suggested that in RAW 264.7 cells, VpOmpU could be recognized by both TLR1/2 and TLR2/6 heterodimers, while in THP-1 cells, VpOmpU could be recognized by the TLR1/2 heterodimer only.

Therefore, to determine the heterodimerizing partner of TLR2, we pulled down the VpOmpU-treated cell lysates with anti-TLR2 antibody, and we observed that both TLR1 and TLR6 coimmunoprecipitated with TLR2 in RAW 264.7 cells (Fig. 5A). To further confirm this result, we immunoprecipitated VpOmpU-treated RAW 264.7 cell lysates with anti-TLR1 and anti-TLR6 antibodies, and we observed coimmunoprecipitation (co-IP) of TLR2 along with both TLR1 (Fig. 5B) and TLR6 (Fig. 5C). VpOmpU also coimmunoprecipitated with TLR2, TLR1, and TLR6 (Fig. 5A to C). These data indicated that TLR2 probably heterodimerizes with both TLR1 and TLR6 in response to VpOmpU in RAW 264.7 macrophages. In the case of THP-1 cells we observed that TLR1, but not TLR6, coimmunoprecipitated with TLR2 in response to VpOmpU treatment (Fig. 5D). To further confirm this result, we did reverse co-IP of VpOmpU-treated THP-1 cell lysates with anti-TLR1 and anti-TLR6 antibodies, and we observed coimmunoprecipitation of TLR2 along with TLR1 (Fig. 5E) but not with TLR6 (Fig. 5F). Consistent with this, VpOmpU coimmunoprecipitated only with TLR2 and TLR1 and not with TLR6 (Fig. 5D to F). These data indicated that in THP-1 cells, TLR2 probably heterodimerizes with TLR1 but not TLR6 in response to VpOmpU.

Therefore, the coimmunoprecipitation data suggested the involvement of both the TLR1/2 and TLR2/6 heterodimers in recognizing VpOmpU in RAW 264.7 cells but involvement of only the TLR1/2 heterodimer in THP-1 cells.

To confirm the above results, we used neutralizing antibodies against TLR1 and TLR6 in THP-1 cells followed by treatment with VpOmpU. We observed reduced production of TNF-α in cells pretreated with TLR1- but not with TLR6-neutralizing antibodies, confirming the involvement of the TLR1/2 heterodimer and not the TLR2/6 heterodimer in VpOmpU-mediated proinflammatory responses in THP-1 cells (Fig. 5G). Also, no decrease in TNF-α was observed after siRNA knockdown of TLR6 in THP-1 cells (Fig. 5H and S2B). Altogether, these results confirm the involvement of the TLR1/2 dimer in the VpOmpU-mediated proinflammatory response in THP-1 cells.

To confirm the TLR heterodimers involved in recognition of VpOmpU in macrophages, we knocked down TLR1 and TLR6 using siRNA in RAW 264.7 cells (Fig. S2C). Upon TLR6 knockdown, a decrease in TNF-α production was observed (Fig. 5I). However, when TLR1 was knocked down, there was no significant decrease in TNF-α production (Fig. 5I).

Although both TLR1/2 and TLR2/6 heterodimers are indicated by coimmunoprecipitation (Fig. 5A to C), the siRNA knockdown (Fig. 5I) implies that TLR6 is the major player in the recognition of VpOmpU in RAW 264.7 cells.

MyD88 and IRAK-1 are involved in TLR-mediated signaling by VpOmpU. The TLR activation signal can be mediated through MyD88-dependent or -independent pathways (23). If MyD88 is recruited to the receptor complex as a result of TLR activation, it most certainly recruits IRAK-1 to the receptor complex (23). Gene expression analysis showed an upregulation of MyD88 in VpOmpU-treated THP-1 and RAW 264.7 cells, indicating its involvement in VpOmpU-mediated TLR-signaling (Fig. 6A). Further, we observed that MyD88 coimmunoprecipitated along with TLR2 when lysates of VpOmpU-treated RAW 264.7 (Fig. 6B) and THP-1 cells (Fig. 6C) were pulled down using anti-TLR2 antibody. These data suggested that VpOmpU-mediated TLR signaling involves MyD88. Further, we have confirmed the involvement of MyD88 by using MyD88-deficient (MyD88$^{-/-}$) transgenic mice, where the TNF-α and IL-6 production in

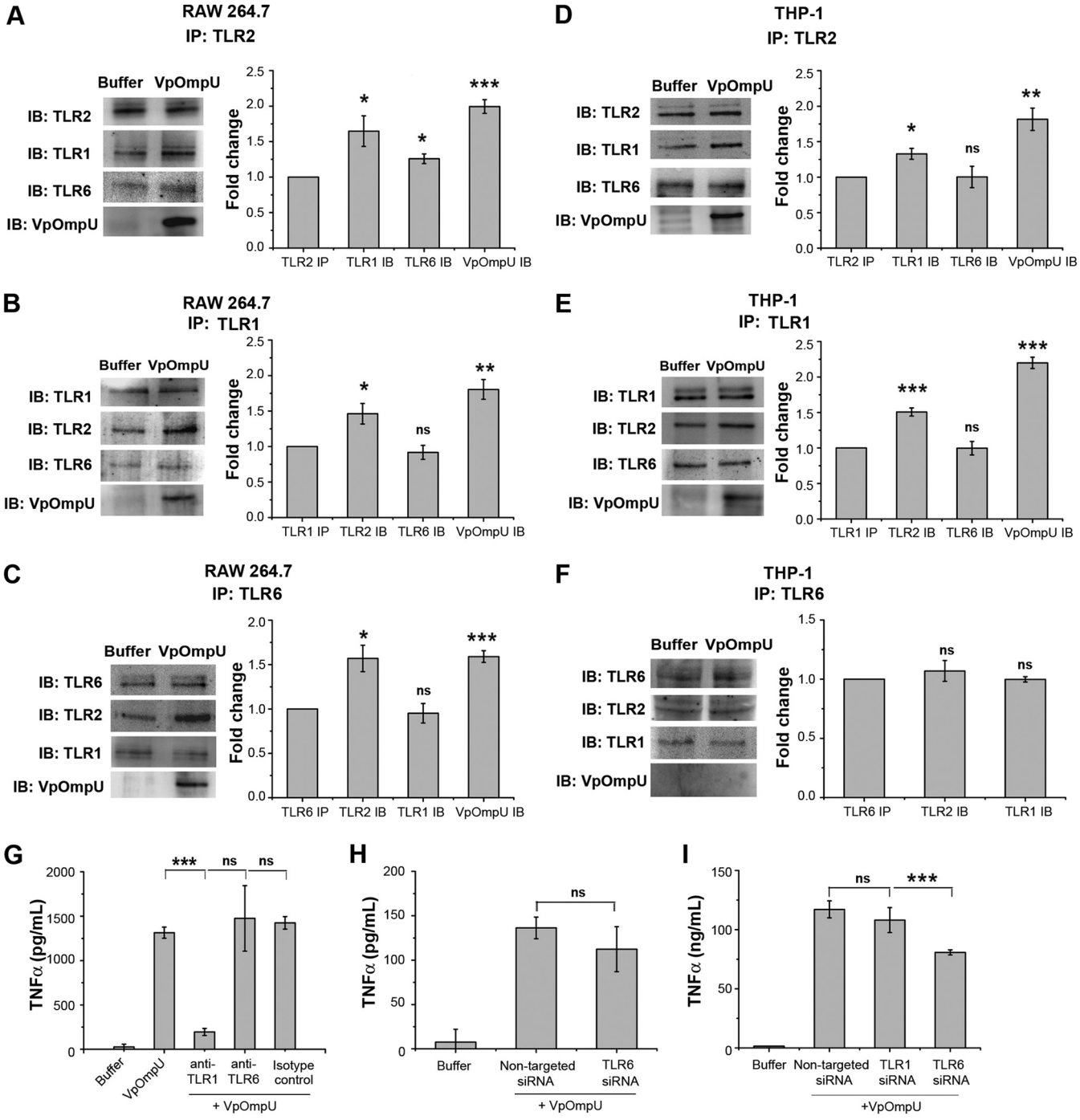

FIG 5 Recognition of VpOmpU by TLR1/2 in THP-1 cells and by TLR1/2 and TLR2/6 in RAW 264.7 cells. (A to C) In RAW 264.7 cells, VpOmpU associates with TLR2, TLR1, and TLR6 as evidenced in coimmunoprecipitation (co-IP) and reverse co-IP studies using anti-TLR2, anti-TLR1, and anti-TLR6 antibodies. (A) TLR1 and TLR6 were coimmunoprecipitated with TLR2 in VpOmpU-treated RAW 264.7 cells as observed by immunoblotting (IB) and densitometric analysis of the bands. (B) TLR2 was coimmunoprecipitated with TLR1 in VpOmpU-treated RAW 264.7 cells as observed by immunoblotting and densitometric analysis of the bands. (C) TLR2 was coimmunoprecipitated with TLR6 in VpOmpU-treated RAW 264.7 cells as observed by immunoblotting blotting and densitometric analysis of the bands. (D to F) VpOmpU associates with TLR1 and TLR2 in THP-1 cells as observed by co-IP and reverse co-IP using anti-TLR2, anti-TLR1, and anti-TLR6 antibodies. (D) TLR1 was coimmunoprecipitated with TLR2 in VpOmpU-treated THP-1 cells as observed by immunoblotting and densitometric analysis of the bands. (E) TLR2 was coimmunoprecipitated with TLR1 in VpOmpU-treated THP-1 cells as observed by immunoblotting and densitometric analysis of the bands. (F) TLR2 did not coimmunoprecipitate with TLR6 in VpOmpU-treated THP-1 cells as observed by immunoblotting and densitometric analysis. For panels A to F, cell lysates were prepared after 15 min of VpOmpU treatment and immunoprecipitated with anti-TLR1, anti-TLR2, or anti-TLR6 antibody, and the IP lysates were further analyzed for TLRs coimmunoprecipitated together to identify the receptor complex. For the densitometric analysis, the band intensities of TLR1, TLR2, TLR6, or VpOmpU in the VpOmpU-treated samples above the respective band intensities in the buffer-treated samples were estimated. Results are expressed as mean ± SEM from three independent experiments (*, $P < 0.05$; **, $P < 0.01$; ***, $P < 0.001$; ns, $P > 0.05$ [versus band intensities in the buffer-treated cells]). (G) Decrease in TNF-α production with anti-TLR1, but not anti-TLR6, neutralizing antibody in VpOmpU-treated THP-1 cells compared to isotype-pretreated VpOmpU-treated cells and cells treated only with VpOmpU. Results are expressed as mean ± SEM from three independent experiments

(Continued on next page)

response to VpOmpU by BMDMs from the MyD88$^{-/-}$ mice was significantly lower than that with the wild-type mice (Fig. 6D).

To examine whether IRAK-1 is involved in VpOmpU-mediated signaling, we used a pharmacological inhibitor of IRAK-1. We observed a considerable decrease in the proinflammatory cytokine production in the VpOmpU-treated cells with the use of the IRAK-1 inhibitor in both RAW 264.7 and THP-1 cells (Fig. 6E).

These observations confirmed that in macrophages and monocytes, the proinflammatory responses generated on recognition of VpOmpU by the TLRs involve MyD88 and IRAK-1.

The NF-κB transcription factor is involved in TLR-mediated signaling of VpOmpU. In general, TLR activation ultimately leads to the activation of transcription factor NF-κB (22). Upon pretreatment of cells with an NF-κB inhibitor (MLN4924) followed by VpOmpU stimulation, a decrease in the production of TNF-α was observed in both RAW 264.7 cells and THP-1 cells compared to VpOmpU-treated cells (Fig. 7A). These data indicated that NF-κB might be involved in VpOmpU-mediated proinflammatory responses.

In an unstimulated cell, NF-κB remains bound to its inhibitor IκB and is present in the cytoplasm. Activation of the IRAK-1/4 complex results in the activation of signaling cascades that lead to the phosphorylation and degradation of IκB, rendering NF-κB free to translocate to the nucleus and transcribe the genes for proinflammatory cytokines. There are five members in the NF-κB subfamily. They either heterodimerize or homodimerize, and depending on the subunits and their nature of dimerization, the cell exerts pro- or anti-inflammatory responses (24). In the majority of cases, p65 and/or c-Rel is the member of the NF-κB family which dimerizes with p50 to transcribe proinflammatory genes. Therefore, phosphorylation and degradation of IκB are crucial for activation of NF-κB (24). In VpOmpU-treated RAW 264.7 and THP-1 cells, we observed phosphorylation and degradation of IκB, indicating the probable activation of NF-κB (Fig. 7B). Further, we also observed nuclear translocation of c-Rel in RAW 264.7 cells and of p65 in THP-1 cells (Fig. 7C).

Altogether, these experiments confirm that NF-κB is involved in VpOmpU-mediated proinflammatory responses.

The AP-1 transcription factor is also involved in VpOmpU-mediated signaling. Apart from NF-κB, another transcription factor, AP-1, is also known to be involved in proinflammatory responses (23). To probe whether AP-1 has a role in VpOmpU-mediated proinflammatory response, we first used a chemical inhibitor against AP-1 (SP600125). We observed a decrease in production of TNF-α in VpOmpU-treated RAW 264.7 and THP-1 cells in the presence of the inhibitor (Fig. 8A), indicating a role of AP-1 transcription in the VpOmpU-mediated proinflammatory response.

The majority of the subunits of the AP-1 transcription factor are in one of two families, Fos and Jun. The members of the Fos and Jun families generally heterodimerize and form AP-1 to function as a transcription factor (25). Nuclear fractions of VpOmpU-treated RAW 264.7 and THP-1 cells were analyzed for the involvement of AP-1 subunits in VpOmpU-mediated proinflammatory processes. By observing the AP-1 subunit levels in nuclear lysates, we came to the conclusions that in VpOmpU-treated RAW 264.7 cells, AP-1 subunits JunB, c-Jun, and c-Fos could be involved and that in THP-1 cells, AP-1 subunits JunB, JunD, c-Jun, and c-Fos could be involved (Fig. 8B).

TLR2 activation by VpOmpU leads to the MAP kinase activation. Generally, MAP kinase activation leads to the activation of AP-1 (23). To probe whether MAP kinases are

FIG 5 Legend (Continued)
(*, $P < 0.05$; **, $P < 0.01$; ***, $P < 0.001$; ns, $P > 0.05$ [versus cells treated with VpOmpU only]). (H) No decrease in TNF-α production in THP-1 cells with knockdown of TLR6 by siRNA, compared to the nontargeted siRNA-transfected control, in response to VpOmpU. (I) Decrease in TNF-α production with siRNA-mediated knockdown of TLR6, but not TLR1, compared to the nontargeted siRNA-transfected control in RAW 264.7 cells in response to VpOmpU. For panels H and I, results are expressed as mean ± SEM from three independent experiments (*, $P < 0.05$; **, $P < 0.01$; ***, $P < 0.001$; ns, $P > 0.05$ [versus VpOmpU-treated cells transfected with nontargeted siRNA]).

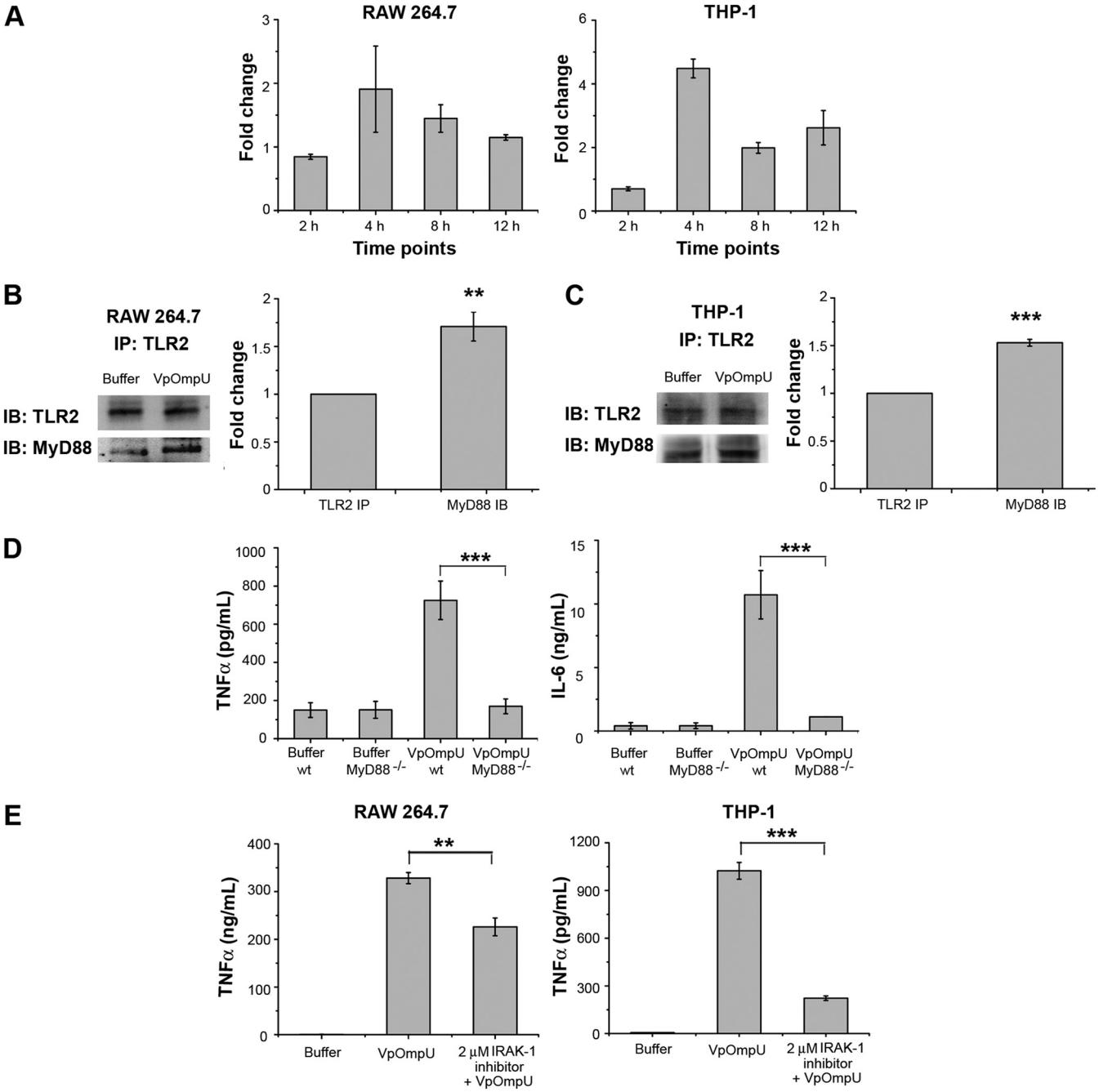

FIG 6 MyD88 and IRAK-1 are involved in VpOmpU-mediated proinflammatory responses. (A) Increase in gene expression of MyD88 in VpOmpU-treated RAW 264.7 and THP-1 cells at different time points. Fold change is calculated as value above that for buffer-treated cells, and results are expressed as mean ± SD from three independent experiments. (B) MyD88 coimmunoprecipitated with TLR2 upon VpOmpU treatment in RAW 264.7 cells as evidenced by immunoblotting and densitometric analysis of the bands. (C) MyD88 coimmunoprecipitated with TLR2 upon VpOmpU treatment in THP-1 cells as evidenced by immunoblotting and densitometric analysis of bands. Results are expressed as mean ± SEM from three independent experiments (*, $P < 0.05$; **, $P < 0.01$; ***, $P < 0.001$; ns, $P > 0.05$ [versus band intensities in the buffer-treated cells]). (D) Decrease in TNF-α and IL-6 production in VpOmpU-treated BMDMs differentiated from MyD88$^{-/-}$ mice compared to the wild-type control. Results are expressed as mean ± SEM from three independent experiments (*, $P < 0.05$; **, $P < 0.01$; ***, $P < 0.001$; ns, $P > 0.05$ [versus VpOmpU-treated BMDMs from wild-type mice]). (E) Decrease in TNF-α production with use of IRAK-1 inhibitor in response to VpOmpU treatment in RAW 264.7 and THP-1 cells. Results are expressed as mean ± SEM from three independent experiments (*, $P < 0.05$; **, $P < 0.01$; ***, $P < 0.001$; ns, $P > 0.05$ [versus cells treated with VpOmpU only]).

involved in VpOmpU-mediated proinflammatory responses in RAW 264.7 and THP-1 cells, we checked the phosphorylation levels of both JNK and p38. We observed phosphorylation (indicative of activation status) of both p38 and JNK in RAW 264.7 (Fig. 9A) and THP-1 (Fig. 9B) cells. Further, we observed a decrease in cytokine production

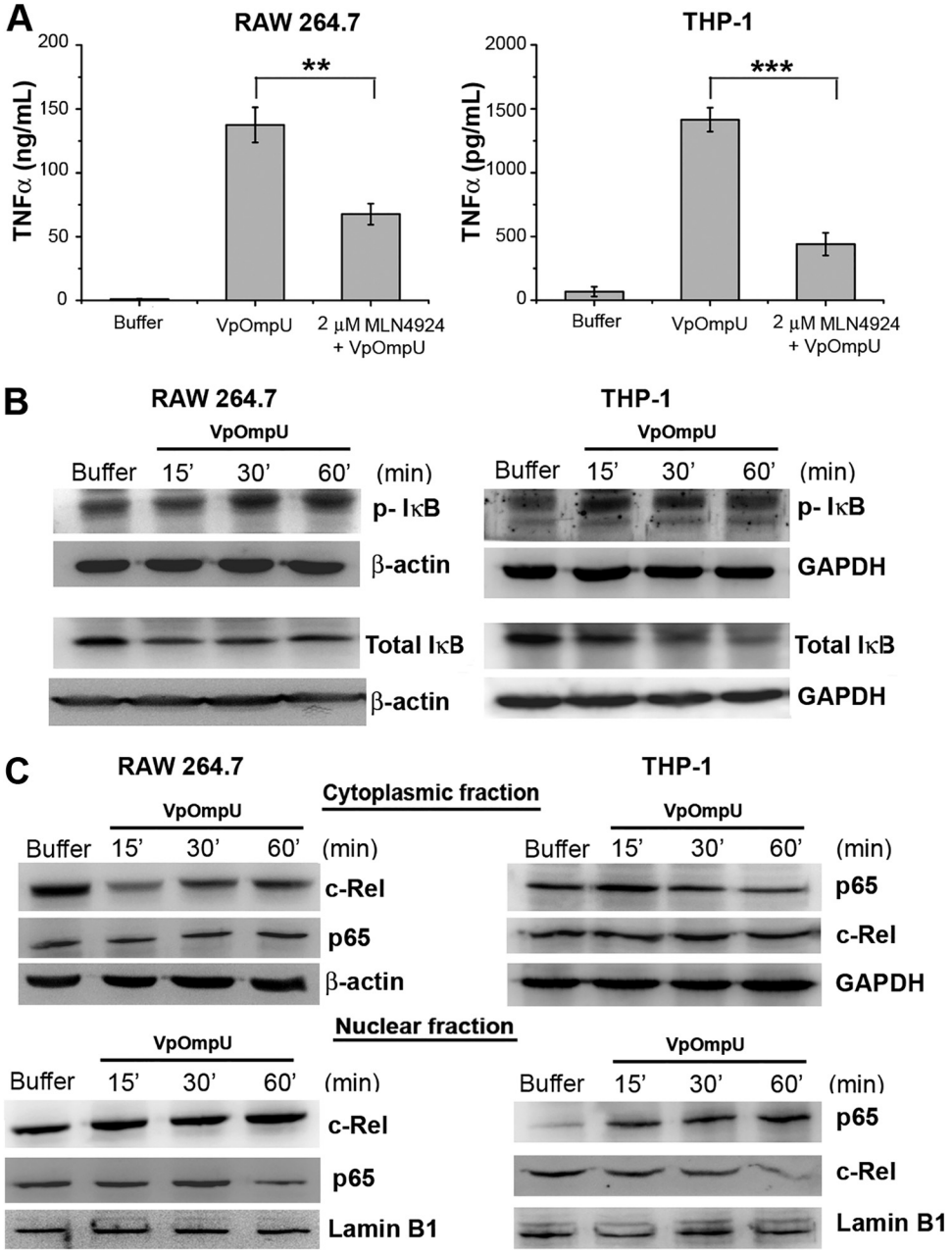

FIG 7 The NF-κB transcription factor is involved in VpOmpU-mediated proinflammatory responses. (A) Decrease in production of TNF-α in response to VpOmpU with the use of an inhibitor of NF-κB (MLN4924) in both RAW 264.7 and THP-1 cells. Results are expressed as mean ± SEM from three independent experiments (*, $P < 0.05$; **, $P < 0.01$; ***, $P < 0.001$; ns, $P > 0.05$ [versus cells treated with VpOmpU only]). (B) Increase in phosphorylated IκB and decrease in total IκB in response to VpOmpU with increase in time in both RAW 264.7 and THP-1 cells. Cells were treated with VpOmpU and incubated for different times. Whole-cell lysates were prepared and analyzed by Western blotting for phosphorylated and total IκB. β-Actin and GAPDH were used as loading controls for the whole-cell lysates. (C) Translocation of NF-κB subunits c-Rel in RAW 264.7 and p65 in THP-1 from the cytoplasm to the nucleus in response to VpOmpU. Lamin B1 was used as a loading control for nuclear lysates, and β-actin and GAPDH were used as loading controls for the cytoplasmic lysates.

in VpOmpU-treated cells pretreated with chemical inhibitors against JNK and p38 (Fig. 9C). To determine whether activation of MAP kinases was TLR2 mediated, we investigated the phosphorylation levels of p38 and JNK in BMDMs from TLR2$^{-/-}$ mice. We found that in the absence of TLR2, MAP kinases (p38 and JNK) were not activated in response to VpOmpU (Fig. 9D and E).

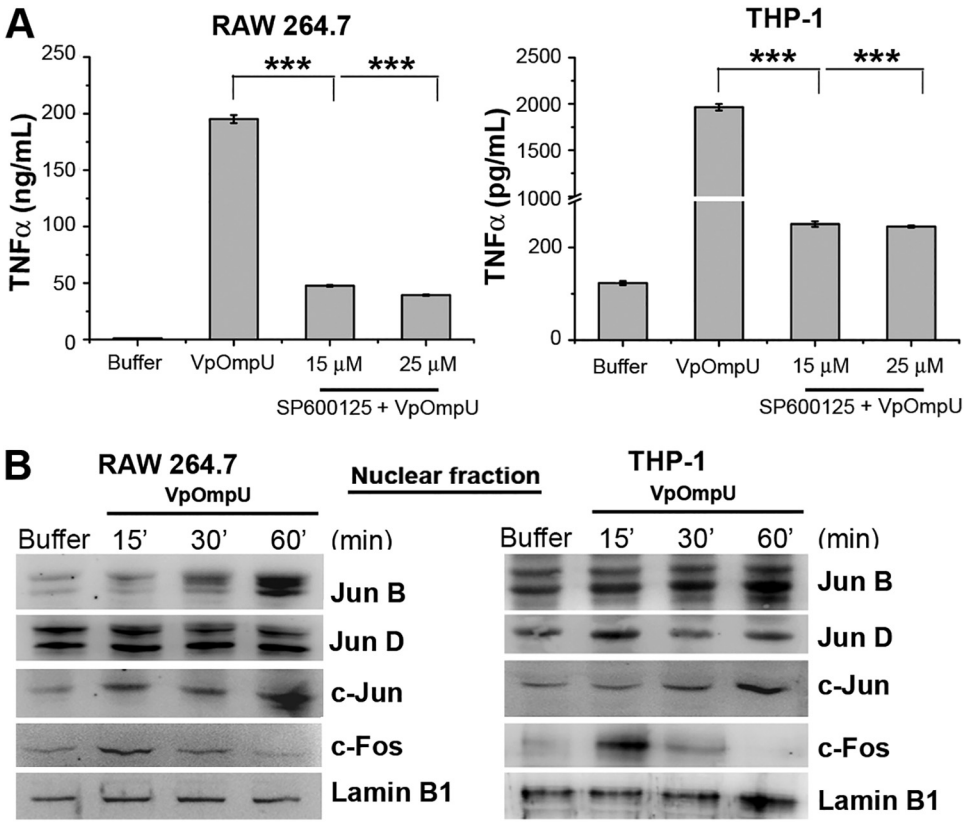

FIG 8 The AP-1 transcription factor is involved in VpOmpU-mediated proinflammatory responses. (A) Decrease in the production of TNF-α in response to VpOmpU in the presence of an AP-1 inhibitor (SP600125) in both RAW 264.7 and THP-1 cells. Results are expressed as mean $\pm$ SEM from three independent experiments (*, $P < 0.05$; **, $P < 0.01$; ***, $P < 0.001$; ns, $P > 0.05$ [versus cells treated with VpOmpU only]). (B) Increase in AP-1 family members in the nuclear lysates of VpOmpU-treated cells, namely, JunB, c-Jun, and c-Fos in RAW 264.7 cells and JunB, c-Jun, c-Fos, and JunD in THP-1 cells. Lamin B1 was used as a loading control for nuclear lysates.

DISCUSSION

OmpU is a major outer membrane protein which is present across the *Vibrio* species. In most of the *Vibrio* species it plays a role in pathogenesis and modulation of host immune function. In *V. alginolyticus* and *V. harveyi*, OmpU has been considered as a vaccine candidate (13, 26). OmpU of *V. parahaemolyticus* (VpOmpU) has also been reported to be immunogenic in yellow croaker fish (17), though this has not been well elucidated.

Many porins, such as PorB of *Neisseria meningitidis* (27) and OmpS1 and OmpS2 of *Salmonella enterica* serovar Typhi (28), have been found to induce proinflammatory responses. In this study, we have characterized the role of VpOmpU in modulating the host's innate immune responses. We have observed that VpOmpU activates macrophages and monocytes as indicated by production of proinflammatory mediators, such as TNF-α and IL-6, in both macrophages and monocytes and of nitric oxide (NO) in macrophages (Fig. 3). Further, to identify the pattern recognition receptor (PRR) which recognizes VpOmpU, we started with the cue that since VpOmpU is present on the outer membrane of *V. parahaemolyticus*, which is a noninvasive bacterium, it must be recognized by the surface PRRs of the cell. Of the surface PRRs, TLRs are mostly involved in the recognition of bacterial ligands (22). TLR1, TLR2, TLR4, TLR5, and TLR6 are the common surface TLRs (29). Generally, upon activation, TLRs form homo- or heterodimers; e.g., TLR2 forms heterodimers with either TLR1 or TLR6, whereas TLR4 forms homodimers (30). Various other outer membrane proteins, such as PorB of *Neisseria meningitidis* (31) and OspA of *Borrelia* spirochetes (32), have been shown to be recognized by TLR1/2 heterodimers. OmpA, an outer membrane protein of *Shigella*

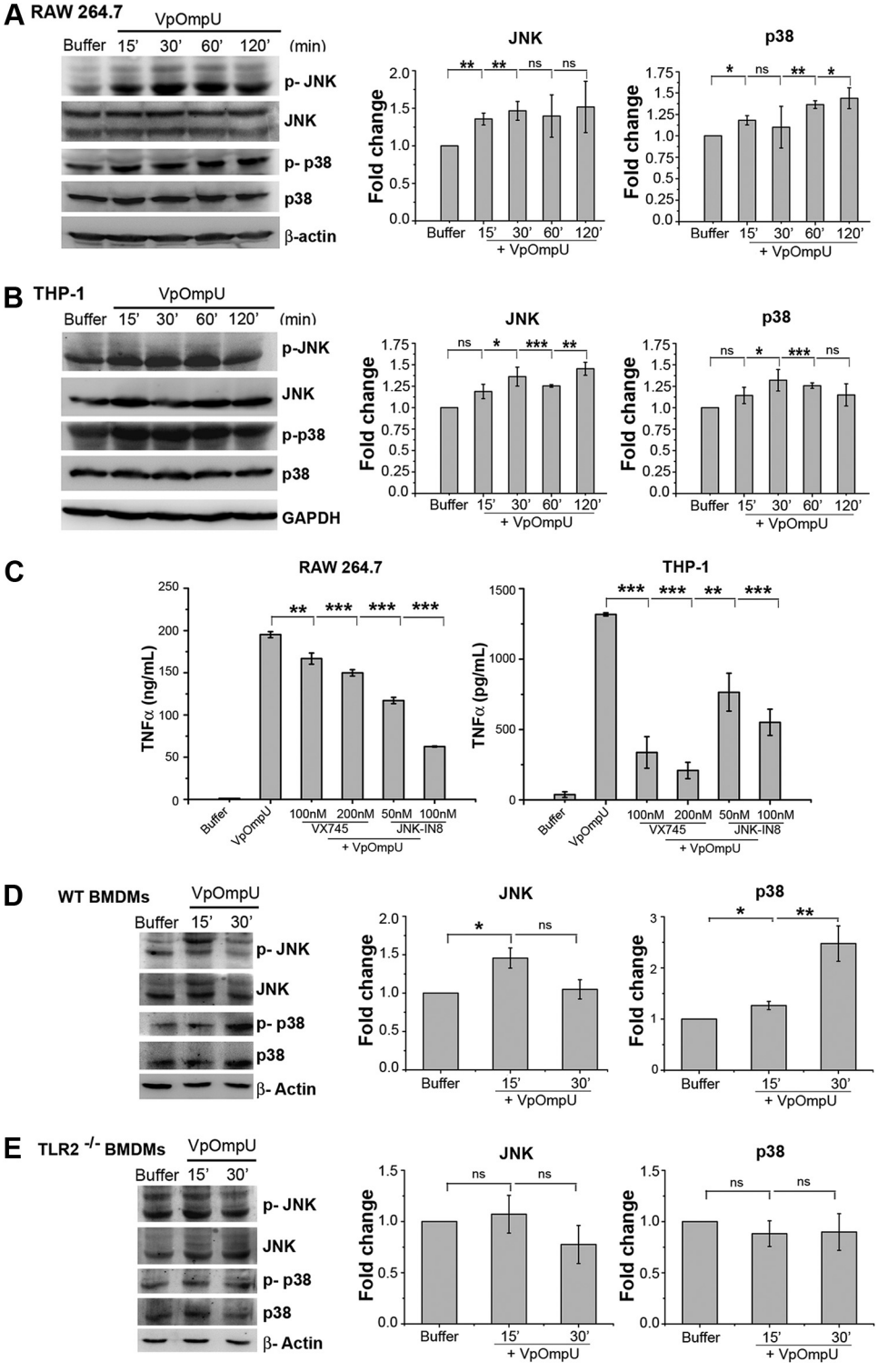

FIG 9 Proinflammatory response by VpOmpU involves TLR-mediated p38 and JNK MAP kinase activation. (A and B) Increased phosphorylation of p38 and JNK in RAW 264.7 (A) and THP-1 (B) cells in response to VpOmpU as evidenced by immunoblotting and densitometric analysis of the bands. Whole-cell lysates were analyzed for the phosphorylation of p38 and JNK at different times following VpOmpU treatment. Total p38 and JNK in the cells were also determined. Densitometric analysis of the immunoblots confirmed increased phosphorylation of p38 and JNK in RAW 264.7 and THP-1 cells in response to VpOmpU. For the densitometric analysis, the band intensities of p-p38 or p-JNK in the samples were calculated as those above the band intensities of p38 or JNK, respectively, and fold changes upon VpOmpU treatment were estimated with respect to the buffer-treated cells. Results are expressed as mean ± SEM from three independent experiments (*, $P < 0.05$; **, $P < 0.01$; ***, $P < 0.001$; ns, $P > 0.05$ [versus band intensities in the buffer-treated cells]). (C) Decrease in TNF-α in response to VpOmpU upon

(Continued on next page)

flexneri (33), and OmpS2 of *S.* Typhi (28) also are known to be recognized by TLR2/6 heterodimers. We observed that VpOmpU mediates its proinflammatory response through TLR2 in both monocytes and macrophages (Fig. 4). Further, to find the binding partner of TLR2, we did coimmunoprecipitation of VpOmpU-treated cell lysates with anti-TLR2 antibody and observed that only TLR1 is present along with TLR2 in VpOmpU-treated THP-1 monocytes, whereas both TLR1 and TLR6 are present along with TLR2 in macrophages. Reverse coimmunoprecipitation with anti-TLR1 and anti-TLR6 antibodies confirmed the result (Fig. 5). This result is particularly intriguing since, to the best of our knowledge, this is the first report of a natural PAMP, i.e., VpOmpU, being recognized by both TLR1/2 and TLR2/6 heterodimers. As mentioned above, while TLR1/2 and TLR2/6 heterodimers have been known to recognize discrete ligands, a previous report indicated the recognition of a synthetic lipoprotein (Pam_2CSK_4, which is a diacylated lipoprotein) by both the TLR1/2 and TLR2/6 heterodimers (34, 35). Buwitt-Beckmann et al. (34) also showed that recognition of a ligand by TLR6 depends not only on the acylation of the ligand but also on the peptide sequence and the overall structure of the protein ligand. However, Farhat et al. (35) showed that this difference in ligand recognition did not alter the downstream signaling elicited by the dimers. They also speculated that this difference in ligand recognition was necessary to increase the array of ligands recognized by the cells.

Bacterial porins of *S. enterica* serovar Typhimurium (36), PorB of *N. meningitidis* (27), OmpA of *Shigella flexneri* (33), P2 porin of *Haemophilus influenzae* (37), and OmpU of *V. cholerae* (38) have previously been reported to induce NF-κB- or AP-1-mediated proinflammatory responses. We have shown in the present study that VpOmpU-mediated activation of TLR signaling leads to activation of the transcription factors NF-κB and AP-1 in both THP-1 monocytes and RAW 264.7 macrophages (Fig. 7 and 8). AP-1 is activated by upstream MAP kinases (Fig. 9). Furthermore, in this study we have also shown that the activation of MAP kinases (p38 and JNK) is TLR2 dependent (Fig. 9). These data suggest that a difference in the recognition of VpOmpU by the TLR1/2 or TLR2/6 heterodimer does not affect the downstream signaling elicited by it.

VpOmpU shares about 70% sequence identity with *V. cholerae* OmpU (VcOmpU) (Fig. 1). Like VcOmpU, VpOmpU is also porin in nature (Fig. 2). Extensive study from our laboratory and others confirmed that VcOmpU is recognized only by TLR1/2 in both monocytes and macrophages (38), whereas our present study shows that VpOmpU can be recognized by both TLR1/2 and TLR2/6 in macrophages, with TLR2/6 being favorable for induction of proinflammatory responses. Further, in the case of VpOmpU, the activation of both MAP kinases (p38 and JNK) is mainly TLR dependent, but in the case of VcOmpU, only p38 MAP kinase activation is dependent on TLR-mediated signaling in macrophages (unpublished data).

Altogether, our study shows that VpOmpU elicits proinflammatory responses via TLR1/2 in monocytes and via TLR2/6 in macrophages. Recognition of VpOmpU by the TLR heterodimer leads to MyD88-IRAK-1-dependent activation of NF-κB and AP-1 transcription factors for such proinflammatory response generation.

FIG 9 Legend (Continued)
pretreatment with inhibitors of the MAP kinases p38 (VX745) and JNK (JNK-IN8) in RAW 264.7 and THP-1 cells. Results are expressed as mean ± SEM from three independent experiments (*, $P < 0.05$; **, $P < 0.01$; ***, $P < 0.001$; ns, $P > 0.05$ [versus cells treated with VpOmpU only]). (D and E) Increased phosphorylation of p38 and JNK in VpOmpU-treated BMDMs from wild-type (WT) mice but no change in phosphorylation status of p38 and JNK in VpOmpU-treated BMDMs from $TLR2^{-/-}$ mice. Densitometric analysis of the immunoblots shows increased phosphorylation of JNK at 15 min and of p38 at both 15 min and 30 min in the wild-type BMDMs and no change in the phosphorylation status of JNK and p38 in the $TLR2^{-/-}$ BMDMs in response to VpOmpU. For the densitometric analysis, the band intensities of p-p38 or p-JNK in the samples were calculated as those above the band intensities of p38 or JNK, respectively, and fold changes upon VpOmpU treatment were estimated with respect to the buffer-treated cells. Results are expressed as mean ± SEM from three independent experiments (*, $P < 0.05$; **, $P < 0.01$; ***, $P < 0.001$; ns, $P > 0.05$ [versus band intensities in buffer-treated cells]). β-Actin and GAPDH were used as the loading controls in the immunoblots of the whole-cell lysates.

MATERIALS AND METHODS

Bacterial strains and chemicals. The *V. parahaemolyticus* strain was obtained from the Microbial Type Culture Collection (MTCC) and Gene Bank facility (MTCC code 451) of the Institute of Microbial Technology, Chandigarh, India. All of the DNA-modifying enzymes were obtained from New England Biolabs (USA). Luria-Bertani (LB) broth and antibiotics were from Himedia, Mumbai, India. Brain heart infusion (BHI) medium was from Fluka, USA. Plasmid and DNA isolation kits were obtained from Qiagen. Ni-NTA agarose was obtained from Qiagen.

PCR amplification and DNA manipulation. The full-length nucleotide sequence encoding the putative OmpU protein of *V. parahaemolyticus* (VpOmpU) was retrieved from the NCBI server (available online at https://www.ncbi.nlm.nih.gov/pubmed) (GenBank accession no. HM042874.1). The N-terminal signal sequence of the VpOmpU protein was determined using SignalP (available online at http://www.cbs.dtu.dk/services/SignalP/). The nucleotide sequence encoding VpOmpU, omitting the N-terminal signal sequence, was amplified by PCR using *V. parahaemolyticus* MTCC 451 genomic DNA as the template. The following primer sequences were designed based on the VpOmpU nucleotide sequence (GenBank accession no. HM042874.1), omitting the sequence for the N-terminal signal peptide: forward primer, 5′-TA*CATATG*GCTGAACTTTACAACCAAG-3′; reverse primer, 5′-CG*GGATCC*TTAGAAGTCGTAACGTAGAC-3′. NdeI and BamHI restriction endonuclease sites (in italic) were incorporated in the forward and reverse primers, respectively, so as to allow cloning of the amplified nucleotide sequence into the target expression vector.

The amplified PCR product was first cloned into the TA cloning vector (pTZ57R/T; Fermentas Life Sciences) and transformed into *E. coli* TOP10 cells (Invitrogen). Transformed cells were screened for the positive plasmid harboring the cloned nucleotide sequence of the VpOmpU gene by PCR, using the gene-specific primers mentioned above. Cloned sequence encoding VpOmpU was excised from the pTZ57R/T vector by restriction digestion with NdeI and BamHI and recloned into the pET-14b bacterial expression vector (Novagen), and the recombinant pET-14b vector (pET-14b/*VpOmpU*) was transformed into the *E. coli* TOP10 cells. The transformants were selected on ampicillin (50 μg/ml)-supplemented LB agar plates. Bacterial colonies were screened for the recombinant pET-14b/*VpOmpU* plasmid by colony PCR using the gene-specific primers. Recombinant pET-14b/*VpOmpU* plasmid was purified, and the construct was verified by DNA sequencing of the cloned nucleotide segment for VpOmpU.

Overexpression and purification of VpOmpU. Recombinant pET-14b/*VpOmpU* plasmid was transformed into *E. coli* Origami B cells. A single colony of *E. coli* Origami B cells harboring the pET-14b/*VpOmpU* plasmid was inoculated into 20 ml LB medium containing ampicillin (50 μg/ml), and the cells were grown at 37°C overnight. For large-scale protein expression, 1 liter of LB medium supplemented with 50 μg/ml ampicillin was inoculated with 20 ml of the overnight-grown seed culture and was grown at 37°C. Protein overexpression was induced by addition of 1 mM IPTG when the optical density at 600 nm (OD_{600}) of the culture medium reached 0.4 to 0.6. After induction for 3 h at 37°C, the cells were harvested by centrifugation at 3,220 $\times$ *g* for 30 min. The cells were resuspended in 10 ml of 20 mM sodium phosphate buffer (pH 7.0) containing bacterial protease inhibitor cocktail (Sigma-Aldrich, USA). The cells were disrupted by sonication. Insoluble inclusion bodies were separated from the soluble fraction of the cell lysate by centrifugation at 18,500 $\times$ *g* for 30 min. The presence of the majority of the recombinant VpOmpU protein in the insoluble inclusion body fraction was observed by SDS-PAGE and Coomassie blue staining. The crude inclusion bodies were washed twice with phosphate-buffered saline (PBS) (20 mM sodium phosphate buffer [pH 7.0] containing 150 mM sodium chloride). Subsequently, the inclusion bodies were solubilized in PBS containing 8 M urea (10 ml of the urea-containing buffer was used to solubilize the inclusion bodies obtained from 1 liter of culture) by constant stirring at 25°C. Insoluble debris was separated by centrifugation at 18,500 $\times$ *g* for 30 min at 4°C. Recombinant VpOmpU protein was further purified from the crude urea-solubilized inclusion body fraction by passage through Ni-NTA agarose affinity chromatography resins (Qiagen) under denaturing conditions in the presence of 8 M urea. The urea-solubilized inclusion body fraction was adjusted with 10 mM imidazole and was applied to Ni-NTA agarose resin preequilibrated with PBS containing 8 M urea (4 ml Ni-NTA agarose resin/10 ml of solubilized inclusion body fraction). After washing with 10 volumes of PBS containing 8 M urea and 40 mM imidazole, the bound protein was eluted with PBS containing 8 M urea and 300 mM imidazole. The purity of the protein was examined by SDS-PAGE and Coomassie blue staining.

Refolding of the recombinant VpOmpU protein. Purified recombinant VpOmpU protein was subjected to refolding by the rapid-dilution method. The purified protein in 8 M urea was diluted into refolding buffer (PBS containing 10% glycerol, 0.5% lauryldimethylamine *N*-oxide [LDAO] [Sigma-Aldrich, USA]) at 25°C with constant shaking for 10 min. The diluted protein was further incubated at 4°C overnight to allow optimal refolding of the protein. Thereafter, the refolding mixture was centrifuged at 18,500 $\times$ *g* for 30 min at 4°C to remove the insoluble aggregates formed during the refolding process. The soluble fraction was immediately subjected to size exclusion chromatography by passage through a Sephacryl S-200 column (1.6 by 60 cm; bed volume, 120 ml; flow rate, 1 ml/min) (GE Healthcare) equilibrated with 10 mM Tris-HCl buffer (pH 7.6) containing 10 mM NaCl and 0.5% LDAO. Eluted fractions containing the VpOmpU protein (eluted at around 40 ml of elution volume) were analyzed by SDS-PAGE and Coomassie blue staining, pooled, and concentrated by ultrafiltration using Millipore Ultra 10-kDa-cutoff filters. The protein concentration was estimated using the Bradford reagent (Sigma-Aldrich, USA), using bovine serum albumin (BSA) as the standard. The final soluble fraction of the purified form of the refolded recombinant VpOmpU protein was analyzed by SDS-PAGE and Coomassie blue staining. The N-terminal 6×His tag of the recombinant protein was removed by treatment with thrombin (1 unit of enzyme/300 μg of protein) for 2 h at 37°C. The reaction was stopped with 2 mM phenylmethylsulfonyl fluoride (PMSF).

Purification of wild-type VpOmpU from the *V. parahaemolyticus* outer membrane fraction. *V. parahaemolyticus* was grown in 2 liters brain heart infusion (BHI) medium until the OD_{600} of the culture reached 1.0. The bacterial culture was subsequently centrifuged at 2,050 × *g* for 30 min. The bacterial cell pellet was resuspended in 20 mM Tris-HCl (pH 7.6), containing protease inhibitor cocktail (Sigma-Aldrich, USA), and the bacterial cells were lysed by sonication and subjected to centrifugation at 18,500 × *g* for 50 min. The supernatant was collected and subjected to ultracentrifugation at 320,000 × *g* for 20 min. The pellet thus obtained was resuspended in PBS and ultracentrifuged at 320,000 × *g* for 20 min. The pellet was further subjected to treatment with 1% *N*-Sarkosyl in PBS for 30 min at 37°C and was ultracentrifuged at 105,000 × *g* for 1 h. The pellet was washed twice with 20 mM Tris-HCl (pH 7.6) at 320,000 × *g* for 20 min and was then subjected to treatment with 4% Triton X-100 in 20 mM Tris-HCl (pH 8.0) for 20 min at 37°C. The supernatant thus obtained contained the outer membrane proteins. The extracted protein fractions were incubated with 10 mM dithiothreitol (DTT) for 10 min at room temperature and were further diluted 5-fold with 20 mM Tris-HCl buffer (pH 7.6) containing 0.1% Triton X-100. The protein sample was loaded onto a DEAE-cellulose column equilibrated with 20 mM Tris-HCl (pH 7.6) containing 0.1% Triton X-100. Bound proteins were eluted with a gradient of 50 to 250 mM NaCl in Tris-HCl (pH 7.6) buffer at a flow rate of 1 ml/min. The eluted fractions were subjected to SDS-PAGE and Coomassie blue staining analysis for detection of the eluted proteins. The eluted fractions were collected, selectively pooled, and subjected to size exclusion chromatography on a Sephacryl S-200 column (1.6 by 60 cm; bed volume, 120 ml; flow rate, 1 ml/min) (GE Healthcare) equilibrated with 10 mM Tris-HCl (pH 7.6) buffer containing 10 mM sodium chloride and 0.5% LDAO. The fractions that eluted at around 36 ml contained the purified form of VpOmpU protein as analyzed by SDS-PAGE and Coomassie blue staining.

Immunological relatedness between the wild-type and recombinant VpOmpU proteins. Polyclonal antiserum was generated in rabbit using the purified refolded form of the recombinant His-tagged VpOmpU protein as the antigen. The antiserum was raised in a New Zealand White rabbit using the Polyclonal Antibody Production Service of Bangalore Genei, India. The antiserum recognized the wild-type VpOmpU extracted from the *V. parahaemolyticus* outer membrane fraction in the immunoblot assay, confirming the antigenic identity/immunological relatedness between the wild-type and recombinant forms of VpOmpU generated in our study.

Far-UV CD. The far-UV circular dichroism (CD) spectra were collected on an Applied Photophysics Chirascan spectropolarimeter equipped with a Peltier-based temperature control system, using a 5-mm-path-length quartz cuvette. Far-UV CD spectra of the purified refolded recombinant VpOmpU and wild-type VpOmpU (extracted from the *V. parahaemolyticus* outer membrane fraction) were recorded between 200 and 260 nm. Protein concentrations were adjusted to 1.5 to 3.0 μM in 10 mM Tris-HCl buffer (pH 7.6) containing 10 mM NaCl and 0.5% LDAO. The resulting spectra were averaged (average of three spectra) and were corrected with the corresponding buffer spectra. All of the spectra were recorded at 25°C.

Liposome-swelling assay. Functional channel-forming activity of VpOmpU (wild-type and refolded recombinant proteins) in the membrane lipid bilayer was determined by the conventional liposome-swelling assay following the method described by Nikaido and Rosenberg (39), with slight modifications. Liposomes were prepared with egg yolk phosphatidylcholine (Sigma-Aldrich, USA) and dicetylphosphate (Sigma-Aldrich, USA) following the method described earlier, with modifications. Phosphatidylcholine (4.7 mg dissolved in 500 μl chloroform) and dicetylphosphate (0.10 mg dissolved in 1 ml of a chloroform-methanol mixture [1:1, vol/vol]) were mixed together in a round-bottom flask, and the lipid film was allowed to generate by evaporation in a vacuum desiccator for 4 h. To this completely dried and solvent-free lipid film, 1 ml of the VpOmpU protein solution (in 5 mM Tris-HCl buffer [pH 7.6]) was added. The refolded recombinant VpOmpU protein was used at up to a 25 μg/ml final concentration, and the wild-type protein was used at up to a 30 μg/ml final concentration. Control liposomes were prepared by mixing the dried lipid film in 5 mM Tris-HCl buffer (pH 7.6) without the protein. Proteoliposomes and the control liposomes were subjected to ultracentrifugation at 350,000 × *g* for 15 min at 4°C and washed thrice with 5 mM Tris-HCl buffer (pH 7.6). The pellets were dried under reduced pressure in a vacuum desiccator overnight and then resuspended in 0.6 ml of same buffer containing 15% dextran 40,000 (Sigma-Aldrich, USA) by incubating for 2 h at 25°C. For the liposome-swelling assay, 20 μl of the proteoliposomes or the control liposomes was mixed rapidly in a cuvette with 580 μl of 30 mM sugar solution (arabinose, glucose, sucrose, and raffinose [Sigma-Aldrich, USA]) in 5 mM Tris-HCl buffer (pH 7.6), and the OD_{400} was continuously monitored for 10 min at intervals of 10 s. The assay was carried out at room temperature in triplicate.

Sequence alignment and protein structural model. An amino acid sequence alignment was generated with CLUSTALW using the server available online (https://www.genome.jp/tools-bin/clustalw) and was visualized with ESPript (http://espript.ibcp.fr/ESPript/ESPript/).

The VpOmpU polypeptide sequence was subjected to a BLAST search in the NCBI server (http://blast.ncbi.nlm.nih.gov/Blast.cgi) against protein sequences having experimentally determined three-dimensional structures in the Protein Data Bank (PDB) (http://www.rcsb.org/pdb/home/home.do). The most suitable template was found to be OmpU of *Vibrio cholerae* (PDB entry 6EHB). Therefore, a homology-based structural model of VpOmpU was generated based on the structural coordinates of 6EHB using the SWISS-MODEL server (http://www.expasy.org/spdbv/). A membrane-inserted structural model of VpOmpU was constructed with the OPM server found online (http://opm.phar.umich.edu/server.php). Protein structural models were visualized with PyMOL (http://pymol.org).

Cell lines and culture conditions. The RAW 264.7 (a murine macrophage cell line) and THP-1 (a human monocytic cell line) cells (NCCS, Pune, India) used in this study were maintained in RPMI 1640 supplemented with 10% fetal bovine serum (FBS), 100 units/ml of penicillin, and 100 μg/ml of strepto-

mycin (Invitrogen, Life Technologies, USA) at 37°C and 5% CO_2. In all of the experiments with VpOmpU, cells were pretreated with 10 μg/ml of polymyxin B (Sigma-Aldrich, USA) for 30 min to prevent any LPS contamination from interfering with the responses.

Cell viability assay. Cells (1×10^5) were plated in 100 μl medium in a 96-well plate and treated with different concentrations of VpOmpU for 24 h. The buffer (10 mM Tris-HCl with 0.5% LDAO) was used as a negative control. The amount of buffer added to the cells was same as that for the highest concentration of VpOmpU. The cell viability was quantified using the MTT assay (EZ Count kit; HiMedia, Mumbai, India) according to the manufacturer's protocol.

Quantification of NO. RAW 264.7 and THP-1 cells were plated at a density of 1×10^6/ml in a 6-well plate and treated with VpOmpU. At different time points, supernatant was collected for quantification of nitric oxide (NO) using Griess reagent (Sigma-Aldrich, USA). Equal volumes of Griess reagent and the supernatant were mixed and incubated in the dark for 15 min, and the optical density was measured at 540 nm. The NO was quantified using a standard curve prepared with different concentrations of sodium nitrite (Sigma-Aldrich, USA), and 1 μg/ml of *E. coli* lipopolysaccharide (LPS) (Sigma-Aldrich, USA) was used as a positive control in the experiments. Buffer (10 mM Tris-HCl with 0.5% LDAO) was used a negative control. For time dependency analysis, buffer was added in an equal amount as for VpOmpU, and for dose dependency studies, the amount of buffer added was equivalent to that for the highest dose of VpOmpU.

Quantification of TNF-α and IL-6. Cells were plated at a density of 1×10^6/ml in a 6-well plate and treated with VpOmpU. At different time points, supernatant was collected. TNF-α and IL-6 were quantified by ELISA (BD Biosciences, USA) by the manufacturer's protocol; 1 μg/ml of *E. coli* lipopolysaccharide (LPS) (Sigma-Aldrich, USA) was used as a positive control in the experiments. Buffer (10 mM Tris-HCl with 0.5% LDAO) was used as a negative control. For time dependency analysis, buffer was added in an equal amount as for VpOmpU, and for dose dependency studies, the amount of buffer added was equivalent to that for the highest dose of VpOmpU.

Gene expression analysis. Cells (2×10^6) were plated in 2 ml medium and treated for different time with 5 μg/ml of VpOmpU. At all time points, buffer (equivalent to the amount of VpOmpU being added) was used as a control. Cells were then harvested, and RNA was isolated according to the manufacturer's protocol using the Nuclepore RNA isolation kit (Genetix). The cDNA was then synthesized using the Verso-cDNA kit (Thermo-Fischer). PCRs were done using the Maxima SYBR green quantitative PCR (qPCR) master mix (Thermo Fischer) and the Eppendorf Realplex master cycler. The primer sequences used were from the primer bank and were synthesized by Integrated DNA Technologies. The fold change of gene expression in VpOmpU-treated cells was calculated as that above expression in the buffer-treated cells for each time point. The threshold cycle (C_T) values of both the buffer-treated and VpOmpU-treated cells were normalized to the respective C_T values of the housekeeping genes.

Analysis of surface expression of TLRs. Cells (1×10^6) were plated in a 6-well plate and treated with 5 μg/ml of VpOmpU for different times. Buffer (10 mM Tris-HCl with 0.5% LDAO)-treated cells were used as a control. Cells were then harvested and washed twice with flow cytometry buffer (PBS supplemented with 1% FBS and 0.05% sodium azide). RAW 264.7 cells were incubated with mouse Fc block for 15 min at 4°C and in THP-1 cells, isotype controls were used. RAW 264.7 and THP-1 cells were then incubated with fluorescein isothiocyanate (FITC)-, phycoerythrin (PE)-, or allophycocyanin (APC)-tagged anti-TLR antibody or the isotype control for 1 h at 4°C. Cells were then washed twice with ice-cold flow cytometry buffer and analyzed on a FACSCalibur flow cytometer (BD Biosciences, USA). FITC-tagged anti-mouse/human TLR2 antibody, PE-tagged anti-mouse TLR1, FITC-tagged anti-human TLR1, and PE-tagged anti-human TLR6 antibodies and the isotype controls were from eBioscience, and APC-tagged anti-mouse TLR6 antibody was from R&D Technologies.

Neutralization of TLRs. Cells were plated in a 96-well plate at a density of 1×10^6 cells/ml. Cells were pretreated for 1 h with 5 μg/ml anti-TLR neutralizing antibodies or the isotype controls and then treated with 5 μg/ml of VpOmpU. Supernatants were collected after 4 h for THP-1 cells and after 24 h for RAW 264.7 cells. TNF-α was then quantified using ELISA. Neutralizing antibodies against mouse/human TLR2 and their isotypes were from BioLegend, and neutralizing antibodies against human TLR1 and TLR6 and the isotypes were from InvivoGen.

Inhibitor studies. Cells were plated at a density of 1×10^6 cells/ml. Cells were then pretreated for 1 h with different pharmacological inhibitors and treated with 5 μg/ml of VpOmpU for 24 h for RAW 264.7 cells and for 4 h for THP-1 cells. The supernatants were then collected and analyzed for TNF-α by ELISA. The inhibitors for IRAK-1, AP-1 (SP600125), JNK (JNK-IN8), and p38 (VX745) were from Sigma-Aldrich, USA, and the inhibitor for NF-κB (MLN4924) was from Boston Biochem, United Kingdom.

siRNA knockdown. For THP-1 cells, 7×10^4 cells were plated in a 24-well plate and transfected using ONTARGETplus siRNA against human TLR2 or human TLR6 or the ONTARGETplus nontargeted siRNA pool (Dharmacon, GE), using DharmaFECT 1 according to the manufacturer's protocol. Knockdown was observed using flow cytometry at 48 h (see Fig. S1A and B in the supplemental material). After 48 h of transfection, cells were treated with 5 μg/ml of VpOmpU for 4 h, after which the supernatants were collected and analyzed for TNF-α using ELISA. For RAW 264.7 cells, 2.5×10^5 cells were plated in a 24-well plate and transfected with ONTARGETplus siRNA against mouse TLR1 or mouse TLR6 or with the ONTARGETplus nontargeted siRNA pool (Dharmacon, GE) using FuGENE HD (Promega) at a ratio of 1:5 (RNA to FuGENE) for 24 h, after which knockdown was analyzed by semiquantitative PCR (Fig. S1C) and cells were treated with 10 μg/ml of VpOmpU for 12 h. Supernatants were then collected, and TNF-α was quantified using ELISA.

BMDMs from wild-type, TLR2$^{-/-}$, and MyD88$^{-/-}$ mice. The protocols for animal handling were approved by our Institutional Animal Ethics Committee (IISERM/SAFE/PRT/2017-2018/001). Six- to 8-week-old mice (C57BL6 wild type, TLR2$^{-/-}$, or MyD88$^{-/-}$) were euthanized, and their femur and tibia

bones were extracted. The femurs and tibias were then cleaned of any muscle tissue and washed with ice-cold PBS. They were then dipped in 70% alcohol for 2 min and transferred to RPMI medium. The epiphyses of the bones were then cut using sterile scissors, and the bones were flushed with RPMI medium, releasing the bone marrow cells into the medium. These bone marrow cells were then differentiated to bone marrow-derived macrophages (BMDMs) using macrophage colony-stimulating factor (M-CSF). Briefly, cells were suspended in bone marrow differentiation medium (RPMI 1640 supplemented with 10% FBS, 100 units/ml of penicillin and streptomycin each, 1 mM sodium pyruvate, 0.1 mM nonessential amino acids [NEAA], 1% β-mercaptoethanol, and 20 ng/ml of M-CSF) and plated in 24-well plates. They were then incubated at 37°C with 5% CO_2. The medium was changed every 2 days, and fresh bone marrow differentiation medium was added. On day 7, the medium was changed to medium without M-CSF, and cells were treated with 5 μg/ml of VpOmpU or the equivalent amount of buffer (10 mM Tris-HCl with 0.5% LDAO) for 24 h. The supernatants were collected and analyzed for TNF-α and IL-6 using ELISA.

Whole-cell lysates and nuclear lysates. Cells were harvested at 2,000 $\times$ *g* and washed twice with PBS. The pellet was then resuspended in whole-cell lysis buffer (50 mM Tris-Cl, 150 mM NaCl, 0.1% SDS, and 0.1% TritonX-100, pH 8) with mammalian protease inhibitor cocktail (Sigma-Aldrich, USA). This mixture was then subjected to sonication at 10 A for 15 s with 3 pulses of 5 s each. It was then centrifuged at 16,000 $\times$ *g* for 30 min, and the supernatant was collected as the whole-cell lysate.

For nuclear lysates, cells were harvested and washed twice with PBS. The pellet volume was measured, and the pellet was dissolved in 5 times the pellet volume in hypotonic buffer (10 mM HEPES [pH 7.9] with 1.5 mM $MgCl_2$ and 10 mM KCl) and centrifuged at 1,850 $\times$ *g* for 5 min at 4°C. The pellet was then dissolved in hypotonic buffer with 0.5 M DTT and mammalian protease inhibitor. After incubation on ice for 15 min, the mixture was sonicated at 10 A for 15 s with 3 pulses of 5 s each and then centrifuged at 3,300 $\times$ *g* for 15 min at 4°C. The supernatant obtained contained the cytoplasmic fraction of the cell. The pellet was resuspended in 70 μl of low-salt buffer (20 mM HEPES [pH 7.9], 1.5 mM $MgCl_2$, 0.02 M KCl, 0.2 mM EDTA, and 25% glycerol) with 0.5 M DTT and mammalian protease inhibitor. To this, 30 μl of high-salt buffer (20 mM HEPES [pH 7.9], 1.5 mM $MgCl_2$, 0.8 M KCl, 0.2 mM EDTA, and 25% glycerol) was added dropwise. After 10 min of incubation on ice, the mixture was sonicated at 10 A for 15 s with 3 pulses of 5 s each and then incubated on ice for 30 min with periodic shaking and subjected to centrifugation at 24,000 $\times$ *g* for 30 min at 4°C. The supernatant obtained contained the nuclear fraction.

Immunoprecipitation and immunoblotting. Whole-cell lysates were prepared after VpOmpU treatment, and 3 μg/ml of antibody was added. This mixture was then subjected to continuous low-speed shaking at 4°C for 3 h. To this, 20 μl of protein A/G beads (Santa Cruz) was added, and the mixture was subjected to low-speed shaking overnight at 4°C. The beads were then pelleted at 6,000 $\times$ *g* for 5 min at 4°C and washed thrice with whole-cell lysis buffer. Beads were then resuspended in SDS loading buffer and boiled for 10 min. This mixture was then subjected to immunoblotting. For immunoblotting, lysates were loaded on SDS-polyacrylamide gels and transferred onto polyvinylidene difluoride (PVDF) membranes using wet transfer. Antibodies against TLR1, TLR2, MyD88, IκB, GAPDH (glyceraldehyde-3-phosphate dehydrogenase), β-actin, p65, c-Rel, JunD, and lamin B1 were from Santa Cruz Biotechnology, and antibodies against TLR6, p-p38, p-JNK, p38, JNK, c-Jun, c-Fos, and JunB were from Cell Signaling Technologies.

The blots were developed using Clarity ECL substrate from Bio-Rad, and the images were acquired using an ImageQuant LAS 4000 instrument (GE Healthcare Life Sciences).

Densitometric analysis. Densitometric analysis of the Western blots was done using the Image J software (https://imagej.nih.gov/ij/). For coimmunoprecipitation studies, the fold changes of the band intensities in the VpOmpU-treated cells above the band intensities in the buffer-treated cells were calculated. For analysis of the phosphorylation status of p38 and JNK, the band intensities of p-p38 or p-JNK above the band intensities of p38 or JNK, respectively, were calculated.

Statistical analysis. Data were expressed as mean $\pm$ standard deviation (SD) or standard error of the mean (SEM). Statistical analysis was done using Student's two-sided *t* test, and *P* values of less than 0.05 were considered significant. Significance is indicated as follows: *, $P < 0.05$; **, $P < 0.01$; ***, $P < 0.001$; and not significant (ns), $P > 0.05$.

SUPPLEMENTAL MATERIAL

Supplemental material for this article may be found at https://doi.org/10.1128/IAI.00809-18.

SUPPLEMENTAL FILE 1, PDF file, 0.2 MB.

ACKNOWLEDGMENTS

Aakanksha Gulati designed and performed experiments, analyzed the data, and wrote the paper. Ranjai Kumar designed and performed experiments and wrote the paper. Arunika Mukhopadhaya designed experiments, analyzed data, supervised the study, and wrote the paper.

We acknowledge the Indian Council of Medical Research (ICMR), Government of India, for a research fellowship to A.G. We acknowledge and thank the Indian Institute of Science Education and Research Mohali for financial support.

REFERENCES

1. Miyamoto Y, Obara Y, Nikkawa T, Yamai S, Kato T, Yamada Y, Ohashi M. 1980. Simplified purification and biophysicochemical characteristics of Kanagawa phenomenon-associated hemolysin of Vibrio parahaemolyticus. Infect Immun 28:567–576.
2. Honda T, Ni Y, Miwatani T, Adachi T, Kim J. 1992. The thermostable direct hemolysin of Vibrio parahaemolyticus is a pore-forming toxin. Can J Microbiol 38:1175–1180. https://doi.org/10.1139/m92-192.
3. Honda T, Ni YX, Miwatani T. 1988. Purification and characterization of a hemolysin produced by a clinical isolate of Kanagawa phenomenon-negative Vibrio parahaemolyticus and related to the thermostable direct hemolysin. Infect Immun 56:961–965.
4. Ceccarelli D, Hasan NA, Huq A, Colwell RR. 2013. Distribution and dynamics of epidemic and pandemic Vibrio parahaemolyticus virulence factors. Front Cell Infect Microbiol 3:97. https://doi.org/10.3389/fcimb.2013.00097.
5. Jones JL, Ludeke CH, Bowers JC, Garrett N, Fischer M, Parsons MB, Bopp CA, DePaola A. 2012. Biochemical, serological, and virulence characterization of clinical and oyster Vibrio parahaemolyticus isolates. J Clin Microbiol 50:2343–2352. https://doi.org/10.1128/JCM.00196-12.
6. Mathur J, Waldor MK. 2004. The Vibrio cholerae ToxR-regulated porin OmpU confers resistance to antimicrobial peptides. Infect Immun 72:3577–3583. https://doi.org/10.1128/IAI.72.6.3577-3583.2004.
7. Duperthuy M, Binesse J, Le Roux F, Romestand B, Caro A, Got P, Givaudan A, Mazel D, Bachere E, Destoumieux GD. 2010. The major outer membrane protein OmpU of Vibrio splendidus contributes to host antimicrobial peptide resistance and is required for virulence in the oyster Crassostrea gigas. Environ Microbiol 12:951–963. https://doi.org/10.1111/j.1462-2920.2009.02138.x.
8. Goo SY, Lee HJ, Kim WH, Han KL, Park DK, Lee HJ, Kim SM, Kim KS, Lee KH, Park SJ. 2006. Identification of OmpU of Vibrio vulnificus as a fibronectin-binding protein and its role in bacterial pathogenesis. Infect Immun 74:5586–5594. https://doi.org/10.1128/IAI.00171-06.
9. Xiong XP, Zhang BW, Yang MJ, Ye MZ, Peng XX, Li H. 2010. Identification of vaccine candidates from differentially expressed outer membrane proteins of Vibrio alginolyticus in response to NaCl and iron limitation. Fish Shellfish Immunol 29:810–816. https://doi.org/10.1016/j.fsi.2010.07.027.
10. Duperthuy M, Schmitt P, Garzón E, Caro A, Rosa RD, Le Roux F, Lautrédou-Audouy N, Got P, Romestand B, de Lorgeril J, Kieffer-Jaquinod S, Bachère E, Destoumieux-Garzón D. 2011. Use of OmpU porins for attachment and invasion of Crassostrea gigas immune cells by the oyster pathogen Vibrio splendidus. Proc Natl Acad Sci U S A 108:2993–2998. https://doi.org/10.1073/pnas.1015326108.
11. Gupta S, Prasad GV, Mukhopadhaya A. 2015. Vibrio cholerae porin OmpU induces caspase-independent programmed cell death upon translocation to the host cell mitochondria. J Biol Chem 290:31051–31068. https://doi.org/10.1074/jbc.M115.670182.
12. Paauw A, Trip H, Niemcewicz M, Sellek R, Heng JM, Mars-Groenendijk RH, de Jong AL, Majchrzykiewicz-Koehorst JA, Olsen JS, Tsivtsivadze E. 2014. OmpU as a biomarker for rapid discrimination between toxigenic and epidemic Vibrio cholerae O1/O139 and non-epidemic Vibrio cholerae in a modified MALDI-TOF MS assay. BMC Microbiol 14:158. https://doi.org/10.1186/1471-2180-14-158.
13. Cai SH, Lu YS, Wu ZH, Jian JC. 2013. Cloning, expression of Vibrio alginolyticus outer membrane protein-OmpU gene and its potential application as vaccine in crimson snapper, Lutjanus erythropterus Bloch. J Fish Dis 36:695–702. https://doi.org/10.1111/jfd.12036.
14. Jung CR, Park MJ, Heo MS. 2005. Immunization with major outer membrane protein of Vibrio vulnificus elicits protective antibodies in a murine model. J Microbiol 43:437–442.
15. Das M, Chopra AK, Cantu JM, Peterson JW. 1998. Antisera to selected outer membrane proteins of Vibrio cholerae protect against challenge with homologous and heterologous strains of V. cholerae. FEMS Immunol Med Microbiol 22:303–308. https://doi.org/10.1111/j.1574-695X.1998.tb01219.x.
16. Sakharwade SC, Sharma PK, Mukhopadhaya A. 2013. Vibrio cholerae porin OmpU induces pro-inflammatory responses, but down-regulates LPS-mediated effects in RAW 264.7, THP-1 and human PBMCs. PLoS One 8:e76583. https://doi.org/10.1371/journal.pone.0076583.
17. Mao Z, Yu L, You Z, Wei Y, Liu Y. 2007. Cloning, expression and immunogenicty analysis of five outer membrane proteins of Vibrio parahaemolyticus zj2003. Fish Shellfish Immunol 23:567–575. https://doi.org/10.1016/j.fsi.2007.01.004.
18. Makino K, Oshima K, Kurokawa K, Yokoyama K, Uda T, Tagomori K, Iijima Y, Najima M, Nakano M, Yamashita A, Kubota Y, Kimura S, Yasunaga T, Honda T, Shinagawa H, Hattori M, Iida T. 2003. Genome sequence of Vibrio parahaemolyticus: a pathogenic mechanism distinct from that of V cholerae. Lancet 361:743–749. https://doi.org/10.1016/S0140-6736(03)12659-1.
19. Pathania M, Acosta-Gutierrez S, Bhamidimarri SP, Basle A, Winterhalter M, Ceccarelli M, van den Berg B. 2018. Unusual constriction zones in the major porins OmpU and OmpT from Vibrio cholerae. Structure 26:708–721 e4. https://doi.org/10.1016/j.str.2018.03.010.
20. Bogdan C. 2001. Nitric oxide and the immune response. Nat Immunol 2:907–916. https://doi.org/10.1038/ni1001-907.
21. MacMicking J, Xie QW, Nathan C. 1997. Nitric oxide and macrophage function. Annu Rev Immunol 15:323–350. https://doi.org/10.1146/annurev.immunol.15.1.323.
22. Akira S, Uematsu S, Takeuchi O. 2006. Pathogen recognition and innate immunity. Cell 124:783–801. https://doi.org/10.1016/j.cell.2006.02.015.
23. Kawai T, Akira S. 2010. The role of pattern-recognition receptors in innate immunity: update on Toll-like receptors. Nat Immunol 11:373–384. https://doi.org/10.1038/ni.1863.
24. Oeckinghaus A, Ghosh S. 2009. The NF-kappaB family of transcription factors and its regulation. Cold Spring Harb Perspect Biol 1:a000034. https://doi.org/10.1101/cshperspect.a000034.
25. Zenz R, Eferl R, Scheinecker C, Redlich K, Smolen J, Schonthaler HB, Kenner L, Tschachler E, Wagner EF. 2008. Activator protein 1 (Fos/Jun) functions in inflammatory bone and skin disease. Arthritis Res Ther 10:201. https://doi.org/10.1186/ar2338.
26. Wang Q, Chen J, Liu R, Jia J. 2011. Identification and evaluation of an outer membrane protein OmpU from a pathogenic Vibrio harveyi isolate as vaccine candidate in turbot (Scophthalmus maximus). Lett Appl Microbiol 53:22–29. https://doi.org/10.1111/j.1472-765X.2011.03062.x.
27. Massari P, Henneke P, Ho Y, Latz E, Golenbock DT, Wetzler LM. 2002. Immune stimulation by neisserial porins is Toll-like receptor 2 and MyD88 dependent. J Immunol 168:1533–1537. https://doi.org/10.4049/jimmunol.168.4.1533.
28. Moreno-Eutimio MA, Tenorio-Calvo A, Pastelin-Palacios R, Perez-Shibayama C, Gil-Cruz C, López-Santiago R, Baeza I, Fernández-Mora M, Bonifaz L, Isibasi A, Calva E, López-Macías C. 2013. Salmonella Typhi OmpS1 and OmpS2 porins are potent protective immunogens with adjuvant properties. Immunology 139:459–471. https://doi.org/10.1111/imm.12093.
29. Kawasaki T, Kawai T. 2014. Toll-like receptor signaling pathways. Front Immunol 5:461. https://doi.org/10.3389/fimmu.2014.00461.
30. Botos I, Segal DM, Davies DR. 2011. The structural biology of Toll-like receptors. Structure 19:447–459. https://doi.org/10.1016/j.str.2011.02.004.
31. Massari P, Visintin A, Gunawardana J, Halmen KA, King CA, Golenbock DT, Wetzler LM. 2006. Meningococcal porin PorB binds to TLR2 and requires TLR1 for signaling. J Immunol 176:2373–2380. https://doi.org/10.4049/jimmunol.176.4.2373.
32. Oosting M, Ter Hofstede H, Sturm P, Adema GJ, Kullberg BJ, van der Meer JW, Netea MG, Joosten LA. 2011. TLR1/TLR2 heterodimers play an important role in the recognition of Borrelia spirochetes. PLoS One 6:e25998. https://doi.org/10.1371/journal.pone.0025998.
33. Bhowmick R, Pore D, Chakrabarti MK. 2014. Outer membrane protein A (OmpA) of Shigella flexneri 2a induces TLR2-mediated activation of B cells: involvement of protein tyrosine kinase, ERK and NF-kappaB. PLoS One 9:e109107. https://doi.org/10.1371/journal.pone.0109107.
34. Buwitt-Beckmann U, Heine H, Wiesmuller KH, Jung G, Brock R, Akira S, Ulmer AJ. 2005. Toll-like receptor 6-independent signaling by diacylated lipopeptides. Eur J Immunol 35:282–289. https://doi.org/10.1002/eji.200424955.
35. Farhat K, Riekenberg S, Heine H, Debarry J, Lang R, Mages J, Buwitt-Beckmann U, Röschmann K, Jung G, Wiesmüller K-H, Ulmer AJ. 2008. Heterodimerization of TLR2 with TLR1 or TLR6 expands the ligand spectrum but does not lead to differential signaling. J Leukoc Biol 83:692–701. https://doi.org/10.1189/jlb.0807586.
36. Galdiero M, Vitiello M, Sanzari E, D'Isanto M, Tortora A, Longanella A, Galdiero S. 2002. Porins from Salmonella enterica serovar Typhimurium activate the transcription factors activating protein 1 and NF-kappaB

through the Raf-1-mitogen-activated protein kinase cascade. Infect Immun 70:558–568. https://doi.org/10.1128/IAI.70.2.558-568.2002.
37. Galdiero S, Capasso D, Vitiello M, D'Isanto M, Pedone C, Galdiero M. 2003. Role of surface-exposed loops of Haemophilus influenzae protein P2 in the mitogen-activated protein kinase cascade. Infect Immun 71: 2798–2809. https://doi.org/10.1128/IAI.71.5.2798-2809.2003.
38. Khan J, Sharma PK, Mukhopadhaya A. 2015. Vibrio cholerae porin OmpU mediates M1-polarization of macrophages/monocytes via TLR1/TLR2 activation. Immunobiology https://doi.org/10.1016/j.imbio.2015.06.009.
39. Nikaido H, Rosenberg EY. 1983. Porin channels in Escherichia coli: studies with liposomes reconstituted from purified proteins. J Bacteriol 153: 241–252.

frontiers in Immunology

ORIGINAL RESEARCH
published: 10 December 2019
doi: 10.3389/fimmu.2019.02822

Salmonella Effector SteA Suppresses Proinflammatory Responses of the Host by Interfering With IκB Degradation

*Aakanksha Gulati, Rhythm Shukla and Arunika Mukhopadhaya**

Department of Biological Sciences, Indian Institute of Science Education and Research Mohali, Sahibzada Ajit Singh Nagar, India

Salmonella enterica serovar Typhimurium is known to cause its virulence by secreting various effector proteins directly into the host cytoplasm via two distinct type III secretion systems (T3SS-1 and T3SS-2). Generally, T3SS-1-delivered effectors help *Salmonella* Typhimurium in the early phases of infection including invasion and immune modulation of the host cells, whereas T3SS-2 effectors mainly help in the survival of *Salmonella* Typhimurium within the host cells including maintenance of *Salmonella*-containing vacuole, replication of the bacteria, and dissemination. Some of the effectors are secreted via both T3SS-1 and T3SS-2, suggesting their role in distinct phases of infection of host cells. SteA is such an effector that is secreted by both T3SS-1 and T3SS-2. It has been shown to control the membrane dynamics of the *Salmonella*-containing vacuole within the host cells in the late phases of infection. In this manuscript, toward characterizing the T3SS-1 function of SteA, we found that SteA suppresses inflammatory responses of the host by interfering with the nuclear factor kappa B pathway. Our initial observation showed that the mice infected with *steA*-deleted *Salmonella* Typhimurium (Δ*steA*) died earlier compared to the wild-type bacteria due to heightened immune responses, which indicated that SteA might suppress immune responses. Furthermore, our study revealed that SteA suppresses immune responses in macrophages by interfering with the degradation of IκB, the inhibitor of nuclear factor kappa B. SteA suppresses the ubiquitination and hence degradation of IκB by acting on Cullin-1 of the Skp-1, Cullin-1, F-box (SCF)-E3 ligase complex. Our study revealed that SteA suppresses a key step necessary for E3 ligase activation, i.e., neddylation of Cullin-1 by interfering with dissociation of its inhibitor Cand-1.

Keywords: ***Salmonella enterica*** **serovar Typhimurium, SteA, proinflammatory responses, IκB degradation, E3 ligase**

OPEN ACCESS

Edited by:
Marina De Bernard, University of Padova, Italy

Reviewed by:
Luís Jaime Mota, New University of Lisbon, Portugal
Susan M. Bueno, Pontifical Catholic University of Chile, Chile

****Correspondence:***
Arunika Mukhopadhaya
arunika@iisermohali.ac.in

Specialty section:
This article was submitted to Microbial Immunology, a section of the journal Frontiers in Immunology

Received: *24 August 2019*
Accepted: *15 November 2019*
Published: *10 December 2019*

Citation:
Gulati A, Shukla R and Mukhopadhaya A (2019) Salmonella Effector SteA Suppresses Proinflammatory Responses of the Host by Interfering With IκB Degradation. Front. Immunol. 10:2822. doi: 10.3389/fimmu.2019.02822

INTRODUCTION

Salmonella enterica serovar Typhimurium utilizes diverse strategies to subvert host defenses by translocating various effectors via a specialized needle-like complex called the type III secretion system (T3SS) (1, 2). The *Salmonella* T3SSs are encoded by small stretches of chromosomes known as *Salmonella* pathogenicity island-1 (SP-1; encoding T3SS-1) and SPI-2 (encoding T3SS-2) (2–5). The T3SS effectors are either encoded or regulated by the SPI-1 or SPI-2 (6). The effectors modulate

different functions of the host and help the bacteria to invade, survive, and replicate in the host cell (5–9).

Before the *Salmonella* enters into the host cell, the T3SS-1 is assembled by the bacteria across the host cell membrane. It generally translocates effectors, which are required for invasion and modulation of host immune responses. T3SS-1 effectors, such as SipA and SipC, bind to actin and help the bacteria in invasion (10–12); SopE and SopE2 modulate both actin rearrangement and host immune responses (13–15). Upon invasion, *Salmonella*-containing vacuoles (SCVs) are formed inside the host cell cytoplasm. Within the SCVs, bacteria replicate. T3SS-2 is formed across the SCV membrane, and the effectors are secreted into the host cell cytoplasm. T3SS-2 effectors are majorly required for maintenance of SCV and replication and spread of the bacteria (4, 7). For example, SifA helps in the formation of *Salmonella*-induced filaments (SIF) (16–18). SIFs connect the SCV to various organelles like ER, Golgi, etc. of the cell, thereby expanding the replicative niche and acquiring nutrients for the replication of *Salmonella* (19–21).

In addition, some of the effectors such as SpvD, SlrP, SteE, SteB, GtgE, etc. are regulated by both SPI-1 and SPI-2 and translocated by both T3SS-1 and T3SS-2, indicating their role in both early and later phases of infection (22, 23). SteA is one such effector molecule (24). Using Nramp1 mice, Lawley et al. have shown that SteA might play a role in the replication of *Salmonella* (25). Geddes et al. have reported that SteA could localize in the trans-Golgi network (22). However, Van Engelenburg and Palmer have later indicated that SteA could localize in *Salmonella*-induced tubules enriched with the trans-Golgi protein GalT (26). Furthermore, Domingues et al. have reported that, in the later phases of infection, SteA binds to phosphatidylinositol 4-phosphate [PI(4)P] to control membrane dynamics of SCV, thereby helping *Salmonella* to localize within SCV and in *Salmonella*-induced tubules (27, 28). Matsuda et al. have indicated that SteA could induce T3SS-1-independent inflammation and cytotoxicity in macrophages (29). McQuate et al. have reported that SteA is important for establishing infection in the early phase and in the prevention of the clearance of *Salmonella* from macrophages (30). However, the SPI-1-regulated role of SteA in *Salmonella* infection is yet to be fully established.

In this study, toward unraveling the T3SS-1 role of SteA, we have shown that SteA suppresses the proinflammatory responses induced due to *Salmonella* Typhimurium infection. We observed that SteA interferes with the activation of nuclear factor kappa B (NF-κB), which is one of the major transcription factors known to be involved in the generation of proinflammatory responses. NF-κB in its inactive state remains in the cytoplasm bound with its inhibitor IκB. IκB degradation is necessary for NF-κB activation and is mediated by its ubiquitination. The E3 ligase is responsible for the ubiquitination of IκB (31). Our study revealed that SteA inhibits activation of Cullin-1, a component of E3 ligase complex and hence ubiquitination and degradation of IκB.

Abbreviations: Δ*steA*, deletion mutant of steA gene; compl, *steA* complemented in the Δ*steA* background; compl-H, 6X His-tagged *steA* complemented in the Δ*steA* background.

MATERIALS AND METHODS

Ethics Statement

All animal experiments were carried out in accordance with the guidelines of the Committee for the Purpose of Control and Supervision of Experiments on Animals (No. 1842/GO/ReBiBt/S/15/CPCSEA). All the protocols for animal handling were approved by the Institutional Animals Ethics Committee of Indian Institute of Science Education and Research, Mohali (IISERM/SAFE/PRT/2016-2018/004, 010, 015).

Bacterial Strains

S. enterica serovar Typhimurium SL1344 strain was a kind gift from Dr. Mahak Sharma (IISER Mohali). SteA in the genome of *Salmonella* Typhimurium was replaced with a Kanamycin cassette by one-step inactivation method following the protocol by Datsenko and Warner (32). Briefly, Kanamycin cassette was amplified from the plasmid pKD13 (a kind gift from Dr. Rachna Chaba, IISER Mohali) using primers—SteA H1P2 and SteA H2P1 (**Table 1**). The amplified Kanamycin cassette with flanking regions corresponding to the flanking regions of the *steA* gene in the *Salmonella* Typhimurium genome was transformed into *Salmonella* Typhimurium expressing the λ-red recombinase via the helper plasmid pKD46 (a kind gift from Dr. Rachna Chaba, IISER Mohali). The colonies were selected on Kanamycin plates and screened by colony PCR. The deletion mutant of Δ*steA* was then transduced to a clean background (*Salmonella* Typhimurium SL1344) using P22 phage (a kind gift from Dr. Rachna Chaba, IISER Mohali). For complementation, *steA* gene of *Salmonella* Typhimurium (www.ncbi.nlm.gov.in) was cloned in pACYC177 (a kind gift from Dr. Rachna Chaba, IISER Mohali) using restriction cloning and was transformed in the deletion mutant of SteA (Δ*steA*) background. The Δ*spi2 Salmonella* Typhimurium 14028 (SV6017) strain was a kind gift from Dr. Francisco Ramos-Morales (University of Seville, Spain) (33). The P22 phage transduction method was used to construct Δ*spi2* SL1344 and Δ*spi2*Δ*steA* SL1344 strains. The primers used in this study are listed in **Table 1**, and the strains and plasmids used in this study are listed in **Table 2**.

Cell Lines and Culture Conditions

RAW 264.7 (a murine macrophage cell line) used in this study was obtained from the National Center for Cell Science, Pune, India, and HEK 293 (a human kidney epithelial cell line) was obtained from American Type Culture Collection. The cells were maintained, respectively, in Roswell Park Memorial Institute (RPMI) 1640 or Dulbecco's modified Eagle medium (DMEM) supplemented with 10% (*v*/*v*) fetal bovine serum (FBS), 100 U/ml of penicillin, and 100 μg/ml of streptomycin (Invitrogen, Life Technologies, USA) at 37°C and 5% CO_2.

Differentiation of Bone Marrow Cells to Bone-Marrow-Derived Macrophages

Balb/c mice 6–8 weeks old were euthanized, and their femur and tibia bones were extracted. The muscle tissue of the bones was then removed off and were then washed with ice-cold phosphate-buffered saline (PBS). They were then dipped in

TABLE 1 | Primers used in this study.

Name of primer		Sequence 5′-3′
SteA H1P2		AGTCTGATTTCTAACAAAACTGGCTAAACATAAACGCTTTATTCCGGGGATCCGTCGACC
SteA H2P1		GACATATAAAGCTATTGAGCAAAATTTGAAGGAGTAGGATATGTGTAGGCTGGAGCTGCTTCG
SteA	Forward	GCGC**CATATG**ATGCCATATACATCAGTTTC
	Reverse	CGCG**GGATCC**TTAATAATTGTCCAAATAGT
SteA-GST	Forward	ATTGTT**GGATCC**CCATATACATCAGTTTCTAC
	Reverse	GTTATT**CTCGAG**TTAATAATTGTCCAAATAGTTATG
SteA-HA	Forward	CCATATT**GGATCC**CCACCATGCCATATACATCAGTTTCTACC
	Reverse	AAGCTAT**CTCGAG**TTAAGCGTAATCTGGAACATCGTATGGGTAATAATTGTCCAAATAGTTATGGTAGCGAG
SteA compl	Forward	ACCT**GGATCC**AAGCAGCATAAGATCAGGCCG
	Reverse	CGT**GACGTC**TTAATAATTGTCCAAATAGTTATGG
SteA compl-H	Forward	ACCT**GGATCC**AAGCAGCATAAGATCAGGCCG
	Reverse	CGT**GACGTC**TTAGTGATGATGATGATGATGATAATTGTCCAAATAGTTATGG
TNFα	Forward	CCCTCACACTCAGATCATCTTCT
	Reverse	GCTACGACGTGGGCTACAG
IL-6	Forward	TAGTCCTTCCTACCCCAATTTCC
	Reverse	TTGGTCCTTAGCCACTCCTTC
IκB	Forward	TTACT**GGATCC**ATGTTTCAGCCAGCTGGGCAC
	Reverse	TCGGTC**GTCGAC**TTATAATGTCAGACGCTGGCC
Rbx-1	Forward	TTACT**GGATCC**ATGGCGGCGGCGATGGATGT
	Reverse	TCGGTC**GTCGAC**CTAATGCCCATACTTCTGGAA
Skp-1	Forward	TTACT**GGATCC**ATGCCTACGATAAAGTTGCAG
	Reverse	TCGGTC**GTCGAC**TCACTTCTCTTCACACCATT
Cullin-1	Forward	CACCATGTCATCAAACAGGAGTCAGAAT
	Reverse	TCGGTC**GTCGAC**TTAAGCCAAGTAACTGTAGGT
SteA Y2H	Forward	ATTGTT**GGATCC**CCATATACATCAGTTTCTAC
	Reverse	GTTATT**GTCGAC**TTAATAATTGTCCAAATAGTTATG

**The highlighted regions indicate the restriction sites.*

70% (*v*/*v*) alcohol for 2 min and were transferred to RPMI 1640 media. Then, using sterile scissors, the epiphyses of the bones were cut, and the bone marrow cells were extracted by flushing the bones with RPMI 1640 media. These bone marrow cells were then differentiated to bone-marrow-derived macrophages (BMDMs) using macrophage colony-stimulating factor (M-CSF). Briefly, cells were suspended in differentiation media [RPMI 1640 supplemented with 10% (*v*/*v*) FBS, 100 U/ml of Penicillin, 100 μg/ml of Streptomycin, 1 mM sodium pyruvate, 0.1 mM nonessential amino acids, 1% (*v*/*v*) β-mercaptoethanol, and 20 ng/ml of M-CSF] and plated in 24-well plates. They were incubated at 37°C with 5% CO_2. The media were changed every 2 days, and fresh differentiation media was added. The adhered cells obtained at day 7 were BMDMs and were used for further experiments.

Infection of Cells

For inducing SPI-1 conditions, as described previously by Cardenal-Munoz and Ramos-Morales (24), bacteria were grown to stationary phase in Luria–Bertani (LB) broth supplemented with 0.3 M NaCl and appropriate antibiotics. Cells were plated in 24- or 6-well plates at a density of 1×10^6 cells/ml for overnight and infected with the stationary phase bacteria at a multiplicity of infection (MOI) of 10:1 (for BMDMs) or 20:1 (for RAW 264.7 and HEK 293 cells) for 30 min. The media containing the bacteria was removed, and fresh media supplemented with 100 μg/ml of gentamicin were added to the wells. After 1 h, this media was replaced with fresh media supplemented with 20 μg/ml of gentamicin for different time points depending on the assay. In all the experiments, the invasion was checked after 2 h of infection by enumerating the bacteria after the cells were lysed with 0.1% (*v*/*v*) Triton-X-100 (Himedia, India) in PBS.

Cell Cytotoxicity Assay

RAW 264.7 and BMDMs were plated at a density of 1×10^6 cells/ml and infected with wild type (wt), Δ*steA*, or compl strains at an MOI of 20:1 or 10:1, respectively. After 8 h of infection, supernatants were collected, and cell cytotoxicity was checked using lactate dehydrogenase release assay (Promega, USA), according to the manufacturer's protocol.

Mice Infection and Scoring

Bacteria grown overnight in LB medium supplemented with 50 μg/ml of streptomycin were subcultured and grown until log phase at 37°C. Balb/c mice 6–8 weeks old were infected intraperitoneally with 5×10^5 or 5×10^7 log-phase bacteria, and the survival of mice was monitored for 24 and 96 h, respectively. *p* values were calculated using Kaplan–Meir test using the software R. In addition, 36 h postinfection (hpi), the

TABLE 2 | Strains and plasmids used in this study.

Strains *Salmonella* Typhimurium	Genotype or description	Reference
wt	Wild-type SL1344	A kind gift from Dr. Mahak Sharma
Δ*steA*	*steA*::Km^R	This study
compl	*steA*::Km^R, pACYC177-*steA*	This study
compl-H	*steA*::Km^R, pACYC177-*steA*-His	This study
14028 Δ*spi2* (SV6017)	*spi2*::Cm^R	A kind gift from Dr. Francisco Ramos-Morales
SL1344 Δ*spi2*	*spi2*::Cm^R	This study
Δ*spi2*Δ*steA*	*spi2*::Cm^R, *steA*::Km^R	This study
Plasmids	**Description**	**Reference**
pKD13	Template used for amplifying Kanamycin Cassette	A kind gift from Dr. Rachna Chaba
pKD46	Plasmid expressing λ-red recombinase	A kind gift from Dr. Rachna Chaba
pACYC177	Bacterial expression plasmid used for complementation	A kind gift from Dr. Rachna Chaba
pACYC177-*steA*	*steA* with its native promoter cloned in pACYC177	This study
pACYC177-*steA*-His	His-tagged *steA* with its native promoter cloned in pACYC177	This study
pGEX4T3	Plasmid expressing GST	A kind gift from Dr. Mahak Sharma
pGEX4T3-*steA*	Plasmid expressing GST-tagged SteA	This study
pcDNA3.1(+)	Mammalian expression plasmid	A kind gift from Dr. Kausik Chattopadhyay
pcDNA3.1(+)*steA*	Mammalian expression plasmid expressing HA-tagged SteA	This study
pGL4.32	NF-κB promoter reporter plasmid	Promega, USA
pRL	Plasmid expressing renilla luciferase	A kind gift from Dr. Rajesh Ramachandran
pGADC1	Yeast expression plasmid with activation domain (AD)	A kind gift from Dr. Shravan Mishra
pGADC1-*IκB*	Yeast expression plasmid with activation domain (AD) fused with IκB	This study
pGADC1-*Rbx1*	Yeast expression plasmid with activation domain (AD) fused with Rbx-1	This study
pGADC1-*Skp1*	Yeast expression plasmid with activation domain (AD) fused with Skp-1	This study
pGADT7	Yeast expression plasmid with activation domain (AD)	A kind gift from Dr. Ram K. Yadav
pGADT7-*Cullin1*	Yeast expression plasmid with activation domain (AD) fused with Cullin-1	This study
pGBDUC1	Yeast expression plasmid with binding domain (BD)	A kind gift from Dr. Shravan K. Mishra
pGBDUC1-*steA*	Yeast expression plasmid with binding domain (BD) fused with SteA	This study

mice infected with 5×10^5 bacteria were scored for their response to stimuli, the extent of decrease in activity, the extent of eye closure and the pilorected fur as compared to the uninfected mice as described previously by Shrum et al. (34). In addition, the core body temperature of mice was checked using a noncontact infrared thermometer at 24 h after infection with 5×10^5 bacteria. The body temperature of mice was also checked before infection, and the difference in temperature of each mice was calculated. The blood of infected mice was collected at 24 and 36 h after infection, and serum was isolated from it. The serum was analyzed for tumor necrosis factor alpha (TNFα), interleukin (IL)-6, IL-1β, interferon gamma (IFN-γ), IL-12, and IL-10 (BD Biosciences, USA) using ELISA according to manufacturer's protocol.

Colonization and Splenic Lysate Preparation

Balb/c mice 6–8 weeks old were infected intraperitoneally with 5×10^5 log-phase bacteria. At 36 hpi, spleens were isolated and homogenized in PBS using a sterile pestle.

For colonization, the homogenate was subjected to lysis with 0.1% (*v*/*v*) Triton-X-100 at 37°C for 30 min. The bacteria were enumerated after serial dilution on LB agar (LA) plates supplemented with 50 μg/ml of streptomycin.

For splenic lysate preparation, the homogenate was pelleted by centrifugation at 2,000×*g* for 5 min and washed twice with PBS. Then, the pellet was treated with 500 μl of ACK lysis buffer [154.95 mM NH_4Cl, 10 mM $KHCO_3$, and 0.1 mM ethylenediaminetetraacetic acid (EDTA); pH 7.2] at room temperature for 5 min. To stop the reaction, 100 μl of FBS was added to it and was centrifuged at 2,000×*g* for 5 min and washed twice with PBS. The pellet was then resuspended in 70 μl of RIPA buffer [50 mM Tris–Cl (pH 8), 150 mM NaCl, 5 mM EDTA, 1% (*v*/*v*) NP-40, 0.5% (*w*/*v*) sodium deoxycholate, and 0.1% (*w*/*v*) sodium dodecyl sulfate] containing 1× mammalian protease inhibitor cocktail (Sigma-Aldrich, USA) and sonicated at 10 Å for three pulses of 5 s each. This was then centrifuged at 24,000×*g* for 30 min. The supernatant thus obtained was the splenic lysate.

TNFα and IL-6 Gene Expression

Balb/c mice 6–8 weeks old were infected intraperitoneally with 5×10^5 log-phase bacteria. At 36 hpi, spleens were isolated and were subjected to ballooning with 400 U/ml Collagenase D in HBSS and incubated at 37°C for 25 min. To stop the reaction, 100 μl of 0.5 M EDTA was added and incubated at 37°C for 5 min. This was then passed through a 40-μm strainer, and 5 ml of ice-cold RPMI 1640 media supplemented

with 10% (*v*/*v*) FBS was added to it. The cells were then harvested at 2,000×*g* for 5 min and washed with PBS. The pellet was resuspended in 3 ml of 30% bovine serum albumin (Sigma-Aldrich, USA). To this, 1 ml of PBS was added slowly along the wall of the conical tube to form a layer and was subjected to density gradient centrifugation (with zero acceleration or deceleration) at 2,200×*g* for 30 min at 12°C. The interface of the two layers contained the mononuclear cells, which were then harvested, and RNA was isolated according to the manufacturer's protocol using the Nucleopore RNA isolation Kit (Genetix, India). The complementary DNA (cDNA) was then synthesized using Verso-cDNA kit (Thermo-Fisher, USA). The PCRs were performed using Maxima SYBR green qPCR master mix (Thermo-Fisher, USA) and the Eppendorf Realplex master cycler. Primer sequences were used from the Harvard primer bank and were synthesized by Integrated DNA Technologies, USA.

Quantification of TNFα

RAW 264.7 and BMDMs were plated at a density of 1×10^6 cells/ml and infected with wt, Δ*steA*, or compl strains at an MOI of 20:1 or 10:1, respectively. The supernatant was collected after 8 h of infection, and TNFα was quantified using ELISA (BD Biosciences, USA) as per the manufacturer's protocol. Furthermore, to confirm equal invasion in all the experiments, cells were lysed after 2 h of infection with 0.1% (*v*/*v*) Triton-X-100 at 37°C for 30 min, and bacteria were enumerated on LA plates.

Transfection of HEK 293 Cells

HEK 293 (a human kidney epithelial cell line) cells (7×10^6) were plated in DMEM in a 90-mm Petri dish for whole-cell lysate preparation, and 2.5×10^4 HEK 293 cells were seeded on coverslips in a 24-well plate for colocalization studies. Cells were then transfected with 3 μg (for whole-cell lysates) or 1 μg (for colocalization) of pCDNA3.1(+) or pCDNA3.1(+)*steA* (**Table 2**) using polyethyleneimine at a ratio of 1:3 (DNA/polyethyleneimine). The media was changed after 8 h of transfection. Then, after 24 or 36 h of transfection, the cells were stimulated with 10 ng/ml of TNFα for 15 or 30 min for whole-cell lysate preparation and 30 min for colocalization studies.

Luciferase Reporter Assay

For HEK 293 Cells

HEK 293 cells (2.5×10^4) were plated in 100 μl of DMEM in a 96-well plate and were transfected with 0.1 μg each of NF-κB reporter plasmid pGL4.1 (Promega, USA) and renilla luciferase plasmid (pRL) (**Table 2**) using Lipofectamine 3000 (Promega, USA) as per the manufacturer's protocol. In addition, in assays for studying the effect of endogenous expression of SteA on NF-κB activation, cells were also transfected with pcDNA3.1(+) or pcDNA3.1(+)*steA* in addition to pGL4.32 and pRL. After 18 h of transfection, the cells were either infected with wt, Δ*steA*, and compl or stimulated with 10 ng/ml of TNFα for 6 and 8 h, respectively.

For RAW 264.7 Cells

RAW 264.7 cells (5×10^4) were plated in 100 μl of RPMI in a 96-well plate and were transfected with 0.15 μg each of NF-κB reporter plasmid pGL4.1 (Promega, USA) and pRL (**Table 2**) using FuGene HD (Promega, USA) as per the manufacturer's protocol. After 12 h of transfection, the cells were infected with wt, Δ*steA*, and compl or stimulated with 500 ng/ml of LPS for 15 h.

The dual luciferase assay kit (Promega, USA) was used according to the manufactures' protocol to analyze the luminescence corresponding to NF-κB activation (firefly luciferase) and the renilla luciferase. The luminescence was detected using a plate reader (BMG Biotech, Germany). The luminescence corresponding to NF-κB activation was normalized to that of renilla luciferase (corresponding to the transfection efficiency). In infection-based experiments, the luminescence was also normalized to the invasion.

Colocalization Studies

After 24 h of transfection in HEK 293 cells and TNFα stimulation for 30 min (as described previously), cells were washed twice with PBS and were then fixed with 2.5% (*w*/*v*) of paraformaldehyde for 30 min at room temperature. Cells were then washed twice with PBS and incubated with anti-IκB (1:750) (Santa Cruz Biotechnologies, USA), anti-HA (1:250) (Biolegend, USA), anti-Cullin-1 (1:250) (Cell Signaling Technologies, USA), or anti-Cand-1 (1:500) (Cell Signaling Technologies, USA) antibodies for 45 min at room temperature. Then, cells were washed thrice with PBS and incubated with Alexa 488-conjugated anti-rabbit immunoglobulin G secondary antibody (1:500) (Life Technologies, USA) and Alexa 568-conjugated anti-mouse immunoglobulin G secondary antibody (1:500) (Life Technologies, USA) for 30 min at room temperature. All the antibody dilutions were prepared in 0.2% (*w*/*v*) Saponin dissolved in PBS. The cells were washed thrice with PBS and were mounted on glass slides using Fluoromount (Sigma-Aldrich, USA). The imaging was performed using a Zeiss confocal microscope (for colocalization of IκB or Cullin-1 with SteA-HA) or Leica confocal microscope (for colocalization of Cand-1 with SteA-HA).

Whole-Cell Lysate Preparation

For Infection

Cells were plated at a density of 1.5×10^6/ml in a six-well plate for overnight. Cells (4.5×10^6) (three wells of 1.5×10^6/ml) were infected with wt, Δ*steA*, or compl for 30 min. Then, the bacteria were removed, and RPMI 1640 media containing 100 μg/ml of gentamicin was added to each well for 30 min. The cells were then washed twice with sterile PBS and were then harvested at 2,000×*g* for 5 min. The pellet was then resuspended in 70–100 μl of whole-cell lysis buffer [50 mM Tris–Cl, 150 mM NaCl, 0.1% (*w*/*v*) sodium dodecyl sulfate (SDS) and 0.1% (*v*/*v*) Triton-X-100, pH 8] with mammalian protease inhibitor cocktail (Sigma-Aldrich, USA) and subjected to sonication at 10 Å for 15 s with a pulse of 5 s each. Then, it was centrifuged at 16,000×*g* for 30 min at 4°C. The supernatant thus obtained was the whole-cell lysate.

In addition, the invasion was also checked by colony-forming unit counting for all the experiments.

For Transfections

After 24 h of transfection in HEK 293 cells (as described previously), cells were washed twice with PBS and were harvested by centrifugation at 2,000×*g* for 5 min. The pellet was then resuspended in 150–200 μl of whole-cell lysis buffer supplemented with mammalian protease inhibitor cocktail. This was then subjected to sonication at 10 Å for 15 s with a pulse of 5 s each. Then, it was centrifuged at 16,000×*g* for 30 min at 4°C, and the supernatant obtained was collected as whole-cell lysate.

Nuclear Lysate Preparation

Cells (4.5×10^6) (three wells of 1.5×10^6/ml) of RAW 264.7 were plated in a six-well plate overnight for each sample and then infected with wt, Δ*steA*, or compl for 30 min. Then, the bacteria were removed, and RPMI 1640 media containing 100 μg/ml of gentamicin were added to each well for 30 min. Cells were then washed twice with sterile PBS and were then harvested at 2,000×*g* for 5 min. The pellet volume was measured, and it was dissolved in five times the pellet volume in hypotonic buffer (10 mM HEPES pH 7.9 with 1.5 mM $MgCl_2$ and 10 mM KCl) and centrifuged at 1,850×*g* for 5 min at 4°C. Then, the pellet was dissolved in hypotonic buffer with 0.5 M dithiothreitol and mammalian protease inhibitor and was then incubated on ice for 15 min. This was then sonicated at 10 Å for 15 s with three pulses of 5 s each and centrifuged at 3,300×*g* for 15 min at 4°C. The pellet was then resuspended in 70 μl of low salt buffer [20 mM HEPES pH 7.9, 1.5 mM $MgCl_2$, 20 mM KCl, 0.2 mM EDTA, and 25% (*v*/*v*) glycerol] with 0.5 M DTT and mammalian protease inhibitor. To this, 30 μl of high salt buffer [20 mM HEPES pH 7.9, 1.5 mM $MgCl_2$, 800 mM KCl, 0.2 mM EDTA, and 25 % (*v*/*v*) glycerol] was added dropwise and incubated on ice for 10 min before subjecting to sonication at 10 Å for 15 s. Then, it was incubated on ice for 30 min with periodic shaking and centrifuged at 24,000×*g* for 30 min at 4°C. The supernatant hence obtained contained the nuclear lysate.

Immunoblotting

The whole-cell lysates or the nuclear lysates were run on SDS-polyacrylamide gel electrophoresis (SDS-PAGE) gel and were transferred to polyvinylidene difluoride membrane using wet transfer. After the transfer, the membrane was incubated with 5% (*w*/*v*) bovine serum albumin (BSA) in TBST [20 mM Tris buffer pH 7.5, 150 mM NaCl, and 0.1% (*v*/*v*) Tween 20] for blocking. Then, it was incubated with various antibodies purchased from different companies. The antibodies against IκB, glyceraldehyde 3-phosphate dehydrogenase (GAPDH), p65, c-Rel, and Lamin B1 were purchased from Santa Cruz Biotechnologies, USA. The antibodies against p-p38, p38, phosphorylated c-Jun N-terminal kinase (p-JNK), JNK, IκB kinase α/β (IKKα/β), Cullin-1, Cand-1, β-TrCP, Skp-1 and Rbx-1 were purchased from Cell Signaling Technologies, USA. The antibodies against His-tag, HA-tag, and proliferating cell nuclear antigen (PCNA) were purchased from Biolegend, USA. The antibody against Nedd8-Cullin was purchased from Abcam, UK. The antibody against LAMP-1 was purchased from Thermo Fisher Scientific, USA.

The horseradish-peroxidase-tagged secondary antibodies and antibody against glutathione-S-transferase (GST) were purchased from Sigma-Aldrich, USA. The immunoblots were developed using Clarity™ ECL Substrate (Bio-Rad, USA) and detected using LAS 4000 (GE Healthcare Technologies, USA).

Densitometric Analysis

The densitometric analysis of the immunoblots was carried out using the Image J software. The band intensities of IκB, IKKα/β, p65, or c-Rel were normalized to the respective band intensities of the loading controls, i.e., glyceraldehyde 3-phosphate dehydrogenase for whole-cell lysates and PCNA for nuclear lysates. The band intensities of phosphorylated p38 and JNK were normalized to the band intensities of the total p38 and JNK. The lane intensities of ubiquitination and the band intensities of Cand-1 were normalized to the band intensities of IκB, and the band intensities of neddylated Cullin was normalized to the band intensities of Cullin-1.

Coimmunoprecipitation Studies

Whole-cell lysates were prepared (as previously described) and were incubated with 1–2 μg of anti-HA, anti-His, anti-Cullin-1, or anti-IκB antibody for 3–4 h with continuous low-speed shaking at 4°C. Then, 20 μl of Protein A/G beads (Santa Cruz Biotechnologies, USA) was added, and it was subjected to continuous low-speed shaking at 4°C for overnight. Then, the beads were washed thrice with whole-cell lysis buffer by centrifugation at 6,000×*g* for 5 min at 4°C. The beads were resuspended in SDS-loading buffer and boiled for 10 min. The samples were then run on SDS-PAGE gel and subjected to immunoblotting.

For IκB Pulldown

HEK 293 cells were transfected with 3 μg of pcDNA3.1(+) or pcDNA3.1(+)*steA* (as described previously). After 24 h of transfection, cells were treated with 20 nM of proteasomal inhibitor, MG132 (Sigma-Aldrich, USA), for 3 h. The cells were then stimulated with 10 ng/ml of TNFα for 20 min, and whole-cell lysates were prepared. The whole-cell lysates were then subjected to coimmunoprecipitation with 2 μg of the anti-IκB antibody as described above.

GST Pulldown Assay

The *steA* gene was cloned in the plasmid pGEX4T3 (**Table 2**) using restriction cloning. The empty pGEX4T3 and pGEX4T3-*steA* were each transformed to *Escherichia coli* Origami B1 cells (Merck, Germany) by chemical transformation method. Then, using these transformants, GST and GST-tagged SteA were overexpressed using 0.1 mM isopropyl β-D-1-thiogalactopyranoside at 18°C for 24 h. The bacteria were pelleted at 2,050×*g* for 30 min at 4°C. The pellet was resuspended in PBS containing bacterial protease inhibitor cocktail (Sigma-Aldrich, USA) and was subjected to sonication at 25 Å for 15 min. Then, this was centrifuged at 18,500×*g* for 50 min at 4°C and analyzed by SDS-PAGE. Both GST and GST-tagged SteA

were found to be present in the soluble fractions. Parallelly, the glutathione beads (Qiagen, USA) were washed twice with lysis buffer [50 mM Tris–Cl, 150 mM NaCl, 0.05% (*v*/*v*) NP-40, pH 7.5]. Then, to 10 ml of the soluble fraction containing GST or GST-tagged SteA, 300 µl of washed glutathione beads were added and incubated at 4°C with shaking. After 2 h of incubation, the beads were pelleted at 1,800×*g* for 5 min and washed four times with lysis buffer. Then, the beads were incubated with 500 µl of 5% (*w*/*v*) BSA in PBS for 90 min. Then, the beads were pelleted and washed four times with lysis buffer. To this, whole-cell lysate of unstimulated RAW 264.7 cells was added and incubated at 4°C for 3–4 h with shaking. Then, the beads were pelleted and washed four times with lysis buffer and resuspended in 40 µl of SDS-loading buffer. This was then boiled for 5 min and subjected to SDS-PAGE and immunoblotting.

Yeast Two-Hybrid Assay

The coding sequences of IκB, Skp-1, Rbx-1, and Cullin-1 from *Mus musculus* were taken from www.ncbi.nlm.gov.in. A cDNA library was prepared according to manufacturer's protocol (Invitrogen, Life Technologies, USA) using RNA isolated (according to the manufacturer's protocol; Genetix, India) from untreated RAW 264.7 cells. IκB, Skp-1, and Rbx-1 were amplified from the cDNA library and cloned in pGADC1 (**Table 2**) plasmid by restriction cloning. Cullin-1 was amplified and cloned in pGADT7 (**Table 2**) by gateway cloning method according to manufacturer's protocol (Thermo-Fisher, USA). The *steA* gene was amplified from the *Salmonella* Typhimurium genome and cloned in pGBDC1 plasmid (**Table 2**) by restriction cloning. The cloned AD and the BD plasmids were cotransformed in yeast (PJ697a) and plated on synthetic complete media deficient in leucine and uracil (SC-Leu, SC-Ura). The colonies thus obtained were then spotted on plates with media deficient in leucine, uracil, and histidine (SC-Leu, SC-Ura, SC-His).

Statistical Analysis

Data were expressed as mean ± standard error of mean (SEM), and *p* values were calculated using Student's two-sided *t* test or by one-way ANOVA followed by Tukey's multiple comparisons test. Significance is indicated as follows: $^{*}p < 0.05$, $^{**}p < 0.01$, $^{***}p < 0.001$, and nonsignificant (ns) when $p > 0.05$.

RESULTS

SteA Affects the Pathogenesis of *Salmonella* Typhimurium

To understand the effect of SteA deletion in mouse model of *Salmonella* infection, we constructed *steA* deletion mutant (Δ*steA*) of *Salmonella* Typhimurium and *steA*-complemented strain (compl) with *steA*-containing plasmid on Δ*steA* background. Furthermore, we infected Balb/c mice with 5×10^5 and 5×10^7 wt, Δ*steA*, and compl *Salmonella* Typhimurium. We have observed that the mice infected with Δ*steA* died earlier than the wt and compl-infected mice (**Figures 1A**, **B**). Furthermore, we have observed that Δ*steA*-infected mice showed symptoms, namely, pilorected fur, decrease in activity, decrease in response to stimulus, and the extent of closing of the eyes that were graded on a scale of 1–4 (34) higher as compared to the control mice (**Figure 1C**). The scoring indicated that the mice infected with the Δ*steA* strain probably died of a heightened immune response. We also checked the body temperatures of mice infected with 5×10^5 wt, Δ*steA*, and compl and found lower body temperatures of Δ*steA*-infected mice, indicating that probably mice were undergoing sepsis (35).

Furthermore, to probe whether there was any increase in the proinflammatory cytokine levels in Δ*steA*-infected mice compared to the controls, we checked TNFα, IL-6, IL-1β, IFN-γ, IL-12, and IL-10 in the serum of the infected mice and found higher TNFα, IL-6, IFN-γ, IL-12, and IL-10 level in the serum of the Δ*steA*-infected compared to wt- or compl-infected mice (**Figure S1**). Furthermore, we have isolated mononuclear cells from the spleen of mice infected with wt, Δ*steA*, and compl strains and analyzed the expression of TNFα and IL-6 genes. We have observed higher expression of both TNFα and IL-6 genes in cells isolated from mice infected with the Δ*steA* strains as compared to the wt- and compl-infected mice (**Figure 1E**). Therefore, in accordance with our hypothesis, it seemed that there was an elevated inflammatory immune response in Δ*steA*-infected mice compared to the controls. Furthermore, to check if the difference in immune response was due to a difference in the colonization pattern of Δ*steA* compared to the wt strain, we have isolated spleen and enumerated the bacteria by colony-forming unit counting. No difference in the colonization of *Salmonella* Typhimurium was observed in the spleen of these respective strain-infected mice (**Figure 1F**). Altogether, these results suggested that during *Salmonella* Typhimurium infection, absence of SteA enhances the host-inflammatory responses.

Increased TNFα Production in Macrophages Infected With Δ*steA*

To further confirm that there is heightened inflammatory response upon infection with Δ*steA*, we infected RAW 264.7 (murine macrophage cell line) and BMDMs with wt, Δ*steA*, and compl strains. After 8 h of infection, supernatants were collected and analyzed for TNFα. In both the cell types, a higher TNFα production was observed when infected with Δ*steA* compared to the wt and the compl-infected cells (**Figure 2A**). We further checked the cell cytotoxicity upon infection with wt, Δ*steA*, and compl strains to probe whether this difference in TNFα production was due to a difference in cell death. However, we did not find any difference in cell cytotoxicity in RAW 264.7 or BMDMs infected with wt, Δ*steA* or compl (**Figure S2**). Therefore, our data confirmed that the *Salmonella* Typhimurium-mediated host-immune responses increase in the absence of SteA.

SteA is secreted by both T3SS-1 and T3SS-2. In addition, recently, it was reported that SteA could be secreted by T3SS-2 as early as 15 min in RAW 264.7 cells (24). Therefore, we wanted to check whether the observed effect of SteA was due to T3SS-2 effector function. To address this, we have used a Δ*spi2* mutant of *Salmonella* Typhimurium and a Δ*steA* mutant

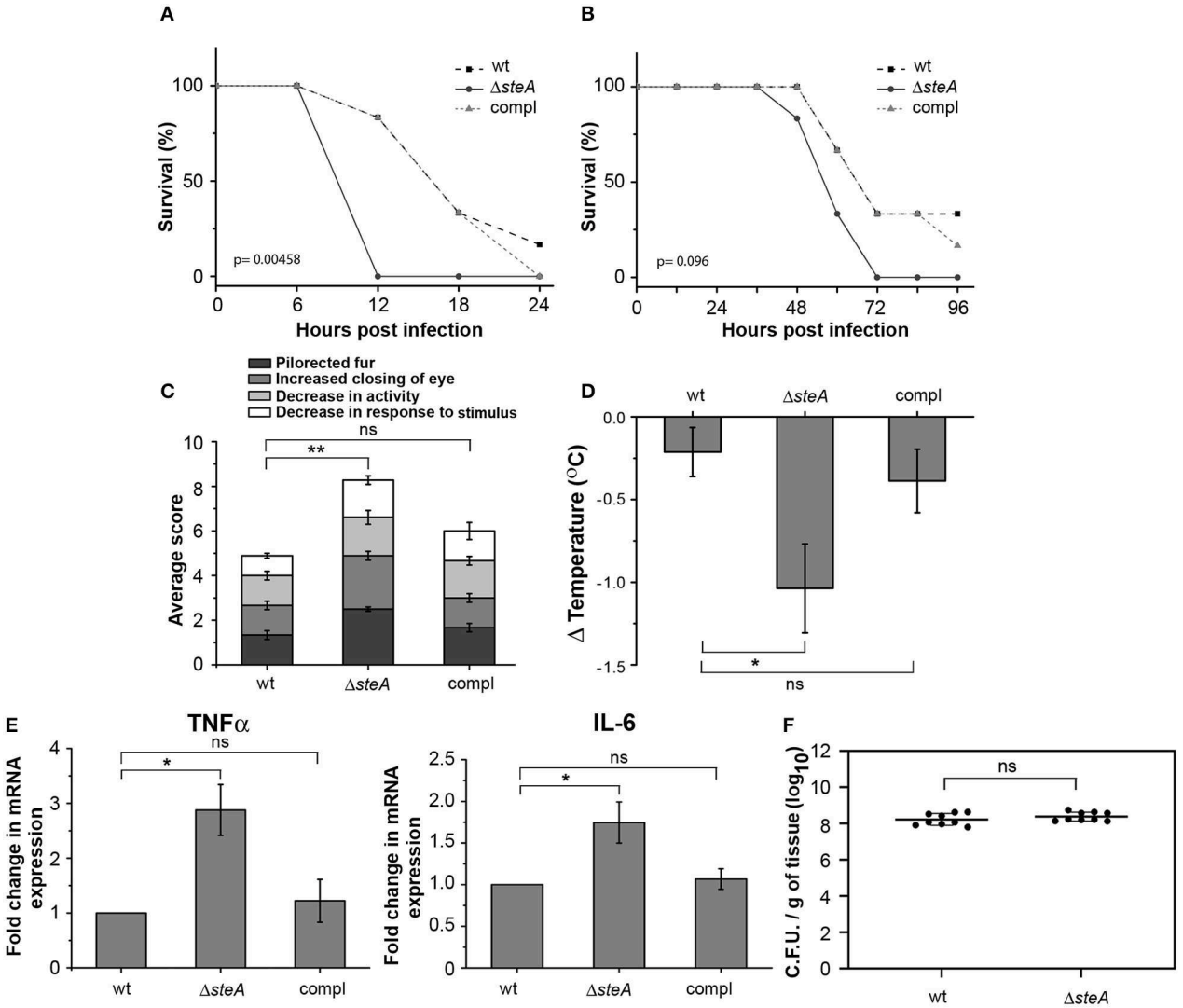

FIGURE 1 | Δ*steA*-infected mice had lower survival and higher immune responses than the wt or compl. **(A,B)** Balb/c mice infected with the *steA* deletion mutant (Δ*steA*) had lower survival than those infected with wild type (wt) and the *steA*-complemented (compl) strain of *Salmonella* Typhimurium. Balb/c mice 6–8 weeks old were infected intraperitoneally with 5×10^7 bacteria and monitored over a period of 24 h **(A)** or with 5×10^5 bacteria and monitored over a period of 96 h **(B)**. After every 6 h **(A)** or 12 h **(B)**, the percentage of survival was calculated as (the number of mice surviving/total mice infected) × 100. The graph represents the percentage of survival of mice infected with wt, Δ*steA*, or compl strains with six mice in each group. *p* values were calculated using Kaplan–Meier survival test. **(C)** Balb/c mice infected with Δ*steA* showed advanced symptoms of a heightened immune response as compared to the wt and the compl-infected mice. Balb/c mice 6–8 weeks old were infected intraperitoneally with 5×10^5 bacteria and scored for symptoms, namely, decrease in activity, decrease in response to stimuli, extent of closing of the eye, and the extent of pilorected fur at 36 h postinfection (hpi). For each experiment, the average of total scores for three or four mice infected with either wt, Δ*steA*, or compl was calculated. Bar graph represents mean ± SEM from three independent experiments. *p* values were calculated using one-way ANOVA of the total scores from three independent experiments (*$p < 0.05$, **$p < 0.01$, ***$p < 0.001$, ns $p > 0.05$ vs. wt-infected mice). **(D)** Body temperatures of Balb/c mice infected with Δ*steA* were lower than wt- or compl-infected mice. Balb/c mice 6–8 weeks old were infected intraperitoneally with 5×10^5 bacteria, and the body temperatures of mice were recorded before infection and at 24 hpi. Then, the difference in body temperature was calculated (ΔTemperature). Bar graph represents mean ± SEM from eight mice in each group. *p* values were calculated using one-way ANOVA of ΔTemperature of eight mice from each group ($n = 8$) (*$p < 0.05$, **$p < 0.01$, ***$p < 0.001$, ns $p > 0.05$ vs. wt-infected mice). **(E)** Tumor necrosis factor alpha (TNFα) and interleukin (IL)-6 gene expression was higher in mononuclear cells isolated from spleen of mice infected with Δ*steA* compared to those infected with wt or compl. The spleens of Balb/c mice infected with 5×10^5 bacteria were isolated at 36 hpi. The mononuclear cells were isolated using density-dependent separation [with bovine serum albumin (BSA)]. RNA was isolated from these cells; then, complementary DNA (cDNA) was prepared and gene expression of TNFα and IL-6 was analyzed by semiquantitative PCR. Fold change in gene expressions was calculated with respect to the gene expression in cells from mice infected with wt. Bar graph represents mean ± SEM from three independent experiments. *p* values were calculated using one-way ANOVA (*$p < 0.05$, **$p < 0.01$, ***$p < 0.001$, ns $p > 0.05$ vs. wt-infected mice). **(F)** No significant difference in the colonization of wt and Δ*steA* *Salmonella* Typhimurium in spleen of infected mice. Bacteria were enumerated in spleen of Balb/c mice infected intraperitoneally with 5×10^5 bacteria at 36 hpi. Graph represents colony-forming units (CFU) enumerated per milligram of spleen tissue from nine mice each (represented as a dot •). *p* values were calculated using Student's *t* test (*$p < 0.05$, **$p < 0.01$, ***$p < 0.001$, ns $p > 0.05$ vs. wt-infected mice).

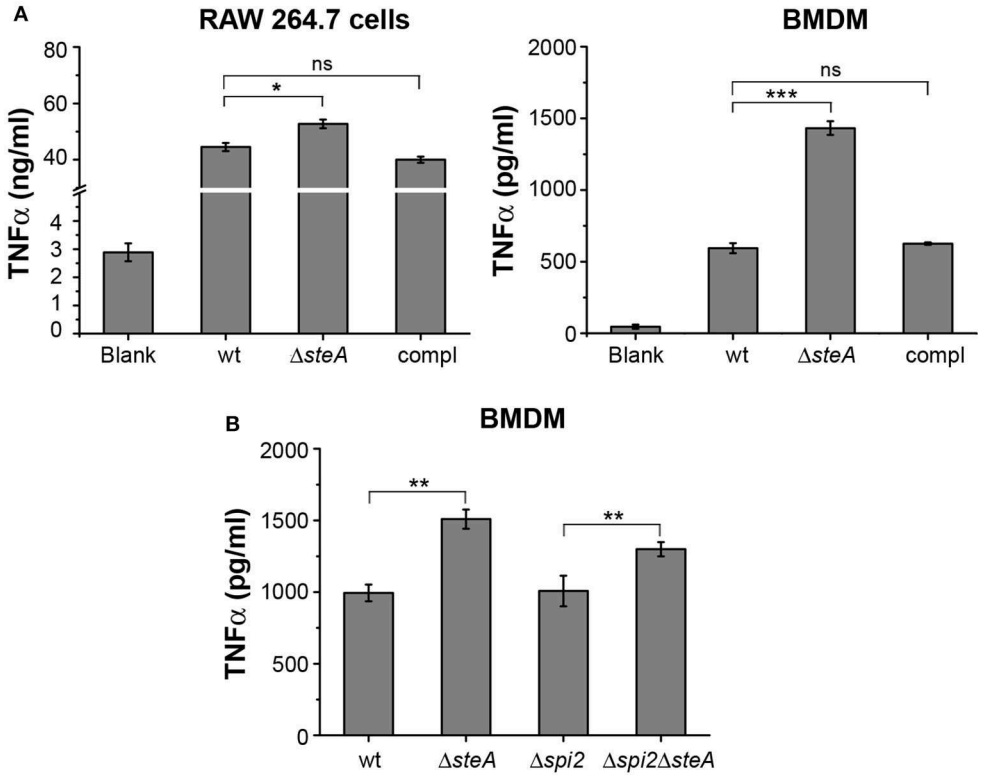

FIGURE 2 | SteA suppresses proinflammatory responses in macrophages during *Salmonella* Typhimurium infection. **(A)** Tumor necrosis factor alpha (TNFα) production was higher in RAW 264.7 macrophages and bone-marrow-derived macrophages (BMDMs) infected with Δ*steA* as compared to the controls. RAW 264.7 cells and BMDMs were infected with wt, Δ*steA*, or the compl [at an multiplicity of infection (MOI) of 20:1 for RAW 264.7 and 10:1 for BMDMs]. The supernatant was collected after 8 h of infection and analyzed for TNFα by ELISA. Bar graph represents mean ± SEM from three independent experiments. *p* values were calculated using one-way ANOVA (*$p < 0.05$, **$p < 0.01$, ***$p < 0.001$, ns $p > 0.05$ vs. wt-infected cells). **(B)** SteA-mediated immune suppression is not affected by the absence of *spi2* gene cluster (Δ*spi2*), indicating that this effect of SteA is not SPI-2 dependent. BMDMs were infected at an MOI of 10:1 with wt, Δ*steA*, Δ*spi2*, and Δ*spi2*Δ*steA*. Supernatant was collected after 8 h, and TNFα was quantified by ELISA. Bar graph represents mean ± SEM from three independent experiments. *p* values were calculated using Student's *t* test (*$p < 0.05$, **$p < 0.01$, ***$p < 0.001$, ns $p > 0.05$ vs. wt or Δ*spi2*-infected cells).

in Δ*spi2* background (Δ*spi2*Δ*steA*). We have treated BMDMs with wt, Δ*steA*, Δ*spi2*, and Δ*spi2*Δ*steA* strains. After 8 h, we collected the supernatants and analyzed for TNFα by ELISA. The cells infected with Δ*spi2*Δ*steA* showed higher TNFα production than Δ*spi2*-infected cells in BMDMs (**Figure 2B**), indicating that SteA-mediated effect on the immune response is not T3SS-2 dependent.

SteA Acts on the NF-κB Pathway to Suppress the Immune Responses

An immune response involves the activation of majorly two transcription factors NF-κB and AP-1. The phosphorylation of mitogen-activated protein (MAP) kinases p38 and/or JNK majorly leads to the activation of AP-1 (36). To check whether MAP kinases could be involved in Δ*steA*-mediated heightened immune response, we infected RAW 264.7 cells with wt, Δ*steA*, and compl strains and checked whether there is an increase in the phosphorylation levels of p38 and JNK MAP kinases in the whole-cell lysates. No difference in the phosphorylation level of p38 and JNK was observed in any of the treatments (**Figures 3A**,**B**). As phosphorylation levels are indicative of activation levels, our study indicated that SteA probably does not interfere in the MAP kinase activation pathway. As activation of the AP-1 transcription factor is dependent on MAP kinase activation, we presumed that probably SteA-mediated effect is not via the AP-1 pathway.

Furthermore, we wanted to check whether SteA has any effect on the activation of NF-κB. In an inactivated state, NF-κB remains bound to its inhibitor IκB, which prevents the translocation of NF-κB to the nucleus. Upon phosphorylation of IκB by upstream kinase IKKα/β, IκB gets ubiquitinated and degraded through proteasome rendering NF-κB free to translocate to the nucleus (31, 37). We observed that in Δ*steA*-infected RAW 264.7 cells and BMDMs, there is increased IκB degradation compared to control infected cells (**Figures 4A**, **B**). NF-κB is known to be activated in HEK 293 cells in response to TNFα. To confirm the observation that SteA affects the degradation of IκB, we endogenously expressed SteA in HEK 293 cells and probed the IκB levels upon stimulation

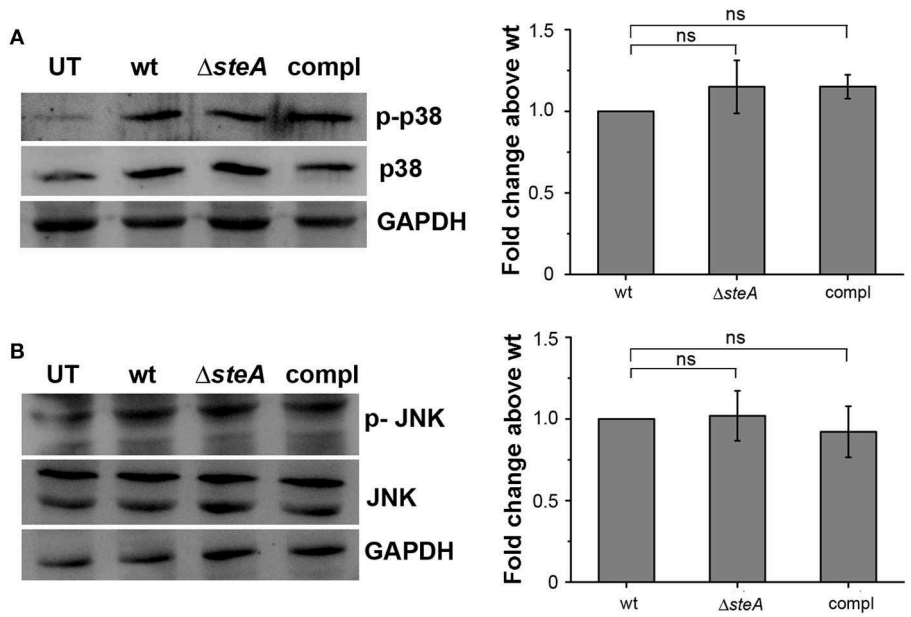

FIGURE 3 | SteA does not affect the mitogen-activated protein (MAP)-kinase activation. **(A,B)** The phosphorylation levels of the MAP kinases p38 **(A)** and c-Jun N-terminal kinase (JNK) **(B)** remained unchanged upon infection with Δ*steA* as compared to the controls. RAW 264.7 cells were infected with wt, Δ*steA*, or compl strains at an multiplicity of infection (MOI) of 20:1, and whole-cell lysates were prepared after 30 min of infection. Whole-cell lysates were probed for phosphorylated levels of p38 and JNK by Western blots and densitometric analysis along with total p38 and JNK levels. Glyceraldehyde 3-phosphate dehydrogenase (GAPDH) was used as a loading control. For densitometric analysis, fold change was calculated with respect to wt. Bar graphs represent mean ± SEM from three independent experiments. *p* values were calculated using one-way ANOVA (*$p < 0.05$, **$p < 0.01$, ***$p < 0.001$, ns $p > 0.05$ vs. wt-infected cells). UT stands for untreated cells.

with TNFα. We observed increased IκB degradation in TNFα-activated cells transfected with the empty plasmid, but in cells expressing SteA, IκB degradation was found to be inhibited (**Figure 4C**). Furthermore, we also observed less IκB in splenic lysates of mice infected with Δ*steA* compared to the control (**Figure 4D**).

More degradation of IκB suggests increased translocation of NF-κB to the nucleus. Among the NF-κB family members, p65 and/or c-Rel are involved in the transcription of proinflammatory genes (37). Thus, to probe if IκB degradation corresponds to the nuclear translocation of NF-κB, we infected RAW 264.7 cells with wt, Δ*steA*, and compl strains and checked the levels of p65 and c-Rel in the nuclear lysates. We observed that the nuclear translocation of both p65 and c-Rel were more in cells infected with Δ*steA* compared to the wt and the compl-infected cells (**Figure 5A**). This observation indicated that the NF-κB activation during *Salmonella* Typhimurium infection increases in the absence of SteA. Furthermore, to confirm that SteA suppresses NF-κB activation, we transfected HEK 293 and RAW 264.7 cells with NF-κB promoter-reporter plasmid and then infected with wt, Δ*steA*, and compl strains. The cells infected with Δ*steA* showed higher NF-κB reporter activity than wt and the compl strains in both HEK 293 and RAW 264.7 cells (**Figure 5B**). Furthermore, we wanted to know if endogenous expression of SteA could also suppress NF-κB activation. Toward this, we endogenously expressed SteA in HEK 293 cells and then transfected with the NF-κB promoter-reporter plasmid. We observed that upon stimulation with TNFα, there is diminished NF-κB reporter activity in endogenous SteA-expressing cells as compared to the cells transfected with empty plasmid (**Figure 5C**).

Altogether, these results confirm that SteA suppresses the immune responses by acting on the NF-κB pathway.

SteA Interferes With the IκB Ubiquitination

IκB phosphorylation by IKKα/β is a prerequisite for IκB degradation. In response to an infection, a signaling cascade leads to the phosphorylation of IKKα/β, which in turn phosphorylates IκB (36). Since we have observed that there is more IκB degradation in Δ*steA*-infected cells compared to the controls (**Figure 4**), we wanted to check whether this was due to increased activation of IKKα/β. No change was observed in the phosphorylation levels of IKKα/β in both RAW 264.7 macrophages and BMDMs infected with wt, Δ*steA*, and compl strains (**Figure 6A**). This result indicated that increased degradation of IκB is probably not due to increased activation of IKKα/β. Hence, SteA seems to act downstream to the activation of IKKα/β for suppression of IκB degradation.

The degradation of IκB requires its polyubiquitination. To probe if SteA was interfering with the polyubiquitination of IκB and subsequently its degradation, SteA-expressing HEK 293 cells were pretreated with a pharmacological inhibitor (MG132),

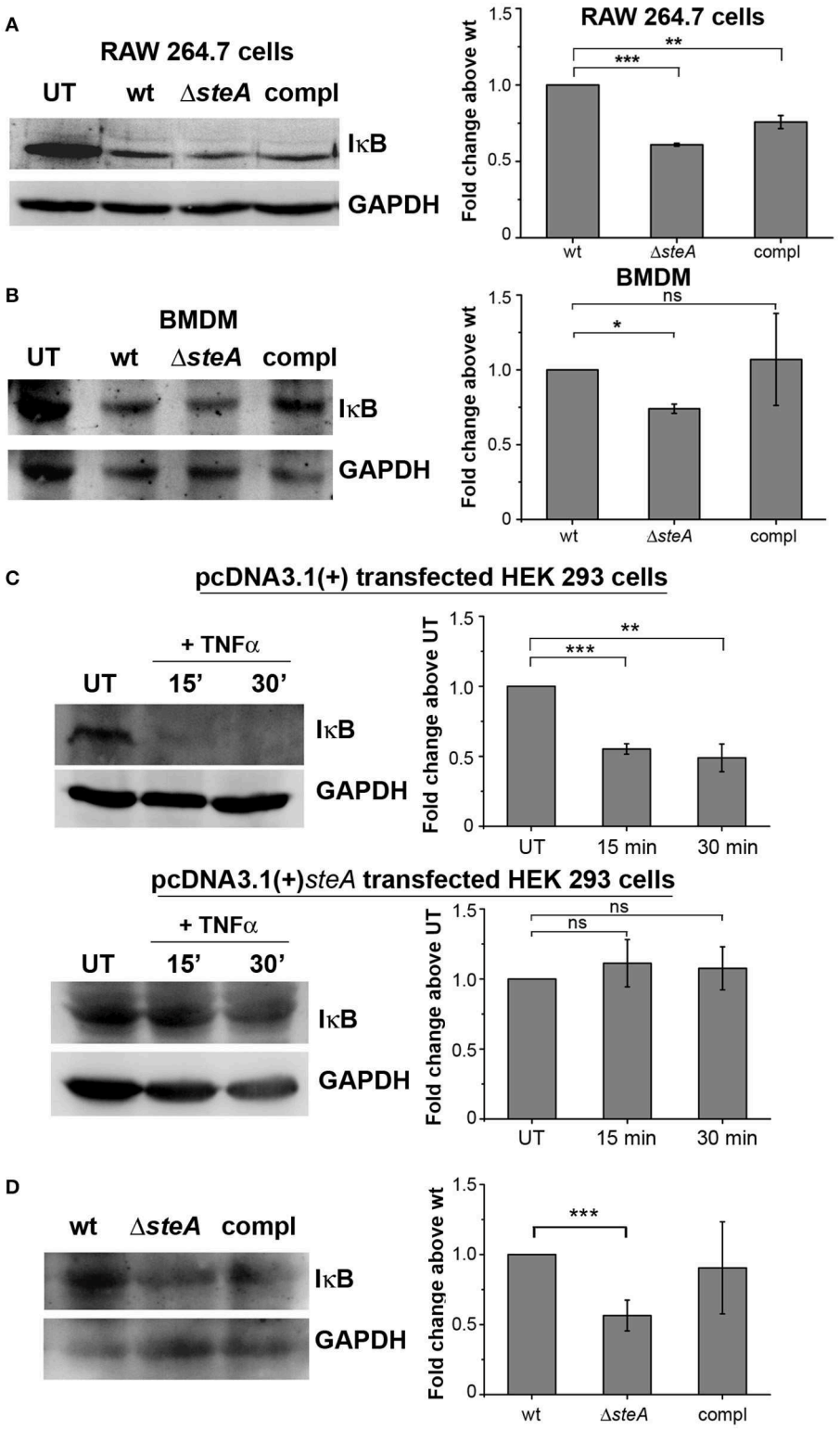

FIGURE 4 | SteA hinders IκB degradation. **(A,B)** IκB degradation was higher in cells infected with Δ*steA* than the wt or compl in both RAW 264.7 cells **(A)** and bone-marrow-derived macrophages (BMDMs) **(B)** as shown by Western blot and densitometric analysis. RAW 264.7 cells and BMDMs were infected with wt, Δ*steA*, or compl at an multiplicity of infection (MOI) of 20:1 and 10:1, respectively, and whole-cell lysates were prepared after 30 min of infection. The levels of IκB were probed by Western blotting. **(A,B)** Glyceraldehyde 3-phosphate dehydrogenase (GAPDH) was used as a loading control in all the experiments. UT stands for untreated cells.

(Continued)

FIGURE 4 | For densitometric analysis, fold change was calculated with respect to wt. Bar graphs represent mean ± SEM from three independent experiments. *p* values were calculated using one-way ANOVA (*$p < 0.05$, **$p < 0.01$, ***$p < 0.001$, ns $p > 0.05$ vs. wt-infected cells). **(C)** Endogenous expression of SteA suppresses the degradation of IκB in HEK 293 cells. HEK 293 cells were transfected with pcDNA3.1(+)*steA* or pcDNA3.1(+) empty plasmid. After 18 h of transfection, cells were stimulated with TNFα for 15 and 30 min. Whole-cell lysates were then prepared, and IκB levels were analyzed by Western blotting and densitometry. GAPDH was used as a loading control in all the experiments. UT stands for untreated cells. For densitometric analysis, fold change was calculated with respect to UT cells. Bar graphs represent mean ± SEM from three independent experiments. *p* values were calculated using Student's *t* test (*$p < 0.05$, **$p < 0.01$, ***$p < 0.001$, ns $p > 0.05$ vs. UT cells). **(D)** IκB levels were lower in splenic lysates of mice infected with Δ*steA* as compared to the control-infected mice. Balb/c mice were infected with wt, Δ*steA*, or compl, and spleen was isolated at 36 hpi. Splenic lysates were then prepared, and the levels of IκB were probed by Western blotting and densitometric analysis. GAPDH was used as a loading control in all the experiments. For densitometric analysis, fold change was calculated with respect to wt. Bar graphs represent mean ± SEM from three independent experiments. *p* values were calculated using Student's *t* test (*$p < 0.05$, **$p < 0.01$, ***$p < 0.001$, ns $p > 0.05$ vs. wt-infected mice).

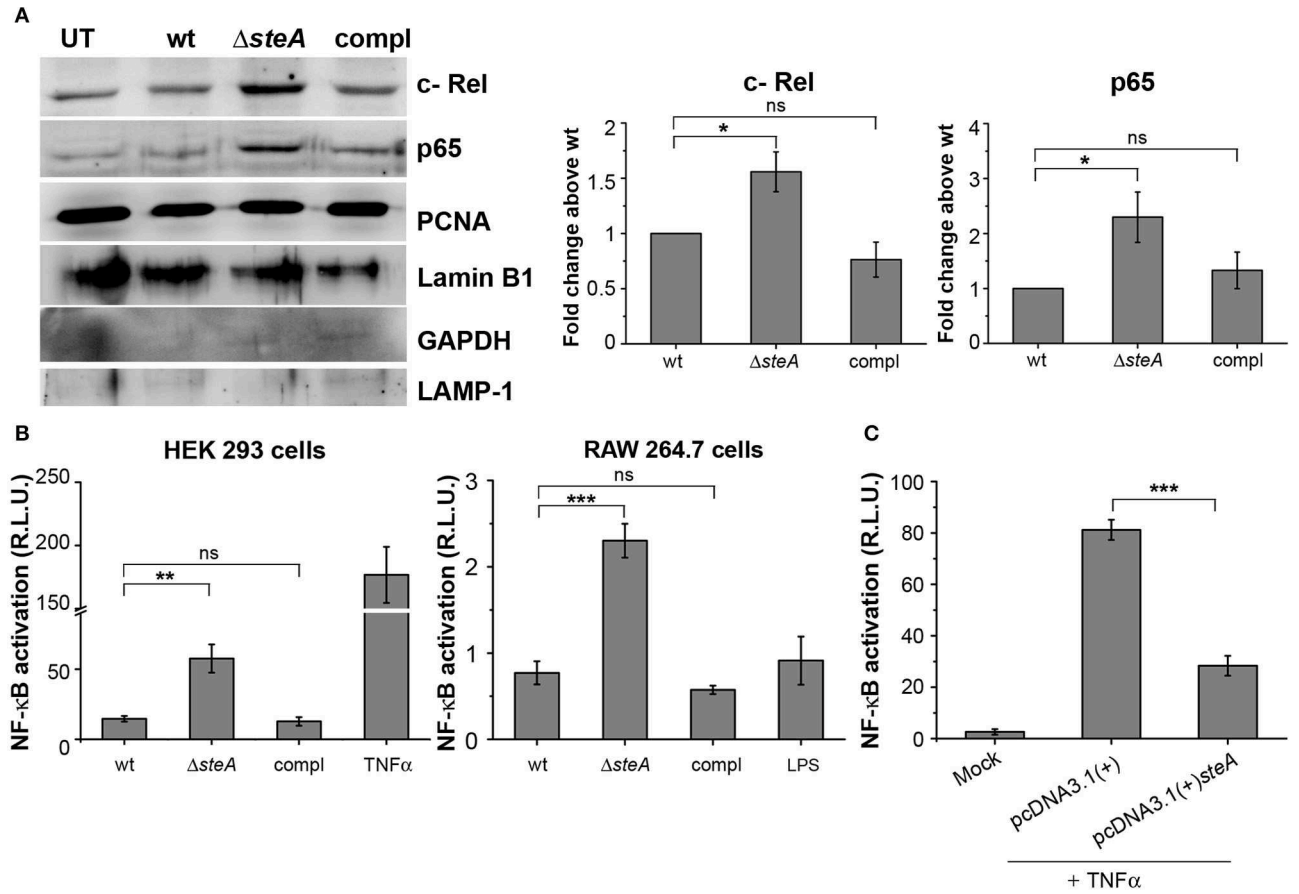

FIGURE 5 | SteA suppresses the nuclear factor kappa B (NF-κB) activation. **(A)** The translocation of NF-κB subunits (p65 and c-Rel) was more in cells infected with Δ*steA* than the controls. Nuclear lysates were prepared following infection of RAW 264.7 macrophages with wt, Δ*steA*, or compl for 30 min. p65 and c-Rel were probed by Western blotting and densitometry. Proliferating cell nuclear antigen (PCNA) and Lamin B1 were used as a loading control for nuclear fractions. In addition, GAPDH and LAMP-1 were used as non-nuclear markers to check the purity of the nuclear lysates. For densitometric analysis, fold change was calculated with respect to wt. **(B)** NF-κB reporter activity was higher upon infection of HEK 293 cells and RAW 264.7 cells with Δ*steA* than the wt or the compl-infected cells. HEK 293 or RAW 264.7 cells were transfected with NF-κB luciferase reporter plasmid and pRL (renilla luciferase) plasmid. After 18 or 12 h of transfection, respectively, cells were infected with wt, Δ*steA*, or compl at an multiplicity of infection (MOI) of 20:1 (HEK 293 cells) or 5:1 (RAW 264.7 cells), and the reporter activity was measured following 8 or 15 h of infection, respectively. Tumor necrosis factor alpha (TNFα) stimulated HEK 293 cells, and lipopolysaccharide (LPS)-stimulated RAW 264.7 cells were taken as positive control for the experiment. **(A,B)** Bar graph represents mean ± SEM from three independent experiments. *p* values were calculated using one-way ANOVA (*$p < 0.05$, **$p < 0.01$, ***$p < 0.001$, ns $p > 0.05$ vs. wt-infected cells). **(C)** Endogenous expression of SteA in HEK 293 cells suppresses the NF-κB reporter activity upon TNFα stimulation. HEK 293 cells were transfected with NF-κB Luciferase reporter plasmid, pRL plasmid, and pcDNA3.1(+)*steA* or pcDNA3.1(+) empty plasmid. After 18 h of transfection, cells were stimulated with TNFα, and the reporter activity was measured after 8 h. Bar graph represents mean ± SEM from three independent experiments. *p* values were calculated using Student's *t* test [*$p < 0.05$, **$p < 0.01$, ***$p < 0.001$, ns $p > 0.05$ vs. pcDNA3.1(+) transfected cells].

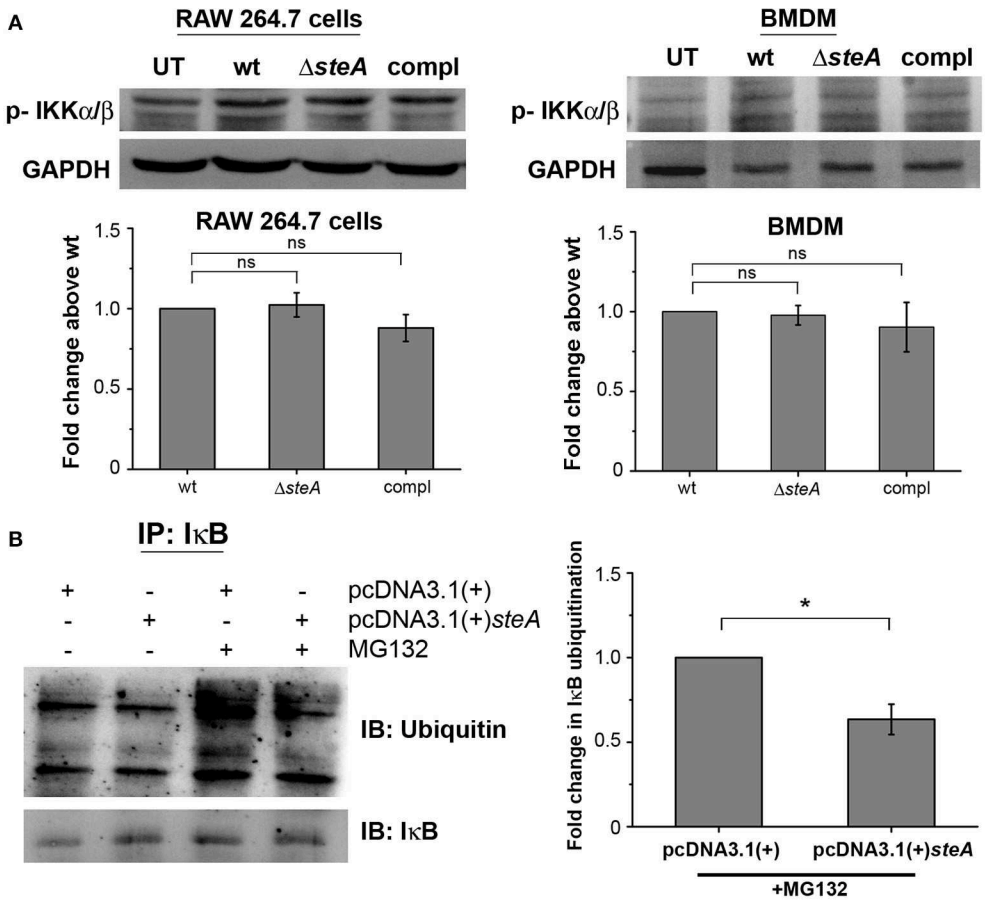

FIGURE 6 | SteA acts on the ubiquitination of IκB but does not affect the activation of upstream kinase (IKK). **(A)** SteA does not affect the activation of IKKα/β. RAW 264.7 cells, and BMDMs were infected with wt, Δ*steA*, or compl at an MOI of 20:1 and 10:1, respectively, and whole-cell lysates were prepared following 30 min of infection. The levels of IKKα/β were probed by Western blotting and densitometry. For densitometric analysis, fold change was calculated with respect to wt. Bar graphs represent mean ± SEM from three independent experiments. *p* values were calculated using one-way ANOVA (**p* < 0.05, ***p* < 0.01, ****p* < 0.001, ns *p* > 0.05 vs. wt-infected cells). **(B)** SteA suppresses the ubiquitination of IκB. HEK 293 cells were transfected with pcDNA3.1(+)*steA* or pcDNA3.1(+) empty plasmid. After 24 h of transfection, cells were pretreated with proteasomal inhibitor MG132 for 3 h and stimulated with TNFα for 20 min. Whole-cell lysates were then prepared and immunoprecipitated with anti-IκB antibody. Ubiquitination was then analyzed by Western blotting and densitometry. **(A,B)** Glyceraldehyde 3-phosphate dehydrogenase (GAPDH) was used as a loading control. For densitometric analysis, fold change was calculated with respect to pcDNA3.1(+) transfected cells. Bar graphs represent mean ± SEM from three independent experiments. *p* values were calculated using Student's *t* test [**p* < 0.05, ***p* < 0.01, ****p* < 0.001, ns *p* > 0.05 vs. pcDNA3.1(+) transfected cells].

which prevents the proteasomal degradation of ubiquitinylated proteins and immunoprecipitated with anti-IκB antibody. We observed that the ubiquitination of IκB was less when SteA was present (**Figure 6B**).

Altogether, these results showed that SteA interferes with the ubiquitination of IκB to suppress the host proinflammatory responses.

SteA Does Not Inhibit the Recruitment of E3 Ligase Components to IκB

For ubiquitination to happen, the phosphorylated IκB is recognized by the Skp-1, Cullin-1, F-box (SCF)-E3 ligase complex. Recruitment of the SCF complex to the phosphorylated IκB happens through F-box protein β-TrCP (31, 38). Therefore, to probe whether SteA could affect the recruitment of the SCF complex to IκB, we immunoprecipitated the lysates of wt and Δ*steA*-infected RAW 264.7 macrophages with anti-β-TrCP antibody and observed the association of SCF complex with IκB both in presence or absence of SteA. This showed that SteA was not interfering with the assembly of the SCF-E3 ligase complex to phosphorylated IκB (**Figure 7A** and **Figure S3A**).

Furthermore, to understand how SteA affects IκB ubiquitination, we checked whether SteA could associate with IκB. Toward this, we overexpressed SteA in HEK 293 cells and checked the localization of SteA with IκB upon stimulation with TNFα using confocal microscopy. We observed that IκB and SteA colocalize upon stimulation in cells overexpressing SteA (**Figure 7B**). Furthermore, to confirm the association of SteA with IκB and SCF complex, we have immunoprecipitated HA-tagged SteA-expressing HEK 293 cell

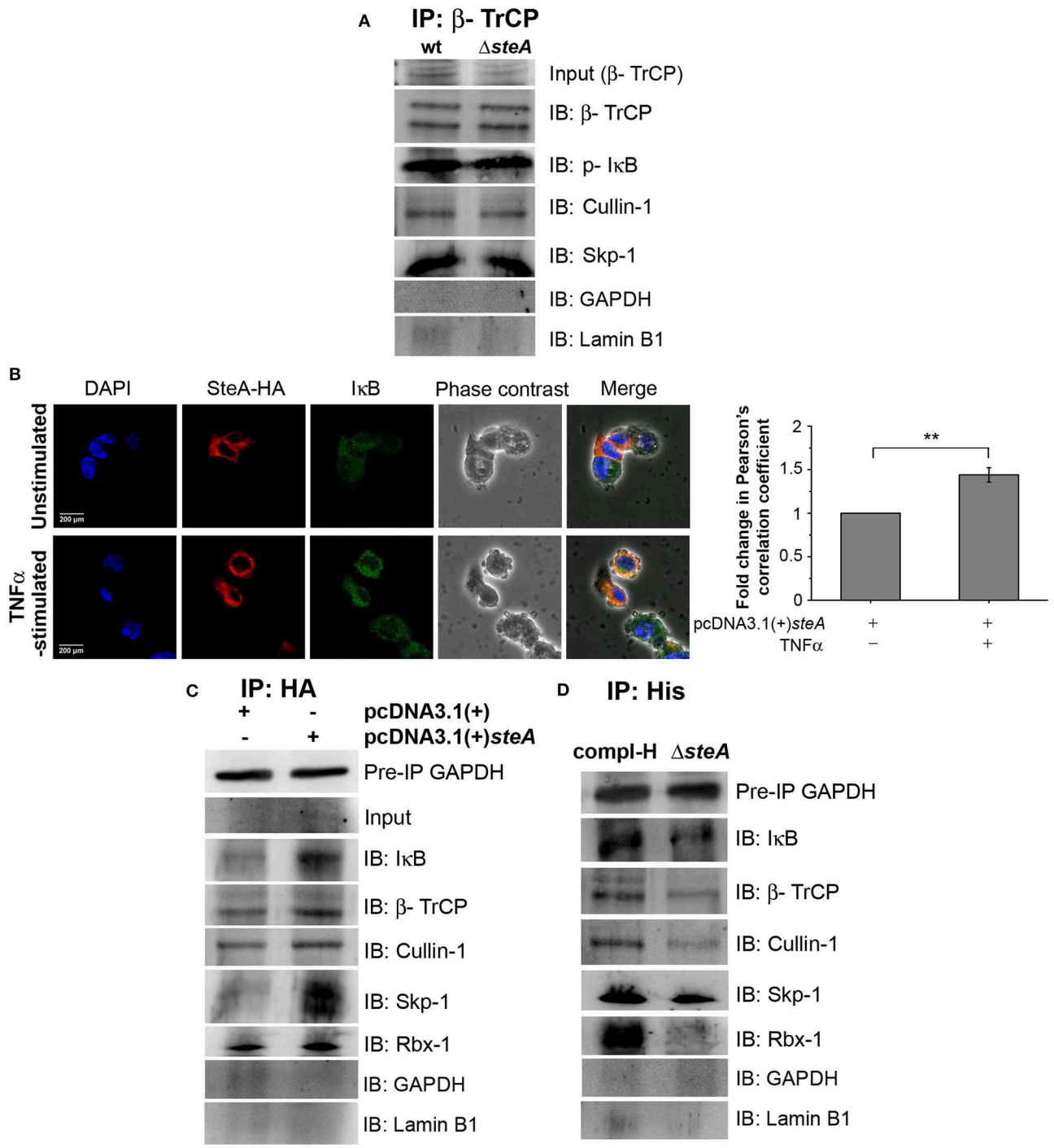

FIGURE 7 | SteA localizes to the SCF-E3 ligase complex. **(A)** The SCF-E3 ligase complex assembled at phosphorylated IκB (p-IκB) in the presence or absence of SteA. RAW 264.7 cells were infected with wt or Δ*steA* strains at an multiplicity of infection (MOI) of 20:1 for 30 min. Whole-cell lysates were then prepared and subjected to immunoprecipitation with anti-β-TrCP antibody. The Skp-1, Cullin-1, F-box (SCF) complex members and p-IκB were then probed by Western blotting. Glyceraldehyde 3-phosphate dehydrogenase (GAPDH) and Lamin B1 were also probed after IP to check the specificity of the pulldowns. **(B)** The colocalization of SteA and IκB increased upon tumor necrosis factor alpha (TNFα) stimulation as compared to the unstimulated control as observed under confocal microscopy. HEK 293 cells overexpressing HA-tagged SteA were fixed after 30 min of TNFα stimulation and were incubated with anti-IκB and anti-HA primary antibodies. Then, the cells were stained with Alexa 488-tagged (for IκB), Alexa 568-tagged (for HA) secondary antibodies, and 4′,6-diamidino-2-phenylindole (DAPI; for the nucleus). The cells were then observed under a confocal microscope. The colocalization was quantified using Pearson's correlation coefficient (PCC) taking 8–10 fields per experiment. Bar graph represents as mean ± SEM from three independent experiments (*$p < 0.05$, **$p < 0.01$, ***$p < 0.001$, ns $p > 0.05$ vs. fold change of PCC in unstimulated cells). **(C,D)** SteA localizes to the SCF-E3 ligase complex on IκB. **(C)** HEK 293 cells were transfected with pcDNA3.1(+)*steA* or pcDNA3.1(+) empty vector. After 18 h

(Continued)

FIGURE 7 | of transfection, cells were stimulated with TNFα for 30 min, and whole-cell lysates were immunoprecipitated with anti-HA antibody. **(D)** RAW 264.7 cells were infected with Δ*steA* and Δ*steA* complemented with His-tagged SteA (compl-H) at an MOI of 20:1 for 30 min. Whole-cell lysates were then prepared and subjected to immunoprecipitation with anti-His antibody. **(C,D)** SCF complex members and IκB were then probed by Western blotting. GAPDH in the preimmunoprecipitation (pre-IP) samples was used as a loading control for the coimmunoprecipitation. GAPDH and Lamin B1 were also probed after IP to check the specificity of the pulldowns.

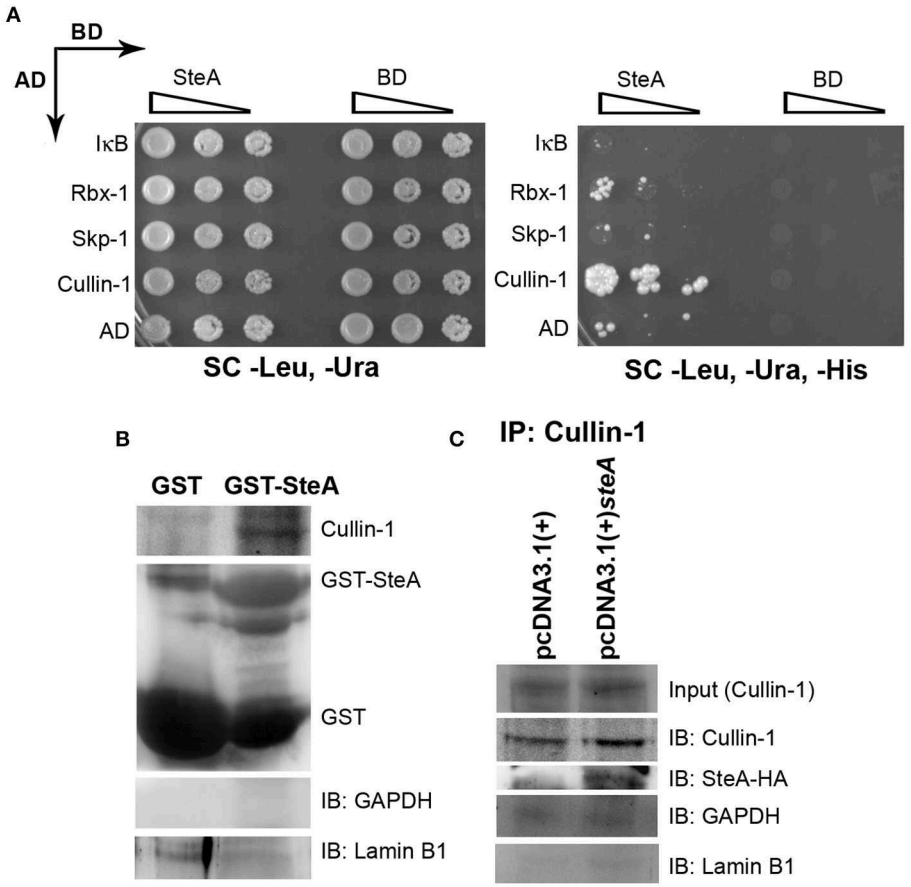

FIGURE 8 | SteA binds to Cullin-1. **(A)** SteA interacts with Cullin-1. The members of the Skp-1, Cullin-1, F-box (SCF) complex and *steA* were cloned in vectors containing activation domain (AD) and binding domain (BD), respectively, for the yeast two-hybrid screen. These were then cotransformed in yeast and selected on synthetic complete (SC)-Leu, SC-Ura, and SC-Leu, SC-Ura, SC-His plates and incubated for 2 days at 30°C. The growth of yeast expressing Cullin-1 and SteA on SC-Leu, SC-Ura, and SC-His plates indicated interaction between SteA and Cullin-1. **(B)** Cullin-1 immunoprecipitates with SteA in the absence of stimulation. Whole-cell lysates of unstimulated RAW 264.7 cells were incubated with glutathione beads labeled with either GST-SteA or GST alone. The beads were then washed, and the proteins bound to GST-SteA or GST were analyzed by Western blotting using anti-Cullin-1 and anti-GST antibodies. **(C)** SteA interacts with Cullin-1. HEK 293 cells were transfected with pcDNA3.1(+)*steA* or pcDNA3.1(+) empty plasmid. After 36 h of transfection, whole-cell lysates were prepared following 30 min of tumor necrosis factor alpha (TNFα) stimulation and immunoprecipitated with anti-Cullin-1 antibody. HA-tagged SteA was detected using anti-HA antibody. **(B,C)** Glyceraldehyde 3-phosphate dehydrogenase (GAPDH) and Lamin B1 were also probed after IP to check the specificity of the pulldowns.

lysates using anti-HA antibody following TNFα stimulation. We have observed that the members of the SCF complex and IκB coimmunoprecipitated with SteA (**Figure 7C** and **Figure S3B**). Furthermore, upon immunoprecipitation of RAW 264.7 cells infected with Δ*steA* and complemented strain expressing His-tagged SteA (compl-H) using anti-His antibody, we observed that SteA coimmunoprecipitated with the SCF complex as well as IκB (**Figure 7D** and **Figure S3C**) even upon infection.

These results indicated that SteA does not inhibit the binding of SCF complex to IκB, and SteA itself binds to the IκB-SCF complex.

SteA Binds to Cullin-1

To better understand how SteA suppresses IκB degradation, we wanted to explore with which component of the SCF complex SteA binds or whether it directly binds to IκB. Toward this, we did a yeast two-hybrid screen for the interaction of SteA

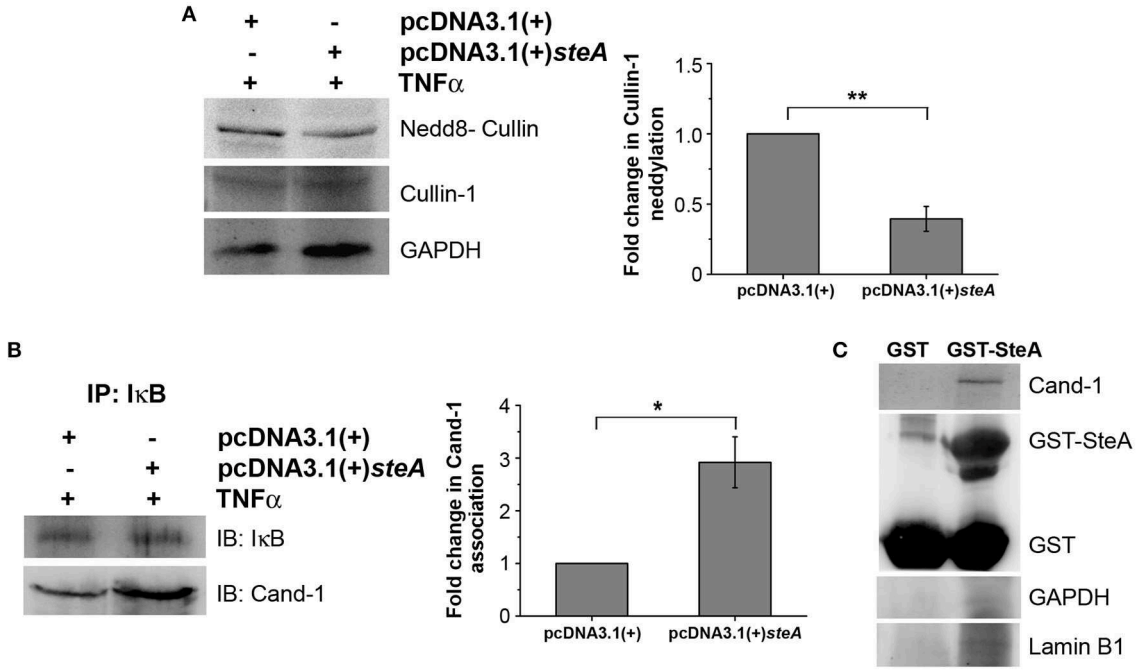

FIGURE 9 | SteA suppresses the neddylation of Cullin-1 and the dissociation of Cand-1. **(A)** Neddylation of Cullin is suppressed in mammalian cells endogenously expressing SteA. HEK 293 cells were transfected with pcDNA3.1(+)*steA* or pcDNA3.1(+) empty plasmid. After 24 h of transfection, whole-cell lysates were prepared following 30 min of tumor necrosis factor alpha (TNFα) stimulation and analyzed by Western blotting using anti-nedd8-Cullin and anti-Cullin-1 antibodies and densitometry. Glyceraldehyde 3-phosphate dehydrogenase (GAPDH) was used as a loading control. **(B)** Cand-1 dissociation from SCF-E3 complex localized at IκB is decreased in the presence of SteA. HEK 293 cells were transfected with pcDNA3.1(+)*steA* or pcDNA3.1(+) empty plasmid. After 24 h of transfection, whole-cell lysates were prepared following 20 min of TNFα stimulation in the presence of proteasomal inhibitor (MG132) and immunoprecipitated with anti-IκB antibody. Cand-1 association was analyzed by Western blotting and densitometry. **(A,B)** For densitometric analysis, fold change was calculated with respect to empty plasmid transfected cells. Bar graphs represent mean ± SEM from three independent experiments. *p* values were calculated using Student's *t* test [$^{*}p < 0.05$, $^{**}p < 0.01$, $^{***}p < 0.001$, ns $p > 0.05$ vs. pcDNA3.1(+) transfected cells]. **(C)** Cand-1 coimmunoprecipitates with SteA even in the unstimulated cells. Whole-cell lysates of unstimulated RAW 264.7 cells were incubated with glutathione beads labeled with either GST-SteA or GST alone. The beads were then washed, and the proteins bound to GST-SteA or GST were analyzed by Western blotting using anti-Cand-1 and anti-GST antibodies. GAPDH and Lamin B1 were also probed after IP to check the specificity of the pulldown.

with IκB and the members of the SCF complex (**Figure 8A**). In this screen, we observed that SteA binds to Cullin-1 but not to IκB, Rbx-1, or Skp-1, indicating that SteA directly interacts with Cullin-1.

Interestingly, we also observed colocalization of SteA with Cullin-1 in both TNFα-stimulated and unstimulated SteA-transfected HEK 293 cells using confocal microscopy, suggesting an association of SteA with Cullin-1 even when SCF complex is not assembled at IκB (**Figure S5A**). Furthermore, we did a GST pulldown assay in whole-cell lysates of unstimulated RAW 264.7 cells using GST-tagged SteA and observed that Cullin-1 was coimmunoprecipitated with GST-tagged SteA (**Figure 8B** and **Figure S4B**). In addition, in HEK 293 cells expressing HA-tagged SteA, we observed that SteA coimmunoprecipitated with Cullin-1 upon immunoprecipitation with anti-Cullin-1 antibody (**Figure 8C** and **Figure S4A**).

Altogether, these data confirmed that SteA interacts with Cullin-1 to suppress IκB degradation.

SteA Binds to Cullin-1 and Prevents Its Neddylation by Interfering With the Dissociation of Cand-1 From Cullin-1

Generally, upon assembly of the SCF complex to IκB, Cullin-1 gets neddylated. This neddylation of Cullin-1 is a crucial step for the activation of the SCF-E3 ligase, which leads to the ubiquitination of IκB (39). Upon neddylation, Cand-1, which is bound to Cullin-1 in the inactivated state, is removed from the E3 ligase complex (40). Therefore, we first checked the neddylation of Cullin-1 in HEK 293 cells transfected with pcDNA3.1(+) and pcDNA3.1(+)*steA* and observed that, upon TNFα stimulation, Cullin-1 was less neddylated in cells expressing SteA (**Figure 9A**). Furthermore, to check if Cand-1 dissociation from the E3 ligase complex was inhibited in the presence of SteA, we stimulated SteA-expressing HEK 293 cells after pretreatment with MG132 and immunoprecipitated with anti-IκB antibody and probed for Cand-1. We observed that Cand-1 dissociation was lesser in the presence of SteA (**Figure 9B**). In addition, in GST pulldown assay, we observed the association of Cand-1 to GST-tagged

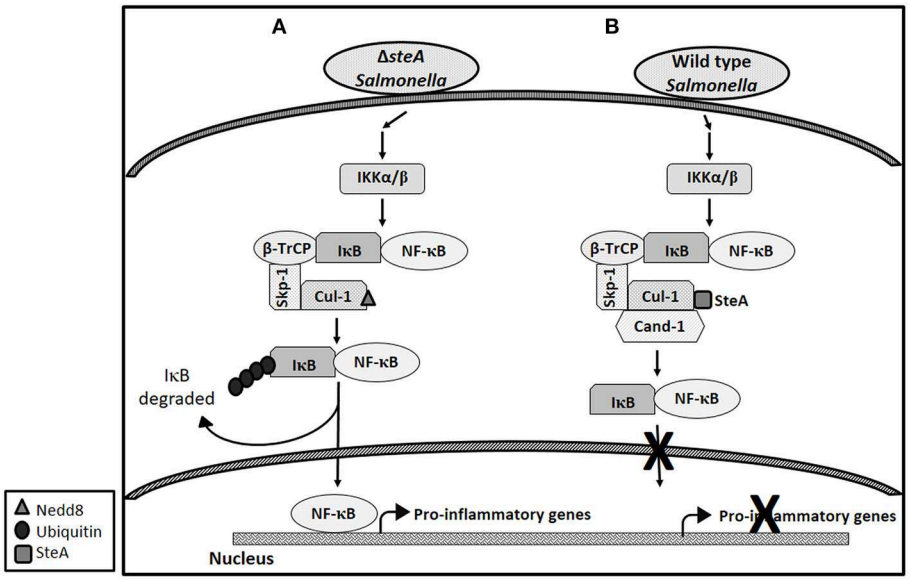

FIGURE 10 | Schematic representation of how SteA suppresses the nuclear factor kappa B (NF-κB) pathway. **(A)** In absence of SteA, *Salmonella* Typhimurium (Δ*steA*) infection triggers a signaling cascade, which leads to the phosphorylation of IKKα/β. IKKα/β then phosphorylates IκB, which is the inhibitor of NF-κB. In the inactivated state, IκB is bound to NF-κB, thus preventing NF-κB to translocate to the nucleus. Phosphorylated IκB is recognized by the F-box protein β-TrCP, which further leads to recruitment of the Skp-1 and Cullin-1 (Cul-1) to form the SCF-E3 ligase complex. Cullin-1 is bound to Cand-1 in the inactive state, and upon neddylation, Cand-1 dissociates from Cullin-1 leading to the complete activation of the E3 ligase. The E3 ligase complex is responsible for the polyubiquitination of IκB. Upon polyubiquitination, IκB undergoes proteasomal degradation, rendering NF-κB free to translocate to the nucleus and transcribe proinflammatory genes. **(B)** During wild-type (wt) *Salmonella* Typhimurium infection (when SteA is present), SteA binds to Cullin-1 (of SCF-E3 ligase) and suppresses the neddylation of Cullin-1 and the dissociation of Cand-1 from Cullin-1, thereby suppressing the polyubiquitination of IκB. This leads to the suppression of NF-κB-mediated proinflammatory responses.

SteA even in unstimulated RAW 264.7 cells, indicating that SteA remains associated with Cullin-1/Cand-1 complex even without stimulation (**Figure 9C** and **Figure S4C**). To further confirm this, we checked the colocalization of SteA and Cand-1 in SteA-transfected HEK 293 cells, and we observed no difference in the colocalization of SteA and Cand-1 with or without TNFα stimulation (**Figure S5B**).

Altogether, this study shows that SteA suppresses the immune responses of the host by suppressing the degradation of IκB. SteA prevents the degradation of IκB by binding to Cullin-1 and thus suppressing the neddylation of Cullin-1, which is necessary for the complete activation of the E3 ligase complex to ubiquitinate IκB (**Figure 10**).

DISCUSSION

In response to a bacterial infection, the immune cells of the host elicit a proinflammatory response and signal other cells of the intrusion. This eventually leads to clearing of the bacteria from the host system. Some pathogens including *Salmonella* Typhimurium have been known to evade the immune system of the host and establish a niche in the macrophages. *Salmonella* Typhimurium makes use of some of the effectors that it translocates directly into the host cells via the type three secretion systems (T3SS) to suppress the host's immune responses. The effectors secreted by T3SSs, mainly T3SS-1, play different roles in immunomodulation of the host (8). Toward characterizing the T3SS-1 role of SteA, we found that mice infected with *steA*-deficient *Salmonella* Typhimurium (Δ*steA*) showed lower survival as compared to the wt *Salmonella* Typhimurium infected mice (**Figures 1A**,**B**). Furthermore, a higher immune response in mice infected with Δ*steA* seemed to be the cause of increased lethality (**Figures 1C–E** and **Figure S1**). Similarly, higher proinflammatory responses were observed when RAW 264.7 murine macrophage cell line and BMDMs were infected with Δ*steA* as compared to wt-infected cells (**Figure 2A**). Furthermore, we confirmed that SteA-mediated suppression of immune response is a T3SS-1 effect using a strain deficient in T3SS-2 (Δ*spi2*) and a Δ*spi2*Δ*steA* double mutant (**Figure 2B**).

The proinflammatory responses are mediated by a multistep signaling cascade involving the activation of the NF-κB pathway or the MAP kinase pathway leading to the activation of transcription factors NF-κB and AP-1 (36). Some of the effectors of *Salmonella* Typhimurium are already known to suppress the host-immune responses. For example, SpvC suppresses the MAP kinase pathway by dephosphorylating JNK and ERK (41), SptP acts on the ERK activation (42, 43), while AvrA suppresses both the NF-κB and the MAP kinase pathway (44–47), hence suppressing inflammation. To be able to understand how SteA suppresses the proinflammatory responses, we first checked the activation levels of p38 and JNK MAP kinases in the whole-cell lysates and the levels of NF-κB family members (p65 and c-Rel) in the nuclear lysates. We observed that SteA does not affect the MAP-kinase activation but acts on the NF-κB pathway

to suppress the immune responses (**Figures 3–5**). To confirm our observation, we transfected HEK 293 and RAW 264.7 cells with NF-κB luciferase reporter plasmid and found the activation of NF-κB to be higher upon infection with Δ*steA* than the wt (**Figure 5B**). Furthermore, upon endogenous expression of SteA in HEK 293 cells, the NF-κB reporter activity was found to be suppressed (**Figure 5C**). Since suppression of the NF-κB pathway is crucial for the survival of *Salmonella* Typhimurium in the host, *Salmonella* Typhimurium secretes various effectors to control it at multiple levels. In the inactive state, NF-κB remains bound to the inhibitor IκB; for the activation of NF-κB, IκB kinase (IKK) phosphorylates IκB and leads to its ubiquitination and degradation rendering NF-κB free. The free NF-κB transcription factor translocates to the nucleus, binds to the DNA, and upregulates transcription of inflammatory cytokine genes (37). Some effectors such as AvrA and SseL are known to interfere with IκB degradation by deubiquitinating IκB (44, 48). Another effector, SpvD, affects the recycling of NF-κB, and PipA acts as a protease, which cleaves RelA, a subunit of NF-κB after its activation (49, 50). Toward exploring how SteA suppresses the NF-κB pathway, we checked the degradation level of IκB in the presence or absence of SteA and observed increased degradation of IκB in the absence of SteA compared to when SteA was present, suggesting that SteA acts on IκB degradation (**Figure 4**). The degradation of IκB is a multistep pathway which is initiated by the phosphorylation of IκB. IκB phosphorylation is dependent on IKK; therefore, there could be increased activation of IKK itself in the absence of SteA, but we observed comparable activation of IKK in cells infected with wt or Δ*steA* strains (**Figure 6A**). Following phosphorylation, the SCF-E3 ligase complex assembles on IκB, leading to the polyubiquitination of IκB and hence its proteasomal degradation (31). One of the effectors, GogB, suppresses ubiquitination by acting on Skp-1, a component of SCF-E3 ligase (51). Our study indicated that SteA also binds to the SCF complex and suppresses the activation of IκB by interfering with the ubiquitination (**Figure 6B**). However, we observed that SteA mainly acts on Cullin-1 of SCF-E3 ligase complex (**Figure 8**). For ubiquitination to happen, the neddylation of Cullin-1 follows the assembly of SCF-E3 ligase complex to IκB. Neddylation of Cullin-1 is a crucial step for the complete activation of the E3 ligase (39). Cullin-1 in the inactive form remains bound to Cand-1; however, upon activation, Cand-1 dissociates from Cullin-1 allowing neddylation to happen (40). Our study indicated that SteA binds to Cullin-1 (**Figure 8**), thus interfering with neddylation of Cullin-1 and the dissociation of Cand-1 from Cullin-1 (**Figure 9**). This further results in suppression of IκB ubiquitination and its degradation.

In response to *Salmonella* Typhimurium infection, proinflammatory responses are generated in the host. This immune response is capable of clearing the infection; also, if unchecked, it may be lethal for the host. However, for *Salmonella* Typhimurium to be able to survive and multiply in the host, these proinflammatory responses need to be suppressed. For this, *Salmonella* Typhimurium secretes an array of effectors which suppress the immune responses at multiple levels and ensures its survival in the host.

Altogether, our study shows that *Salmonella* Typhimurium effector SteA suppresses the proinflammatory responses generated against *Salmonella* Typhimurium by suppressing the neddylation of Cullin-1 and hence suppressing the degradation of IκB, eventually leading to the suppression of NF-κB activation (**Figure 10**).

DATA AVAILABILITY STATEMENT

All datasets generated for this study are included in the article/**Supplementary Material**. The raw datasets will be available on request.

ETHICS STATEMENT

The animal study was reviewed and approved by the Institutional Animals Ethics Committee (IAEC) of the Indian Institute of Science Education and Research, Mohali.

AUTHOR CONTRIBUTIONS

AG designed and performed experiments, analyzed the data, and wrote the paper. RS performed experiments and analyzed the data. AM designed experiments, analyzed data, supervised the study, and wrote the paper.

FUNDING

This work was funded by a research grant from the Science and Engineering Research Board (SERB), Department of Science and Technology (DST), India (Grant No. EMR/2016/007788) and IISER Mohali. We acknowledge the Indian Council of Medical Research (ICMR) for funding AG and IISER Mohali for funding RS.

ACKNOWLEDGMENTS

We thank Dr. Rachna Chaba (IISER Mohali, India) and her lab members for helping us with the preparation of deletion mutants and Dr. Shravan K. Mishra (IISER Mohali, India) and his lab members for helping with yeast two-hybrid-based experiments. We thank Dr. Kausik Chattopadhyay, Dr. Mahak Sharma, Dr. Rajesh Ramachandran, and Dr. Ram K. Yadav from IISER Mohali, India, and Dr. Francisco Ramos-Morales from the University of Seville, Spain for providing us with various strains or plasmids.

SUPPLEMENTARY MATERIAL

The Supplementary Material for this article can be found online at: https://www.frontiersin.org/articles/10.3389/fimmu.2019.02822/full#supplementary-material

REFERENCES

1. Kubori T, Matsushima Y, Nakamura D, Uralil J, Lara-Tejero M, Sukhan A, et al. Supramolecular structure of the *Salmonella typhimurium* type III protein secretion system. *Science*. (1998) 280:602–5. doi: 10.1126/science.280.5363.602
2. Galan JE. Interaction of Salmonella with host cells through the centisome 63 type III secretion system. *Curr Opin Microbiol*. (1999) 2:46–50. doi: 10.1016/S1369-5274(99)80008-3
3. Galan JE. Molecular genetic bases of Salmonella entry into host cells. *Mol Microbiol*. (1996) 20:263–71. doi: 10.1111/j.1365-2958.1996.tb02615.x
4. Ochman H, Soncini FC, Solomon F, Groisman EA. Identification of a pathogenicity island required for Salmonella survival in host cells. *Proc Natl Acad Sci USA*. (1996) 93:7800–4. doi: 10.1073/pnas.93.15.7800
5. Shea JE, Hensel M, Gleeson C, Holden DW. Identification of a virulence locus encoding a second type III secretion system in *Salmonella typhimurium*. *Proc Natl Acad Sci USA*. (1996) 93:2593–7. doi: 10.1073/pnas.93.6.2593
6. Ramos-Morales F. Impact of *Salmonella enterica* type III secretion system effectors on the eukaryotic host cell. *ISRN Cell Biol*. (2012) 2012:36. doi: 10.5402/2012/787934
7. Hensel M, Shea JE, Waterman SR, Mundy R, Nikolaus T, Banks G, et al. Genes encoding putative effector proteins of the type III secretion system of Salmonella pathogenicity island 2 are required for bacterial virulence and proliferation in macrophages. *Mol Microbiol*. (1998) 30:163–74. doi: 10.1046/j.1365-2958.1998.01047.x
8. McGhie EJ, Brawn LC, Hume PJ, Humphreys D, Koronakis V. Salmonella takes control: effector-driven manipulation of the host. *Curr Opin Microbiol*. (2009) 12:117–24. doi: 10.1016/j.mib.2008.12.001
9. Eichelberg K, Galan JE. Differential regulation of *Salmonella typhimurium* type III secreted proteins by pathogenicity island 1. (SPI-1)-encoded transcriptional activators InvF and hilA. *Infect Immun*. (1999) 67:4099–105.
10. McGhie EJ, Hayward RD, Koronakis V. Cooperation between actin-binding proteins of invasive Salmonella: SipA potentiates SipC nucleation and bundling of actin. *EMBO J*. (2001) 20:2131–9. doi: 10.1093/emboj/20.9.2131
11. Lilic M, Galkin VE, Orlova A, VanLoock MS, Egelman EH, Stebbins CE. Salmonella SipA polymerizes actin by stapling filaments with nonglobular protein arms. *Science*. (2003) 301:1918–21. doi: 10.1126/science.1088433
12. Myeni SK, Zhou D. The C terminus of SipC binds and bundles F-actin to promote Salmonella invasion. *J Biol Chem*. (2010) 285:13357–63. doi: 10.1074/jbc.M109.094045
13. Friebel A, Ilchmann H, Aepfelbacher M, Ehrbar K, Machleidt W, Hardt WD. SopE and SopE2 from *Salmonella typhimurium* activate different sets of RhoGTPases of the host cell. *J Biol Chem*. (2001) 276:34035–40. doi: 10.1074/jbc.M100609200
14. Hapfelmeier S, Ehrbar K, Stecher B, Barthel M, Kremer M, Hardt WD. Role of the Salmonella pathogenicity island 1 effector proteins SipA, SopB, SopE, and SopE2 in *Salmonella enterica* subspecies 1 serovar Typhimurium colitis in streptomycin-pretreated mice. *Infect Immun*. (2004) 72:795–809. doi: 10.1128/IAI.72.2.795-809.2004
15. Bruno VM, Hannemann S, Lara-Tejero M, Flavell RA, Kleinstein SH, Galan JE. *Salmonella typhimurium* type III secretion effectors stimulate innate immune responses in cultured epithelial cells. *PLoS Pathog*. (2009) 5:e1000538. doi: 10.1371/journal.ppat.1000538
16. Stein MA, Leung KY, Zwick M, Garcia-del Portillo F, Finlay BB. Identification of a Salmonella virulence gene required for formation of filamentous structures containing lysosomal membrane glycoproteins within epithelial cells. *Mol Microbiol*. (1996) 20:151–64. doi: 10.1111/j.1365-2958.1996.tb02497.x
17. Beuzon CR, Meresse S, Unsworth KE, Ruiz-Albert J, Garvis S, Waterman SR, et al. Salmonella maintains the integrity of its intracellular vacuole through the action of SifA. *EMBO J*. (2000) 19:3235–49. doi: 10.1093/emboj/19.13.3235
18. Brumell JH, Goosney DL, Finlay BB. SifA, a type III secreted effector of *Salmonella typhimurium*, directs Salmonella-induced filament. (Sif) formation along microtubules. *Traffic*. (2002) 3:407–15. doi: 10.1034/j.1600-0854.2002.30604.x
19. Brumell JH, Tang P, Mills SD, Finlay BB. Characterization of Salmonella-induced filaments. (Sifs) reveals a delayed interaction between Salmonella-containing vacuoles and late endocytic compartments. *Traffic*. (2001) 2:643–53. doi: 10.1034/j.1600-0854.2001.20907.x
20. Vorwerk S, Krieger V, Deiwick J, Hensel M, Hansmeier N. Proteomes of host cell membranes modified by intracellular activities of *Salmonella enterica*. *Mol Cell Proteom*. (2015) 14:81–92. doi: 10.1074/mcp.M114.041145
21. Knuff K, Finlay BB. What the SIF is happening-the role of intracellular salmonella-induced filaments. *Front Cell Infect Microbiol*. (2017) 7:335. doi: 10.3389/fcimb.2017.00335
22. Geddes K, Worley M, Niemann G, Heffron F. Identification of new secreted effectors in *Salmonella enterica* serovar Typhimurium. *Infect Immun*. (2005) 73:6260–71. doi: 10.1128/IAI.73.10.6260-6271.2005
23. Niemann GS, Brown RN, Gustin JK, Stufkens A, Shaikh-Kidwai AS, Li J, et al. Discovery of novel secreted virulence factors from *Salmonella enterica* serovar Typhimurium by proteomic analysis of culture supernatants. *Infect Immun*. (2011) 79:33–43. doi: 10.1128/IAI.00771-10
24. Cardenal-Munoz E, Ramos-Morales F. Analysis of the expression, secretion and translocation of the *Salmonella enterica* type III secretion system effector SteA. *PLoS ONE*. (2011) 6:e26930. doi: 10.1371/journal.pone.0026930
25. Lawley TD, Chan K, Thompson LJ, Kim CC, Govoni GR, Monack DM. Genome-wide screen for Salmonella genes required for long-term systemic infection of the mouse. *PLoS Pathog*. (2006) 2:e11. doi: 10.1371/journal.ppat.0020011
26. Van Engelenburg SB, Palmer AE. Imaging type-III secretion reveals dynamics and spatial segregation of Salmonella effectors. *Nat Methods*. (2010) 7:325–30. doi: 10.1038/nmeth.1437
27. Domingues L, Holden DW, Mota LJ. The Salmonella effector SteA contributes to the control of membrane dynamics of Salmonella-containing vacuoles. *Infect Immun*. (2014) 82:2923–34. doi: 10.1128/IAI.01385-13
28. Domingues L, Ismail A, Charro N, Rodriguez-Escudero I, Holden DW, Molina M, et al. The Salmonella effector SteA binds phosphatidylinositol 4-phosphate for subcellular targeting within host cells. *Cell Microbiol*. (2016) 18:949–69. doi: 10.1111/cmi.12558
29. Matsuda S, Haneda T, Saito H, Miki T, Okada N. *Salmonella enterica* Effectors SifA, SpvB, SseF, SseJ, and SteA contribute to type III secretion system 1-independent inflammation in a streptomycin-pretreated mouse model of colitis. *Infect Immun*. (2019) 87:e00872–18. doi: 10.1128/IAI.00872-18
30. McQuate SE, Young AM, Silva-Herzog E, Bunker E, Hernandez M, de Chaumont F, et al. Long-term live-cell imaging reveals new roles for Salmonella effector proteins SseG and SteA. *Cell Microbiol*. (2017) 19:e12641. doi: 10.1111/cmi.12641
31. Kanarek N, London N, Schueler-Furman O, Ben-Neriah Y. Ubiquitination and degradation of the inhibitors of NF-kappaB. *Cold Spring Harb Perspect Biol*. (2010) 2:a000166. doi: 10.1101/cshperspect.a000166
32. Datsenko KA, Wanner BL. One-step inactivation of chromosomal genes in *Escherichia coli* K-12 using PCR products. *Proc Natl Acad Sci USA*. (2000) 97:6640–5. doi: 10.1073/pnas.120163297
33. Baison-Olmo F, Cardenal-Munoz E, Ramos-Morales F. PipB2 is a substrate of the Salmonella pathogenicity island 1-encoded type III secretion system. *Biochem Biophys Res Commun*. (2012) 423:240–6. doi: 10.1016/j.bbrc.2012.05.095
34. Shrum B, Anantha RV, Xu SX, Donnelly M, Haeryfar SM, McCormick JK, et al. A robust scoring system to evaluate sepsis severity in an animal model. *BMC Res Notes*. (2014) 7:233. doi: 10.1186/1756-0500-7-233
35. Mai SHC, Sharma N, Kwong AC, Dwivedi DJ, Khan M, Grin PM, et al. Body temperature and mouse scoring systems as surrogate markers of death in cecal ligation and puncture sepsis. *Intensive Care Med Exp*. (2018) 6:20. doi: 10.1186/s40635-018-0184-3
36. Kawai T, Akira S. The role of pattern-recognition receptors in innate immunity: update on Toll-like receptors. *Nat Immunol*. (2010) 11:373–84. doi: 10.1038/ni.1863
37. Oeckinghaus A, Ghosh S. The NF-kappaB family of transcription factors and its regulation. *Cold Spring Harb Perspect Biol*. (2009) 1:a000034. doi: 10.1101/cshperspect.a000034
38. Deshaies RJ. SCF and Cullin/Ring H2-based ubiquitin ligases. *Annu Rev Cell Dev Biol*. (1999) 15:435–67. doi: 10.1146/annurev.cellbio.15.1.435

39. Petroski MD, Deshaies RJ. Function and regulation of cullin-RING ubiquitin ligases. *Nat Rev Mol Cell Biol*. (2005) 6:9–20. doi: 10.1038/nrm1547
40. Goldenberg SJ, Cascio TC, Shumway SD, Garbutt KC, Liu J, Xiong Y, et al. Structure of the Cand1-Cul1-Roc1 complex reveals regulatory mechanisms for the assembly of the multisubunit cullin-dependent ubiquitin ligases. *Cell*. (2004) 119:517–28. doi: 10.1016/j.cell.2004.10.019
41. Mazurkiewicz P, Thomas J, Thompson JA, Liu M, Arbibe L, Sansonetti P, et al. SpvC is a Salmonella effector with phosphothreonine lyase activity on host mitogen-activated protein kinases. *Mol Microbiol*. (2008) 67:1371–83. doi: 10.1111/j.1365-2958.2008.06134.x
42. Murli S, Watson RO, Galan JE. Role of tyrosine kinases and the tyrosine phosphatase SptP in the interaction of Salmonella with host cells. *Cell Microbiol*. (2001) 3:795–810. doi: 10.1046/j.1462-5822.2001.00158.x
43. Lin SL, Le TX, Cowen DS. SptP, a *Salmonella typhimurium* type III-secreted protein, inhibits the mitogen-activated protein kinase pathway by inhibiting Raf activation. *Cell Microbiol*. (2003) 5:267–75. doi: 10.1046/j.1462-5822.2003.t01-1-00274.x
44. Collier-Hyams LS, Zeng H, Sun J, Tomlinson AD, Bao ZQ, Chen H, et al. Cutting edge: salmonella AvrA effector inhibits the key proinflammatory, anti-apoptotic NF-kappa B pathway. *J Immunol*. (2002) 169:2846–50. doi: 10.4049/jimmunol.169.6.2846
45. Ye Z, Petrof EO, Boone D, Claud EC, Sun J. Salmonella effector AvrA regulation of colonic epithelial cell inflammation by deubiquitination. *Am J Pathol*. (2007) 171:882–92. doi: 10.2353/ajpath.2007.070220
46. Jones RM, Wu H, Wentworth C, Luo L, Collier-Hyams L, Neish AS. Salmonella AvrA coordinates suppression of host immune and apoptotic defenses via JNK pathway blockade. *Cell Host Microbe*. (2008) 3:233–44. doi: 10.1016/j.chom.2008.02.016
47. Du F, Galan JE. Selective inhibition of type III secretion activated signaling by the Salmonella effector AvrA. *PLoS Pathog*. (2009) 5:e1000595. doi: 10.1371/journal.ppat.1000595
48. Le Negrate G, Faustin B, Welsh K, Loeffler M, Krajewska M, Hasegawa P, et al. Salmonella secreted factor L deubiquitinase of *Salmonella typhimurium* inhibits NF-kappaB, suppresses IkappaBalpha ubiquitination and modulates innate immune responses. *J Immunol*. (2008) 180:5045–56. doi: 10.4049/jimmunol.180.7.5045
49. Rolhion N, Furniss RC, Grabe G, Ryan A, Liu M, Matthews SA, et al. Inhibition of nuclear transport of NF-kB p65 by the Salmonella type III secretion system effector SpvD. *PLoS Pathog*. (2016) 12:e1005653. doi: 10.1371/journal.ppat.1005653
50. Sun H, Kamanova J, Lara-Tejero M, Galan JE. A family of salmonella type III secretion effector proteins selectively targets the NF-kappaB signaling pathway to preserve host homeostasis. *PLoS Pathog*. (2016) 12:e1005484. doi: 10.1371/journal.ppat.1005484
51. Pilar AV, Reid-Yu SA, Cooper CA, Mulder DT, Coombes BK. GogB is an anti-inflammatory effector that limits tissue damage during Salmonella infection through interaction with human FBXO22 and Skp1. *PLoS Pathog*. (2012) 8:e1002773. doi: 10.1371/journal.ppat.1002773

Conflict of Interest: The authors declare that the research was conducted in the absence of any commercial or financial relationships that could be construed as a potential conflict of interest.